Synthesis of Amphiphilic Stimuli-responsive Block Copolymers and their Structural Characterization to generate smart membranes

Maryam Bozorg

Hamburg 2021

University of Hamburg

Faculty of Mathematics, Informatics and Natural Sciences

Institute of Physical Chemistry, Department of Chemistry

Dissertation submitted to the University of Hamburg in fulfillment of the requirements for the degree of doctor rerum naturalium (Dr. rer. nat.)

PhD advisor: Prof. Dr. Volker Abetz

Reviewr 1: Prof. Dr. Volker Abetz

Reviewer 2: Priv. Doz. Dr. Christoph Wutz

Date of defense: 18.06.2021

UHH
Universität Hamburg
DER FORSCHUNG | DER LEHRE | DER BILDUNG

The submitted dissertation was prepared under the supervision of Prof. Dr. Volker Abetz at the Institute of Physical Chemistry (Department of Chemistry, MIN Faculty), University of Hamburg. The study was conducted between April 2013 and December 2017 and the dissertation was submitted in March 2021.

Contents

Figures

Tables

Abbreviations

$[i]$	concentration of compound i
A	amplitude of cumulant fit of field autocorrelation function
AFM	atomic force microscopy
AIBN	Azobisisobutyronitrile
ATRP	atom transfer radical polymerization
b	block
B_{max}	increase in LCST at ion saturation due to ion adsorption
BHT	butylated hydroxytoluene
BIBB	α-bromoisobutyryl bromide
BriBA	α-Bromoisobutyric acid
CRP	controlled radical polymerization
CTA	chain transfer agent
CTAB	cetyltrimethylammonium bromide
CuBr	copper(I) bromide
D	diffusion coefficient
2DCOS	two-dimensional correlation spectroscopy
DCC	*N*,*N*′-dicyclohexylcarbodiimide
DCM	dichloromethane
DLS	dynamic light scattering
DMAC	*N*,*N*-dimethylacetamide
DMAP	4-dimethylamino pyridine
DMF	*N*,*N*-Dimethylformamide
dNbpy	4,4′-dinonyl-2,2′-bipyridine
DOX	dioxane
DSC	differential scanning calorimetry
E	redox potential
EO	ethylene oxide
EBiB	ethyl α-bromo isobutirate
f	fraction of occupied independent binding sites

FTIR	Fourier-transform infrared spectroscopy
G	Free Gibbs energy
g^{1}	field autocorrelation function
grad	gradient
H	enthalpy
HPC	hydroxypropyl cellulose
I	initiator
I	normalized scattering intensity
$\mathrm{k_{act}}$	rate coefficient of activation
$\mathrm{k_{app}}$	apparent rate coefficient of ATRP
K_{A}	ion association constant to the polymer
$\mathrm{K_{ATRP}}$	rate coefficient of ATRP
$\mathrm{k_{B}}$	Boltzman constant
$\mathrm{k_{deact}}$	rate coefficient of deactivation
K_{eq}	equilibrium constant
$\mathrm{k_{i}}$	rate coefficient of chain initiation
$\mathrm{k_{p}}$	rate coefficient of chain propagation
L	ligand
LCST	lower critical solution temperature
LiBr	Lithium Bromide
M	monomer
MEHQ	monomethyl ether hydroquinone
MEO$_2$MA	di ethylene oxide methyl ether methacrylate
MI	macroinitiator
M_{n}	number-average molecular weight
$M_{n,th}$	Theoretical number-average molecular weight
M_{w}	weight-average molecular weight
MW	molecular weight
n_{0}	refractive index of the solvent
N	total degree of polymerization
NMP	nitroxide mediated polymerization
NMR	nuclear magnetic resonance spectroscopy

ODT	order-to-disorder transition
OEGMA	oligo ethylene glycol methacrylate (synonym: OEOMA)
OEOMA	oligo ethylene oxide methacrylate (synonym: OEGMA)
p	monomer conversion
p_n	polymer chain with the degree of polymerization “n”
P2VP	poly(2-vinylpyridine)
P4VP	poly(4-vinyl pyridine)
PDEAAM	poly(*N*,*N*-diethyl acrylamide)
PDMAEMA	poly[2-(dimethyl amino)ethyl methacrylate]
PEG	poly(ethylene glycol) (synonym: PEO)
PEGMA	poly (ethylene glycol methacrylate) (synonym: POEOMA)
PEO	poly(ethylene oxide) (synonym: PEG)
PEO-N3	azide-end-capped poly(ethylene oxide)
PIPOX	poly-2-isopropyl-2-oxazoline
PMDETA	*N*,*N*,*N*′,*N*″,*N*″-pentamethyl diethylenetriamine
PMEO$_2$MA	poly(di(ethylene oxide) methyl ether methacrylate)
POEOMA	poly (oligo ethylene oxide methacrylate) (synonym: PEGMA)
PMMA	polymethyl methacrylate
PNIPAM	poly(*N*-isopropylacrylamide)
PRE	persistent radical effect
PS	polystyrene
PS-Br	bromide functionalized polystyrene
PS-OH	hydroxy functionalized polystyrene
PSD	particle size dispersity
PVCL	polyvinyl caprolactam
PVME	polyvinyl methyl ether
q	wave vector
r	random

R_g	radius of gyration
R_h	hydrodynamic radius
R_p	polymerization rate
RAFT	reversible addition fragmentation chain transfer
S	entropy
SAX	Small angle X-ray scattering
SDS	sodium dodecyl sulfate
SEC	size exclusion chromatography
SEM	Scanning Electron Microscopy
SET	single electron transfer
SNIPS	self-assembly non-solvent induced phase separation
stat	statistic
Sul	sulfolane
t	time
T	temperature
T_b	boiling point
T_{cp}	cloud point
Tg	glass transition temperature
THF	tetrahydrofuran
UCST	upper critical solution temperature
UV-Vis	ultraviolet–visible
z	number of nearest neighbours per repeat unit in the polymer
υ	molar volume
$\bar{\Gamma}$	averaged relaxation rate
δ	chemical shift (in NMR results)
δ	Hansen solubility parameter
δ_d	dispersion solubility parameter
δ_p	polarity solubility parameter
δ_H	Hydrogen bonding solubility parameter
ε_{AB}	interaction energies per repeat unit of A–B
η	viscosity

λ	wavelength
μ_2	second moment of cumulant fit of field autocorrelation function
χ	Flory-Huggins-Staverman-parameter
$Đ$	Molecular weight dispersity
π^*	polarizability of the solvent

1 Zusammenfassung

Funktionspolymere (stimuli responsive polymers, engl.) haben viel Aufmerksamkeit in der Forschung und Industrieanwendungen auf sich gezogen wegen ihrem großem Potenzial als sogenannte smart materials (intelligente Werkstoffe). Diese sind insbesondere weitverbreitet in Bio-Anwendungen wie z.B. in Arzneimittel oder Gewebe-Engineering, sowie auch in Mikroroboter, Sensoren, Antriebe, und Membrane mit umschaltbaren Porengröße. Poly oligo Ethylenoxid Methacrylate (POEOMAs) sind populär wegen ihrer Biokompatibilität und verstellbarer Thermoempfindlichkeit. Diese Polymere weisen ein großes Bereich unterer kritischen Lösungstemperaturen (LCST) auf, zwischen 26−90 °C in Wasser, abhängig von der Anzahl der Ethylenoxide (EO) in der Seitenkette. Die LCST kann linear angepasst werden durch die einfache Copolymerisation zweier OEOMAs mit verschiedener Anzahl von EOs und durch die Einstellung der Copolymer-Zusammensetzung. Außerdem, ist die Abhängigkeit der LCST von Additive wie Salz oder Wasser geringer für POEOMAs im Vergleich zu anderen Funktionspolymere, was diese umso mehr interessanter für physiologische Anwendungen macht. Die Synthese und Lösbarkeitsverhalten der POEOMAs werden in dieser Arbeit gründlich untersucht. Darüber hinaus, wird der Einfluss verschiedener Additive wie Salze, Netzmittel, und Ethanol als organischer polares Lösungsmittel studiert. Ergebnisse von dynamischer Lichtstreuung zeigen (DLS), dass die LCST abhängig von der Struktur des Copolymers ist und sich leicht durch die Additive verändert. Gute Co-Lösungsmittel wie Ethanol können die LCST durch die Auflösung der kollabierten Copolymer-Ketten erhöhen. Derselbe Einfluss wird für Netzmittel beobachtet, welche die Polymerlösung durch die Verhinderung der Aggregation stabilisieren. Über eine gewisse Konzentration des Netzmittels, abhängig von der Polymerarchitektur, ist die Lösung temperaturübergreifend stabil und kein LCST wird aufgewiesen.

Block-Copolymerisation wird oft benützt um die Eigenschaften zu verbessern und den Anwendungsbereich von Polymere zu erweitern. Außerdem, können Block-Copolymere sich selbst in Bulk zusammenstellen oder in einem selektiven Lösungsmittel um nanostrukturierte, schaltbare Materialien zu bilden. Block-Copolymerisation von OEOMAs mit einem herkömmlichen Monomer wie Styren reduziert nicht nur die Herstellungskosten drastisch und macht sie somit viel interessanter für Industrieanwendungen, sondern verleiht diesen auch

Amphiphilie und damit die Möglichkeit in der Herstellung intelligenter Membrane eingesetzt zu werden.

Polystyren-*b*-Poly[di(ethylenoxid) Methylethermethacrylat] (PS-*b*-PMEO$_2$MA) Diblock Copolymere und Polystyren-*b*-Poly[di(ethyleneoxid) Methylethermethacrylat]-*stat*-Oligo(ethylenoxid) Methylethermethacrylat] [PS-*b*-P(MEO$_2$MA-*stat*-OEOMA)] Diblock Terpolymere mit hohem Molekulargewicht und niedriger Dispersität werden zum ersten Mal synthetisier durch eine Kombination aus streng kontrollierter anionischen Polymerisation and Atom Transfer Radical Polymerization (ATRP). Obwohl kontrollierte Polymerisationstechniken wie ATRP sich als einfache Methoden für die Synthese von POEOMA und derer Block-Copolymere erwiesen, können diese meistens der Polymere nicht hohe Molekularmassen auf einer kontrollierten Art zuteilen. Deshalb sind für Anwendungen in welchen ein hohes Molekulargewicht notwendig ist, wie z.B. in Membrane für Nano- und Ultrafiltration, präzisere Methoden wie die anionische Polymerisation vorteilhafter. In dieser Arbeit wird eine Kombination aus anionischer Polymerisation mit ATRB angewendet um Block-Copolymere zu synthetisieren. Diese Methode ermöglicht Polystyren Majoritäts-Blöckee mit hohem Molekulargewicht und einer sehr geringen Dispersität. Außerdem ermöglicht es die Synthese von POEOMAs durch ATRP. Als Ergebnis davon, können durch diese flexible Methode statistische und Gradient-Copolymere als zweiter Block synthetisiert werden.

PS-*b*-POEOMAs Block Copolymere weisen geregelte selbst zusammengestellte hexagonal gepackte Zylinder ihres eigenen Minoritätsblocks (POEOMA) in Bulk-Morphologie auf. Die Block Copolymere mit hohem Molekulargewicht (>100 kDa) und einer hohen Anzahl an hydrophilem Block (PMEO$_2$MA or P(MEO$_2$MA-*stat*-OEOMA)) weisen eine senkrecht orientierte zylindrische Morphologie auf, während geringeres Molekulargewicht, oder ein geringerer Anteil an hydrophilem Block ein Gemisch aus senkrechten und waagerechten Zylinder erzeugt. Diese bemerkenswerte Selbst-Zusammenaufstellung der PS-*b*-POEOMA bietet die Möglichkeit sehr aussichtreichen Anwendungen für dieser außerordentlichen Block-Copolymere in Nanolithographie und Membrantechnologie. Um das Potenzial dieser Block-Copolymere für Membranvorbereitung zu untersuchen, wurde eine Kombination aus selbst-zusammenaufstellbaren und nicht-lösbarer induzierten Phasenseparation (SNIPS) Technik auf PS-*b*-PMEO$_2$MA und PS-*b*-P(MEO$_2$MA-*stat*-OEOMA) angewendet. Hoch geordnete integral asymmetrische Membrane mit Temperaturempfindlichkeit und verstellbare Porengröße wurden hergestellt. Der Einfluss verschiedener Parameter wie Lösungsmittelvermischung, Lösungskonzentration, Evaporationsdauer, Molekulargewicht des Block-Copolymers und Block-Anteil, sowie auch der Einfluss des Fällungsmittels auf die Oberflächenstruktur der hergestellten Membrane wurden studiert. Die resultierende geregelte Struktur mit hoher Selektivität der oberen Membranschicht mit einer porösen, schwammartigen Struktur der Unterschicht weist somit eine vielversprechende Anwendbarkeit des PS-*b*-POEOMA in der Membranherstellung durch SNIPS als eine unkomplizierte Methode. Solche Membrane können in der Wasserreinigung, Proteintrennung sowie auch weitere Bio-Anwendungen angewendet werden.

2 Abstract

Stimuli responsive polymers have attracted a lot of attention in academic research and industrial application due to their potential for application as smart materials. They are especially popular in bio applications such as drug delivery or tissue engineering as well as microrobots, sensors, actuators, and membranes with switchable pore size. Poly (oligo (ethylene oxide) methacrylates) (POEOMAs) are specially interesting due to their biocompatibility and adjustable thermoresponsivity. These polymers show a vast range of lower critical solution temperature (LCST) between 26-90 °C in water depending on the number of ethylene oxide (EO) in the side chain. The LCST can be linearly adjusted by simple copolymerization of two OEOMAs with different number of EO and adjusting the copolymer composition. Furthermore, the dependence of the LCST on additives such as salt or alcohol is lower for POEOMAs compared to other thermoresponsive polymers, which makes them more interesting for physiological applications. The synthesis and solubility behaviour of POEOMAs is investigated thoroughly in this work. Furthermore, the effect of various additives including different salts, surfactants and ethanol as an organic polar solvent is studied. According to dynamic light scattering (DLS) results, the LCST depends on the structure of the copolymer and it is changing slightly by the additives. Good cosolvents like ethanol can increase the LCST through dissolving the collapsed copolymer chains to some extent. The same effect is observed for surfactants that make the polymer solution more stable by preventing aggregation. Above a certain concentration of surfactant, depending on the polymer architectural structure, the solution is stable at all temperatures and no LCST is observed.

Block copolymerization is often used to improve the properties and widen the application of polymers. Furthermore, block copolymers can self-assemble in bulk or in a selective solvent to form nanostructured switchable materials. Block copolymerization of OEOMAs with a common monomer such as styrene, not only decreases their preparation costs drastically and makes them much more interesting for industrial applications, but also provides them with amphiphilicity and enables them to be used in smart membranes' production.

polystyrene-*b*-poly[di(ethylene oxide) methyl ether methacrylate] (PS-*b*-PMEO$_2$MA) diblock copolymers and polystyrene-*b*-poly[di(ethylene oxide) methyl ether methacrylate]-*stat*-oligo(ethylene oxide) methyl ether methacrylate] [PS-*b*-P(MEO$_2$MA-*stat*-OEOMA)] diblock

terpolymers with high molecular weight and low dispersity are synthesized for the first time by a combination of highly controlled anionic polymerization and atom transfer radical polymerization (ATRP). Although controlled polymerization techniques like ATRP prove to be straightforward methods for the synthesis of POEOMA and their block copolymers, they mostly fail to provide polymers with high molecular weights in a controlled manner. Therefore, for applications in which a high molecular weight polymer is needed, such as in membranes for nano- and ultrafiltration, more precise methods such as anionic polymerization is preferred. In this work, the combination of anionic polymerisation and ATRP is used to synthesize the block copolymers. This method produces polystyrene (PS) major blocks with high molecular weight and very low dispersity and enables the synthesis of POEOMA via ATRP. As a result, one can benefit from the flexibility of ATRP to synthesize random and gradient copolymers of OEOMAs as the second block.

PS-*b*-POEOMAs block copolymers show well-ordered self-assembled hexagonally packed cylinders of their minority block (POEOMA) in bulk morphology. The block copolymers with higher molecular weight (>100 kDa) and higher amount of the hydrophilic block (PMEO$_2$MA or P(MEO$_2$MA-*stat*-OEOMA)) show a perpendicularly oriented cylindrical morphology, while lower molecular weight, or lower ratio of the hydrophilic block result in a mixture of perpendicular and horizontal cylinders. The remarkable self-assembly of PS-*b*-POEOMA offers very promising applications for these extraordinary block copolymers in nanolithography and membrane technology. To study the potential of these block copolymers in membrane preparation, the combination of self-assembly and non-solvent induced phase separation (SNIPS) technique is applied on PS-*b*-PMEO$_2$MA and PS-*b*-P(MEO$_2$MA-stat-OEOMA). Highly ordered integral asymmetric membranes with temperature responsivity and adjustable pore size are fabricated. The influence of different parameters such as solvent mixture, solution concentration, evaporation time and block copolymers' molecular weight and block ratio as well as the effect of precipitant on the surface structure of the fabricated membranes are studied. The resulted well-ordered structure with high selectivity at the top layer of the membrane film with a spongy porous structure at the supporting layer presents the promising application of Ps-*b*-POEOMA in membrane fabrication via SNIPS as a simple fast forward technique. Such membranes can find usage in water treatment as well as protein separation and further bio applications.

3 Theoretical background

3.1 Stimuli responsive polymers

Stimuli-responsive materials respond rapidly to a change in the environment (stimulus) by altering a specific characteristic in themselves. Therefore, they are often called “smart materials”. The most common stimulus are PH, temperature, and electrolyte concentration. However, there are polymers specially in biomedical application which respond to specific antigen–antibody interactions, enzymes, and glucose. Also, the polymeric systems that respond to physical changes such as light, electric, magnetic, and sonic fields, have gathered a lot of attention in the area of controlled release. Thiol-responsive and redox-responsive polymers are very popular due to their reversible dynamic covalent chemistry [1]–[3].

Stimuli-responsive materials are attracting a lot of attention in various research fields due to their promising applications in biomedicine [2][4], drug delivery [2][5]–[8], microfluidic devices [9], tissue engineering [10], sensors [11][12], actuators [13][14], microrobots [15], oil and gas recovery [16], membranes with switchable pore sizes [6][17][18], smart self-cleaning coatings [19] and textile applications [7][10].

The idea of stimuli responsive polymers is inspired by nature which triggered scientists to expand this field of research. The simplest example is sunflowers which turn toward the sun or the leaves of mimosa pudica which collapse suddenly when touched. Mimicking the functions of such organisms, there is a great effort made by scientists to provide stimuli-responsive polymers which have scientific significance and promising applications [10]. The progress in polymer science, especially controlled polymerization provides versatile routes to synthesize various stimuli responsive polymers for sophisticated applications.

Temperature-responsive polymers

Temperature-responsive polymers or thermoresponsive polymers are polymers that exhibit a drastic change in their physical properties when the temperature changes [20]. The physical properties like shape, size, colour, solubility, viscosity or wettability of thermoresponsive materials vary in response to mild temperature fluctuation [21], but the most studied characteristic is the solubility in water.

These polymers show a miscibility gap and as a result, an upper critical solution temperature (UCST) or lower critical solution temperature (LCST) in their temperature- composition diagram. If the polymer shows UCST, the components of the polymer mixture are miscible in all compositions above UCST. And if the polymer shows LCST, the components of the polymer mixture are miscible in all compositions below LCST (Fig.1).

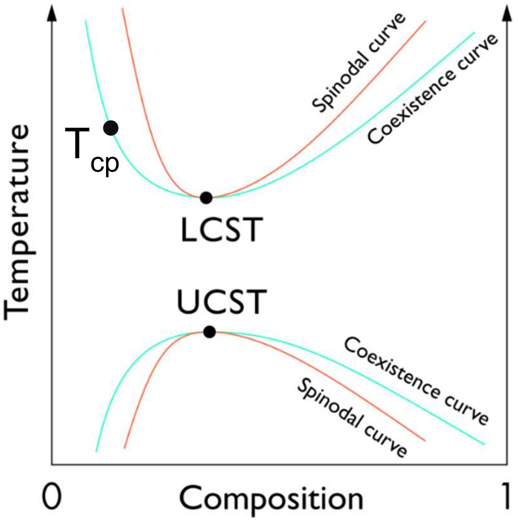

Fig. 1 A typical phase diagram of a polymer solution including LCST and UCST.

Thermoresponsive polymer chains adopt an expanded coil conformation in solution. At the phase separation temperature (T_{cp}) they collapse to form compact globules. This process is called "coil to globule transition" and can be observed directly by methods of turbidimetry [22], static and dynamic light scattering [23][24], Fourier-transform infrared spectroscopy (FTIR) [25][26], Nuclear magnetic resonance spectroscopy (NMR) [27], two-dimensional correlation spectroscopy (2DCOS) [25][28], etc. The drop in viscosity can be indirectly observed. When mechanisms which reduce surface tension are absent, the globules aggregate, subsequently causing turbidity and the formation of visible particles.

Polymers which show LCST in water are very popular due to their various applications specially in biomedicine. The interest in this group is mainly due to the change in their hydrophilicity upon temperature change. The sudden change of the polymer from hydrophilic to hydrophobic is based on hydrogen bonds between the polymer and the surrounding water molecules at low temperatures. The polymer chains are hydrated and solubilized, resulting in a one-phase system. When the temperature increases, the hydrogen bonds are weakened, and the polymer chains get dehydrated. Therefore, they can't be solubilized anymore, leading to polymer aggregation [29]. A polymer solution below the LCST is a clear, homogeneous solution while a polymer solution above the LCST looks cloudy.

Temperature-induced phase separation of a polymer solution can be explained by simple thermodynamics:

$$\Delta G_{mix} = \Delta H_{mix} - T.\Delta S_{mix} \tag{3.1}$$

Where ΔG_{mix} is free Gibbs energy of mixing, ΔH_{mix} enthalpy of mixing, T temperature and ΔS_{mix} entropy of mixing. Polymers dissolve in a solvent when the free Gibbs energy of the system decreases while mixing. Binding of water molecules to the polymer chains result in a favourable enthalpy of mixing ($\Delta H_{\mathrm{mix}} < 0$) but also leads to an enhanced ordering, which contributes unfavourably to the entropy of mixing ($\Delta S_{\mathrm{mix}} < 0$). At higher temperatures, the entropy term ($T\Delta S$) becomes predominant, and the free energy of mixing turns positive, which leads to phase separation. Therefore, it is clear that the LCST phase transition is entropy driven. Specifically, the main driving force is the entropy of the water. When the polymer is not in solution the water is less ordered and has a higher entropy. This is called the "hydrophobic effect" [30]. It is noteworthy that while LCST is an entropically driven effect, UCST is an enthalpically driven effect [20] [29] [31].

It is worth notifying that although in literature, the terms "LCST" and "cloud point (T_{cp})" are used interchangeably, these two terms are not equivalent. Cloud point or phase transition temperature is the temperature at which a polymer solution with a specific concentration is phase transitioned from the soluble state to the collapsed aggregated state. These phenomenon results in changing a clear solution to a cloudy mixture. According to Fig. 1, T_{cp} can be located at any position on the coexisting (binodal) curve. Therefore, it is necessary to mention the polymer concentration while determining the T_{cp}. Accordingly, the LCST is the minimum temperature value of the binodal curve. Hence, the LCST is the lowest value of T_{cp} in the phase diagram. It should also be mentioned that the cloud point curve in the entire phase diagram does not exactly coincide with the binodal curve. This variance in T_{cp} and the binodal curve is related to kinetic aspects of determining the T_{cp} versus the thermodynamic binodal curve [29].

For all thermoresponsive polymers, the cloud points upon cooling and heating of a polymer solution do not overlap due to the time-consuming process of equilibrium. The temperature interval between the cloud points upon cooling and heating is called hysteresis. The cloud points are dependent on the cooling and heating rates, and hysteresis decreases with lower rates. Therefore, the accuracy of analytical techniques plays a crucial role in studying the thermoresponsivity of polymers. Studies show that the hysteresis is influenced by temperature, viscosity, glass transition temperature and the ability to form additional intra- and inter-molecular hydrogen bonds in the phase separated state [31].

The most studied thermoresponsive polymer is poly(*N*-isopropylacrylamide) (PNIPAM) which shows LCST around the physiological temperature (32 °C) that makes it extremely popular for biomedical applications. Therefore, for a long time, PNIPAM has had the title of "gold standard" for thermoresponsive polymers [32]–[34]. Further examples of thermoresponsive polymers are poly(*N,N*-diethyl acrylamide) (PDEAAM) with an LCST over the range of 25 to 32 °C [35], poly[2-(dimethyl amino)ethyl methacrylate] (PDMAEMA) with an LCST of around 50 °C [36][37][38], hydroxypropyl cellulose (HPC) with an LCST around 45 °C [39], polyvinyl caprolactam (PVCL) with an LCST between 25 and 35 °C [40][41], poly-2-isopropyl-2-oxazoline (PIPOX) an LCST around 36 °C [42][43], polyvinyl methyl ether (PVME) with an LCST of 37 °C [44][45] and poly(ethylene glycol) (PEG), also called poly(ethylene oxide) (PEO) whose LCST is around 85 °C [46][47].

Among thermoresponsive polymers with LCST behaviour, POEOMAs have attracted a lot of attention among researchers due to their adjustable LCST. The thermoresponsivity of these polymers and their advantages over other polymers of similar thermoresponsive behaviour is explained in the next section.

POEOMAs

POEOMAs are nonlinear poly(ethylene oxide) (PEO) or poly(ethylene glycol) (PEG) analogues. They can be up to 85 wt.% composed of ethylene oxide units (EO) which makes them water soluble and biocompatible. POEOMAs first appeared in scientific literature during the 1980s [48][49]. The motivation for investigating such polymers was the design of novel macromolecular as well as the possibility to access high-molecular-weight PEG-based polymers using relatively mild synthetic conditions [50]. POEOMAs combine the properties of PEG and PNIPAM (the most utilized polymers in bio applications) in a single macromolecule and therefore are considered as ideal structures to use in biomedicine. The cloud point of these polymers does not depend much on the solution concentration in water above approx. 1 g/L, which is an important factor for application in biotechnology. Moreover, being produced from a commercially available monomer, POEOMA containing polymers are favorable to be used as smart biomaterials in biosensors, artificial tissues, smart gels for chromatography and hyperthermia-induced drug delivery. For POEOMAs, the phase transition temperature depends slightly on molecular weight, main-chain end-groups, tacticity and ionic strength. Though, the changes in LCST are generally rather small [21], [28], [50]–[52]. The end group of the PEG chain is, in most cases, a methoxy function but ethoxy- or hydroxy-terminal groups are also frequent. Among these possible structures, the oligo(ethylene glycol) methyl ether methacrylates series is particularly appealing as most of its members are commercially available [50].

POEOMAs can exhibit an adjustable LCST between 26 and 90 ºC by simple copolymerization of OEOMAs with different number of EO in the side chain. The LCST can be precisely adjusted by the copolymer composition considering that the comonomers have similar structure containing a methacrylate moiety and ethylene oxide units [50][53]. Moreover, the phase transition of these copolymers is reversible, in comparison to PNIPAM which shows an irreversible phase transition [23][51]. The solubility behavior of PNIPAM also shows a significant dependency to its end group [54]. Furthermore, The presence of the amide group at the side chain of PNIPAM might cause hydrogen bonding with other polyamides like proteins and result in bio-adhesion [55]. PNIPAM also produces low molecular weight amines during hydrolysis which complicates its usage in biotechnological applications [56].

The outstanding solubility behavior of POEOMA is due to its hydrogen bonding with water and lack of strong polymer-polymer interactions in the collapsed state. Like PNIPAM, the phase transition of POEOMA is attributed to the competition between hydrophilic polymer-water interactions and hydrophobic polymer-polymer interactions. At temperatures below the LCST, polymer-water interactions are thermodynamically favorable which makes the polymer soluble in water. Above LCST, the polymer-polymer interactions become more favored which result in polymer's self-aggregation and phase transition in the form of globules or micelles depending on the structure of POEOMA copolymer [28][50] [57]. Maeda *et al.* discovered that both C=O and C−H groups are hydrated in poly di(ethylene oxide) methyl ether methacrylate (PMEO$_2$MA) aqueous solution, but due to the crowded position of carbonyl groups near the backbone, only about half of these moieties are hydrated. By increasing the temperature above LCST, the fraction of hydrogen-bonded carbonyl groups decreases. Moreover, the complete breakage of the H-bond between the ether oxygens with water are reported. The fraction of hydrogen-bonding methoxy oxygens changes from one below LCST to zero after LCST. These results indicate that the hydrogen bond breakage is the main reason for phase separation of POEOMAs [58][59].

A similar behavior is observed for the solubility of P(MEO$_2$MA-*stat*-OEGMA$_{475}$) copolymers in water which shows a sharp change of the hydrodynamic radius at the LCST and a gradual change above LCST. The phase transition of P(MEO$_2$MA-*stat*-OEGMA$_{475}$) is happening due to multiple chain aggregation without pre-connection of individual polymer chains. Self-aggregation of P(MEO$_2$MA-*stat*-OEGMA$_{475}$) is mainly based on the conformation change of ethylene oxide side chains. They first collapse to be near the hydrophobic backbone and then distort to bring hydrophilic ether oxygen groups to the "outer shell" of polymer chains as far as possible. As a result of disturbing the balance between hydrophobic and hydrophilic interactions, the single dehydrated polymer chains aggregate into more stable micelles and cause a sharp change at the LCST [28].

P(MEO$_2$MA-*stat*-PEGMA$_{2080}$) copolymer in aqueous dilute solution undergoes a similar phase separation mechanism. However, compared to other random copolymers of MEO$_2$MA and OEOMA, this copolymer shows a weird two stage thermally induced phase separation. Instead of loose aggregates formed at the phase transition, the copolymer chains associate at the first thermal transition, followed by a rearrangement process at the second thermal transition to form stable micellar structures consisting of a methacrylate core stabilized by the longer ethylene oxide chains at the shell [60]. A more detailed study shows four conformation changes of: "unimers−clusters −micelles−aggregates" during the two-step phase transition. Like other POEOMAs, the dehydration of the long hydrophilic ethylene oxide side chains take place before the dehydration of carbonyl groups and backbones during the whole phase transition process. Therefore, the driving force of the phase transition of P(MEO$_2$MA-*stat*-PEGMA$_{2080}$) should be the hydration changes of the side chains. However, detailed FT-IR analysis explain that the peculiar behavior in the phase transition process could be attributed to the complex transition between hydrated C=O, semi-dehydrated C=O and dehydrated C=O [61].

A two-step phase transition is also observed by Yao and Tam for the behavior of PMEO$_2$MA-*block*-(PMEO$_2$MA-*stat*-POEGMA$_{300}$) block copolymers. They observed that by changing the ratio of MEO$_2$MA/OEGMA$_{300}$ from 80/20 to 70/30 the copolymer's solution behavior changes from showing one thermal transition to two [62]. A similar phenomenon has also been observed by Gibson *et al.* for the mixture of two POEGMA chains with different molecular weights. The independent phase transitions are described by the weak molecular weight dependence of the polymers' cloud point [63].

By increasing the number of blocks, Kudo *et al.* observed a multi-step phase separation for the hexa-block copolymer of P[MEO$_2$MA-*block*-(MEO$_2$MA-*stat*-OEOMA)]. They synthesized this hexa-block by semi-batch RAFT polymerization with addition of more OEOMA every two hours and therefore, the concentration of OEOMA in the reaction flask increased in batches, not gradually. Upon sequential dehydration, each block of the hexa-block copolymer showed its own temperature responsive behavior. The thermoresponsivity in each step was reversible with 2 °C hysteresis. Overall, the behavior of the block copolymer showed slight similarity to gradient copolymers [64]. To the best of our knowledge, this is the only study mentioning the solubility behavior of gradient POEOMA copolymers with similar comonomer structure.

Studies on the solubility behavior of gradient copolymers consisting of a hydrophilic and a hydrophobic monomer show that the solubility behavior changes drastically, depending more on the interaction of the comonomers with water and their hydrophobicity rather than their sequential order in the copolymer structure [65][66]. On the other hand, the thermal phase transition of other temperature responsive gradient copolymers consisting of monomers with similar chemical structure and therefore, similar hydrophobicity has shown considerable differences from the respective random and block copolymers and dependent on their sequential order in the gradient structure. This characteristic makes such gradient copolymers a great potential in biomimetic applications [27], [67]–[74].

Various studies are done on the effect of additives on the solubility behavior of thermoresponsive polymers [47], [75]–[83] including POEOMAs [84]–[88], but so far there is no comprehensive study to compare the effect of different additives on the phase transition of thermoresponsive copolymers with different structure.

In this study, the synthesis of gradient copolymers of MEO_2MA and OEOMA via semi-batch ATRP is investigated. The injection procedure of the second monomer (OEOMA) is optimized to reach the best sequence control and gradient structure. Moreover, the solubility behavior of gradient and random copolymers with different compositions as well as their behavior in the presence of various additives are compared. As additives, different anions and cations, as well as ethanol as an organic polar solvent and sodium dodecyl sulfate SDS (anionic surfactant) and cetyltrimethylammonium bromide CTAB (cationic surfactant) are used and the effect on the solubility behavior of random and gradient copolymers of MEO_2MA and OEOMA are investigated. The knowledge of the copolymer's responsivity towards different additives is essential for in vivo applications, as well as separation and membrane technology [81][89]. While adjusting the phase transition behavior of POEOMAs by changing the structure seems to be expensive, time consuming and complicated, an easier way to alter the dynamic thermal transition is an addition of slight amounts of additives to the system.

3.2 Controlled synthesis of polymers

The choice of a synthetic route to obtain a certain polymer depends on several factors, such as the chemical properties of the monomers, the desired degree of polydispersity and the targeted molecular architecture (homopolymers, block copolymers, grafted polymers, etc.). Among the various synthesis methods, radical polymerization is the most used method in industrial- and laboratory-scale synthesis of polymer. The reason is the tolerance of this method to protic compounds such as water, high reaction rate and high polymerization temperature. However, the growing radical species in radical polymerization usually suffer from bimolecular termination reactions such as radical recombination and disproportionation. Therefore, radical polymerization is mostly unsuitable for accurate polymer synthesis in a controlled manner [90].

To alter the radical polymerization technique to synthesize tailor made polymers, controlled radical polymerization (CRP) has attracted a lot of attention in the last decades. The main concept of CRP lies in lowering the (instantaneous) concentration of a growing radical species by introducing a covalent dormant species that exists predominantly over, and in fast equilibrium with, the growth-active radical species. Such a dynamic and rapid equilibrium minimizes the probability of the radical bimolecular termination and gives an equal opportunity of propagation to all polymer (or dormant) terminals via the frequent interconversion between the active and the dormant species. These aspects therefore result in nearly uniform chain length (molecular weight) and polydispersity. Another factor to consider is the “persistent radical” effect. A persistent radical is a relatively stable radical that does not react with its own kind but does combine with the growing radicals [90]. Consequently, every radical–radical termination is accompanied by the irreversible accumulation of persistent radicals resulting in a progressively increase of their concentration by time. Thus, the concentration of radicals as well as the probability of termination decreases by time. In systems obeying the persistent radical effect, a steady state of growing radicals is founded by the activation–deactivation process rather than initiation– termination in conventional radical polymerization [91].

The most common CRP techniques include nitroxide mediated polymerization (NMP), reversible addition fragmentation chain transfer (RAFT) and atom transfer radical polymerization (ATRP) [92]. NMP is based on a reversible termination mechanism between the propagating radicals and the nitroxide. This termination mechanism acts as a control agent, and results in a macro-alkoxy amine as the predominant species (Fig. 2). The macro-alkoxy amine as dormant species functionality generates back the propagating radical and the nitroxide by a simple homolytic cleavage when temperature increases. If the reaction parameters are accurately optimized, an equilibrium between dormant and active species, (the activation–deactivation equilibrium) is formed [93].

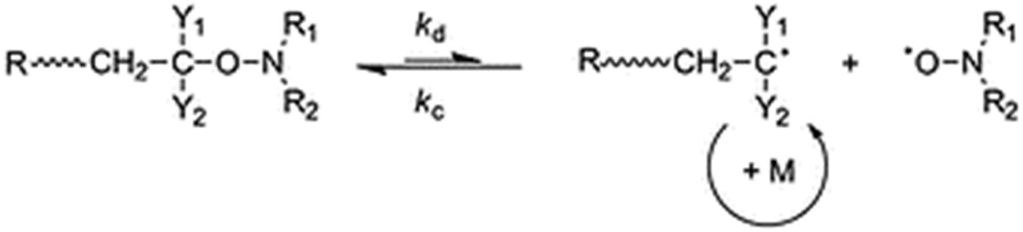

Fig. 2 Activation–deactivation equilibrium in nitroxide-mediated polymerization (NMP) [93].

RAFT polymerization like the other methods of CRP, is based on an equilibrium between active and dormant species. However, despite NMP and ATRP, the dormant species in RAFT are not achieved by reversible deactivation but by degenerative transfer. In a RAFT polymerization system, a source of radicals is required to start the reaction, since the overall number of radicals stays constant during activation-deactivation process [93]. Mostly the typical initiators for radical polymerization such as Azobisisobutyronitrile (AIBN) are used.

Initiation, chain propagation and chain termination in RAFT polymerization are similar to those in conventional radical polymerization. Therefore, the main step in this reaction is reversible addition-fragmentation equilibrium [94]. In a typical RAFT polymerization mechanism (Fig. 3), after the activation step (Fig. 3, step I and II), the radical species are added to the RAFT agent to enter the equilibrium between active and dormant species (Step III and V). The chain transfer step is the degeneration of chain transfer agent (CTA) in a reversible transfer of the functional chain-end group between the dormant chains and the propagating radicals. In a successful process, the rate of addition/fragmentation equilibrium is higher than that of the propagation. Therefore, there are less than one monomer unit added per activation cycle. As a result, all chains will have a similar degree of polymerization at a given time [93].

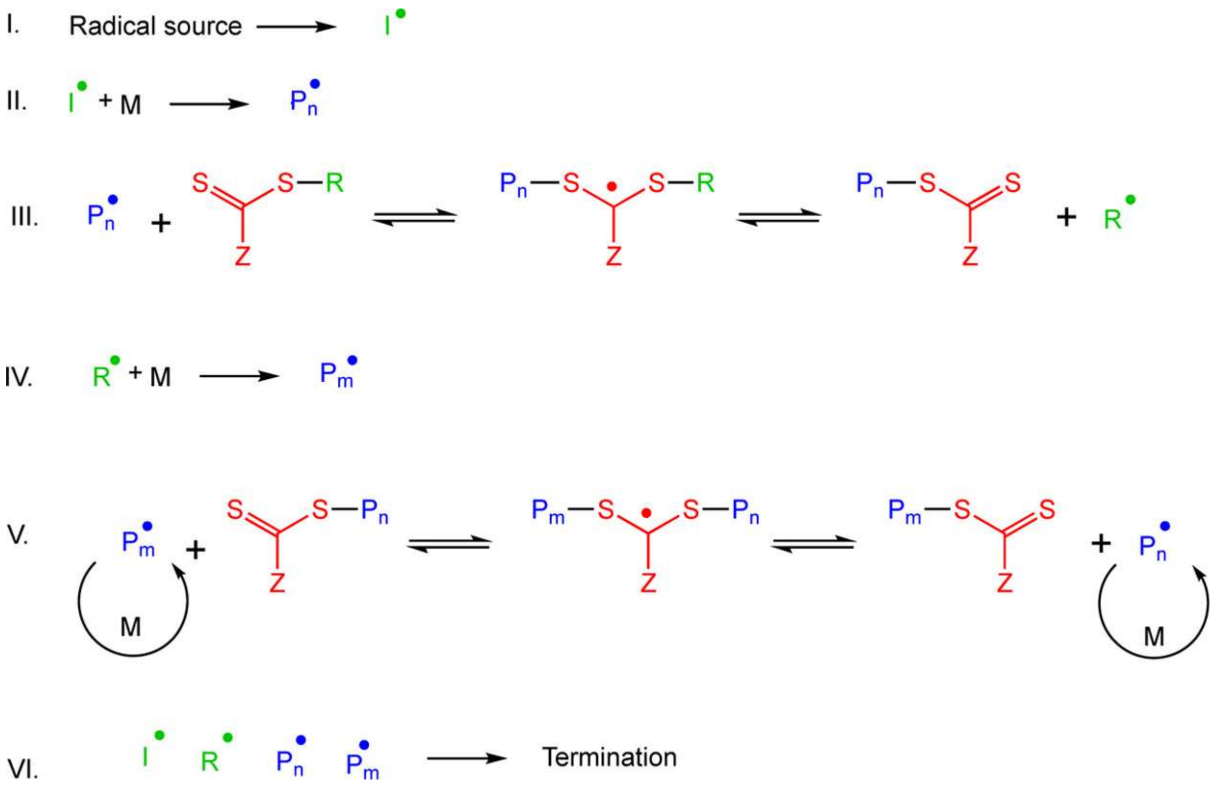

Fig. 3 The mechanism of reversible addition fragmentation chain transfer (RAFT) polymerization [95].

ATRP employs transition metals especially copper (I) as catalyst to temper the reversible activation-deactivation between the dormant species and propagating radicals [96]. By means of a redox reaction between a solubilized transition metal and an alkyl halide, an equilibrium is generated between propagating radicals and dormant polymer chains (Fig. 4). The equilibrium is controlled by the relative rates of the forward (k_{act}) and back (k_{deact}) reactions and termination is eliminated as a result of the low instantaneous radical concentration [97]. Before a termination occurs in ATRP, radicals add to only a few monomer molecules prior to be converted to dormant species. Therefore, radical lifetime is extended from seconds in typical radical polymerization to days, or even months in ATRP, by alternating short periods of activity and longer dormant periods. Thus, the fraction of dead chains is very small, because of the intermittent activation/ deactivation [98].

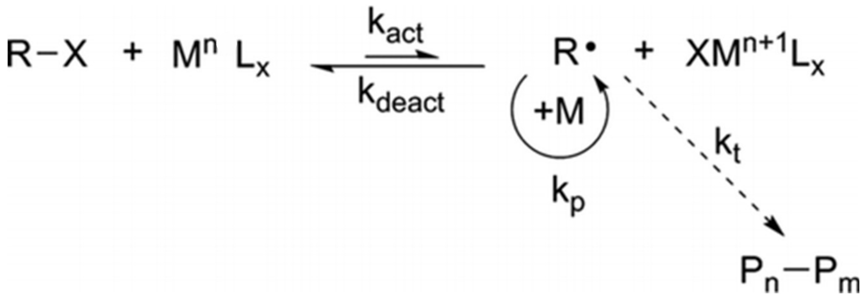

Fig. 4 The mechanism of atom transfer radical polymerization (ATRP) [97].

Other methods to gain control over polymerization include anionic polymerization and cationic polymerization. These techniques make use of an anion or a carbocation as initiator, resulting in a propagating ionic polymer chain. The key characteristics of such polymerizations is that the chain termination and transfer reactions are essentially eliminated, leaving only initiation and (chain) propagation reactions in the polymerization mechanism. The high rate of initiation accompanied with the absence of termination results in low polydispersity index [99].

Controlled polymerization techniques not only enable the synthesis of tailor-made homopolymers, but also block, random or alternative copolymers with defined molecular architecture, block chemistry and composition, molecular weight and polydispersity [100]. In this research, Anionic polymerization, ATRP and the combination of Anionic polymerization and ATRP are utilized to synthesize well defined homo and copolymers with tailor made molecular weight and structure. These methods are explained in more details in the following sections.

3.2.1 Anionic polymerization

Nowadays living anionic polymerization enables the controlled synthesis of polymers with very low dispersity ($Đ < 1.1$). Anionic polymerization is one of the most effective methods for precise polymer synthesis and is based on the sequential addition of monomers. In 1956 Szwarc *et. al* [101] demonstrated the mechanism of anionic polymerization of styrene, which had a great impact on further research of anionic polymerization of vinyl monomers. The term “living polymer” describes the products of the anionic polymerization, which are able to add monomers to the polymer chains after the initial batch of monomers are consumed. More precisely it means that the polymer chains do not undergo irreversible chain breaking reactions, termination or chain transfer [92][101]. Therefore, the molecular weight of the polymers (M_n) synthesized via anionic polymerization depends exclusively on the quantity of the reacted monomer and the initiator concentration, or in another words, the degree of polymerization increases linearly with conversion [102][103]. The absence of side reactions enables anionic polymerization to generate polymers of well-defined architecture and molecular weight. In general, however, living anionic polymerization was at first limited to nonpolar hydrocarbon monomers such as styrene and 1,3-dienes, but now it has been developed to polar monomers such as (meth)acrylates and other functional derivatives [90].

The decisive factor in anionic polymerization is a much faster initiation reaction than propagation ($k_i \gg k_p$). Therefore, all polymer chains propagate with the same speed. In order to compose a rapid initiation, radical anions [104][105] or carbanions [106][107] are used. The most common representatives are Organolithium reagents, which have a very high reactivity despite their tendency to aggregate [108]. Due to the instability of these reagents in polar solvents, the polymerization should be performed at very low temperatures (-78 ° C). The mechanism of anionic polymerization using sec-butyllithium as initiator is plotted in Fig. 5.

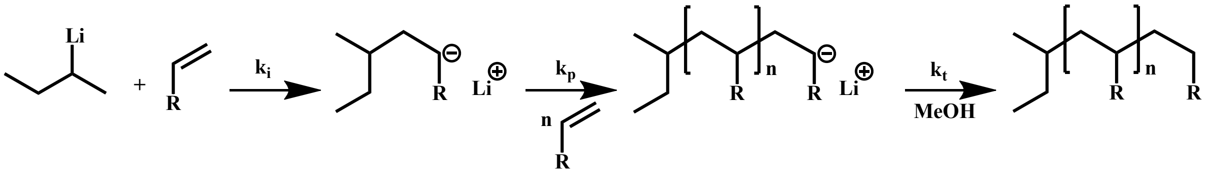

Fig. 5 The reaction mechanism of anionic polymerization using sec-butyllithium as initiator. “R” is representing an electron-withdrawing group. It is assumed that the initiation is much faster than propagation ($k_i \gg k_p$).

Anionic polymerization is often used when high molecular weight polymers with very narrow distribution, are desired [109]. For examples in integral asymmetric block copolymer membranes [17] [110] patterning, or nanolithography [111]. Although anionic polymerization is very promising in the synthesis of tailor made high molecular weight homo- and block copolymers, it shows some limits due to the high sensitivity of the anions towards impurities. Any small trace of air or humidity reacts very fast with anions and affects the molecular weight and polydispersity of the final product. Hence, it is necessary to use high vacuum technique to remove oxygen and water from the system and purify the ingredients to the highest degree of purity possible using sophisticated laboratory equipments and advanced practical skills [112].

Such drawback complicates the upscaling of anionic polymerization to industrial synthesis of polymers and limits its application only in small scale chemistry labs. Furthermore, anionic polymerization is only possible for monomers that the negative charge can be stabilized by adjacent electron-withdrawing groups or mesomeric effects. Moreover, the monomers cannot contain functional groups which are prone to a nucleophilic attack of the highly reactive anions (often carbanions) or which include acidic protons. As a result, the range of polymers and copolymers which can be synthesized via anionic polymerizations is quite limited.

3.2.2 Atom transfer radical polymerization (ATRP)

Atom transfer radical polymerization (ATRP) was first introduced independently by Krzysztof Matyjaszweski and Jin-Shan Wang [113] and by Mitsuo Sawamoto [114] in 1995. ATRP has been a successful method to synthesize polymers with a relatively high molecular weight and a narrow size distribution. The basic principle of the ATRP as explained previously in section 3.2, is the reversible deactivation of active radical chains to a dormant species. Because of the equilibrium between a dormant and an active state, the radical concentration is kept low and termination reactions are suppressed [115].

ATRP is initiated by the transfer of a halogen atom from an alkyl halide (R-X) to a transition metal complex at a lower oxidation state (M^nL_x). The oxidation state of the transition metal changes from I to II and a radical ($R^\bullet$) is formed via single electron transfer (SET). The transition metal complex in its lower oxidation state is the activator of this process [116]. The generated alkyl radical ($R^\bullet$) starts the polymerization of a vinyl monomer (M) which could terminate via recombination or disproportionation or deactivate through reversible catalyst deactivation [117]. The mechanism of ATRP is controlled by the equilibrium between the propagating radicals and the dormant species [118][119]. The activation of the dormant species occurs periodically with the rate constant of activation k_{act}. The control over polymerization is achieved by the deactivation reaction being much faster than activation reaction ($k_{deac} \gg k_{act}$) and therefore, the radical concentration is kept as low as possible. In addition, the persistent radical effect (PRE) supports the control over reaction. During the ATRP there are two different radicals, the transient and the persistent radicals. The transient radicals undergo self-termination, while the persistent radicals only terminate with transient radicals. This self-termination of transient radicals affects the concentration of persistent radicals which increase and take control over the reaction. The system orders itself due to the self-termination of the transient radicals. The ordering happens so fast that the effect of the transient radicals is hardly noticeable in the final product. For ATRP the bond of a transient radical and a persistent one can be split up again, this should be the transition from dormant species to active species. Due to the early termination of the growing polymer chains via recombination or disproportionation, an accumulation of the persistent radicals $X^{\bullet}$ occurs, which itself can only be terminated by combining it with the growing Species (k_{deact}). With increasing the concentration of the persistent radicals, its probability of reaction with the active polymer chain and self-locking of the termination reaction increases. The ATRP is thus based on a balance between active and deactivated (dormant) species [120].

Alkyl halides are generally used as initiators. They can be cleaved homolytically to emerge alkyl radicals that start the radical polymerization. The halide group is often bromine or chlorine which show a good molecular weight control. Fluorine cannot be used, since the bonding between carbon and fluorine is too strong to undergo a homolytic cleavage [118]. The reactivity of the initiator is affected by carbonyl, phenyl or cyano groups in the α position, which activates the halogen-carbon bond and thus demonstrate a reciprocal relationship between the dissociation energy of the halogen-carbon bond and the reactivity of the initiator [121][122]. Usually, initiators are used which have a structure similar to that of the monomer to be polymerized. For example, α-bromoisobutyrates for methacrylates, α-bromopropionates for acrylates, and 1-bromoethylbenzene for styrene, but aromatic sulfonyl chlorides are also quite common [120]. In addition, there is the possibility of introducing activated halogens into the chain end of a polymer obtained by a different polymerization technique to use this macroinitiator to initiate the ATRP.

Copper complexes have proven to be the most efficient catalyst systems in ATRP as they can be used to polymerize a wide range of monomers in various media [123]. A wide variety of multidentate nitrogen-containing ligands are used to increase the solubility of the metal catalyst, which at the same time influence the stability and reactivity of the catalyst. The decisive factor here is the redox potential of the catalyst, since atom transfer not only expands the coordination geometry of the complex, but reversible electron transfer should take place quickly [124]. A diverse range of complexing ligands has been applied for ATRP and Fig. 6 lists the most common nitrogen-based ligands for the complexation of copper ions by the increase in their activity. In general, the activity of the ligands decreases in this order: alkylamine ≈ pyridine > alkyl imine, aryl imine > arylamine, and tris(2-(dimethylamino)ethyl)amine seems to be one of the most active ligands [120] [121].

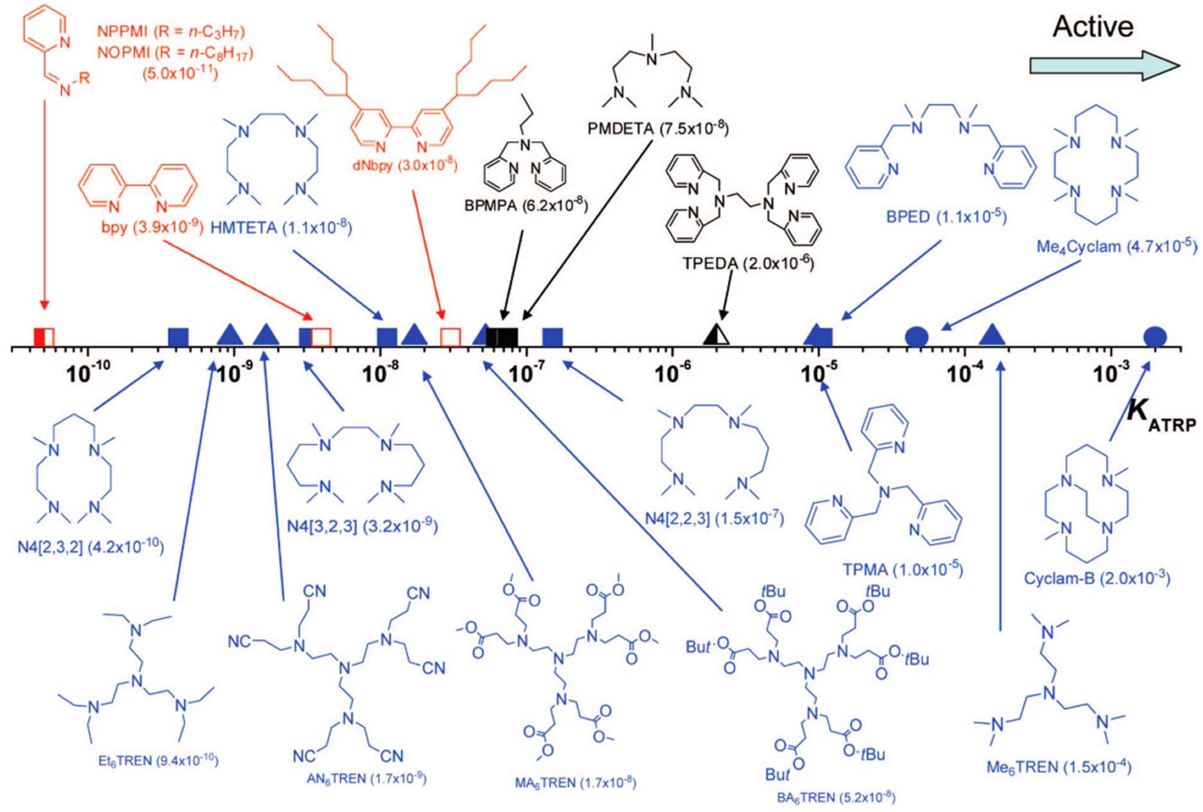

Fig. 6 ATRP equilibrium constants (K_{ATRP}) for various nitrogen-based ligands with the initiator ethyl α-bromo isobutirate (EBiB) in the presence of CuBr in acetonitrile at 22 °C. Colour key: (red) N2; (black) N3 and N6; (blue) N4. Symbol key: (solid) amine/imine; (open) pyridine; (left-half-solid) mixed; (□) linear; (Δ) branched; (O) cyclic [121].

Several types of olefinic monomers can be polymerized using ATRP and even statistically copolymerized depending on the copolymerization parameters. In addition, the ATRP is characterized by an extremely high tolerance towards functional groups; Except for carboxylic acids and CH-azide groups that can only be polymerized with the use of protective groups, since in the presence of an acid, the amine-based ligands of the catalyst could be protonated.

Terminations usually occur at the beginning of the polymerization. If a sufficient amount of Cu^{II} is formed as a deactivator and the radical concentration is therefore very low, there is hardly any unwanted termination and the majority of the polymer chains continue to grow successfully. Assuming that the contribution of termination is insignificant due to the persistent radical effect and that the equilibrium is set quickly, which is necessary to have low polydispersity, the rate law for the ATRP can be drawn up according to equation (3.2).

$$R_p = k_{app}[M] = k_p[M][P^*] = k_p K_{eq}[M][I]_0 \times \frac{[Cu^I]}{[Cu^{II}]} \tag{3.2}$$

Where R_p is the polymerization rate, k_{app} the apparent constant rate of polymerization, k_p constant rate of polymerization, [M] the monomer concentration, [P*] the concentration of radicals, K_{eq} the equilibrium constant, $[I]_0$ the starting concentration of initiator, [Cu^I] the concentration of deactivators and [Cu^{II}] the concentration of activators.

A linear change in the conversion over time with a semilogarithmic plot indicates a constant concentration of the growing species during the polymerization and first-order kinetics with respect to the monomer (eq (3.3)). The linear change guarantees fast initiation and relatively slow propagation as well as a low rate of termination. In most cases, the rate of polymerization is also first-order with respect to the initiator and catalyst, whereas the kinetics of deactivation is more complicated [118].

$$\frac{R_p}{[M]} = \frac{1}{t} ln\left(\frac{[M]_0}{[M]}\right) = k_p K_{eq} \frac{[I]_0[Cu^I]}{[Cu^{II}]} = k_{app} \tag{3.3}$$

The equilibrium rate of ATRP increases with the catalyst activity. If no chain termination or chain transfer happens and the initiation is fast enough, the dispersity of ATRP can be described as:

$$\frac{M_w}{M_n} = 1 + \frac{1}{DP_n}\left(\frac{k_p[P_nX]}{k_{deact}[X-Cu^{II}]}\right)\left(\frac{2}{p} - 1\right) \tag{3.4}$$

The polydispersity depends on the concentration of dormant species P_nX, deactivator $X\text{-}Cu^{II}$, the rate constant of propagation kp, and deactivation k_{deact}, and monomer conversion p [116].

3.2.3 Combination of anionic polymerization and ATRP

Combination of anionic polymerization and ATRP provides a versatile route to synthesize well-controlled block copolymers with high molecular weights and stimuli-responsivity. The hydrophobic major block is mostly synthesized via anionic polymerization, which allows to produce high molecular weight polymers with very low polydispersity ($Đ < 1.1$). ATRP offers a straightforward route to synthesis a vast number of polymers for the minor block. Therefore, the drawback of the limited choice of suitable monomers for anionic polymerizations is avoided and the scope of accessible high molecular weight smart materials is widened remarkably.

Recent research offers several ways to combine anionic polymerization and ATRP [125], including:

- **Click chemistry**; The most common reaction in this group is the cycloaddition of azides to alkynes which recently has become the most popular click reaction, and is widely used in biology, chemistry, and material science. In an example, an azido end-functionalized poly(2-vinylpyridine)-*block*-poly(ethylene oxide) (P2VP-*b*-PEO-N3) diblock copolymer was synthesized by anionic polymerization. In a second step, poly(*N,N*-dimethylaminoethyl methacrylate) (PDMAEMA) and poly(oligo(ethylene glycol) methacrylate) (POEGMA) were synthesized via ATRP using an alkyne functionalized initiator. The resulting polymers were attached to the P2VP-*b*-PEO-N3 diblock copolymer using the 1,3-dipolar Huisgen cycloaddition (click chemistry) [126]. By using the efficient click reaction, various novel architectures of macromolecules such as dendrimers, dendronized linear polymers, hydrogels, supra-polymers and novel conjugated polymers can be created [125].

- **Mechanistic transformation of anionic polymerization to ATRP**; This method transforms living anionic polymerization to controlled/"living" atom transfer radical polymerization (ATRP) by end functionalization of anionically synthesized polymers to use them as macroinitiator for ATRP [127][128][129]. High yield end functionalization reaction is needed to introduce a halide at the end of polymer chains and make them suitable for further ATRP reaction. Often the high molecular weight of the synthesized polymers and steric hindrance is a problem in the success of this method.

In this research, the mechanistic transformation of anionic polymerization to ATRP is used to synthesize polystyrene-*block*-poly(diethylene oxide methyl ether methacrylate) [PS-*b*-PMEO$_2$MA] and polystyrene-*block*-poly(oligo ethylene oxide methyl ether methacrylate(s)), [PS-*b*-POEOMA(s)]. PS is first synthesized via anionic polymerization and used as a macroinitiator to synthesize PMEO$_2$MA or POEOMA via ATRP, after end-functionalization. The experimental work is explained in section 5.2 and the results are discussed in section 6.3.

3.3 Block copolymers' phase separation

Block copolymers are made of at least two different polymers which are connected via chemical bonds in one polymer chain. Block copolymers combine the properties of constituting blocks and can even show new characteristics. The properties of block copolymers depend on the building blocks they are made of, the way different blocks are connected into one macromolecule (Fig. 7), the molecular weight of each block and the strength of incompatibility between different blocks [130][131].

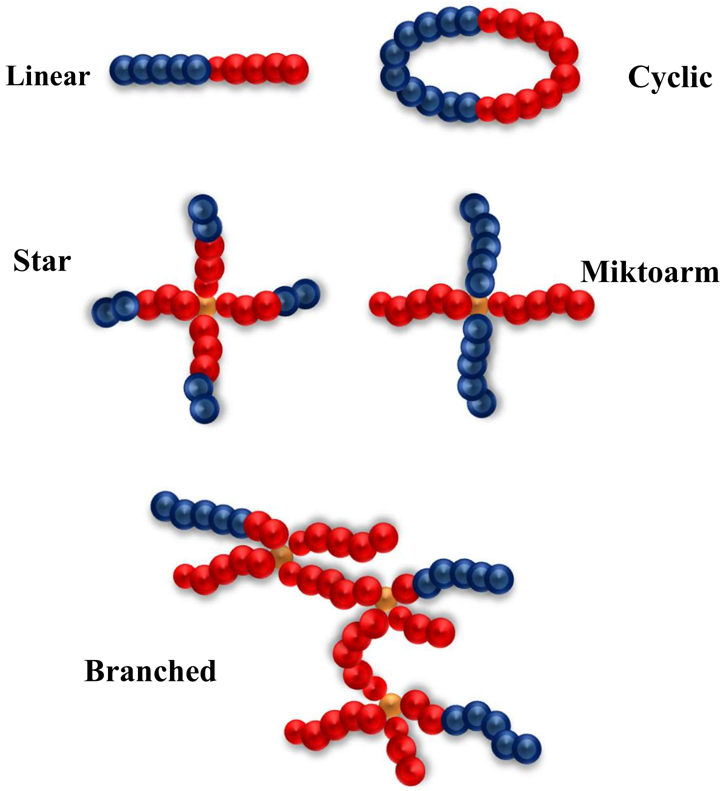

Fig. 7 Different structures of block copolymers

Due to the incompatibility of the covalently bonded polymer blocks, block copolymers are able to self-assemble and phase separate into well-defined microphase structures. The driving force for the self-assembly of block copolymers is an unfavourable mixing enthalpy coupled with a small mixing entropy, while the covalent bond connecting the polymer blocks prevents macroscopic phase separation and results in microphase separation instead [132]. The main microphase separated morphologies of a diblock copolymer are plotted in Fig. 8 (a) including spheres, cylinders, gyroid and lamellae [100][131][133]. The theoretical phase diagram for the diblock copolymer is illustrated in Fig. 8 (b). "f" is the volume fraction of one of the blocks (f_A or f_B, with $f_A + f_B = 1$).

The term χN, is the multiplication of Flory-Huggins-Staverman-parameter χ and the total degree of polymerization N and represents the degree of incompatibility between the blocks [130]. The parameters f and N are altered by polymerization techniques and influence the translational and configurational entropy, while the χ parameter is determined by the selection of the A-B monomer pair [134]. The interaction parameter is temperature dependant and the relationship between χ_{AB} and temperature (T) is given in eq (3.5) [132]:

$$\chi_{AB} = \left(\frac{z}{k_B T}\right)\left[\varepsilon_{AB} - \frac{1}{2}(\varepsilon_{AA} + \varepsilon_{BB})\right] \tag{3.5}$$

where z is the number of nearest neighbours per repeat unit in the polymer, k_B is the Boltzman constant, $k_B T$ is the thermal energy, and ε_{AB}, ε_{AA}, and ε_{BB} are the interaction energies per repeat unit of A–B, A–A, and B–B, respectively. For diblock copolymers with no strong specific interactions, such as hydrogen bonding, χ_{AB} is generally positive and small, and varies inversely with temperature. χN determines the degree of microphase separation of the diblocks. By increasing the temperature or decreasing χN, the incompatibility between the constituent blocks decreases, while the combinatorial entropy increases, and the copolymers show order-to-disorder transition (ODT) and become disordered (homogeneous instead of phase separated). The temperature, at which the ODT occurs, is referred to as T_{ODT} [132].

The condition in which the chains of the diblock copolymer are arranged in minimum free energy configurations, represents the equilibrium state in a block copolymer [135]. If χ or N are small enough (resulting in $\chi N << 10$) the entropic factor dominates, and the block copolymer is in a disordered (homogeneous) state. By increasing N or χ, the free energy balance is shifted, resulting in the development of local composition fluctuations. When $\chi N \approx 10$, there is a balance between entropic and energetic effects. Further increase of χN induces a first-order transition to an ordered state where entropically favoured but energetically costly curved and disordered microstructures are exchanged for a periodic mesophase (the order-disorder transition, ODT). More increase of χN results in sharper microdomain boundaries while the number of A-B segment-segment contacts decrease at the expense of additional chain stretching. If $\chi N > >10$, energetic factors dominate and the ordered microstructures with narrow interfaces and almost flat composition profiles are formed [134]. For a fixed value of χN above the order-to-disorder transition, with an increase of “f” the order-to-disorder transition starts from closely packed spheres (S_{CP}), passing through body-centered cubic spheres (S), hexagonally packed cylinders (C) and bicontinuous gyroid (G) to lamella (L). For further increase of the value of f_A, morphological inverted morphologies are formed [132].

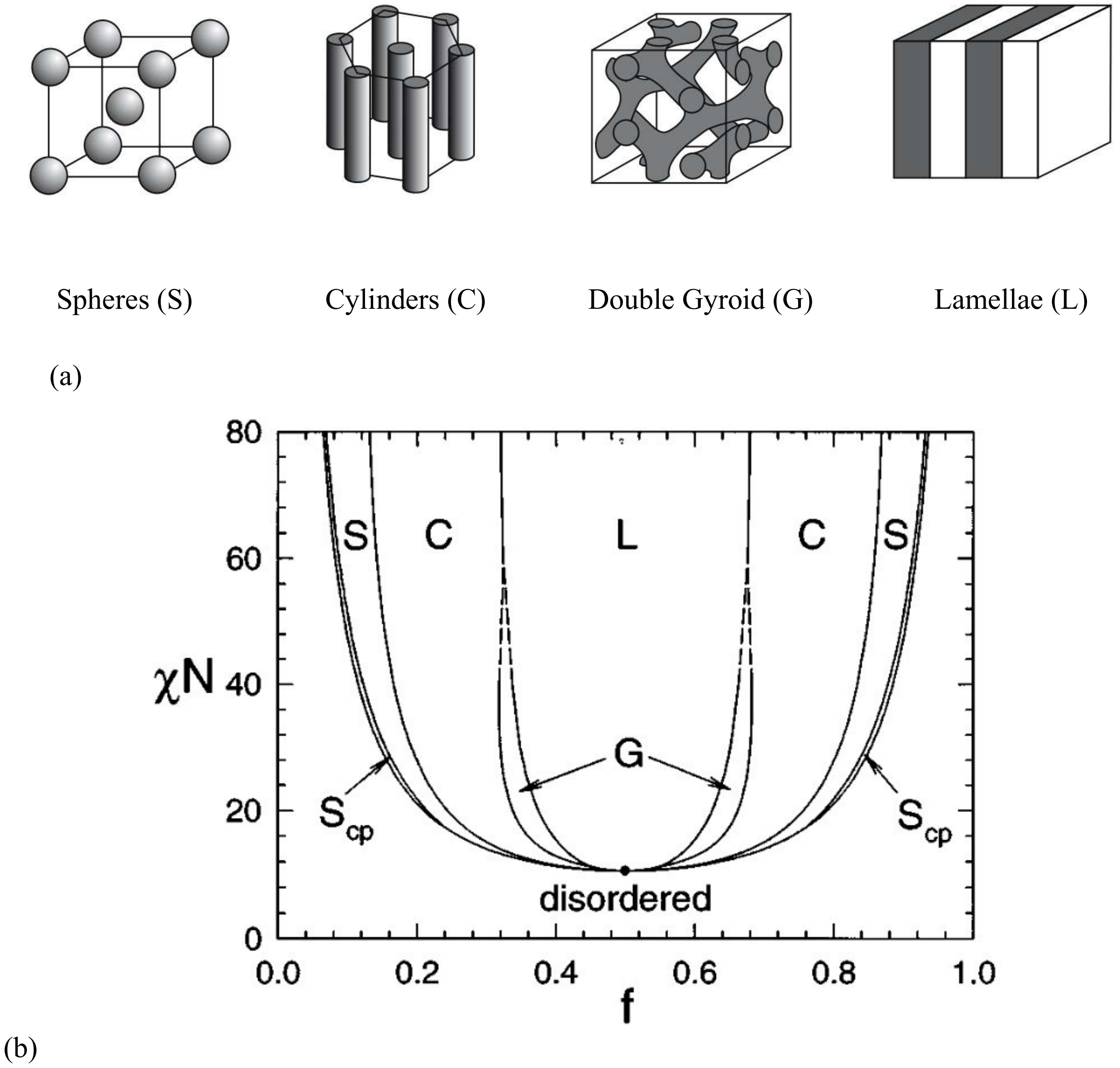

Fig. 8 Schematic representation of microphase separated morphologies in a diblock copolymer (a) Theoretical phase diagram of a conformationally symmetric diblock copolymer (segments of both blocks have similar size and flexibility), predicted by self-consistent mean field theory (b) where S shows spheres, S_{cp}, closely packed spheres, C cylinders, G double gyroid and L lamellae. The x axis (f) is the volume fraction; the y axis (χN) is the degree of incompatibility as represented in terms of the Flory–Huggins–Staverman segmental interaction parameter, χ and the total degree of polymerization, N [100][131][136].

In section 6.4, the self-assembly of PS-*b*-PMEO$_2$MA and PS-*b*-P(MEO$_2$MA-*stat*-OEOMA) block copolymers in cylindrical morphology is investigated. The χ parameter of these diblock copolymers is calculated based on their Hansen solubility parameters and the relation of the microphase structure to the molecular weight and the composition of the diblock copolymers is studied.

3.4 Membrane fabrication via self-assembly non-solvent induced phase separation (SNIPS)

Fabrication of porous membranes with high permeability combined with high selectivity has attracted great attention owing to their potential applications in various fields including sensing, catalysis, filtration, separation, drug delivery, etc [137].

Self-assembly non-solvent induced phase separation (SNIPS) is one of the most successful membrane fabrication techniques to date. The technique makes use of the microphase separation of incompatible block copolymers and their capability of self-assembly, accompanied by macrophase separation induced by the solvent-non-solvent exchange. This offers a tuneable one-step process for preparing isoporous asymmetric membranes, without requiring post-treatment [138]–[140]. The asymmetry eliminates the trade-off between selectivity and permeability, as the isoporous top layer provides high selectivity and the macroporous supporting structure provides high permeability [141]. The difference between symmetric and asymmetric membranes lays in their cross-section. Symmetrical membranes properties do not change throughout cross-section, while asymmetric membranes are thin, selective layers with microporous supportive layers that give the membrane mechanical strength [142]

In practice, the preparation of membranes via SNIPS is relatively simple, a polymer solution is poured onto a substrate, drawn out into a film, and after a set amount of time, put in a non-solvent bath. The steps of this method are very briefly explained in Fig. 9. In this technique, first the diblock copolymer is dissolved in a solvent or a mixture of at least two solvents at a certain concentration. Each solvent chosen should be selective for one of the blocks and generally the solvent selective for the major block has lower boiling point and evaporates faster. This aids in the formation of the isoporous surface layer via self-assembly of the different polymers [141] Although the immiscibility through repulsive interactions are present in solution, they are mediated by the presence of the solvent(s), avoiding phase separation of the polymers. While dissolved, the polymers form a disordered, micellar structure (Fig. 10 a). These micelles consist of a core of the insoluble blocks surrounded by a flexible fringe of soluble blocks. Usually these micelles show a spherical structure with narrow size distribution, but the structure can also change under particular conditions [143].

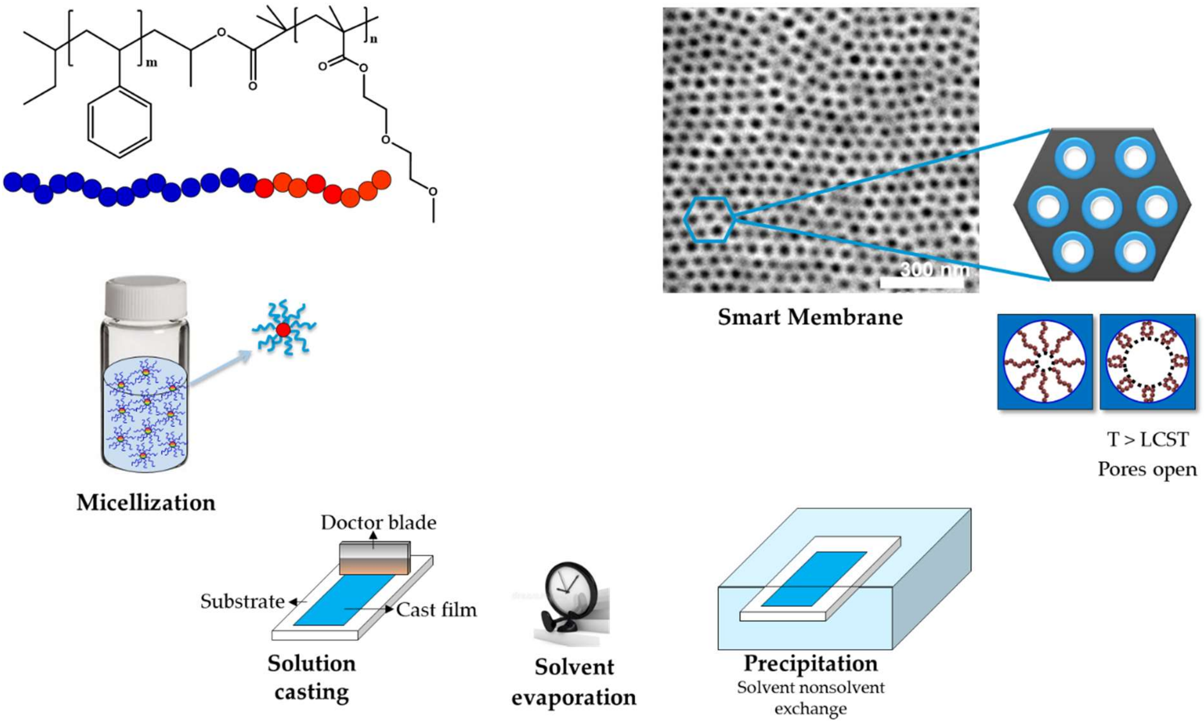

Fig. 9 The scheme of Self-assembly non solvent induced phase separation technique for membrane fabrication out of PS-*b*-PMEO$_2$MA.

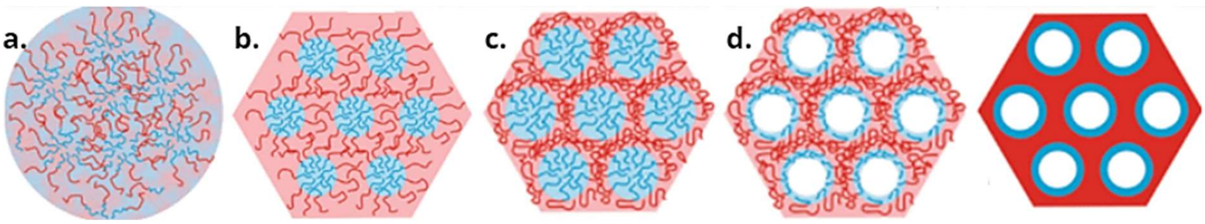

Fig. 10 Schematic overview of the SNIPS procedure, a) Disordered or weakly segregated diblock copolymer in mixed selective solvents (red: polystyrene rich domains, blue: poly(4-vinyl pyridine) rich domains); b) microphase separation with polystyrene rich matrix after film casting; c) solidification of the matrix due to solvent evaporation; d) open pores in the poly(4-vinylpyridine) rich domains after non-solvent induced phase separation; Taken from [110].

The homogenous polymer solution is then cast on glass plate or non-woven using a doctor blade. At this moment, the more volatile solvent starts to evaporate and provides a gradient of concentration perpendicular to the surface of the polymer film. This change of concentration causes the block copolymers to self-assemble in a structure similar to their bulk morphology.

If proper time for evaporation is given, hexagonally packed cylinders form perpendicular to the film surface. When casting the polymer solution on the substrate, the evaporation of solvent(s), causes repulsive interactions to increase until the polymers reach an order-to-disorder transition. This effect occurs due to the local concentration of the polymer at the solvent-air interface being significantly higher than in solution [144]. Microphase separation of the polymer chains then occur and well-defined nanostructured domains at the solution-air interface are formed (Fig. 10 b-d). During the formation of the domains, the spatial scale is determined by the polymer chain length and the morphology by the composition of the casting solution [145].

After predetermined duration of solvent evaporation, the substrate covered with polymer film is immersed into a non-solvent coagulant, which causes the solvent-nonsolvent exchange. For amphiphilic polymer solutions, the non-solvent molecules can diffuse into the membrane structure via the hydrophilic polymer chains and accumulate as droplets, named the polymer-lean phase (Point B in Fig. 11). Solvent from the surrounding hydrophobic polymer chains dissolves into the polymer-lean phase and causes growth of the droplet size. When the solvent is rapidly extracted from the polymer solution, either instantaneous or delayed liquid-liquid de-mixing (difference in ternary diagrams shown in Fig. 12) occurs depending on the polymer solution parameters such as the viscosity (Point C in Fig. 11), solvent non-solvent affinity and the speed of solvent-nonsolvent exchange [141]. If the solvent and non-solvent are completely miscible, instantaneous de-mixing favours formation of finger-like pore structures, whereas delayed de-mixing due to the slight immiscibility of solvent and non-solvent tends to create a sponge-like structure [146]–[148]. The large amount of non-solvent induces a phase inversion, causing precipitation of the polymer, kinetically trapping the structure in a non-equilibrium state (Point D in Fig. 11) [141], [149] As a result, the top layer structure (generally around 100 nm) freezes immediately by precipitation. The penetration of the nonsolvent through the cylinder channels formed, causes the rest of the polymer film to precipitate as well, forming a spongy or finger like porous structure at the bottom of the thin highly ordered layer.

It should be noted that at a ternary phase diagram, the composition of polymer, solvent and non-solvent in each separated phase at equilibrium state can be verified by a tie line passing through the solidification point. Thus, the initial composition of the polymer solution, the position of the binodal line and the composition pathway have a sincere effect on the membrane morphology [150][151]. Nonetheless, in macromolecular systems, equilibrium does not always take place, although the phase diagram represents an equilibrium state. Therefore, the phase separation in these systems is influenced by kinetic parameters as well. While kinetics of the transport process affects the membrane final structure, the main focus of research in SNIPS technique is mainly on the thermodynamic analysis of phase separation [150].

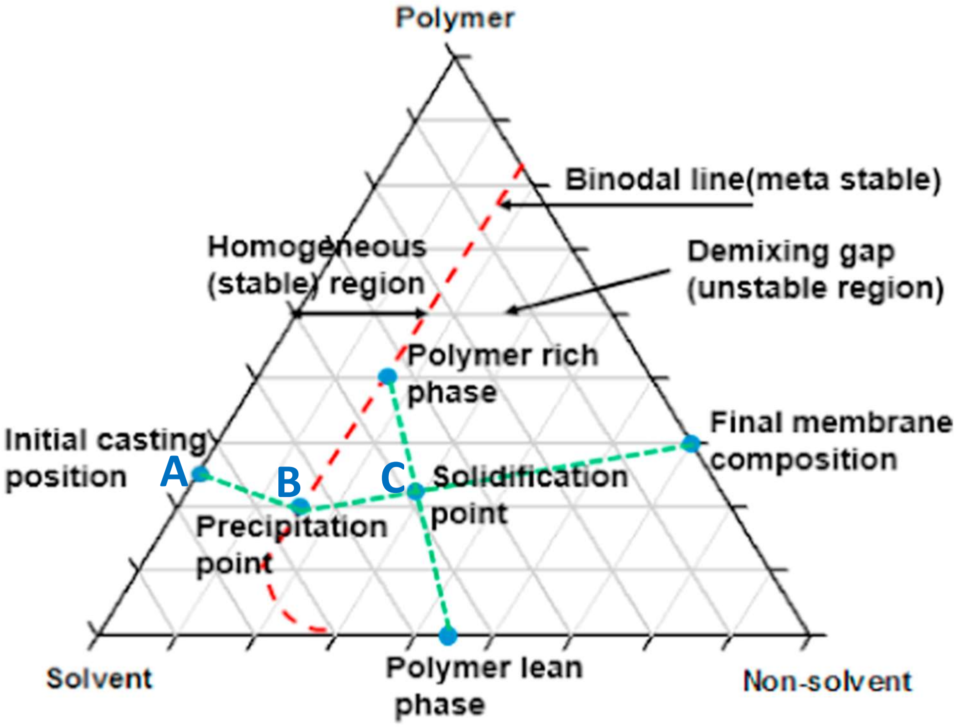

Fig. 11 Schematic phase diagram of the ternary system during membrane formation. The ternary diagram is divided into two regions by the cloud point curve (red dashed line): a homogenous stable region where all species are present in a single phase, and a two phase region where the system is divided into separate phases, a polymer rich and a polymer lean phase, which are in thermodynamic equilibrium. Point A shows the initial casting position, which is the cast solution on the substrate. At point B, the cast polymer film is immersed into a non-solvent coagulant, which causes the solvent-nonsolvent exchange. Point C represents the solidification point. where the polymer viscosity increases, and it is considered a solid. At point D, the polymer is fully precipitated, and the final structure is achieved [150].

However, the membrane fabrication is a complex interplay of different parameters, including the polymers used, molecular weight of the polymer blocks, the solvent composition, casting solution concentration and evaporation time. Prerequisites to prepare a membrane are that the different polymer chains have sufficient repulsive interaction to be strongly segregating, and at least one of the polymers has a high glass transition temperature to ensure mechanical stability. Should an additive be used during casting, it must be easily removeable by simple purifications such as rinsing [152]. In section 6.5, each of the steps in the formation of the asymmetric membrane from PS-*b*-PMEO$_2$MA and PS-*b*-P(MEO$_2$MA-*stat*-OEOMA) will be discussed. Furthermore, the effects of different casting parameters on the resulting membrane surface structure will be investigated thoroughly.

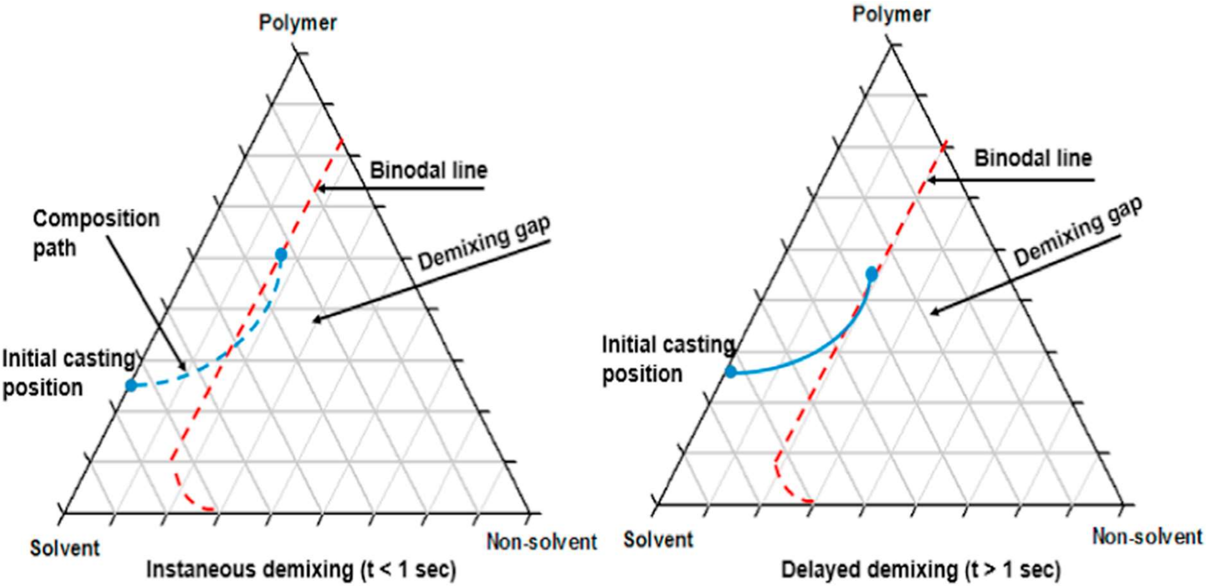

Fig. 12 Composition pathways of a cast polymer film during immersion step, Instantaneous demixing versus delayed demixing. Instantaneous demixing results in finger-like pore structures, while delayed de-mixing tends to create a sponge-like structure [150].

Although the knowledge and the possibilities of the preparation of membranes with defined pore structure rises, it is still a challenge to obtain membranes with chemical resistance, anti-fouling properties and high mechanical strength with high flux and selectivity. Thus, further improvements of membrane fabrication techniques are needed. A key of further development is also the better understanding between structure-surface properties. This research attempts to optimize the casting parameter for membrane fabrication of PS-*b*-PMEO$_2$MA and PS-*b*-P(MEO$_2$MA-*stat*-OEOMA) via SNIPS as well as providing an insight about the tactics such membranes could be altered in surface structure, mean pore size and pore size distribution.

4 Motivation and Objective

Stimuli responsive polymers are very popular for applications in switchable devices, especially in the form of block copolymers due to their self-assembly as smart materials. One of these sophisticated applications is in the fabrication of isoporous integral asymmetric membranes with switchable pore sizes. The highly regular microporous structure of those membranes originates from the block copolymers self-assembly. Therefore, block copolymers with high molecular weight are preferred. The best results so far have been obtained with asymmetric block copolymers of polystyrene (PS) exhibiting molecular weights above 100 kDa and a composition of 75-85 wt% PS (in this case, the PS block forms the membrane matrix while the minor block which is mostly poly(4-vinyl pyridine) (P4VP) forms the pores) [138]. Therefore, the focus of this work is on the synthesis of novel high molecular weight styrenic block copolymers with a similar asymmetric composition, which have a major PS block and a minor stimuli responsive block.

So far, due to the lack of straightforward synthetic options, the molecular weight of the synthesized stimuli responsive block copolymers has been limited to around 10-30 kDa which makes their self-assembly and furthermore, membrane fabrication very complicated if not impossible. Moreover, the resulted films of such copolymers are not suitable to use in industrial and engineering applications as the films are mostly brittle and lack required mechanical resistance. Therefore, one of the main goals of this work is to pursue synthetic pathways for stimuli responsive, amphiphilic block copolymers with high molecular weight. Such pathways need to provide block copolymers preferably using non-complicated scientific methods or laboratory techniques and offer the possibility of further scaleup for promising commercial applications.

Poly (oligo ethylene oxide methacrylate)s (POEOMAs) prove to be an extraordinary group of stimuli responsive polymers with state-of-the-art applications specially in biomedicine and membrane fabrication. However, their solubility behaviour and thermoresponsivity has not yet been fully investigated. In detail study of the mechanism of temperature responsivity as well as the role of different affecting parameters such as inter and intra-molecular interactions or the presence of additives would help the development of stimuli-responsive materials for altered applications. That is because the temperature is one of the most common stimuli to trigger the desired conformational changes in materials utilized in switchable devices. Therefore, it is aimed in this work to contribute to the discussion about mechanistic aspects of temperature-induced characteristic changes of POEOMAs on a molecular level.

Likewise, the self-assembly of the stimuli-responsive block copolymers in bulk is of great interest for their further application in membrane fabrication via self-assembly non solvent induced phase separation (SNIPS) technique. This technique is based on freezing the already assembled block copolymers in a desired structure, via precipitating them in a non-solvent. The order and the shape of the self-assembled nanostructured materials dictate the surface structure and porosity of the polymeric membrane films. It is worth to mention that although SNIPS is a very fast and cheap method for membrane fabrications, but since there are many factors besides the self-assembly of the block copolymers affecting the membrane structure, therefore optimization of the casting procedure in SNIPS needs well planned experimental efforts and full consideration of all parameters involved. Since the majority of studies on SNIPS technique are based on the common block copolymer PS-*b*-P4VP, successful attempts of preparing well-structured membrane films from other stimuli responsive polymers could pave the way for widening the range of materials applicable in this field and as a result, further possibilities for applying such a promising technique. Therefore, optimization of the SNIPS parameters for fabrication of highly porous integral asymmetric membranes out of PS-*b*-POEOMAs is one of the major goals in this work.

As a summary the main objectives of this work include the synthesis of asymmetric stimuli-responsive amphiphilic block copolymers with high molecular weights, Understanding and fine tuning of the Stimuli-responsiveness of the polymers (specially the temperature responsivity of POEOMAs) and the investigation, manipulation, and use of the Self-assembly of the block copolymers to create smart highly porous membranes via optimized SNIPS technique.

5 Experimental

5.1 Synthesis of poly (oligo ethylene oxide methyl ether methacrylate) homopolymers, random and gradient copolymers

5.1.1 Materials

The monomers, di ethylene oxide methyl ether methacrylate (MEO_2MA) (Aldrich, 95%) and oligo ethylene oxide methyl ether methacrylate (OEOMA) (Aldrich Mn=500) were purified by passing through a basic alumina column to remove the inhibitors such as monomethyl ether hydroquinone (MEHQ) and butylated hydroxytoluene (BHT) (antioxidant inhibitor and radical absorbents to stabilize monomers for storage).

The catalyst, copper (I) bromide (CuBr) (Sigma-Aldrich >98%) was purified by mixing with glacial acetic acid, followed by filtration. It was then washed three times with absolute ethanol and two times with diethyl ether. The colorless solid product was dried overnight under vacuum at room temperature and was stored under nitrogen. The initiator, ethyl α-bromoisobutyrate (EBiB) (Sigma-Aldrich 98%), the ligands, 4,4′-dinonyl-2,2′-bipyridine (dNbpy) (Alfa Aesar 97%), *N,N,N′,N″,N″*-pentamethyl diethylenetriamine 99% (PMDETA) (TCI 98%), the reaction solvents, anisole (Merck 99%), ethanol (Acros,99.5%) as well as other chemicals like copper (II) bromide ($CuBr_2$) (Sigma-Aldrich 99%), tetrahydrofuran (THF) (VWR 99.5%) and cyclohexane (Grüssing 99%) were used as received without further purification.

5.1.2 Homopolymerization of di ethylene oxide methyl ether methacrylate (MEO_2MA) and oligo ethylene oxide methyl ether methacrylate (OEOMA)

Thoroughly degassing is required before starting an ATRP reaction. It is necessary to avoid the contact of CuBr with oxygen, unless the catalyst will be oxidized and precipitated and therefore, excluded from the reaction. The ATRP reaction carries on very slowly or stops in absence of catalyst.

The reaction scheme for homopolymerization of MEO_2MA is plotted in Fig. 13. The polymerization was done with $[\text{Monomer}]_0$: $[\text{Initiator}]_0$: $[\text{CuBr}]_0$: [Ligand] ($[M]_0$: $[I]_0$: $[Cu^I]_0$: [L]) of 100:1:0.5:1 for PMDETA as a ligand and ($[M]_0$: $[I]_0$: $[Cu^I]_0$: [L]) of 100:1:0.5:2 for dNbyp. For a general ATRP reaction, CuBr and a magnetic stirring bar were added to a 50 ml two necked flask connected to a Dimroth condenser and Schlenk line. It was then evacuated and backfilled with nitrogen at least 3 times and each time it stayed about 15 min under vacuum. The monomer and the initiator were added to a 50 ml Schlenk flask. The solvent and the ligand were added to another 50 ml Schlenk flask. The liquids were degassed via 3 freeze-pump-though cycles. They stayed at each cycle 20 min under vacuum and afterwards under nitrogen before addition to the reaction flask. The solvent and the ligand were then added to the reaction flask containing CuBr via a degassed airtight syringe and mixed for half an hour till the CuBr/ligand complex was built. The monomer and the initiator were added subsequently with a degassed airtight syringe and the reaction started by sinking the reaction flask in a preheated oil bath at 60˚C. The reaction carried on under nitrogen flow. Samples were taken with a degassed syringe at exact time intervals for kinetic study. At the planned time, the reaction was stopped by opening the flask to the air and cooling it via sinking the reaction flask in ice bath. The reaction solution was diluted with THF and passed through a neutral aluminum oxide column to remove the catalyst. The extra amount of solvent was removed via rotary evaporator. The polymer was then purified by precipitating the concentrated polymer solution in cyclohexane and dried under vacuum overnight.

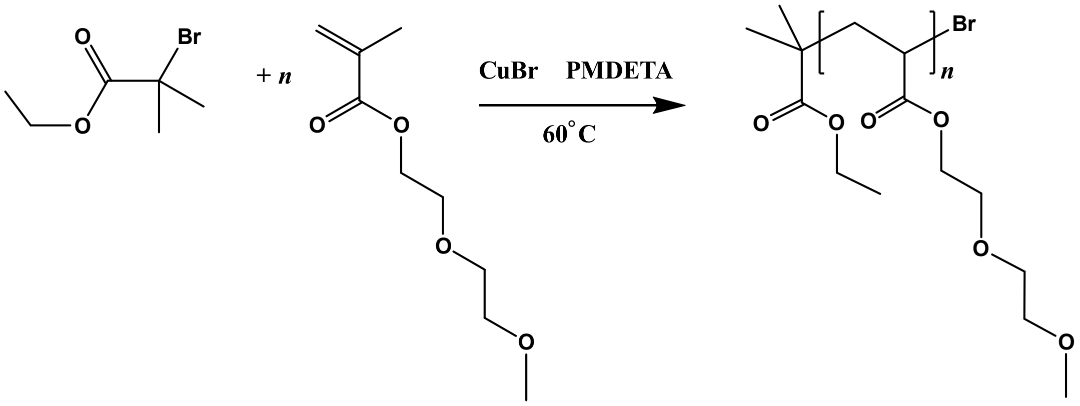

Fig. 13 Homopolymerization of MEO_2MA via ATRP using CuBr/PMDETA as catalyst complex; the reaction is done in 40 vol% at 60˚C.

5.1.3 Random copolymerization of MEO_2MA and OEOMA via ATRP

The procedure for random copolymerization is exactly as homopolymerization (see section 5.1.2); instead of one monomer, two monomers (MEO_2MA and OEOMA) with a defined molar ratio were added depending on the planned copolymer composition.

5.1.4 Gradient copolymerization of MEO_2MA and OEOMA via ATRP

Gradient copolymerization of MEO_2MA and OEOMA was performed with the ratio of $[M]_0$: $[I]_0$: $[CuI]_0$: [L]: 100:1:0.5:1 (where $[M]_0$ is a mixture of MEO_2MA and OEOMA with a defined molar ratio) using PMDETA as a ligand and anisole as a solvent (Fig. 14). To achieve a better quality of gradient structure, several injection programs were used to optimize the composition change along copolymer chain. In the optimization step, the aspired ratio of two monomers was considered as [MEO_2MA]: [OEOMA]: 80:20. It was subsequently changed according to the desired composition for further syntheses.

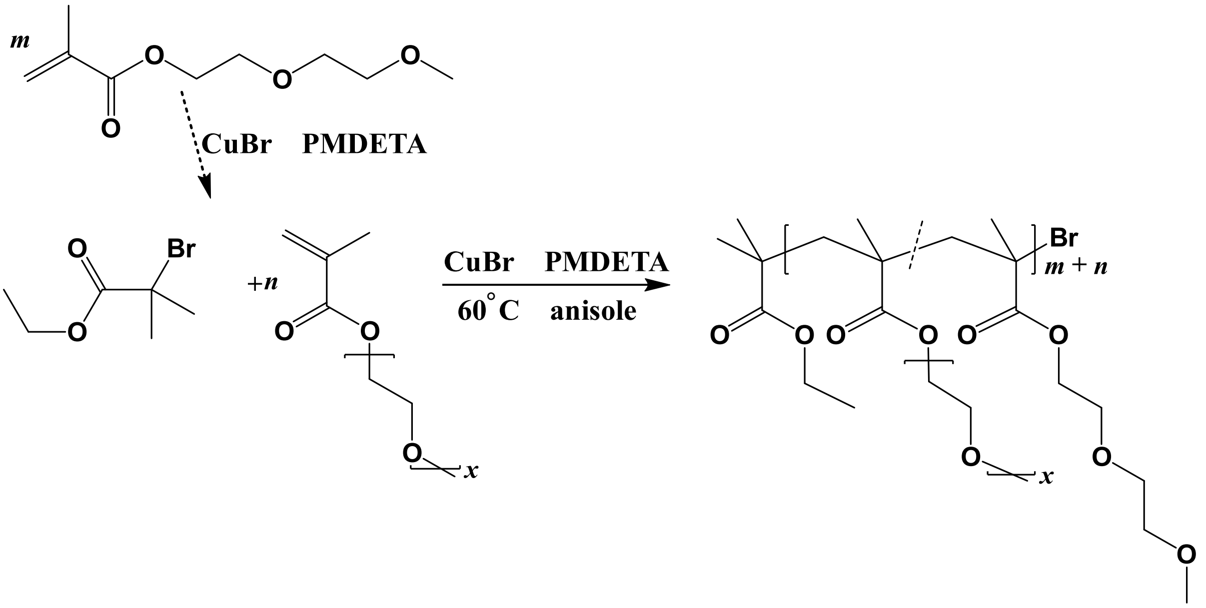

Fig. 14 Gradient copolymerization of MEO_2MA and OEOMA via ATRP using CuBr/PMDETA as catalyst complex; the reaction is done in 40 vol% at 60˚C in anisole.

To achieve the gradient composition of the two monomers in the copolymer product, a programmable single syringe pump was applied. The injection procedures used for gradual addition of OEOMA solution to the reaction solution, differed in the overall injection time as well as the number of steps and the injection volume of each step. The different injection programs were calculated for the given injection volume and injection time with an increasing injection speed in order to compensate the increasing viscosity of the reaction solution and the decreasing reaction rate. Based on the results of the first syntheses, the injection program was adjusted to achieve the gradient copolymer with desired composition and good gradient quality.

The exact injection procedures and their effect on gradient structure will be explained in detail in section 6.1.3.

In order to avoid a very fast reaction at the beginning due to the high concentration of catalyst, CuBr/L complex and the reaction solvent were divided in two different monomer flasks with the same equivalent ($[M]_0$: $[Cu^I]_0$: [L] of 100:0.5:1). This also helped to keep the ratio between catalyst/ligand and monomer constant during the reaction. To prevent a reaction in the syringe, no initiator was added to the solution in the syringe and the whole amount of initiator was added at the start to the reaction flask.

Fig. 15 shows the addition procedure of different reagents. In general, the reaction procedure was as it was mentioned in section 5.1.2 for homopolymerization, with an extra step of monomer solution preparation. The reaction flask was prepared and charged with MEO_2MA, while another flask of OEOMA was prepared in the same way (only without initiator). MEO_2MA and the initiator were not added to the CuBr solution before the reaction started but degassed separately.

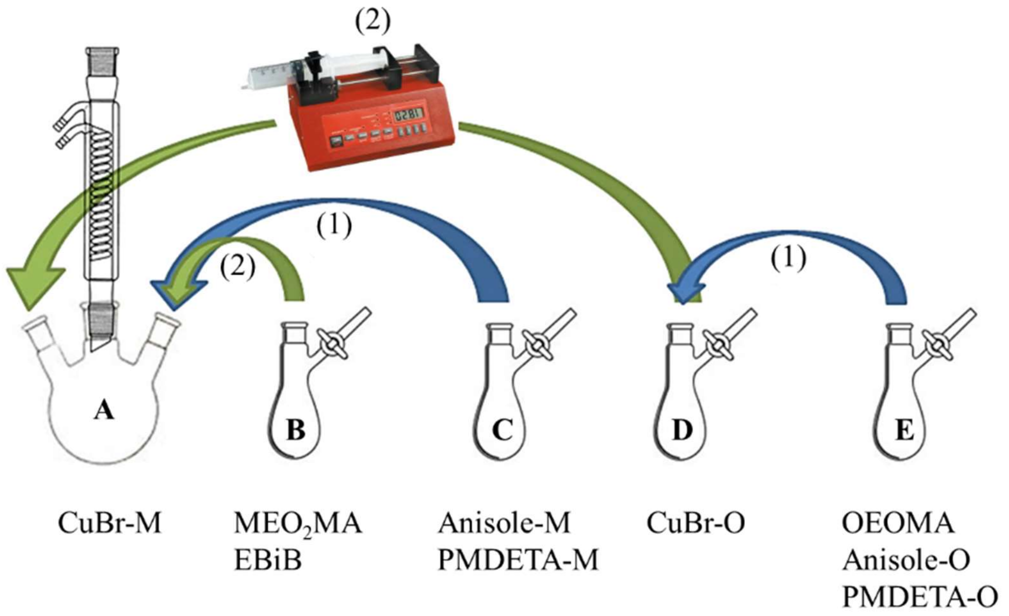

Fig. 15 The addition procedure of different reagents for gradient copolymerization; M assigns for equivalent of MEO_2MA and O for OEOMA. First the stage (1) was performed, and the contents of flask E and C were added to flask D and A respectively. At the stage (2), the contents of flask D and B were added to flask A. The transfer from flsk D to A was done during reaction via the syringe pump.

Both flasks containing CuBr (Fig. 15– A and D) were degassed via evacuation and backfilling with nitrogen as mentioned before. The mixtures of liquids were degassed via three freeze-pump-though cycles. To dissolve the solids and build up the copper complex, solution C (the equivalent amount of anisole and PMDETA to MEO_2MA) and E (the equivalent amount of anisole and PMDETA to OEOMA) were added to flask A (reaction flask, containing the equivalent amount of CuBr to MEO_2MA) and D (containing the equivalent amount of CuBr for OEOMA) respectively and mixed for 30 minutes. The solution in flask D (OEOMA and CuBr/PMDETA complex dissolved in anisole, all equivalent to OEOMA) is then taken into a degassed airtight syringe and adjusted in the syringe pump. The reaction was started by adding the MEO_2MA and the EBriB from flask B to the reaction solution A and immersing the flask into an oil bath (T = 60 °C). The injection program of the OEOMA solution was started simultaneously. Samples of 0.7 ml were taken from the reaction solution at exact time intervals to follow the composition change during reaction. These samples were diluted via ice cold THF and passed through a small column of neutral alumina followed by precipitating in cyclohexane. They were studied via SEC and NMR measurements after drying under vacuum overnight.

After the respective reaction time, the reaction was quenched as described for homopolymerization (section 5.1.2) and the final product was purified by passing through neutral alumina column and precipitation in Cyclohexane as mentioned before.

5.2 Synthesis of polystyrene-*block*-poly (oligo ethylene oxide methyl ether methacrylate) amphiphilic diblock copolymers

Polystyrene (PS) block was synthesized via anionic polymerization. It was then functionalized via two different methods to produce brominated PS macroinitiator (PS-Br) with the highest functionalization yield. In the first method, polystyrene anion reacted with styrene oxide to produce polystyrene with oxy-anion chain-end, which was later turned to brominated polystyrene by reacting with α-bromoisobutyryl bromide. In the second method, hydroxyl functionalized PS was produced via reaction of polystyrene anion with ethylene or propylene oxide. It was then turned to brominated PS macroinitiator via Steglich esterification.

The synthesis is shown very briefly in Fig. 16. The second block (PMEO$_2$MA or P(MEO$_2$MA-*stat*-OEOMA)) was synthesized via ATRP, using PS-Br as a macroinitiator.

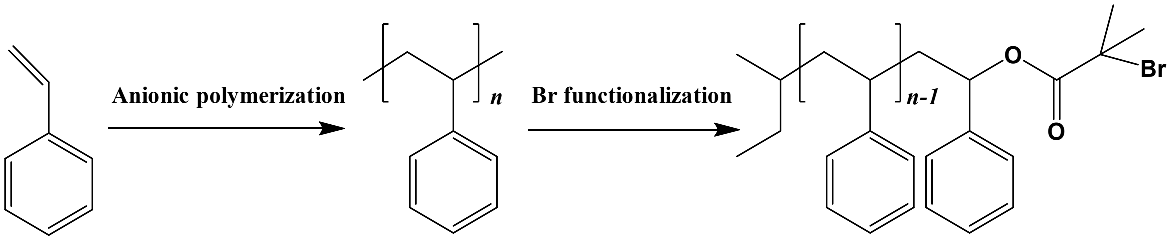

Fig. 16 Synthesis of brominated polystyrene macroinitiator.

5.2.1 Materials

All chemicals were purchased with the possible highest purity and were used without further purification unless noted.

Di-*n*-butyl magnesium, 1 M solution in heptane, *sec*-butyl lithium, 1.4 M solution in hexane, styrene oxide (97%), propylene oxide, 99%, *N,N'*-dicyclohexylcarbodiimide (DCC, 99%), 4-dimethylamino pyridine (DMAP, ≥99%), styrene (≥99%) toluene (>99.7%) and dichloromethane (DCM, >99.7%) were purchased from Sigma-Aldrich. Further materials used were α-bromoisobutyryl bromide, (BIBB) (TCI, >98%), α-bromoisobutyric acid (BIBA) (Acros, 98%), *N,N,N',N'',N''*-pentamethyl diethylenetriamine (PMDETA) (TCI, 98%), tetrahydrofuran (THF) (VWR, 99.5%), cyclohexanone (Grüssig, 99%) and dioxane (Burdick & Jackson, 99%).

Styrene was passed through basic aluminum oxide column to remove the inhibitor and dried over di-*n*-butyl magnesium and stored under argon atmosphere. Further, it was freshly distilled via high vacuum distillation and degassed via a freeze-pump-thaw cycle prior to use. The details of purification procedure are explained below.

First, Styrene was dried over di-*n*-butyl magnesium. For this step, a 500 ml high vacuum flask with a high vacuum Teflon stopcock valve was connected to the high vacuum line and heated to 600˚C. It was then evacuated and backfilled with argon 3 times. The flask was let to cool down to room temperature under vacuum. 20 ml of 1M solution of di-*n*-butyl magnesium in heptane was added to the flask while it was open to argon. The valve was placed back and the flask was evacuated very slowly till heptane evaporated completely and di-*n*-butyl magnesium stayed as a solid in the flask. The flask was filled with argon and separated from the line but stayed under argon with a hose from argon line. The stopcock was removed, and 100 ml styrene was added to this flask after passing through a basic aluminum oxide column to remove the inhibitor mono methyl ether hydroquinone (MEHQ). The stopcock was then closed, and styrene was mixed with di-*n*-butyl magnesium overnight. Styrene was then degassed via a freeze-pump-thaw cycle and stored under argon in the fridge. Styrene was freshly distilled via high vacuum distillation and degassed via a freeze-pump-thaw cycle prior to use.

THF was stayed over molecular sieve (4 Å) overnight. It was freshly distilled to the reaction flask which was pre-dried via heating at 600˚C under vacuum for 30 min and cooled down. Further, THF was degassed via a freeze-pump-thaw cycle and titrated with 1.4 M solution of *sec*-butyl lithium in hexane at -30˚C. The addition of *sec*-butyl lithium continued very slowly till the yellow color of the THF anion lasted for at least 20 min, which showed that THF was sufficiently pure to conduct anionic polymerization. The mixture was stirred overnight to let the remaining of *sec*-butyl lithium react in order to avoid any side effect on the polymerization.

Styrene oxide, propylene oxide and α-bromoisobutyryl bromide were dried over calcium hydride (CaH_2), freshly distilled in pre-dried ampullas and degassed via a freeze-pump-thaw cycle prior to use. Di ethylene oxide methyl ether methacrylate (MEO_2MA) (Sigma-Aldrich, 95%) and oligo ethylene oxide methyl ether methacrylate (OEOMA) (Sigma-Aldrich M_n=500) as well as Copper (I) bromide (CuBr) (Sigma-Aldrich >98%) were purified as mentioned in section 5.1.1.

5.2.2 Anionic polymerization of styrene

250 ml dried and purified THF was degassed one more time via a freeze-pump-thaw cycle and kept frozen. 20 ml of styrene was distilled from the ampulla into the frozen THF. The reaction flask was then warmed up to -70˚C via adding ethanol slowly to the liquid nitrogen bath that the reaction flask was sunk in. To reach the molecular weight of $M_n = 100$ k Da, the equilibrium amount of *sec*-butyl lithium (0.130 ml, 1.0 eq. of 1.4 M solution in cyclohexane) was added rapidly using a degassed airtight syringe to the reaction flask which was stirred vigorously. The orange color of styrene anion appeared immediately. The reaction continued at -70˚C for 1 hr. under argon. For further studies, a sample was taken from the reaction solution via cannulation and immediately precipitated in degassed methanol.

According to the functionalization method used to prepare brominated polystyrene (PS-Br) macroinitiator, 0.064 ml, 10 eq of degassed styrene oxide or 0.127 ml, 20 eq of degassed propylene oxide were added rapidly via a degassed syringe to terminate anionic polymerization.

5.2.3 Synthesis of brominated polystyrene macroinitiator

5.2.3.1 Polystyrene functionalization using α-Bromoisobutyryl bromide

BIBB was used in one procedure to functionalize polystyrene. In this procedure, the anionic polymerization was terminated via styrene oxide to produce polystyrene with oxy-anion chain-end as it can be seen in

Fig. 17. As mentioned before (section 5.2.1), 0.064 ml (10 eq) of degassed styrene oxide was added via a degassed airtight syringe to the vigorously stirring reaction flask. The reaction was carried out at -30 ˚C for 3 hr. After addition of styrene oxide, the reaction solution turned colorless which indicates the reaction of styrene anions. After 3 hr. when the reaction with styrene oxide was complete, another sample was taken from the reaction solution via cannulation in degassed methanol. Degassed BIBB (0.064 ml, 10 eq) was then added rapidly and under vigorous stirring to the system via a degassed airtight syringe. This changed the color

of the reaction solution to yellow. The reaction went on for another 1 hr. at -30 ˚C and then overnight at room temperature. PS-Br macroinitiator was obtained by two times precipitation of reaction solution in cold methanol followed by filtration and washing with methanol and then drying under vacuum at room temperature overnight.

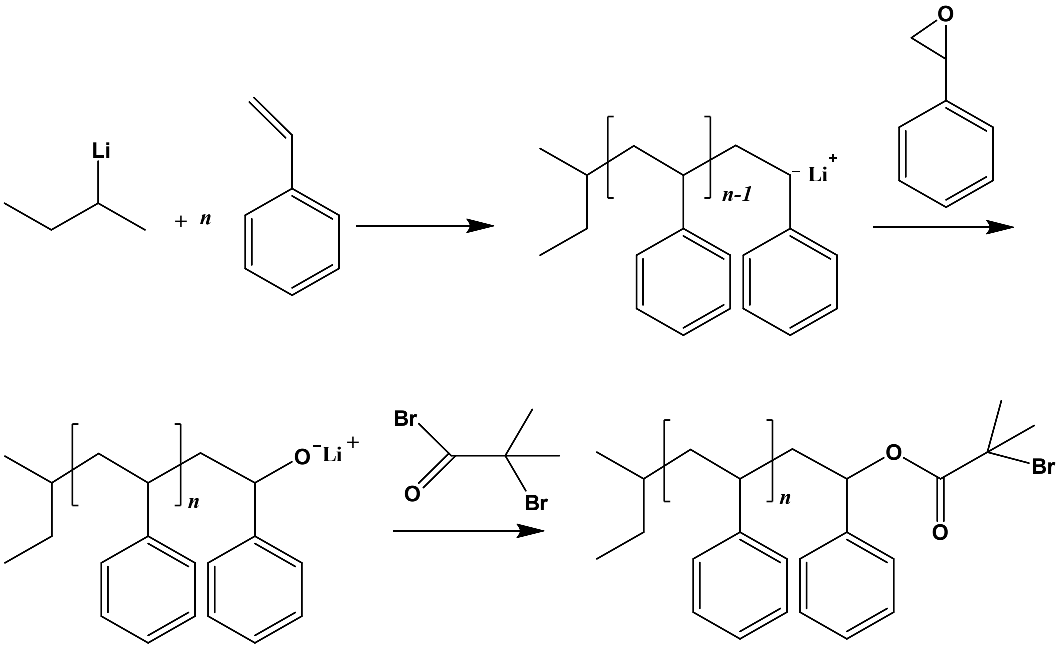

Fig. 17 The synthesis of brominated polystyrene macroinitiator using α-Bromoisobutyryl bromide.

5.2.3.2 Polystyrene functionalization via Steglich esterification

Within the second procedure to synthesize brominated polystyrene, first, hydroxy functionalized polystyrene (PS-OH) was provided via anionic polymerization. PS-OH was then functionalized via Steglich esterification using α-Bromoisobutyric acid (BriBA), *N,N'*-Dicyclohexylcarbodiimide (DCC) and 4-(Dimethylamino)pyridine (DMAP). The procedure is as shown in Fig. 18.

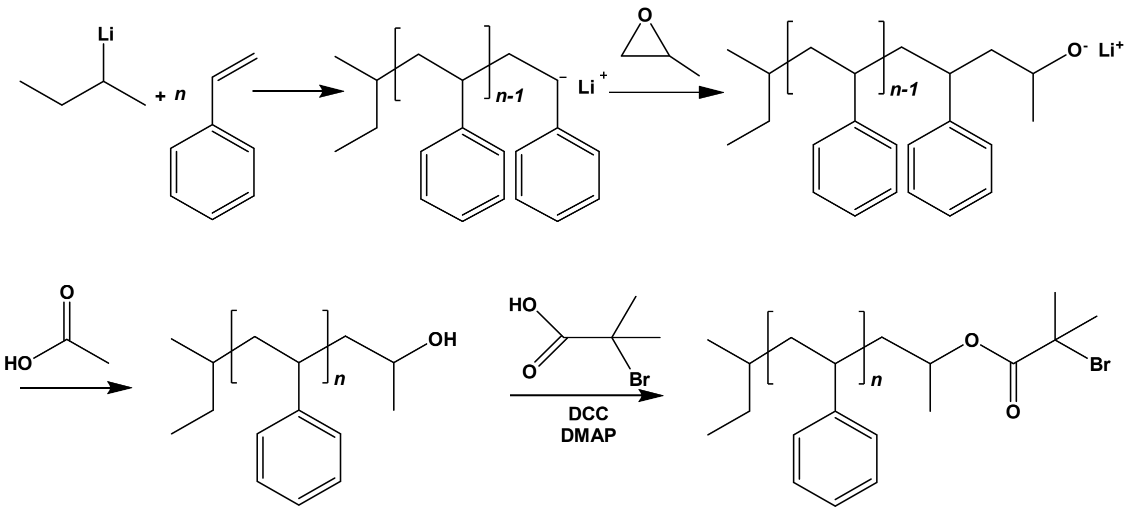

Fig. 18 The synthesis of brominated polystyrene macroinitiator via Steglich esterification.

Following the anionic polymerization explained in section 5.2.2, as mentioned, 0.127 ml (20 eq) of degassed propylene oxide was added rapidly under vigorous stirring via degassed syringe to terminate anionic polymerization. After addition of propylene oxide, like styrene oxide, the reaction solution turned colorless, which showed the full reaction of styrene anions indicating there was no more styrene anion in the system. The reaction is let to proceed for 3 hr. at -30 ˚C. A degassed solution of 5 wt.% (0.208 ml, 20 eq) acetic acid in methanol was added rapidly while vigorous stirring to the reaction solution to produce hydroxy functionalized polystyrene from polystyrene with oxy-anion chain-end. After 1 hr. the cooling bath was removed, and the system was let mixing at room temperature overnight. PS-OH was then obtained by two times precipitation from cold methanol followed by filtration and carefully washing with methanol. PS-OH was dried under vacuum at room temperature for at least two days to remove any excess of solvents inside. Like the previous procedure of functionalization with BIBB (section 5.2.3.1), samples were taken via cannulation in degassed methanol after each step of functionalization.

For Steglich esterification of PS-OH with the molecular weight of M_n= 100 k Da, PS-OH (8 gr), BIBA (0.5344 gr, 40 eq) and DMAP (0.0394 gr, 4.04 eq) with a magnetic stirring bar were added to a 250 ml Schlenk flask, evacuated for at least 1 hr. and backfilled with nitrogen afterwards. Dried and degassed DCM (53.3 ml) was then added to the flask under nitrogen and the solution was mixed for 30 min till the whole PS-OH fully dissolved and made a clear solution. It was afterward sunk in an ice bath while the stirring continued.

In a 10 ml pear shape Schlenk flask, DCC (0.6669 gr, 40.4 eq) was added with a magnetic stirring bar. The flask was evacuated for 30 min and backfilled with nitrogen. Dried and degassed DCM (3.33 ml) was added to dissolve DCC. The amount of DCM as a solvent was adjusted in a way to make 15 wt.% PS-OH solution after addition of DCC solution. The solution of DCC in DCM was then added dropwise to the abovementioned ice-cold PS-OH solution via a degassed syringe. After the addition was complete, the ice bath was removed, and the reaction continued overnight at room temperature.

PS-Br was obtained as a colorless solid by four times precipitation from cold methanol to remove the excess of non-reacted chemicals. It was then washed thoroughly with methanol and dried under vacuum at room temperature for 2 days.

By changing the molecular weight of PS-OH, the amount of other reagents used in the functionalization reaction changed. For example, when the PS-OH's molecular weight decreased to 50 kDa, the amount of other chemicals changed as follows: BIBA (20 eq), DMAP (2.02 eq) and DCC (40.4 eq). The amount of DCM was in any case adjusted in a way to make 15 wt.% PS-OH solution after addition of DCC solution.

5.2.4 ATRP of OEOMA(s) using PS-Br macroinitiator to synthesize polystyrene-*block*-poly (oligo ethylene oxide methyl ether methacrylate)

The polymerization was performed with $[M]_0 : [MI]_0 : [Cu^I]_0 : [L]$ ($[\text{Monomer}]_0 : [\text{Macro-Initiator}]_0 : [\text{CuBr}]_0 : [\text{Ligand}]$) of 700 : 1 : 2 : 4. The procedure of chemical addition for the synthesis in dioxane and toluene as solvent mixture is shown in Fig. 19.

PS-Br (2 gr) was added to a 100 ml two-necked flask (Fig. 19 – A) containing a magnetic stirring bar, connected to a Dimroth condenser and Schlenk line. It was then evacuated for at least 1 hr. CuBr (2.5 mg, 2eq) was added to a 50 ml Schlenk flask (Fig. 19 – B), evacuated, and backfilled with nitrogen 3 times; it stayed each time at least 15 min under vacuum.

The monomer (MEO_2MA or OEOMA), the ligand (PMDETA) and the solvent (60 vol.%) were added to another 50 ml Schlenk flask (Fig. 19 – C). Different solvents were used for ATRP of

OEOMAs using PS-Br macroinitiator. The effect of solvent in ATRP reaction will be explained in detail in chapter 6.3.2. The best result however was achieved by using dioxane/toluene with the volume ratio of 3:1. A part of dioxane was added to the monomer flask (Fig. 19 – C) to makes 60 vol.% of monomer and ligand solution. In the last 50 ml Schleck flask (Fig. 19 – D) the amount of solvent (the rest of dioxane together with toluene) to dissolve PS-Br (10 wt.% solution) was added separately. The liquids were degassed via 3 freeze-pump-though cycles. Each time they stayed at least 30 min under vacuum. The solution of monomer and ligand (Fig. 19 – C) was then added to the CuBr flask (Fig. 19 – B) under nitrogen via a degassed airtight syringe. The mixture was stirred for 0.5 hr. under nitrogen to make a clear solution in which the CuBr/ligand complex was built.

On the other hand, the degassed solvent (Fig. 19 – D) was added to PS-Br flask (Fig. 19 – A) under nitrogen and stirred till PS-Br was fully dissolved. The CuBr complex flask including monomer and the PS-Br flask were then degassed again via 3 via 3 freeze-pump-though cycles. Each time they stayed at least 30 min under vacuum. The degassing was done for another cycle if there were gas bubbles observed while defreezing. The solutions were finally defreezed and stayed under nitrogen prior to start of the reaction.

The reaction started by adding CuBr solution (Fig. 19 - B) with a degassed airtight syringe to PS-Br solution (Fig. 19 – B) under nitrogen rapidly while vigorous stirring, followed by sinking the reaction flask in a preheated oil bath at 80 ˚C. Samples of 1 ml were taken with degassed syringe at exact time intervals for kinetic study. Each sample was purified via dilution in ice cold THF, passing through a small column of neutral alumina and precipitating two times in ice cold methanol. The product was then washed thoroughly with methanol and dried under vacuum at room temperature overnight. The reaction stopped by opening the reaction flask to air and cooling it in ice bath. The diblock copolymer was then purified as it was mentioned for kinetic samples.

The synthesis of diblock terpolymers [PS-*b*-P(MEO$_2$MA-*stat*-OEOMA)] was the same as mentioned above; just two monomers (MEO$_2$MA and OEOMA) were simultaneously added to the monomer-ligand flask instead of one monomer. The reaction scheme is presented in Fig. 20.

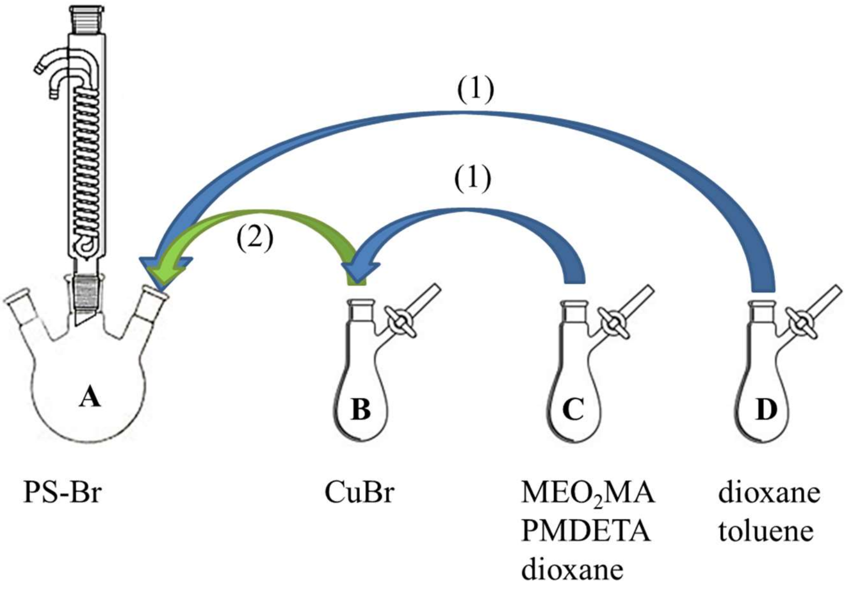

Fig. 19 The procedure of reagent preparation and addition to reaction flask for synthesis of PS-*b*-PMEO$_2$MA via ATRP using PS-Br as macroinitiator. At the stage (1) the contents of flasks D and C are added to flask A and B respectively. In the second stage (2), the CuBr in flask B is added to flask A following by sinking flask A (reaction flask) in a preheated oil bath and start of reaction.

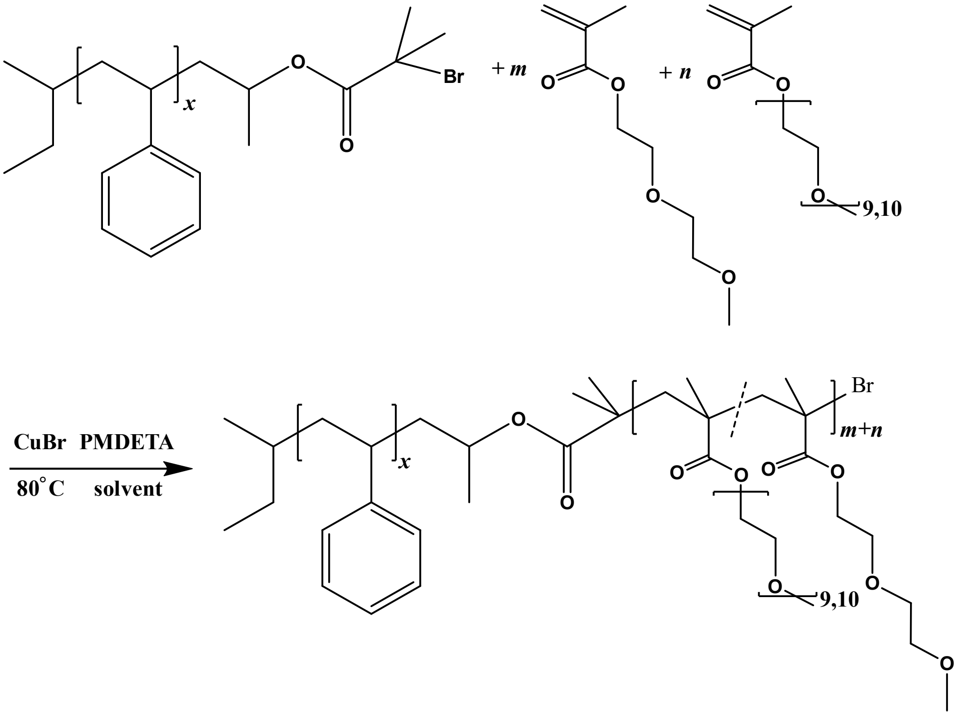

Fig. 20 Synthesis of PS-*b*-P(MEO$_2$MA-*stat*-OEOMA) via ATRP using PS-Br as macroinitiator.

5.3 Preparation of solvent evaporated films for bulk structure studies

The films were prepared from polymer solutions in Tetrahydrofuran (THF, VWR 99.5%). THF was filtered through a PTFE hydrophobic membrane filter (0.2 µm) prior to use. Different diblock copolymers were dissolved in THF to make 5.0 wt.% solutions. The solutions were shaken for 48 hr. to make sure that all polymer was dissolved, and a homogenous solution was made. They were then transferred to a desiccator saturated with THF vapor via a small bowl of solvent at the bottom of it. The solutions were kept in the desiccator till the whole THF was evaporated. This procedure lasted for a period of three weeks. The formed films were then obtained by cracking the glass vials. They were kept for 48 hrs. under vacuum at room temperature to remove any remaining solvent.

5.4 Solution Casting and membrane production

5.4.1 Materials

All the solvents and non-solvents used for casting were purchased with the highest purity possible and used without further purification. The solvents used for casting are as follows:

N,N-Dimethylformamide **(**DMF, Sigma-Aldrich, 99,8%), THF (VWR, 99.5%), dioxane (Burdick & Jackson) 99% and sulfolane (Sul, Sigma-Aldrich, 99%). The possibility of solution casting for membrane production is also studied using acetonitrile (Sigma-Aldrich, 99,8%) as one of the solvents which led to unsuccessful results.

5.4.2 Casting procedure

The solutions were prepared in dust-free glass vials which were rinsed with filtered THF (using PTFE hydrophobic membrane filter, 0.2 µm) and dried in an oven at 70˚C overnight prior to use. The polymers and solvents used for solution preparation were weighed precisely with analytical balance. Only filtered solvents (PTFE hydrophobic membrane filter, 0.2 µm) were used. The solutions were mixed for 48 hr. with magnet stirring mixers at room temperature to assure the homogeneity of the polymer solutions.

Solutions were prepared by dissolving the PS-*b*-PMEO$_2$MA or PS-*b*-P(MEO$_2$MA-*stat*-OEOMA) diblock copolymers in various solvents, solvent ratio, and certain concentrations. The block copolymers were dissolved in the binary/ternary mixtures of DMF/THF: 50/50, 60/40, 70/30, DOX/DMF: 70/30, THF/DOX/DMF: 35/35/30 and THF/DMF/Sul = 75/13.8/11.2. The solutions were let to rest 1 h prior to casting by turning off the magnetic stirring, so air bubbles can get out.

Casting was done in ambient condition; the temperature was 22ºC and humidity was controlled by a dehumidifier and was adjusted at 30-34%. The polymer solution was cast on a glass plate via a doctor blade at 200 µm air gap height. The glass plates were rinsed with filtered THF and dried carefully to avoid dust on them. 0.2-0.3 ml of solution was used for each casting. The solution was injected on the glass plate at the edge of the casting knife and the casting started immediately. As soon as the casting knife reached the end of the glass plate, the stopwatch started. After a defined evaporation time, the glass plate was immersed into the precipitation bath containing 2 L of precipitant (Milli-Q water or diethyl ether). As soon as the film separated from the glass plate, it was taken out of the bath carefully and dried at room temperature for 0.5-1 hr. Then the films were dried overnight in a vacuum oven at 25 °C.

5.5 Characterization methods

5.5.1 Size exclusion chromatography (SEC)

SEC was used to obtain the products' molecular weight (M_n and M_w) and size distribution (Đ). The measurements were performed on a system PSS Agilent Technologies 1260 Infinity including SECcurity auto-injector and an isocratic SECcurity pump. The system was operated by WinGPC Unichrom software.

For characterization of homopolymers, gradient and random copolymers containing only MEO_2MA and OEOMA, a pre-column (8 mm × 50 mm) and three analytical columns (mesh size 1 × 30 Å and 2 × 1000 Å) with a polyester copolymer network (GRAM) as stationary phase, was used. The elugramms were recorded by a refractive index and a UV-Vis detector, working at a wavelength of 280 nm. A 0.1 M solution of Lithium Bromide (LiBr) (Acros Organics) in *N,N*-dimethylacetamide (DMAC) (HPLC Optigrade, Promo-chem) with a flow rate of 1.0 mL min^{-1} at a temperature of 50 ˚C was utilized as eluent. Methyl benzoate was added as internal standard to the analyzed polymer solutions which had a polymer concentration of 2 mg/mL. The injection volume was 100 µL. For determination of relative MWs and Đ-values, the system was calibrated with narrowly distributed PMMA standards with the molecular weights between 2.2 and 1190 kDa.

To determine the molecular weight and dispersity index of PS macroinitiators and the relative molecular weight and dispersity index of diblock copolymers, the SEC measurements were performed on a system PSS Agilent Technologies 1260 Infinity including a pre-column (8 mm × 50 mm) and three analytical columns (1000 Å, 10000 Å, 1000 000 Å). The system used cross-linked styrene divinylbenzene (SDV) as stationary phase and a refractive index and a UV-Vis detector, working at a wavelength of 260 nm. THF with a flow rate of 1.0 mL/min at a temperature of 30 ˚C was used as eluent and toluene was added as internal standard. The injection volume was 100 µL and the analyzed polymer solutions had a concentration of 2 g/L. The calibration was done via narrowly distributed PS standards to determine relative MWs and Đ-values.

5.5.2 Proton nuclear magnetic resonance spectroscopy (^{1}H NMR)

For the determination of the monomer conversion in the ATRP polymerizations for kinetic studies as well as the composition of copolymers, the success of PS end-functionalization to PS-OH and PS-Br and the calculation of the yield for functionalization reaction, ^{1}H NMR was used. The ^{1}H NMR measurements were conducted on a Bruker Avance II 400 MHz spectrometer at 300 K with Bruker TopSpin Software. For a typical ^{1}H NMR spectrum, 16 scans were recorded, and a relaxation delay of 5 s was applied. Solutions were measured in $CDCl_3$ at concentrations of ≈ 20 g/L. For end-functionalized polymers (PS-OH and PS-Br), signal-to-noise ratio was increased by recording 1024 scans per spectrum and the solution concentrations to 50 g/L. The internal solvent signal of $CDCl_3$ was used as reference ($\delta = 7.260$ ppm). The spectra were analyzed with the software MestReNova 7.1.

5.5.3 Dynamic Light Scattering (DLS)

The thermoresponsivity of POEOMA polymers and the hydrodynamic radii of PS-*b*-POEOMA copolymers were studied via DLS. DLS measurements were performed using an ALV/CSG-3 Compact Goniometer System with an ALV/LSE-7004 multiple tau digital correlator working with pseudo cross correlation and the ALV Digital Correlator Software 3.0 (ALV-GmbH, Langen, Germany).

All measurements considering the thermoresponsivity of POEOMAs were performed at an angle of 90 °. While the measurements for investigating PS-*b*-POEOMA hydrodynamic radii were performed with the angle changing from 40-140°. The measurement duration was 120 s with a post wait time of 10 s. A Nd:YAG laser emitting at 532 nm was used as a light source. The viscosity and refractive index of the solvent were automatically corrected by the DLS software according to the temperature. For the measurements with ethanol as additive, extra correction on the viscosity and refractive index was done based on the solvent mixture [153][154][155][156]. For the organic solvents used in the measurement of the hydrodynamic radii of diblock copolymers, the solvent/solvent mixture's viscosity and refractive index at 25 °C was considered. In case of salt solutions, since the change of viscosity and refractive index after salt addition was not significant, no further correction has been applied.

The polymer solutions were prepared with the concentration of 1 mg/mL for the thermoresponsivity studies and 0.1 wt.% for hydrodynamic radii measurements. The samples were shaken overnight to ensure complete dissolution. Each solution was filled in a dust-free glass tube through a microporous regenerated cellulose filter with the average pore diameter of 200 nm (for aqueous solutions) or hydrophobic PTFE filters with average pore diameters of 0.45 µm (for organic solutions). The DLS samples were let to rest at least 1h prior to measurement to assure that the possible dust particles present in the system settle and do not interfere with the measurement. To investigate the effect of different additives, the solution of the certain additive with an exact concentration was prepared beforehand and added to the polymer instead of pure solvent.

Temperature-dependent DLS measurements were performed at temperature steps of 2 ˚C with 3 runs per temperature level, except for more detailed measurements which were done with 1 ºC temperature steps. A Julabo F25 thermostat functioning with a mixture of water and ethylene glycol with a temperature accuracy of 0.01 ˚C was used as heating system. There was a 3 min time interval for the temperature stabilization prior to each measurement.

A MATLAB program was used to analyze the electric field autocorrelation functions $g^1(q,t)$ by means of a cumulant fit up to the second order for a monomodal distribution, equation (5.1),

$$ln\left(g^1(q,t)\right) = ln\,A - \overline{\Gamma} \times t + \frac{\mu_2}{2} \times t^2 \tag{5.1}$$

, where A is the amplitude, $\overline{\Gamma}$ is the average decay rate, t is the time, μ_2 is the second moment, and $\frac{\mu_2}{\overline{\Gamma}^2}$ presents a measure of the relative width of the size distribution (particle size dispersity, *PSD*):

$$PSD = \frac{\mu_2}{\overline{\Gamma}^2} \tag{5.2}$$

The translational diffusion coefficient D was determined from $\overline{\Gamma} = Dq^2$ with

$$q = \frac{4\pi n_0 sin\left(\frac{\theta}{2}\right)}{\lambda_0} \tag{5.3}$$

where q is the absolute value of the scattering vector, n_0 is the refractive index of the solvent, θ is the scattering angle, and λ_0 is the vacuum wavelength of the laser. The hydrodynamic radius was calculated from the Stokes−Einstein equation.

$$R_h = \frac{k_B T}{6\pi\eta} \tag{5.4}$$

with k_B being the Boltzmann constant, T is the temperature, η is the solvent viscosity and D is the apparent diffusion coefficient, respectively [157].

5.5.4 Differential scanning calorimetry (DSC)

A differential scanning calorimeter, DSC 204 F1 Phoenix, Netzsch was used to determine the glass transition temperatures T_g of the diblock copolymers. The measurements were performed at 1 bar under nitrogen atmosphere in the temperature range between 20°C and 180°C. The heating and cooling rates were 10 °C/min. During a first heating interval, the thermal history of the PS-*b*-POEOMA block copolymers was erased by heating up the samples from room temperature to 180 °C followed by cooling them down to 20 °C. The thermal properties were analyzed using the DSC data of the last cooling interval. For each measurement, about 5 mg of the diblock copolymer was weighed into a 40 µL aluminum crucible, which was capped afterwards using a pierced lid. The data processing was performed by the Netzsch software Protheus analysis.

5.5.5 Atomic force microscopy (AFM)

The surface topographies of polymer films obtained after solvent evaporation as well as the cast films were characterized using a JPK NanoWizard®3 atomic force microscope in the intermittent contact mode (air) with scan rates of 0.6-0.8 Hz. The images were detected using a standard gold tip with a radius of 10 nm. The obtained data were processed with the JPK Data Processing software. After completely drying the films, a small piece of each film was cut using a sharp blade and stuck on a Menzel-glass for analysis.

5.5.6 Scanning Electron Microscopy (SEM)

Surface and cross section morphology of the cast films were investigated by SEM (GEMINI LEO 1550) at an acceleration voltage of 3 kV. The samples were sputter coated with 2 nm of platinum prior to measurement using a PECS by Gatan sputter coater. The images were detected using and Inlens SE detector.

5.5.7 Small angle X-ray scattering (SAX)

SAXS images were recorded using our in-house SAXS apparatus equipped with an Incoatec^{TM} X-ray source IµS and Quazar Montel optics. The wavelength of the X-ray probe was 0.154 nm and the sample-detector distance was 1.6 m. The patterns were recorded with a Rayonix^{TM} SX165 CCD-Detector and the accumulation time per SAXS measurement was 600 s. An empty sample holder was measured to subtract the background. All samples were measured at ambient temperature.

6 Results and Discussion

6.1 Synthesis of di- and oligo(ethylene oxide) methacrylate homopolymer, random and gradient copolymers via atom transfer radical polymerization (ATRP)

6.1.1 Kinetics studies of PMEO$_2$MA synthesis via ATRP

The synthesis route was optimized based on the research of Lutz *et al.* [158] and Matyjaszewski *et al.* [53]. Lutz *et al.* reported a well-controlled ATRP of OEOMAs in pure ethanol. The polarity of ethanol establishes fast polymerization kinetics [158], but since OEOMA monomers have a low polarity, their polymerization can also be successfully done in apolar solvents like anisole as reported by the work of Matyjaszewski's *et al.* [53].

To choose the best reaction conditions for the gradient copolymerization of OEOMAs via ATRP, first the homopolymerization of MEO$_2$MA was optimized first. Several test reactions with different solvents, ligands and reaction time were conducted. Samples were taken at exact time intervals and analyzed via NMR and SEC.

The majority of the test reactions were conducted to optimize the homopolymerization of MEO$_2$MA. Since methacrylate is the reactive part of OEOMA monomers, the two monomers used in this study (MEO$_2$MA and OEOMA) have nearly the same reactivity. The length of the ethylene oxide (EO) side chain does not affect the reactivity ratio of two monomers in the system while, first, it is not long enough to cause any steric hindrance, change of polarity, etc. and second, the vicinity of the MMA part which contains two EO is the same in both monomers. This assumption will be further proven by studying the homopolymerization of OEOMA and the random copolymerization of MEO$_2$MA and OEOMA. Thus, kinetic studies of the homopolymerization of MEO$_2$MA provides enough information to plan the gradient copolymerization of MEO$_2$MA and OEOMA. Fig. 21 shows the NMR spectrum of MEO$_2$MA monomer and its change during polymerization. The monomer conversion is calculated by comparing the integral over the vinyl protons of the remaining monomers (A & B; 5.45-6.12 ppm) to the integration over the region C (3.9-4.4 ppm) which represents the esteric carbon of the homopolymer and the remaining monomer [159], [158]. As the polymerization proceeds, the A&B peaks representing the monomer's double bond disappear; Moreover, the sharp peak of C representing the esteric carbon of monomer is replaced by a broad peak representing the esteric carbon of the polymer.

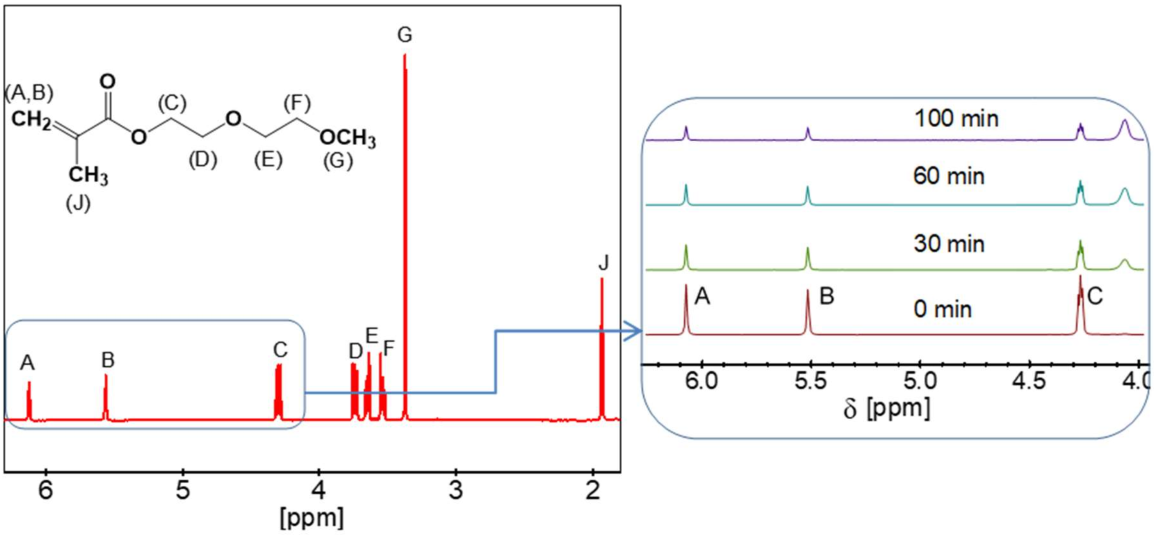

(a) (b)

Fig. 21 (a) The ^{1}H NMR spectrum of MEO$_2$MA; (b) The change of the ^{1}H NMR spectrum with time during the reaction. As the reaction goes on, the peaks at the region 5.45-6.12 ppm (A&B) tend to get smaller and eventually disappear. The peak at the region 3.9-4.4 ppm (C) which is corresponding to esteric carbon of monomer also gets replaced by the broad peak at the same region designated to the esteric carbon of polymer.

To analyze and compare the control over different reaction systems, the semi-logarithmic plot of monomer conversion i.e. ln([M]$_0$/[M]) is plotted versus reaction time in Fig. 22. The reaction time was 100 min for all reactions, except for the one with ethanol as the solvent and PMDETA as the ligand which was stopped after 80 min due to its faster reaction rate. In order to produce consistent data, the reactions with dNbyp as a ligand were done with the ratio of [Monomer]$_0$: [Initiator]$_0$: [CuBr]$_0$: [Ligand] ([M]$_0$: [I]$_0$: [Cu^I]$_0$: [L]) = 100:1:0.5:1 of and with PMDETA with the ratio of ([M]$_0$: [I]$_0$: [Cu^I]$_0$: [L]) = 100:1:0.5:2 as explained in chapter 5.1.2. The semi-logarithmic kinetics plots are linear for all of the polymerizations indicating that the polymerization rate is proportional to the monomer concentration (first order polymerization with respect to monomer) and moreover, the radical concentration is constant during the polymerization, according to eq (6.1) [160].

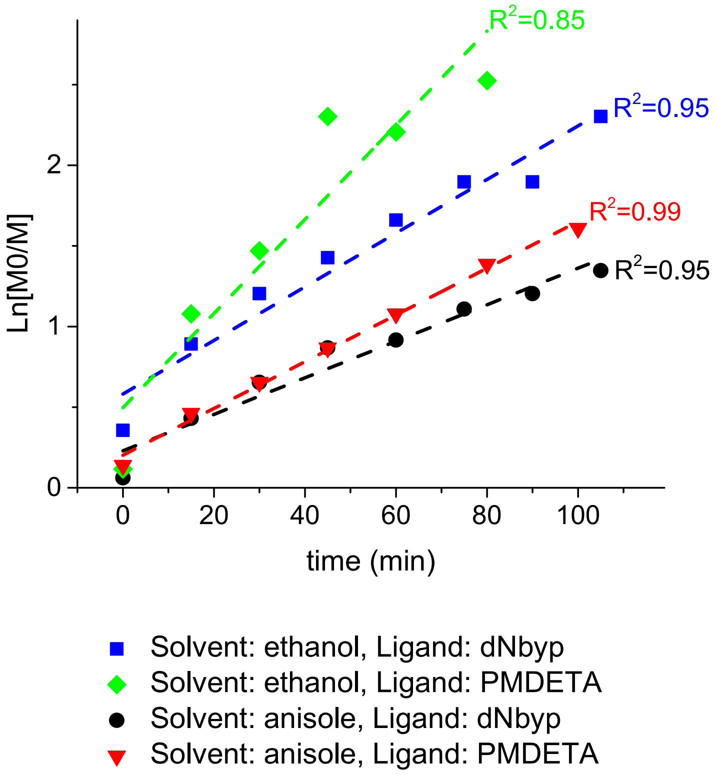

Fig. 22 Comparison of semi-logarithmic plot of monomer conversion vs. time in ATRP homopolymerization of MEO_2MA with different solvents and ligands. The best control is obsereved for anisole as solvent and PMDETA as ligand. The worst control as well as the fastest reaction is observed for ethanol as solvent and PMDETA as ligand. $[M]_0:[I]_0:[Cu^I]_0:[L]=100:1:0.5:1$ for all reactions.

$$\frac{R}{[M]} = \frac{1}{t} ln\left(\frac{[M]_0}{[M]}\right) = k_p K_{eq} \frac{[I]_0[Cu^I]}{[Cu^{II}]} = k_{app} \tag{6.1}$$

where R is the reaction rate, $[M]$ is the monomer concentration, t is time, $[M]_0$ is the concentration of monomer at the start of reaction, k_p is the constant rate of propagation, K_{eq} is the constant rate of equilibrium, $[I]_0$ is the concentration of initiator at the beginning of reaction, $[Cu^I]$ and $[Cu^{II}]$ are the concentration of cupper ions and k_{app} is the apparent constant rate of reaction.

The highest slope in the semi-logarithmic kinetics plots is observed for the system of ethanol and PMDETA showing the highest apparent reaction rate with lower degree of control over reaction compared to the other systems.

The best control over reaction is observed using anisole as a solvent and PMDETA as a ligand. Compared to anisole, the reaction with ethanol is faster and less controlled. This can be explained by the higher relative polarity of ethanol (0.654) compared to anisole (0.198); (relative polarity, normalized from measurements of solvent shifts in absorption spectra) [161].

Among different solvents used to conduct ATRP synthesis, good control is mostly resulted from bulk polymerization or nonpolar solvents; using polar solvents especially water, often leads to limited control and poor livingness while the reaction is incredibly fast [162], [163].

Wang and Armes explained that, by increasing the solvent polarity, a higher concentration of mononuclear copper catalyst is produced which increases the radical concentration and the polymerization rate. As a result, the molecular weight distribution is broadened distinctly [159]. According to other studies, increasing the solvent's polarity increases the k_{act} while decreasing k_{deact} with approximately the same ratio since $\Delta\log k_{act} \approx -\Delta\log k_{deact}$. Therefore, changing to a more polar solvent increases K_{ATRP} as $K_{ATRP} = k_{act}/k_{deact}$ and results in overall faster and less controlled reaction [163], [164].

By applying the linear solvation energy relationship of Kamlet and Taft, Horn and Matyjaszewski [164] indicated that the effect of solvent on k_{act} could be mainly explained by dipolarity/polarizability (π^*) of the solvent, which accounts for the stabilization of a charge or dipole by means of nonspecific interactions. In addition, they mentioned that for some solvents like methanol, ethanol and isopropanol, Lewis acid−base interactions between the solvent and the copper species should also be considered.

Furthermore, by quantum chemical calculations of the energies of the solvated states of the actual species involved in the activation process, Horn and Matyjaszewski showed that more polar solvents stabilize the Cu^{II} product complex to a higher degree than the Cu^{I} starting complex. They hence concluded that starting materials, transition state, and products of the activation step are more stable, i.e. better solvated or in another word more active, in more polar solvents. Therefore, the different soluability of the Cu^{I} and Cu^{II} species are the main reason for the effect of solvent on the activation rate [164]. Although the effect of solvent on the reaction rate and the control over reaction is unneglectable, it is less pronounced than the effect of the ligand or initiator [163], [164]. The ligand affects the activity of the transition-metal ion by changing its solubility and as a result, its redox potential in different solvents.

Studies on ATRP kinetics show that the redox potential of the metal complex is one of the parameters controlling the reaction. A higher redox potential of the Cu^I complex, results in a higher equilibrium concentration of the propagating radicals and therefore faster polymerization [162] , [163] , [165] , [166].

It should also be noted that the redox properties are remarkably affected by the solvent. Moreover, the solvent effect on the redox potential appears to be higher for complexes of copper with ligands having higher degrees of freedom, compared to more rigid structures with lower degrees of freedom [163]. The impact of the solvent also depends on the catalyst complex. In a study by Horn and Matyjaszewski [164], the effect of solvent on K_{ATRP} is less distinct for Cu^IBr/HMTETA compared to Cu^IBr/ Me6TREN and Cu^IBr/TPMA. In an ATRP polymerization of MA with Cu^IBr/Me6TREN, as the medium is changed from 60 to 20 vol. % MA in DMSO, K_{ATRP} increases 19 fold. While in case of Cu^IBr/HMTETA the increase is just 5 times [164].

Cyclic voltametric measurements of the redox potential for different copper complexes show that the reducing power of a copper complex depends on the ligand structure rather than the solvent. By increasing the number of coordination sites of a ligand, the redox potential of its copper complex increases. Therefore, the redox potential increases with the number of N-atoms: bidentate ligand < tridentate ligand < tripodal ligand. Moreover, aliphatic amines stabilize Cu^{II} species better than Cu^I species compared to aromatic amines while they are more nucleophilic. This leads to better complexation, since Cu^{II} is a stronger Lewis acid than Cu^I and complexes better with stronger nucleophiles (alkyl amines vs. pyridines) [167].

Comparing the ligands that are used in this research, PMDETA has a higher redox potential considering its faster reaction in both ethanol and anisole, which is in agreement with literature. For example $E_{1/2,PMDETA}$=-0.075 V compared to $E_{1/2,dNbyp}$ =-0.050 V in acetonitrile [167]. Incidentally, the reaction with PMDETA in anisole is still well controlled based on its first order kinetics, sustained also by the SEC results.

The SEC results of different reaction conditions (Fig. 23 and Table 1) prove the good control over polymerization reaction and show low Đ for all of the systems excluding the polymerization using ethanol as a solvent and PMDETA as a ligand. The abovementioned system shows a small shoulder at higher molecular weights which is related to faster activation reactions than deactivation in ATRP equilibrium and therefore a small portion of bimolecular termination is observed close to the end of reaction. The addition of $Cu^{II}Br$ or a decrease in the $Cu^{I}Br$ concentration does not help decreasing the propagating radicals' concentration nor improving the control over reaction noticeably.

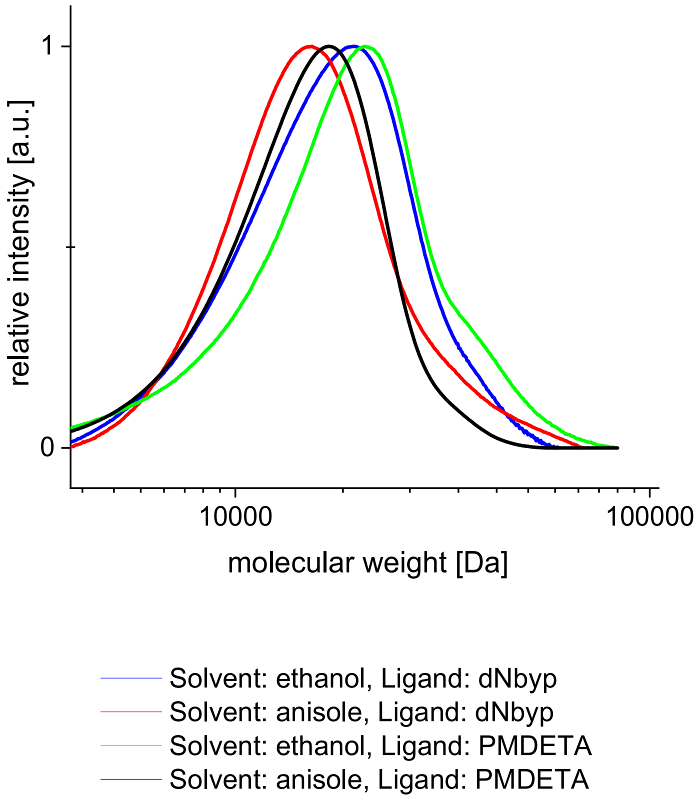

Fig. 23 The SEC graphs of MEO_2MA homopolymerization with different solvents and ligands; The best control is obsereved for anisole as solvent and PMDETA as ligand. The worst control as well as the fastest polymerization is observed for ethanol as solvent and PMDETA as ligand.

Table 1 shows that the SEC measured apparent molecular weight of the polymers synthesized in anisole is in good agreement with the theoretical calculation, while for the ethanol systems the molecular weight achieved is slightly lower than from theoretical calculation. Among the test polymerizations conducted, the one in ansiole using PMDETA as a ligand shows a very good control while being fast. Considering the fact that lower molar amount of PMDETA is needed to provide a good control compared to dNbyp and the easier way of handling such small amounts (because PMDETA is liquid while dNbyp is solid), the final choice was to carry out the ATRP polymerization of MEO$_2$MA and further copolymerizations in anisole using PMDETA as a ligand.

Table 1 Detailed experimental conditions and results of ATRP test reactions for PMEO$_2$MA synthesis.

Entry	Solvent	Ligand	$[M]_0$:$[I]_0$:$[Cu^I]_0$:$[L]$[a]	Conv.[b]	Time (min)	M_n^{theory}[c] (hDa)	M_n^{SEC} (kDa)	$Đ$
1	ethanol	PMDETA	100:1:0.5:1	0.92	80	17.316	1.4953	1.4253
2	ethanol	dNbyp	100:1:0.5:2	0.85	100	15.999	1.2026	1.357
3	anisole	PMDETA	100:1:0.5:1	0.75	100	14.116	1.3664	1.235
4	anisole	dNbyp	100:1:0.5:2	0.65	100	12.234	1.2856	1.2212

[a] $[M]_0$:$[I]_0$:$[Cu^I]_0$:$[L]$: $[MEO_2MA]_0$:$[EBiB]_0$:$[Cu^IBr]_0$:[Ligand]: the ratio of the ingredients at the start of reaction.

[b] Monomer conversion is determined by ^1H NMR (as explained in Fig. 21).

[c] M_n^{theory}: theoretical number-average molecular weight is calculated via eq. (6.2).

$$M_{n,th} = Conv.\frac{M_m * [M]}{[I]} \tag{6.2}$$

$M_{n,th}$: theoretical molecular weight

$Conv.$: conversion

M_m: monomer's molecular weight

$[M]$: molar amount of monomer

$[I]$: molar amount of initiator

The growth of molecular weight vs. conversion as well as the shift of SEC peaks over time for the reaction using anisole and PMDETA is plotted in Fig. 24. It shows that after a conversion around 0.3, the molecular weight increases linearly with conversion and it is in agreement with the theoretical prediction. The fast increase of molecular weight at the beginning is explained by low deactivator concentration, which results in rapid early growth of a small amount of polymer chains. It is also visible in Fig. 24, that the Đ value decreases at the beginning of the reaction and then stays constant, indicating a fast exchange between active and dormant species. According to SEC results in Fig. 24, the narrow SEC peaks are shifted gradually to higher molecular weight, which indicates that termination and chain transfer reactions are not occurring since no high molecular tail or shoulder is observable.

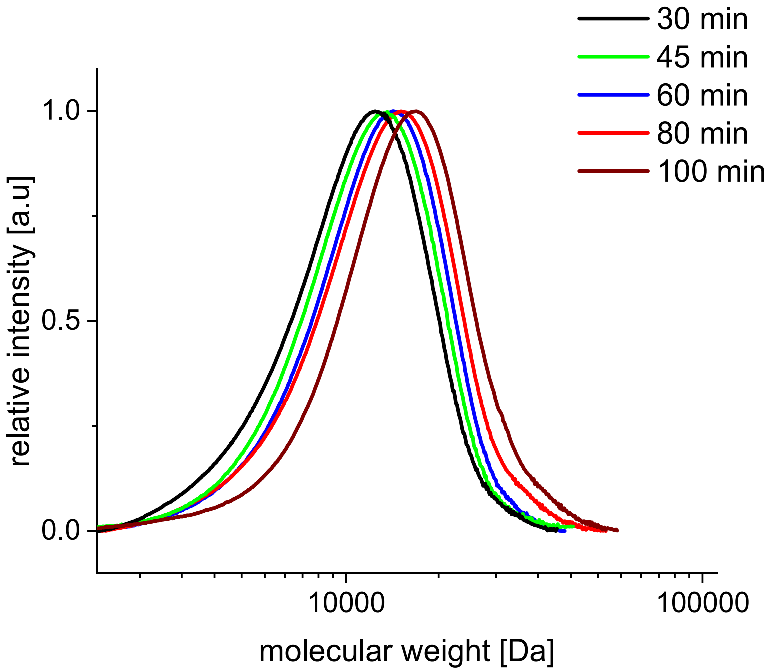

(A)

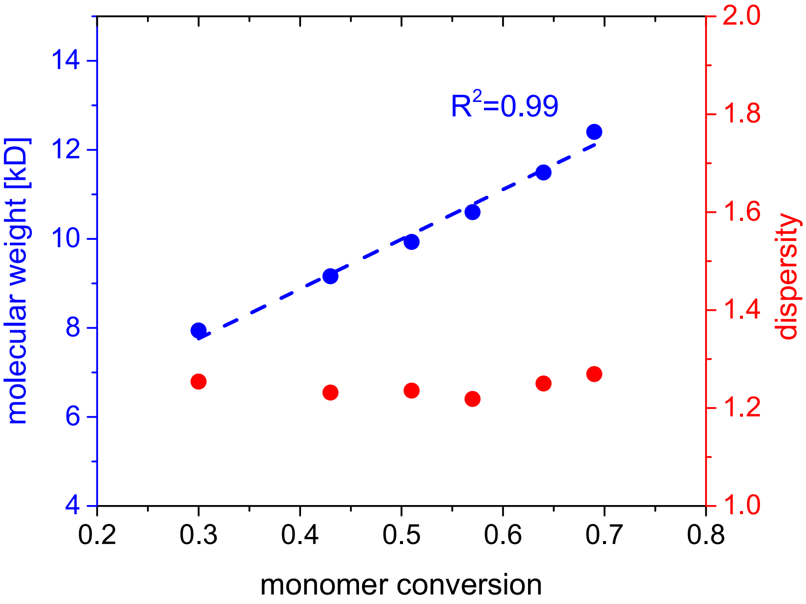

(B)

Fig. 24 SEC results of MEO$_2$MA polymerization in anisole using PMDETA as a ligand (A). The change of molecular weight versus conversion at different time intervals (B). The SEC peaks are shifted to a higher molecular weight while the reaction is progressing. The molecular weight changes linearly as the conversion increases while the dispersity stays almost constant.

The PMDETA-anisole system provides the desired characteristics of high initiation efficiency, low polydispersity, and a moderate apparent polymerization rate. This system should permit fast initiation, fast deactivation of the propagating radicals by Cu^{II} species, and reduced side reactions of the P_n-Br growing chains formed by halogen exchange, thereby providing a good control during ATRP [160].

6.1.2 Synthesis of POEOMA and P(EMO$_2$MA-*stat*-OEOMA) compared to PMEO$_2$MA synthesis via ATRP

Since MEO$_2$MA and OEOMA differ only in the side chain, their reactivity ratios are very similar. This is also proven by the very similar ATRP kinetics of these monomers to and their statistic copolymerization at similar reaction conditions as can be seen in Fig. 25, Fig. 26 and Fig. 27. All reactions are performed in anisole with PMDETA as a solvent and with ta reagent ratio of $[M]_0$: $[I]_0$: $[CuI]_0$: $[L] = 100:1:0.5:1$. The similar kinetics of these reactions will provide the possibility of forced gradient polymerization, this will be explained in section 6.1.3.

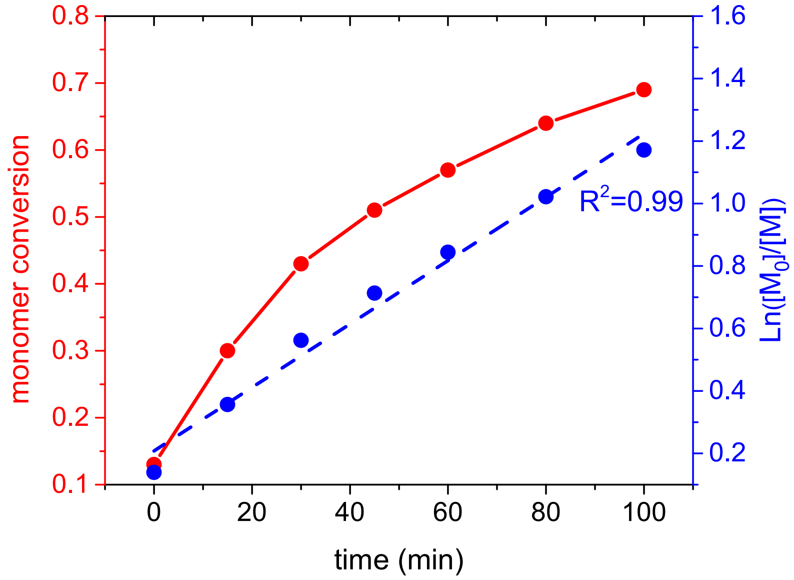

Fig. 25 The monomer conversion versus reaction time and the semi-logarithmic plot of monomer conversion i.e. $\ln([M]_0/[M])$ versus reaction time for the ATRP homopolymerization of MEO$_2$MA. All reactions were done with the reagent ratio of $[M]_0 : [I]_0 : [CuI]_0 : [L] = 100 : 1 : 0.5 : 1$ and the reaction time was 100 min.

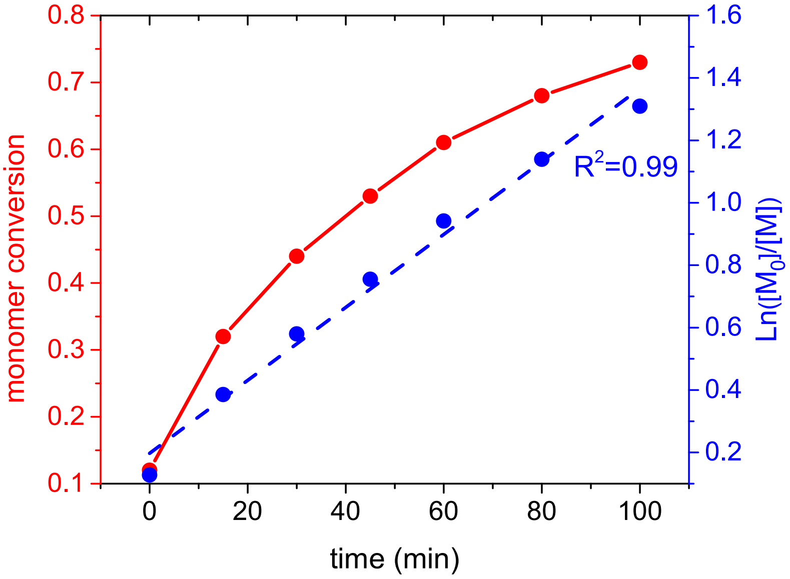

Fig. 26 The monomer conversion versus reaction time and the semi-logarithmic plot of monomer conversion i.e. ln($[M]_0$/[M]) versus reaction time for ATRP homopolymerization of OEOMA. All reactions were done with the reagent ratio of $[M]_0 : [I]_0 : [CuI]_0 : [L] = 100 : 1 : 0.5 : 1$ and the reaction time was 100 min.

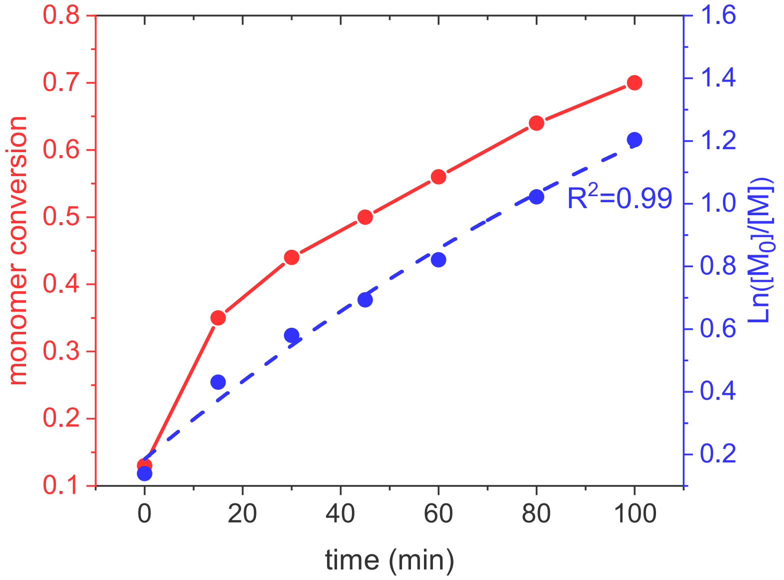

Fig. 27 The monomer conversion versus reaction time and the semi-logarithmic plot of monomer conversion i.e. ln($[M]_0$/[M]) versus reaction time for ATRP statistic copolymerization of MEO_2MA and OEOMA with molar ratio of 80:20. All reactions were done with the reagent ratio of $[M]_0 : [I]_0 : [CuI]_0 : [L] = 100 : 1 : 0.5 : 1$ and the reaction time was 100 min.

6.1.3 Random and gradient copolymerization of MEO$_2$MA and OEOMA

As mentioned in section 6.1.2, similar reactivity ratios of MEO$_2$MA and OEOMA, make it optimal to obtain a gradient copolymer with high gradient quality via forced gradient copolymerization. This technique involves a semi-batch reaction, in which one of the monomers is added continuously from an external reservoir, e.g. via a syringe pump, into the polymerization mixture. The forced gradient method combined with a living polymerization allows precision design and synthesis of gradient compositions with high sequence control [67].

The growth of molecular weight vs. conversion as well as the shift of SEC peaks over time for the random and gradient copolymerization are plotted in Fig. 28 and Fig. 29, respectively. Similar to the homopolymerization of MEO$_2$MA, after a conversion of around 30%, the molecular weight increases linearly with conversion while the Đ value decreases at the beginning and then stays constant during the reaction, indicating a fast exchange between active and dormant species. According to SEC results in Fig. 28 and Fig. 29, the narrow SEC peaks are shifted gradually to higher molecular weight, which indicates that termination and chain transfer reactions are not happening since no high molecular tail or shoulder is observed. This proves a good control in both gradient and random copolymerization and guarantees copolymers with a controlled molecular weight and low poly dispersity index.

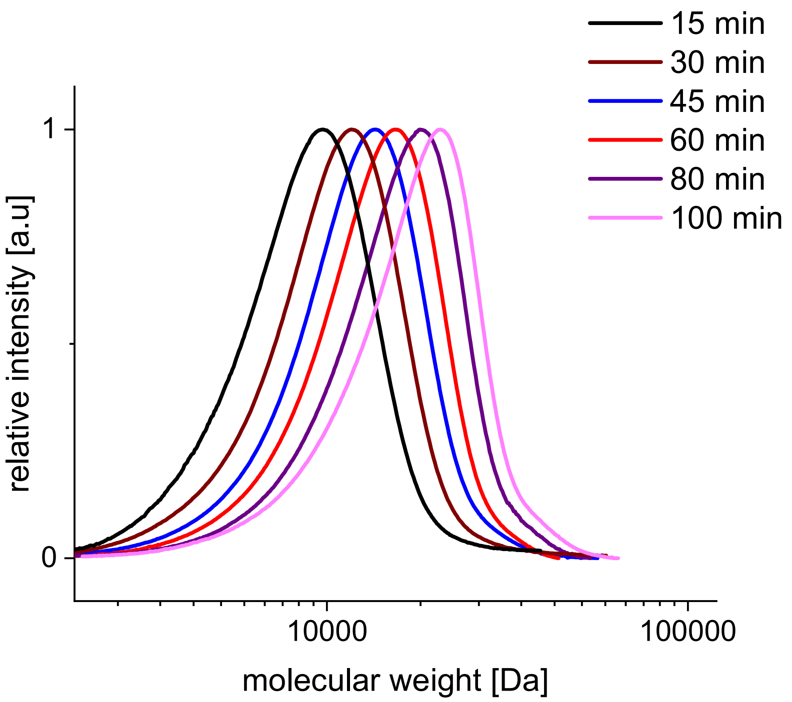

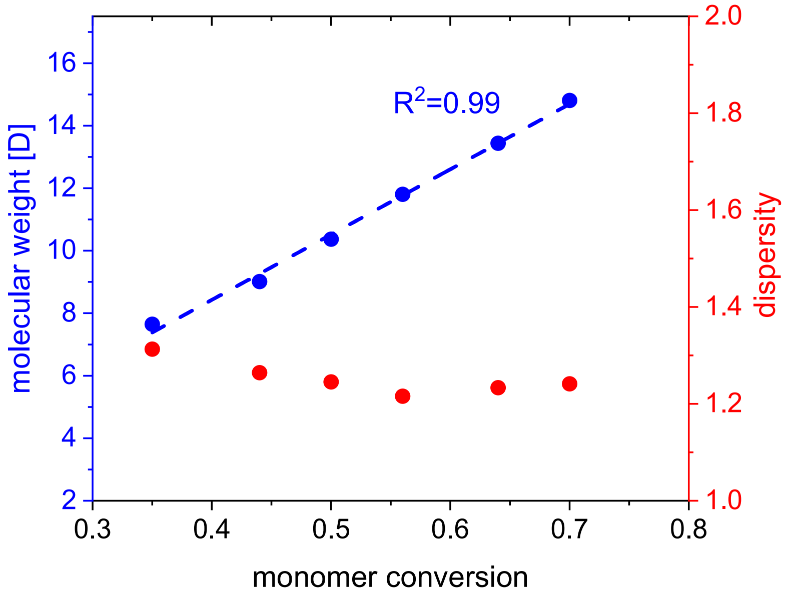

Fig. 28 SEC results of MEO$_2$MA and OEOMA random copolymerization in anisole using PMDETA as a ligand. The upper graphs are the SEC traces at different time intervals. The lower graphs are the molecular weight growth and dispersity change vs. conversion. The SEC peaks are shifted to higher molecular weight while the reaction is progressing. The molecular weight changes linearly versus conversion while the dispersity stays almost constant.

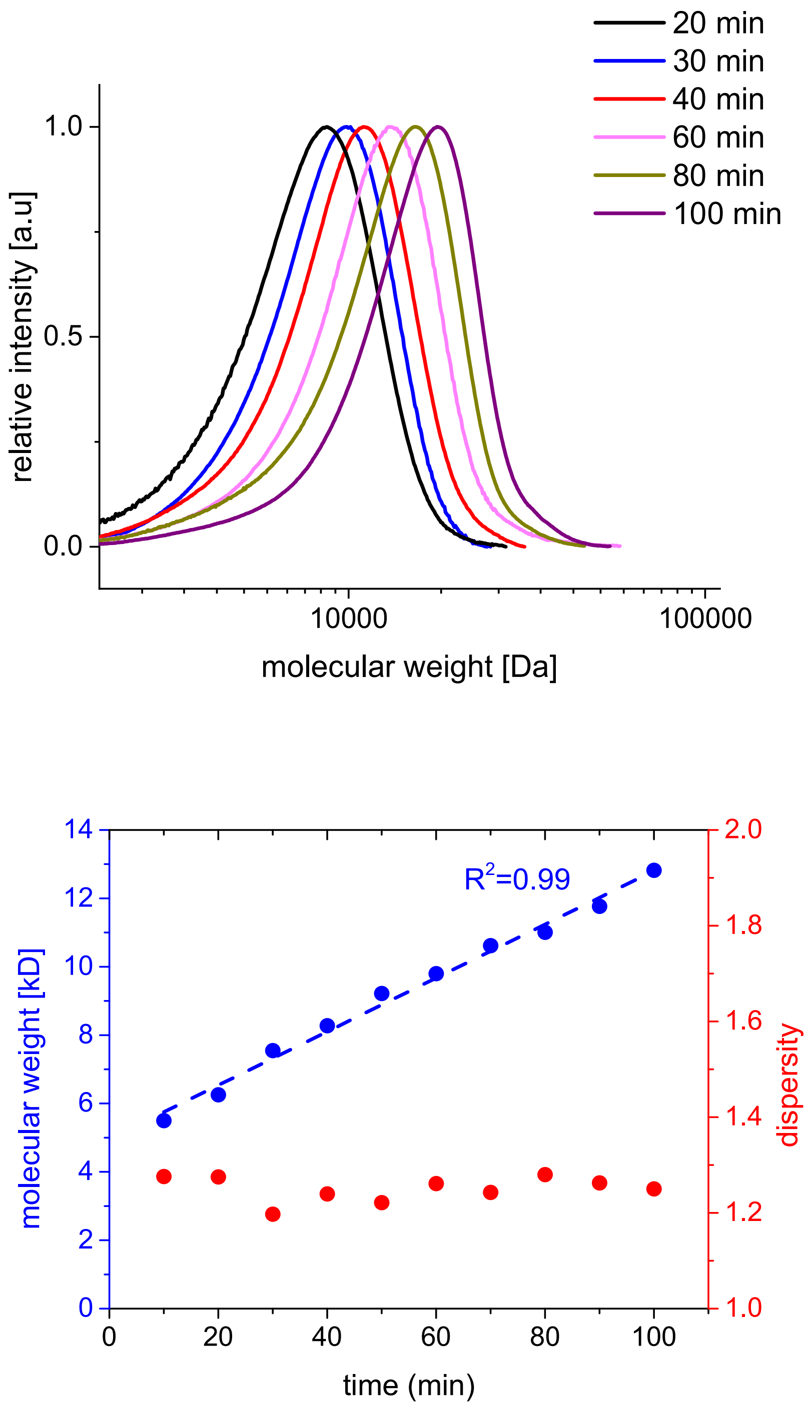

Fig. 29 SEC results of MEO_2MA and OEOMA gradient copolymerization in anisole using PMDETA as a ligand. The upper graphs are the SEC traces at different time intervals. The lower graphs are the molecular weight growth and dispersity change vs. conversion. The SEC peaks are shifted to higher molecular weight while the reaction is progressing. The molecular weight changes linearly versus conversion while the dispersity stays almost constant. The molecular weight growth is slower for the gradient copolymerization compared to random copolymerization due to the lower concentration of monomers during reaction.

To follow the change of copolymer structure during reaction, the copolymers' compositions are studied via ^{1}H NMR spectroscopy. Samples are taken at exact time intervals and measured after purification via column chromatography and precipitation in cyclohexane as mentioned in section 5.1.4. The ^{1}H NMR spectra of MEO$_2$MA, PMEO$_2$MA and P[MEO$_2$MA-*stat*-OEOMA] are represented in Fig. 30. The zoomed-in spectra of the reaction samples for the random copolymerization MEO$_2$MA and OEOMA are shown in Fig. 31.

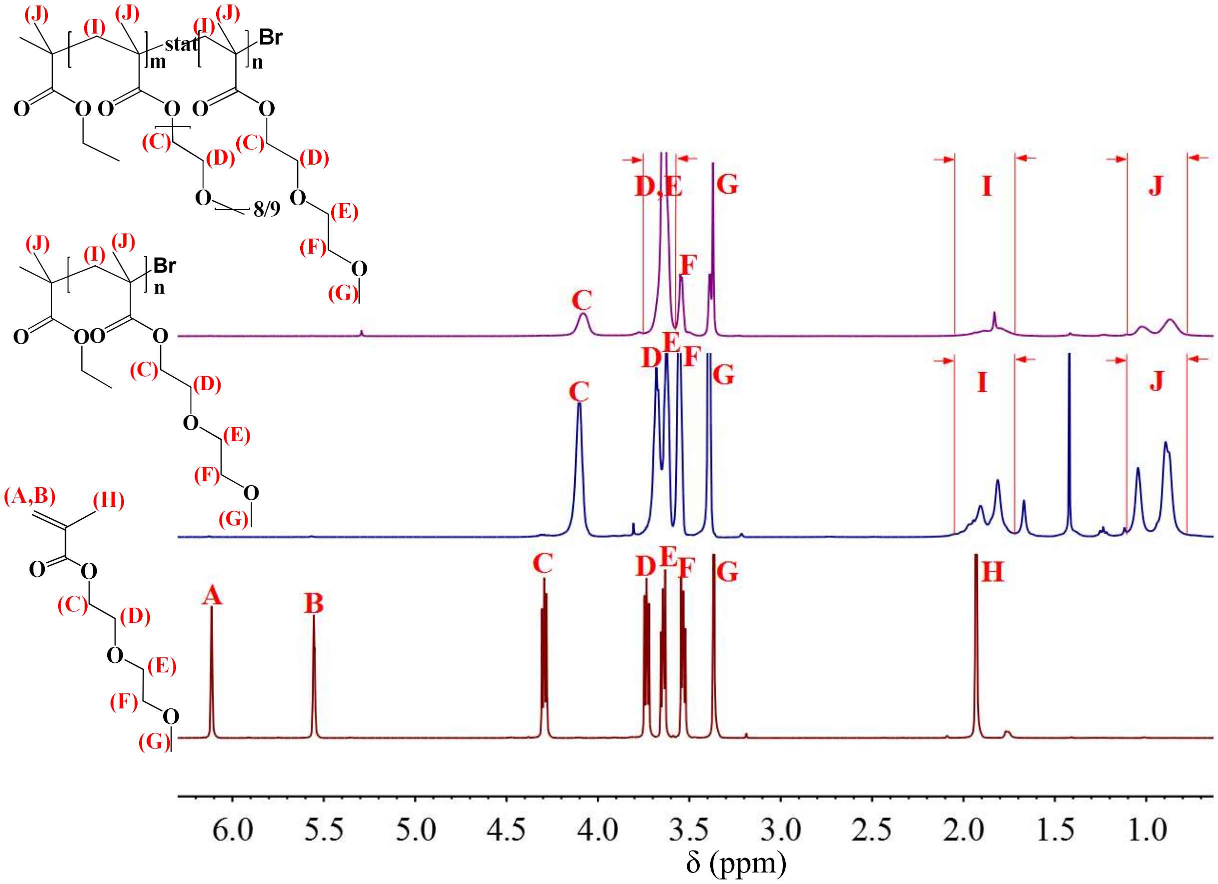

Fig. 30 The ^{1}H NMR spectra of MEO$_2$MA and its homopolymer as well as its copolymer with OEOMA.

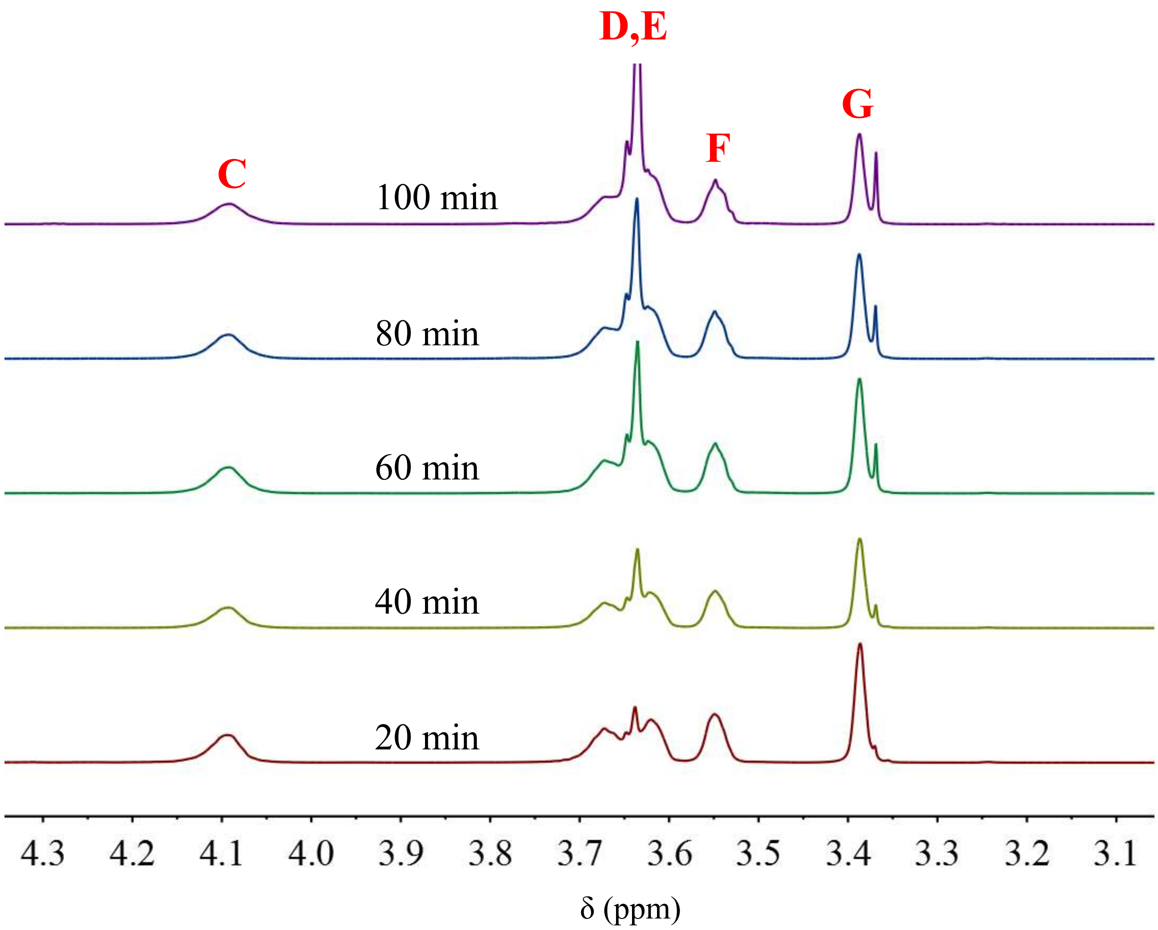

Fig. 31 The zoomed-in ^{1}H NMR spectra of the samples during the random copolymerization of MEO$_2$MA and OEOMA. The change of the peaks in the range D, E shows how the copolymer composition is changing by time.

As discussed in section 6.1.1, the signal between 3.9 and 4.2 ppm is associated with the first methylene group of the side chain and thereby two protons per repeating unit. The integration of the signal in the range of 3.9-4.4 ppm normalized to the integral in the range of 3.5-3.9 ppm thus yields the average number N of the remaining protons in the oligo(ethylene oxide) chains. For a composite of the two monomers M(EO)$_2$MA (M) and O(EO)$_n$MA (O), this results in the following expression:

$$A = N_M \times x + N_O \times y \qquad (6.3)$$

wherein x and y are the molar fractions of M and O, respectively. As the sum of these fractions must be equal to one, equation (6.3) can be transformed to link either x or y to the integral A:

$$N_M \times (1 - y) + N_O \times y = A \qquad (6.4)$$

$$\Leftrightarrow y = \frac{A - M_M}{N_O - N_M} \tag{6.5}$$

The values of N_j (j = M, O) are linked to the number n_j of ethylene oxide units by equation (6.6), taking out the first two protons of each side chain.

$$N_j = 4 \times n_j - 2 \tag{6.6}$$

with $n_M = 2$ and $n_O = 9.08$. The latter was calculated from the molecular weight indicated from MEOMA's molecular weight (Mn = 500 g/mol). Combining equations (6.5) and (6.6) hence gives equation (6.7), which was used to calculate the composition of the gradient and random copolymers. [158]

$$y = \frac{A - 6}{34.32 - 6} = \frac{A - 6}{28.32} \tag{6.7}$$

Fig. 32 shows the change of the copolymer's composition for a random copolymer of MEO_2MA and OEOMA. The composition remains constant during reaction, which shows a perfect random copolymerization of the two monomers [82].

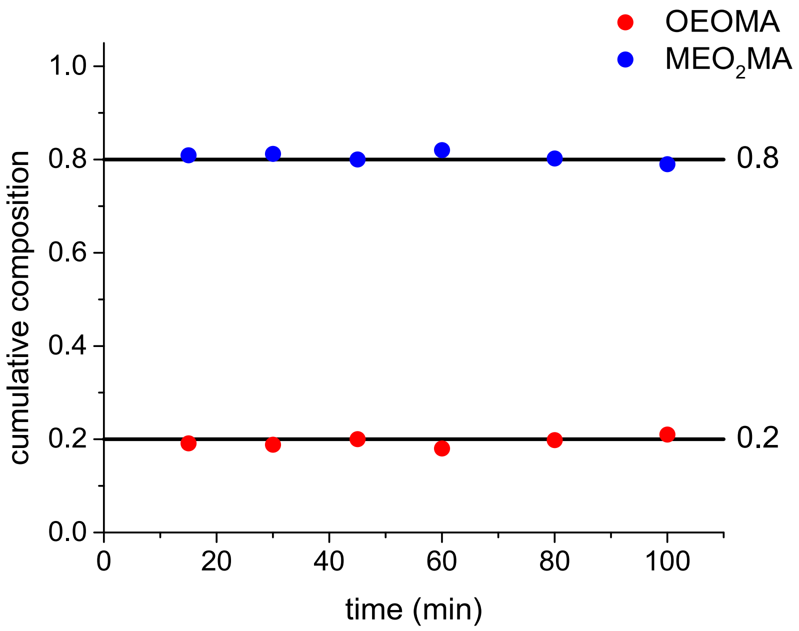

Fig. 32 The composition change for random copolymerization of two monomers with the ratio of MEO_2MA:OEOMA : 80:20.

Since the reactivity of the two monomers is very similar, a gradient copolymerization in a batch system is impossible [168], as it is also proven by the perfect random copolymerization of the two monomers in a batch system (Fig. 32). Therefore, the gradient copolymerization was done via ATRP semi-batch polymerization. Three different injection programs (P1-P3) are used in this work to inject the OEOMA solution into the reaction system (Fig. 33). In all the programs, the injection speed is increased stepwise during the reaction leading to a parabolic curve of the injected volume against time. The reason for injecting OEOMA into the system is its lower proportion in copolymer's desired composition compared to MEO_2MA and its higher viscosity. Since the two monomers have almost the same structure and they differ only in the side chain, their reactivity ratios are the same and almost equal to one. This is also proven by the kinetic studies of OEOMA homo-polymerization (Fig. 27). The similar reactivity ratios of MEO_2MA and OEOMA make it easier to adjust the injection program according to the desired composition.

In the first synthesis (P1), the injection was carried out for the first 80 min of the total reaction time of 100 min. In the second synthesis (P2), the starting injection speed was decreased 30% while the injection time was reduced to 70 min leading to a steeper injection volume curve. The third reaction (P3) is done like the first one (injecting for 80 min of 100 min reaction time) but with 30% higher starting speed and less injection steps which changes the injection volume curve toward a linear graph.

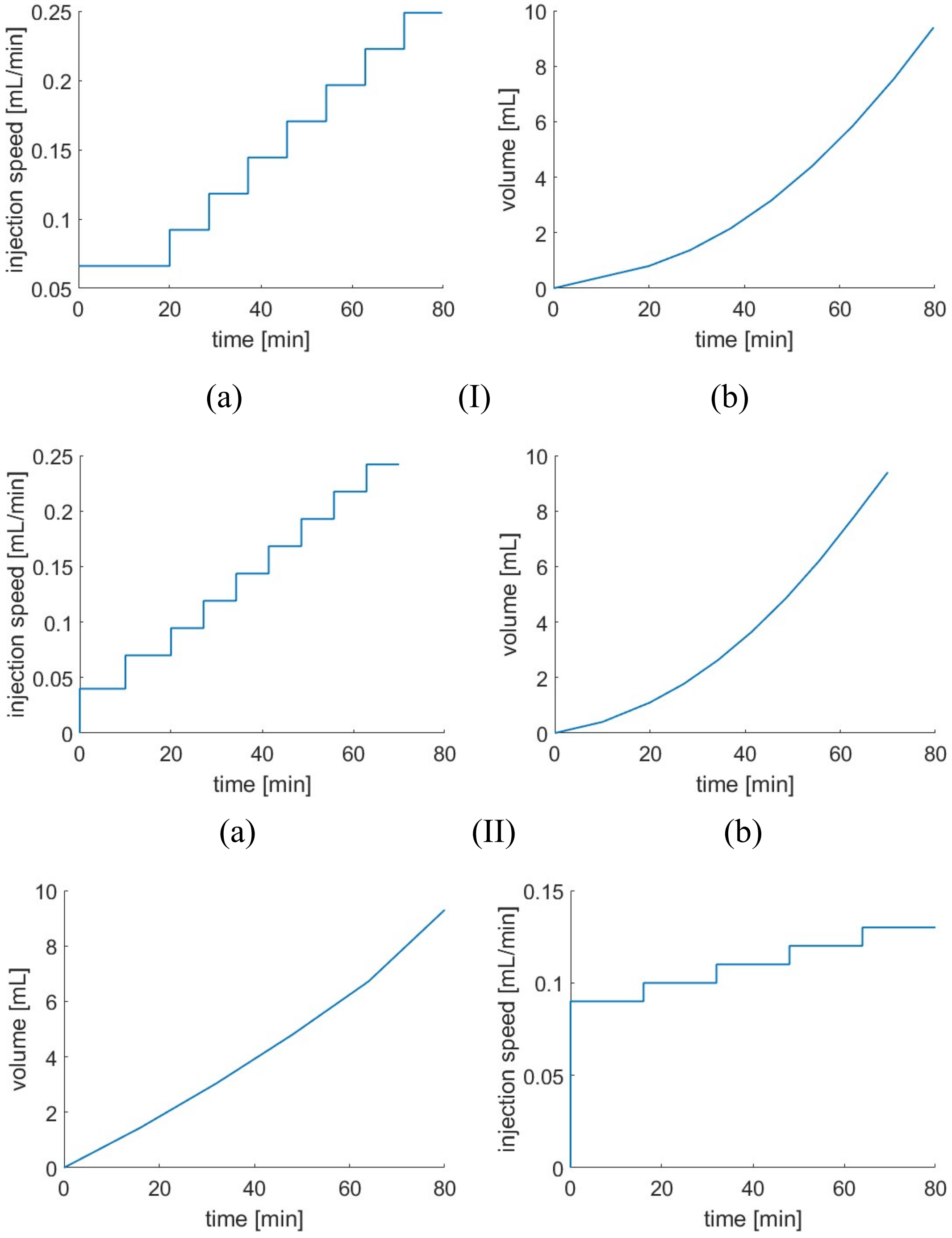

(a) (I) (b)

(a) (II) (b)

(a) (III) (b)

Fig. 33 The injection program of OEOMA for different gradient copolymerization systems, as (a) injected speed vs. time and (b) injection volume vs. time for: (I) Injection program P1 resulting in gradient copolymer P1; (II) Injection program P2 resulting in gradient copolymer P2; (III) Injection program P3 resulting in gradient copolymer P3.

The composition development during the reaction for the three polymerizations is shown in Fig. 34. The plots of all syntheses show a gradual, almost linear increase of OEOMA and decrease of MEO$_2$MA in the copolymer composition, which indicates a gradient structure for all systems. In the first syntheses P1 and P2, the change of composition at the beginning of reaction was very small which leads us to increase the starting injection speed for the last reaction. It should also be noted that for both P1 and P2, the aspired copolymer composition (OEOMA: MEO$_2$MA of 80:20) was not achieved. The final composition was 87:13 for P1 and 85:15 for P2. In the last reaction P3, a perfect linear graph of composition vs. time is observed and the copolymer reached the desired composition. The developments of the composition qualitatively follow the injection program. Since the chain growth is directional with only one active end, the increasing incorporation of OEOMA during the reaction indicates an increasing OEOMA concentration from one chain end to the other. Hence, the synthesized polymers exhibit the aspired gradient structure.

A direct conclusion about the kinetics or the control over the reaction is difficult because of the continuous injection of monomer. A kinetic study of polymerization control via conversion calculation is hence not possible. However, the implied high control over the reaction is reflected in the SEC analysis and the molecular weight development (Fig. 28 and Fig. 29). Furthermore, the molecular weight change for gradient and random copolymerization versus time is linear showing a good control over the reaction. The lower molecular weight of the gradient copolymer compared to the random copolymer is also a proof for the gradient structure, because less OEOMA was added to the polymer chain compared to the random copolymer.

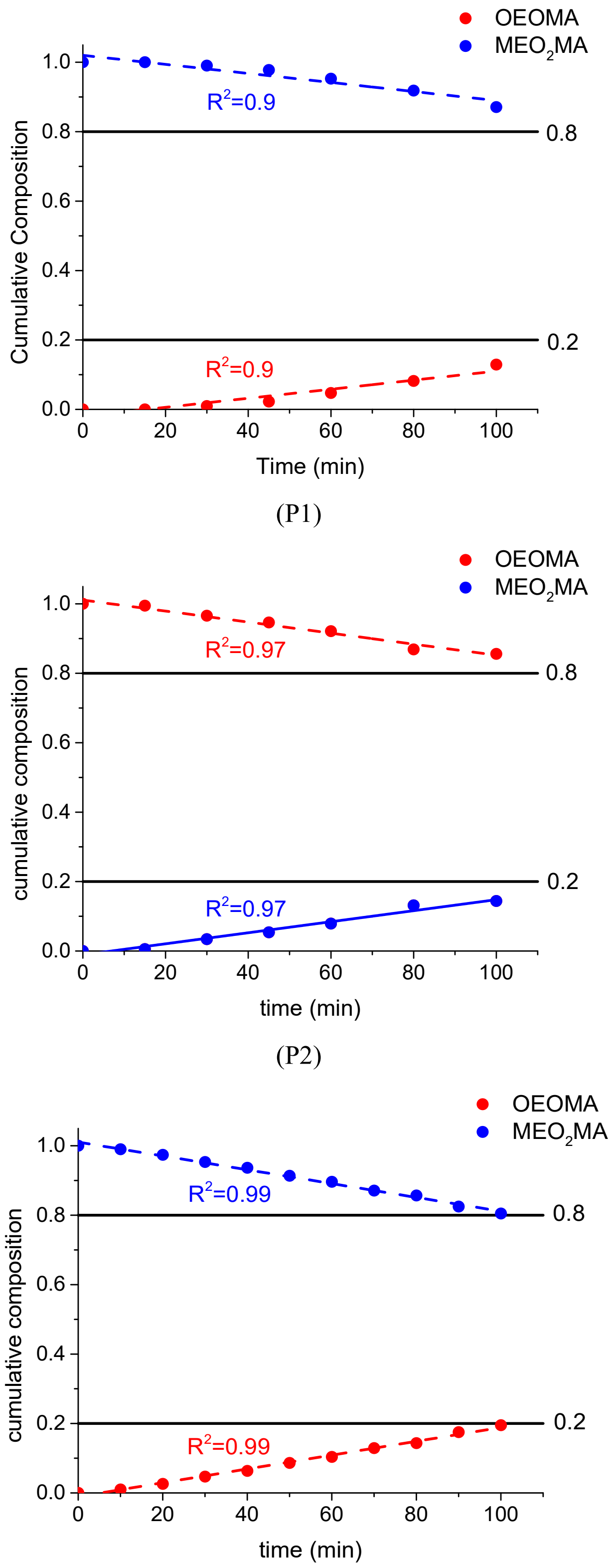

(P1)

(P2)

(P3)

Fig. 34 The composition development during ATRP gradient copolymerization (injection program P1-P3)

6.2 Solubility behavior of random and gradient copolymers MEO_2MA and OEOMA in water

6.2.1 Solubility study of POEOMAs in pure water

The solubility behavior of a temperature responsive polymer is most often studied by turbidimetry, while this gives good information about the cloud point, it cannot explain the transition procedure [57][22]. By using DLS, we are able to follow the changes in the particles' size, size distribution and scattering intensity, and therefore, study the solution behavior in more details. Fig. 35 shows the solubility behavior of $PMEO_2MA$ synthesized in anisole with PMDETA in a dilute aqueous solution. As seen in the graph, both normalized scattering intensity (I) and hydrodynamic radius (R_h) increase sharply above the LCST, then they increase gradually to reach a maximum and then decrease very slowly (the red graph).

The amphiphilic structure of $PMEO_2MA$ is the reason for its thermoresponsive behavior. Below the LCST, the ether oxygens of the side chains form hydrogen bonds with water. On the other hand, the apolar carbon-carbon backbone causes a competitive hydrophobic effect. This results in a balance between energetically favorable polymer-water interactions and unfavorable polymer– polymer interactions which together grants solubilization. By increasing the temperature above the LCST, this balance is disrupted as the hydrogen bonds break and hydrophobic polymer–polymer interactions become thermodynamically favored as compared to polymer-water interactions [50]. Therefore, the hydrophobicity of the polymer increases as the temperature gets higher and this results in aggregation of polymer chains and phase separation [53]. This also explains why the LCST increases by increasing the amount of ethylene oxide in the side chain of POEOMA, as more EO unities result in increasing the amount of hydrogen bonds and therefore stronger polymer-water interaction.

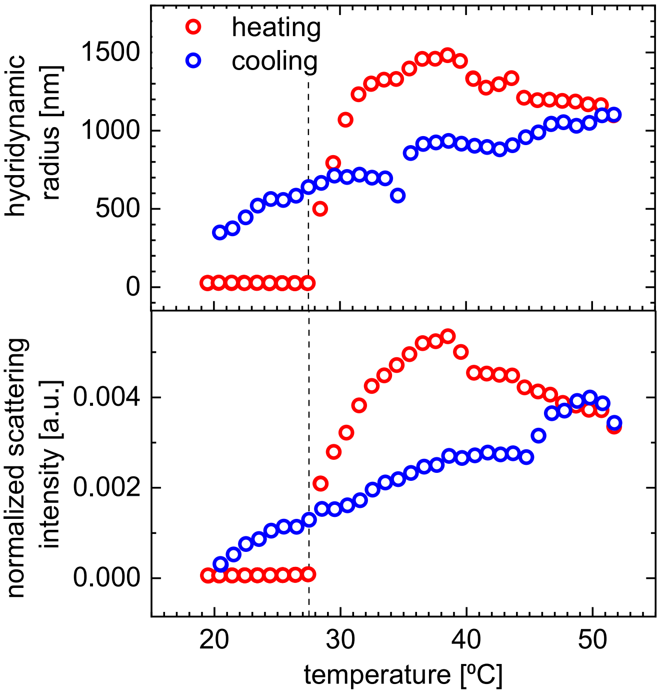

Fig. 35 DLS measurement of PMEO$_2$MA (Mn = 13.66 kDa, Đ = 1.23) in water. The red points show the heating cycle and blue points the cooling cycle. The vertical dashed line points out the abrupt change in hydrodynamic radius and normalized scattering intensity and indicates the LCST at 27.5 ºC.

As demonstrated in Fig. 35, at temperatures below LCST, the polymer is dissolved in the form of unimers with a R_h of around 20 nm. When the temperature reaches LCST, as was explained before, the polymer chains form aggregates and R_h suddenly increases to 1300 nm at 32 ºC. The size growth continues until R_h reaches 1500 nm, due to binding more PMEO$_2$MA chains to the aggregate. The aggregate size then starts to decrease while more and more water molecules are expelled and PMEO$_2$MA chains get dehydrated and as a result, the aggregates slightly shrink. It should also be noted that there is no size change observed for PMEO$_2$MA before LCST, proving that the coil of PMEO$_2$MA does not collapse (mainly by the distortion of backbones) into a crumpled structure at low temperatures. This is totally different from PNIPAM which shows a precontraction of individual polymer chains before the phase transition [28][24].

It is also obvious from Fig. 35 that there is a hysteresis in the heating and cooling cycle of the solubility behavior of PMEO$_2$MA, which is due to the small delay in the dissolution of large precipitated globular particles. This is attributed to the procedure of DLS measurements, which excludes any type of stirring while measuring and makes it more difficult for the large globules to dissolve fast. However, the hysteresis according to literature is still much less than for PNIPAM which is treated as the gold standard of temperature responsive polymers [50][28].

Wu and coworkers explain the large hysteresis in the solution behavior of PNIPAM as a result of the intramolecular and intermolecular $\mathrm{NH}\cdots\mathrm{O}=\mathrm{C}$ hydrogen bonding interactions that are formed in the collapsed state. These strong hydrogen bonds hinder the rehydration of PNIPAM during the cooling process and result in a pronounced hysteresis [24]. In contrast, a reversible dehydration is observed for POEOMAs due to the lack of strong H-bond donor in the molecular structure of these polymers and as a result, there is no possibility of stabilizing H-bonds formation in the collapsed state [50].

Fig. 36 compares the solubility behavior of a random and a gradient copolymer of $\mathrm{MEO_2MA}$ and OEOMA with approximately 20 mol% OEOMA. Both copolymers were chosen based on their similar molecular weight and dispersity index for better comparison, as the LCST shows a slight decrease by increasing the molecular weight [53]. According to Fig. 36, the LCST of the random copolymer (50.7 °C) is almost 15 °C higher than the one for the gradient copolymer (36.6 °C). Around 8 °C hysteresis is observable in the gradient copolymer, a value similar to the $\mathrm{PMEO_2MA}$ homopolymer. But the hysteresis for the random copolymer is still lower than 5 °C. The behaviors of gradient and random copolymers also differ significantly above the LCST. The random copolymer shows a large broad transition in the normalized scattering intensity (4.7×10^{-5} -1.6×10^{-3} a.u.) and in the hydrodynamic radius (20 - 1280 nm), while the change in gradient copolymers (I: 2.7×10-5 - 5.2×10^{-4} a.u., R_h: 24 - 292 nm) is rather sharp but with a lower increase. This data indicates the formation of micelles rather than globular aggregates in the case of gradient copolymers which are held in solution by the hydrophilic OEOMA segments that are not yet aggregated [53].

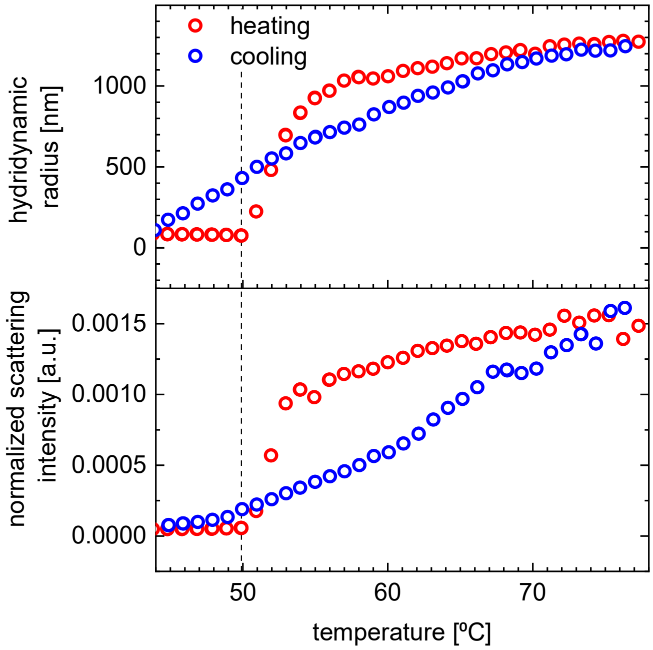

(a)

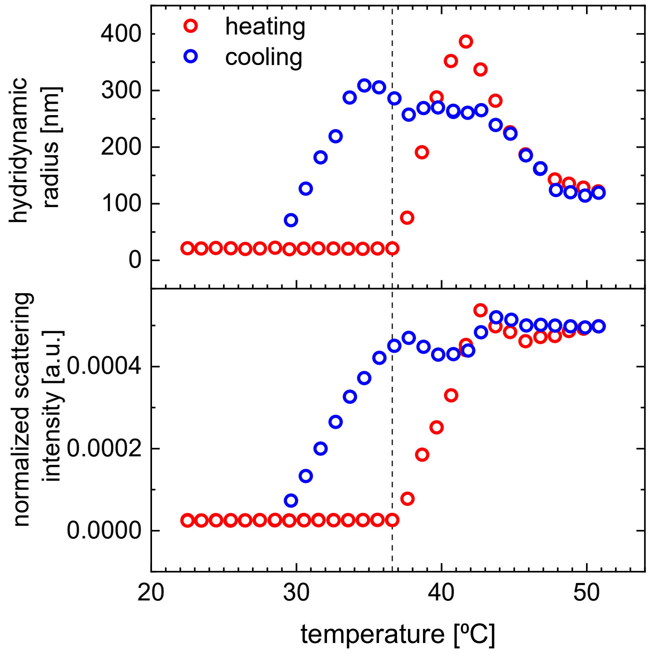

(b)

Fig. 36 DLS measurement of the random copolymer P(MEO$_2$MA$_{81}$-*r*-OEOMA$_{19}$), M$_n$ = 15.96 kDa, Đ = 1.17 (a) and gradient copolymer P(MEO$_2$MA$_{80.5}$-*g*-OEOMA$_{19.5}$), M$_n$ = 15.21 kDa, Đ = 1.24 (b) in water. The red points show the heating cycle and blue ones the cooling cycle. The vertical dashed lines point out the abrupt change in hydrodynamic radius (upper graphs) and normalized scattering intensity (lower graphs) and indicates the LCST.

As mentioned before, there are no strong intermolecular hydrogen bonding interactions between polymer chains. Therefore, the phase transition occurs mainly because of multiple chain aggregation without a precontraction process of individual polymer chains. Moreover, the self-aggregation process of P(MEO_2MA-*co*-OEOMA) is mainly dominated or driven by the conformation changes of oxyethylene side chains, which collapse first to get close to the hydrophobic backbones and then distort to expose hydrophilic ether oxygen groups to the "outer shell" of polymer chains as much as possible[21][28][57][58]. According to Sun and Wu [28], P(MEO_2MA-*co*-OEOMA) random copolymers exhibit "hydrated chains, dehydrated chains, loosely aggregated agglomerates and finally densely aggregated agglomerates" during the phase transition. As there is no precontraction process before phase transition, the conformation of hydrophobic backbones with the slowest response does not change much and the micelle size stays constant. It should be noted that the cores in the micelles are only physically or loosely cross-linked by hydrogen bond bridges between ether oxygen groups and water molecules. By increasing the temperature above the LCST, due to the increased molecular motion and decreased density, the amount of water molecules which participate in hydrogen bonding decreases or in another word, more water molecules expel from micelles. Therefore, the micelles get more densely aggregated which results in a gradual change as seen in DLS [28].

The case is significantly different for the gradient copolymer based on its phase behavior in water (Fig. 36 (b)). The change of R_h and I are rather sharp than broad and, in the amount, less pronounced than the random copolymer. Above the LCST, when the temperature is increased further, R_h decreases first and then stays constant. This could be attributed to the formation of micelles rather than large agglomerates. Peng *et al.* [60] reported a similar behavior in case of poly(MEO_2MA-*co*-$PEOMA_{2080}$) due to the association of the polymer chains as a result of the dehydration while increasing the temperature, followed by a rearrangement process and micelle formation [60]. In the system of P(MEO_2MA-*grad*-OEOMA), there are no long $PEOMA_{2080}$ side chains to stabilize the micelles in the system, whereas the dense OEOMA at one end of the polymer chain can help the micelle stabilization to some extent. The decrease in R_h is explained by further dehydration and water expelling from the system, which results in shrinking the micelles and decreasing the particle size while the scattering intensity stays constant. This is to a certain degree similar to the behavior of block copolymers [62][64], but without showing multiple transition temperatures, while micelles cannot stay in the system long enough to reach a second LCST.

The solubility behavior of several gradient and random copolymers with various comonomer compositions were studied via DLS and the change of hydrodynamic radii and normalized scattering intensities are plotted in Fig. 37. For simplicity, just the heating cycles are shown. The solubility behavior depends strongly on the copolymer structure and therefore is similar for all random copolymers or all gradient copolymers, in a similar manner shown in Fig. 36 and Fig. 37, respectively. For both random and gradient structures, the LCST increases with a higher portion of OEOMA in the comonomer composition. This change is plotted in Fig. 38. By increasing the mol% of OEOMA, the LCSTs of gradient and random copolymers get closer to each other. The higher slope of LCST versus composition for gradient copolymers shows the higher dependency of LCST to OEOMA's ratio for gradient copolymers rather than random copolymers.

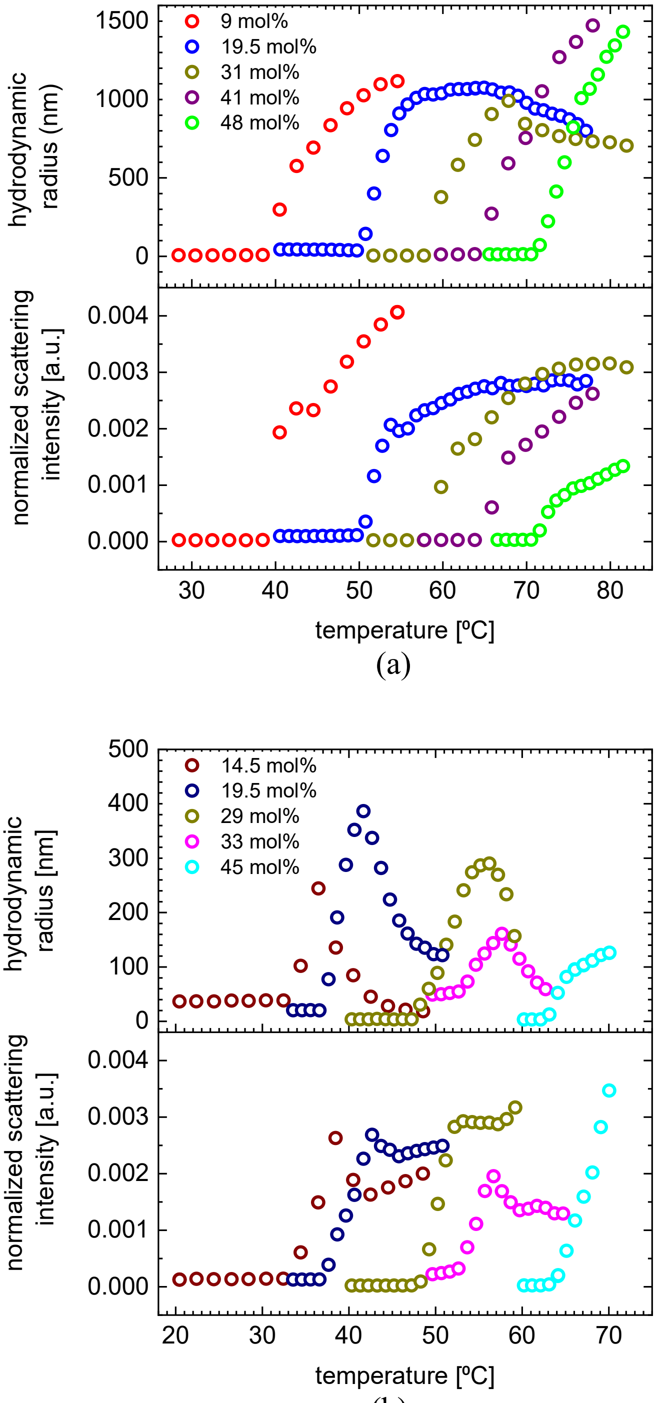

(a)

(b)

Fig. 37 DLS graphs of the (a) random and (b) gradient copolymers with different compositions measured in water. In the upper graphs the hydrodynamic radii and in the lower graphs the normalized scattering intensity versus the temperature is shown. The mol% of OEOMA in each copolymer is indicated on the graph. The LCST of random copolymers is always higher than the LCST of gradient copolymers with similar composition. The solubility behavior strongly depends on the copolymer structure and therefore differs a lot from gradient to random structure.

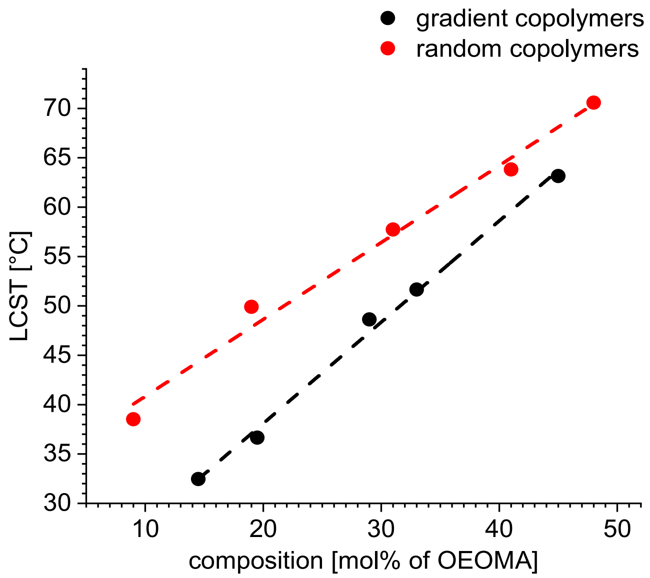

Fig. 38 The change of LCST versus the copolymer composition for gradient and random copolymers. As the amount of OEOMA in the polymer increases, the LCST of gradient and random copolymers get closer to each other.

6.2.2 The effect of additives on the solubility behavior of random and gradient copolymers of di- and oligo (ethylene oxide) methacrylate in water

6.2.2.1 The effect of anions and cations

Hofmeister discovered and explained the effect of salts on the denaturation of proteins in aqueous solution for the first time [169] [170]. The results of his work are still used as a guide to study the thermodynamics of the effect of salts on macromolecule solubility [78] [171] [172] [173] [174]. Salts are well-known to have a high impact on the behavior of thermoresponsive polymers in solution [81]. Both the cation and the anion of the salt are considered to influence the solubility behavior of macromolecules [170]. To study the effect of different anions on the solubility behavior of gradient and random copolymers, sodium salts of these anions are used. The order of anions in the Hofmeister series is as follows, with decreasing denaturation ability from left to right. The bold anions were studied in this research.

$$\mathrm{CO_3^{2-}} > \mathbf{SO_4^{2-}} > \mathrm{H_2PO_4^-} > \mathbf{F^-} > \mathbf{Cl^-} > \mathbf{Br^-} \approx \mathrm{NO_3^-} > \mathbf{I^-} > \mathrm{ClO_4^-} > \mathbf{SCN^-}$$

The results of DLS measurement (normalized scattering intensity and hydrodynamic radius versus temperature) in the presence of sodium sulfate (Na_2SO_4) for random and gradient copolymer of MEO_2MA and OEOMA are plotted in Fig. 39 and Fig. 40 respectively. The results of DLS measurements in presence of other salts studied in this work, are plotted in Fig. A1- Fig. A9 (to investigate the effect of anions on solubility behavior) and Fig. A10 - Fig. A15 (to investigate the effect of cations on solubility behavior).

As a summary of these results, Fig. 41 shows the change of the LCST for gradient and random copolymers of MEO_2MA and OEOMA with 20% OEOMA in their chains in the presence of different salts. The concentration of all the salts was set to 0.5 M. Although a generally lower amount of salt is present in most biological systems, this high concentration was necessary because for some of the salts, concentrations lower than 0.5 M, did not lead to a change in the LCST of the copolymers in water. Surprisingly, there is no distinguishable trend in the behavior of different cations on the LCST for both random and gradient copolymers.

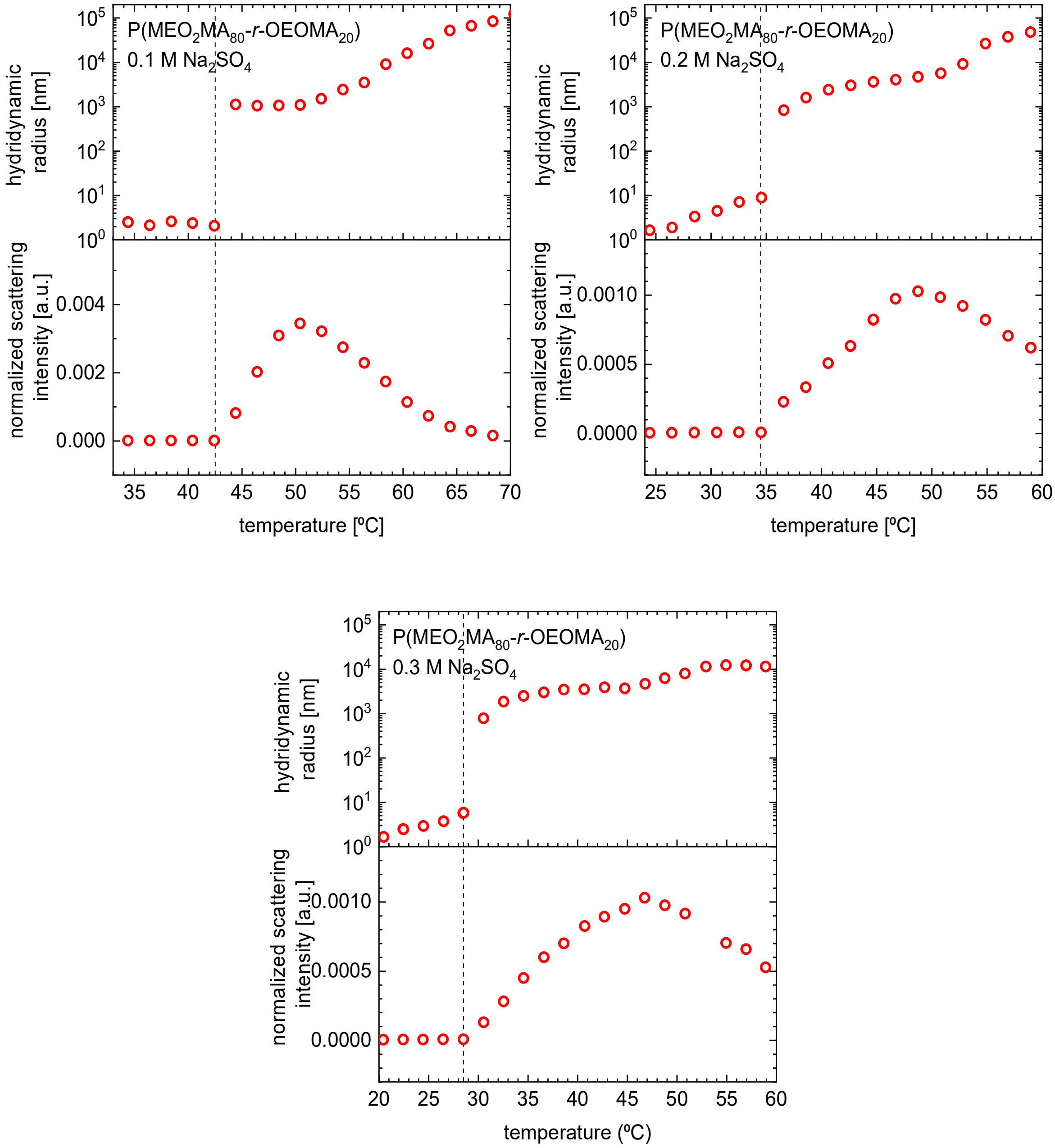

Fig. 39 DLS measurements of the random copolymer P(MEO$_2$MA$_{80}$-*r*-OEOMA$_{20}$), M_n = 15.96 kDa, Đ = 1.17 in Na$_2$SO$_4$ aqueous solution. The vertical dashed lines point out the abrupt change in hydrodynamic radius (upper graph) and normalized scattering intensity (lower graph) and indicates the LCST.

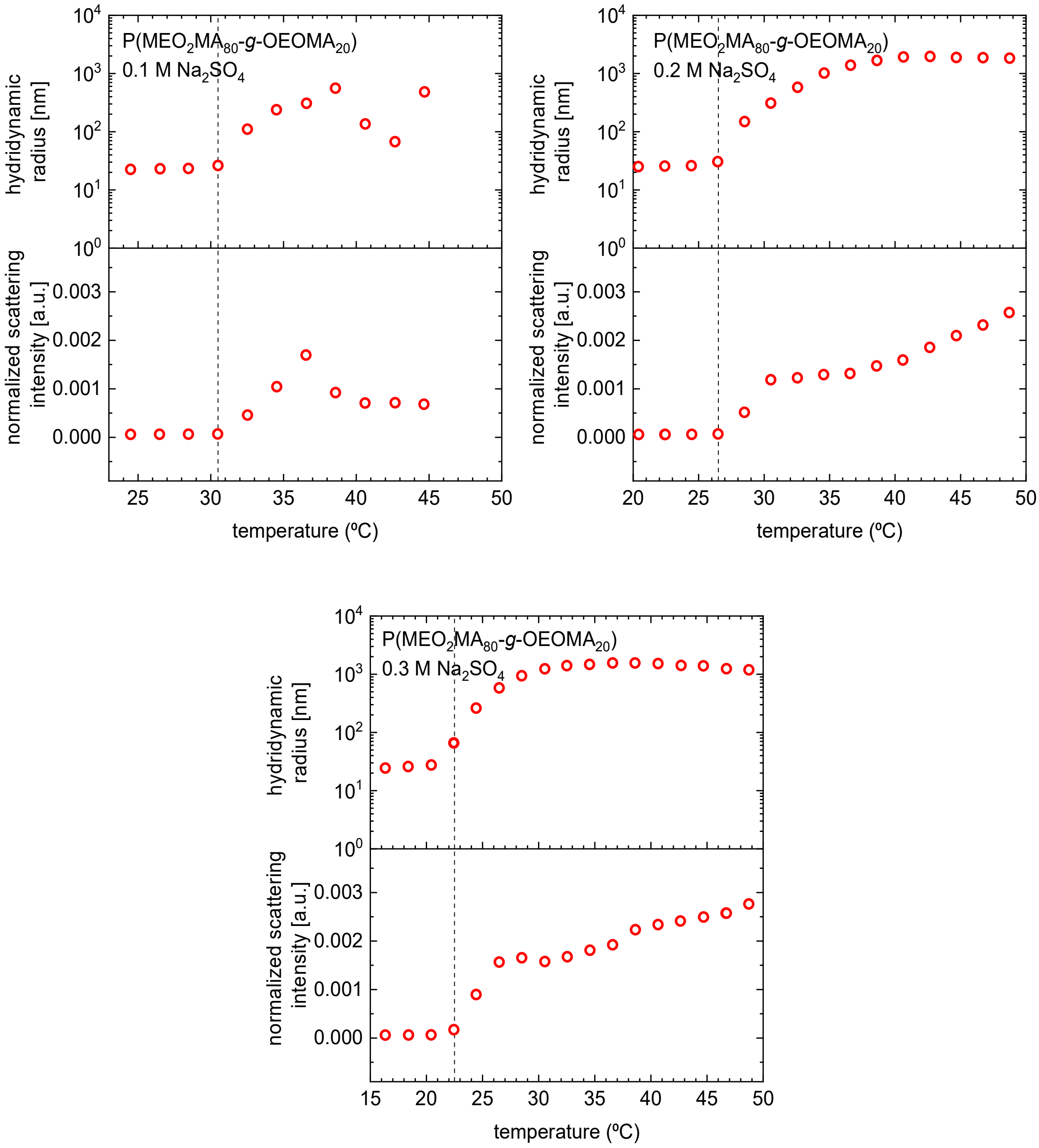

Fig. 40 DLS measurements of the gradient copolymer P(MEO$_2$MA$_{80}$-g-OEOMA$_{20}$), M_n = 15.21 kDa, Đ = 1.24 in Na$_2$SO$_4$ aqueous solution. The vertical dashed lines point out the abrupt change in hydrodynamic radius (upper graph) and normalized scattering intensity (lower graph) and indicates the LCST.

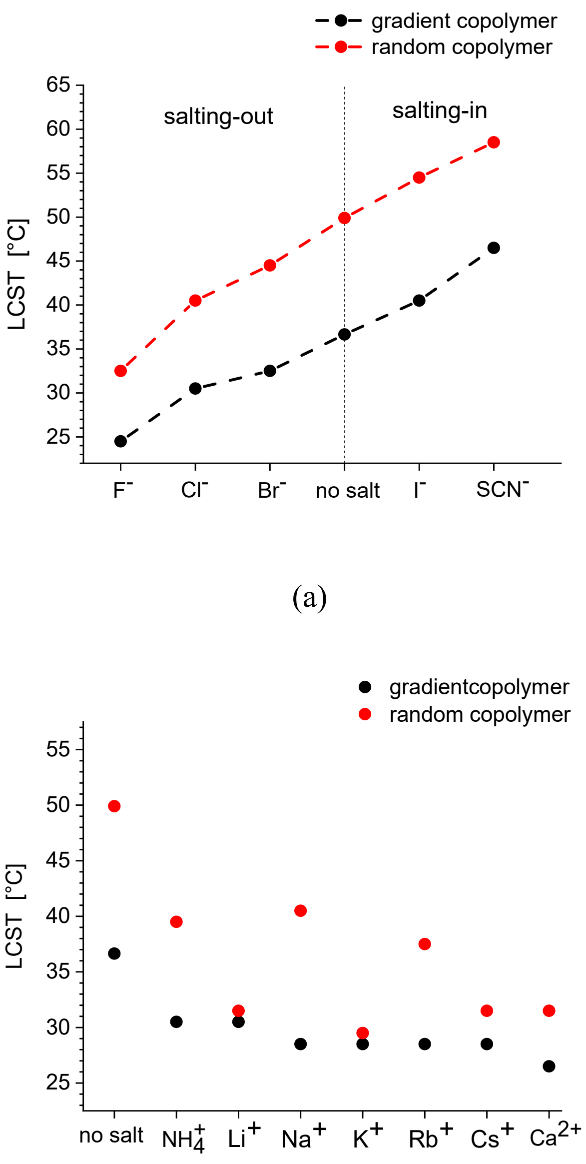

(a)

(b)

Fig. 41 The effect of anions (a) and cations (b) on the LSCT of random and gradient copolymers. The salt concentration in all measurements is 0.5 M. The anions are studied as sodium salt and the cations as chloride salts.

The effect of anions on the solubility behavior of gradient and random copolymers is in agreement with the Hofmeister series and similar to their effect on the solubility of PNIPAM [77]. F^-, $Cl^-$and Br^- decrease the LCST and therefore, show a salting-out effect while I^- and SCN^-increase the LCST and show a salting-in effect. The biggest change in solubility is observed for SO_4^{2-} which makes the copolymer precipitate immediately after it is added to the solution and therefore, it is not plotted in Fig. 41. The next maximum of change is observed for F$^-$ with the most salting out effect that decreases the LCST around 17.5 ºC for random and gradient copolymer. The biggest salting in effect is observed for SCN$^-$, which causes 8.5 ºC increase in LCST for the random copolymer and 10 ºC increase for the gradient copolymer.

The salting-out effect is assumptively related to the high surface charge density of the kosmotropic anions; this increases the surface tension in the inner hydration shell of the polymer, leading also to a relatively rigid and well-ordered anion hydration shell. As a result, the kosmotropic salts show a highly negative hydration entropy [175]. Therefore, in the presence of kosmotropic anions, less water molecules are available to hydrate the polymer and the LSCT decreases. Furthermore, in the presence of salt, the solvent polarity increases which enforces the hydrophobic–hydrophobic interactions. On the other hand, the salting-in effect is related to the high polarizability of the chaotropic salts which results in lower negative hydration entropy. This can partially distruptthe rigid cage-like water structure and as a result, more water molecules can hydrate the polymer. Moreover, chaotropic anions can bind directly to the polymer and increase its surface charge and thus its solubility [81].

According to Zhang *et al.* [77], the change of LCST after adding salt to a polymeric solution could be modeled based on three facts:

1- If the concentration of an inorganic salt is not too high, the surface tension of water at the hydrophobic/aqueous interface changes linearly with salt concentration.
2- At the first hydration shell of a macromolecular solute the polarization of water molecules is also dependent linearly on the salt concentration.

Each of these two effects can be the cause of polymer precipitation depending on whether the anion is a kosmpotrope or a chaotrope.

3- For the most weakly hydrated anions, enthalpically favorable anion-polymer interactions can result in a salting-in effect.

As a result, the change of LCST by addition of salt could be described by:

$$T = T_0 + \kappa\,[A^-] + \frac{B_{max}K_A[A^-]}{1+K_A[A^-]} \tag{6.8}$$

T_0 is the LCST with no salt, κ is a constant with the unit of temperature/molarity, which is proportional to the surface tension, or hydration entropy of the anion. B_{max} is the increase in LCST related to anion binding at saturation and K_A is the binding constant of the anion to the polymer.

The binding isotherm $\frac{B_{max}K_A[A^-]}{1+K_A[A^-]}$ is attributed to the direct ion binding to the polymer (third fact) which is considered to be a saturation phenomenon and is relevant just for the chaotrope salts. For kosmotrope salts, the LCST is related linearly to the salt concentration as:

$$T = T_0 + \kappa\,[A^-] \tag{6.9}$$

Fig. 42 shows the effect of salt concentration of different salts on the LCST of gradient and random copolymers. From these graphs it is visible that the effect of salt concentration on the LCST of gradient copolymers is sharper than for random copolymers in NaSCN's salting in effect. The calculated amount of κ as well as B_{max} and K_A are presented in Table 2. It is also obvious from Fig. 42, that the increase of κ for both gradient and random copolymer is in agreement with the order in the Hofmeister series. Moreover, except for SO_4^{2-} which shows a considerably lower value of κ for the random copolymer when compared to the gradient copolymer, for the rest of anions, κ and as a result the effect of anion on the LCST is similar for gradient and random copolymers.

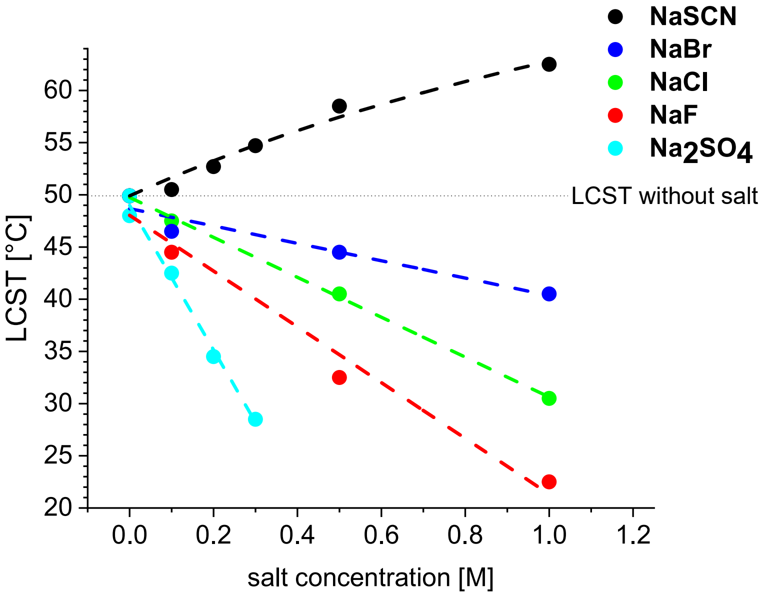

(a)

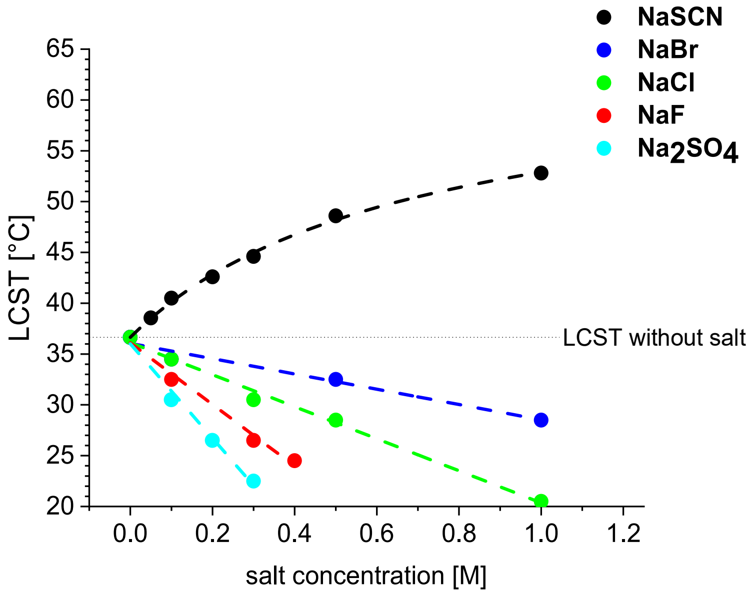

(b)

Fig. 42 The effect of salt concentration of different sodium salts on the LCST of random (a) and gradient (b) copolymers containing 20 mol% OEOMA measured via DLS in water. All the salts in this study show a salting out effect except for NaSCN which shows salting in effect.

Table 2 Fitted values of κ, B_{max} and K_A from LCST measurements for gradient and random copolymer

	κ [M^{-1}]		B_{max} [^{o}C]		K_A [M^{-1}]	
anion	Random copolymer	Gradient copolymer	Random copolymer	Gradient copolymer	Random copolymer	Gradient copolymer
$\mathbf{SO_4^{2-}}$	-69	-46	____	____	____	____
$\mathbf{F^-}$	-27	-30	____	____	____	____
$\mathbf{Cl^-}$	-19	-16	____	____	____	____
$\mathbf{Br^-}$	-8	-7	____	____	____	____
$\mathbf{SCN^-}$	-2.5	-12	34.5	69.2	0.65	0.68

6.2.2.2 The effect of surfactant

Fig. 43 shows the change of LCST for gradient and random copolymer after addition of SDS (anionic surfactant) and CTAB (cationic surfactant). The surfactant concentration is chosen to be lower than or close to the critical micelle concentration (CMC) (~8.1 mM for SDS [176] and for ~1 mM for CTAB [177][178]). In general, addition of a surfactant increases the LCST, due to its effect on stabilizing the formed polymeric micelles or globules in the solution. The surfactant molecules interact with the polymer and anchor on the surface of the formed micelles or globules in solution and increase the repulsion between adjacent polymer-bound micelles [76]. This can also explain the lower increase of particle size above the LCST when increasing the surfactant concentration (Fig. A16 - Fig. A19). Based on Fig. 43, the LCST increases linearly with increasing surfactant concentration until it reaches the boiling point of the solvent. This result is completely different from PNIPAM, which shows the abnormal behavior of not precipitating in the presence of SDS until the concentration of SDS reaches the critical aggregation concentration (CAC) [179]. The increase in LCST is larger for CTAB than for SDS, which is different from the general trend observed for PNIPAM [180]–[182]. For PNIPAM in general, the LCST increases in the order of nonionic < cationic < anionic which is the general surfactant adsorption on the polymer [76]. The reason could be the longer alkyl chain for CTAB which according to the literature can also influence the increase of the LCST after addition of surfactant [181][183]. Although it was mentioned that the effect of ionic structure is more relevant than the length of the alkyl chain, this is not in agreement with our observation for POEOMAs.

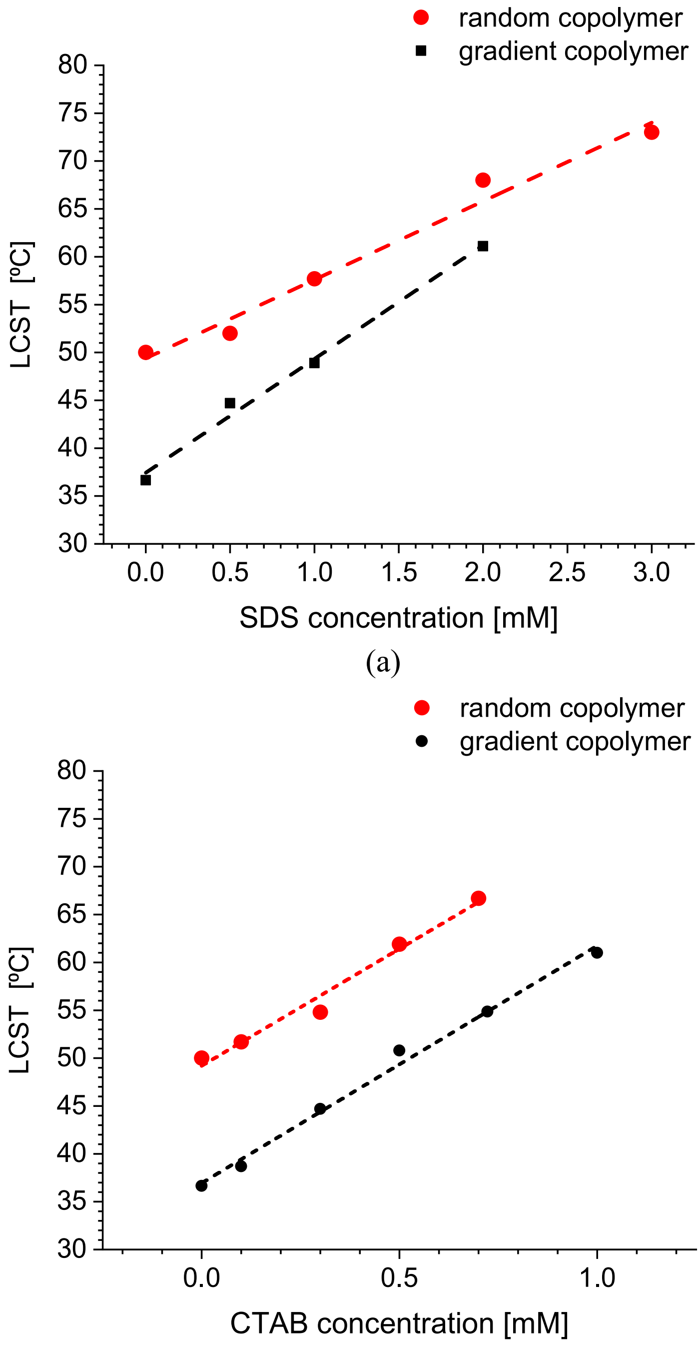

(a)

(b)

Fig. 43 The change of LCST for gradient and random copolymers containing 20 mol% OEOMA versus surfactant concentration. The upper graph (a) shows the effect of SDS and the lower graph (b) of CTAB. The LCST is increasing drastically as the surfactant concentration increases.

6.2.2.3 The effect of ethanol

The change of LCST of the gradient and random copolymers of MEO$_2$MA and OEOMA with 20 mol% OEOMA in presence of ethanol as a cosolvent is plotted in Fig. 44. The results of DLS measurements for gradient and random copolymers in the presence of various amount of ethanol in aqueous solution, are plotted in Fig. A20 - Fig. A21. The LCST increases with an increasing amount of ethanol until the polymer is completely soluble and does not show any LCST below the solvents' boiling point. The change of LCST is exponential for the random copolymer and linear for the gradient copolymer. This behavior is in agreement with copolymers of similar structure in the literature [184]. Addition of ethanol as a good solvent for POEOMAs increases their solubility. Moreover, the competitive interaction with polymer between water and alcohol enhances the solubility, thus increases the LCST.

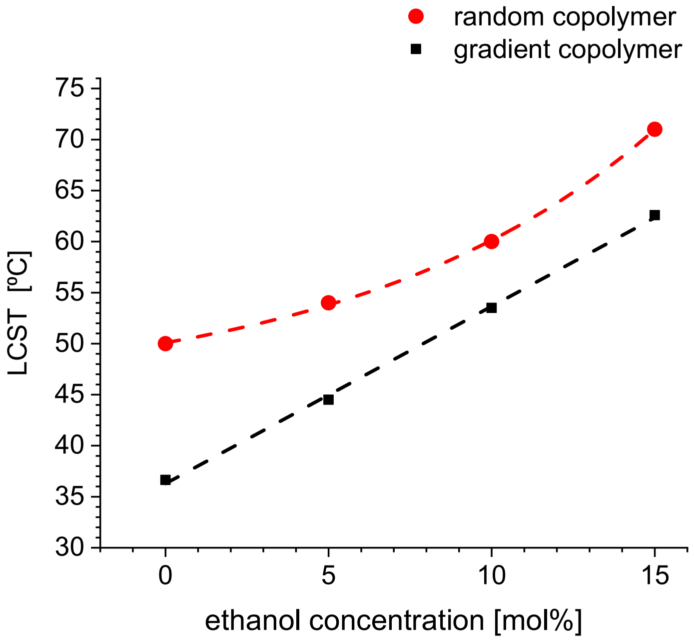

Fig. 44 The change of LCST for random and gradient copolymers containing 20 mol% OEOMA by adding absolute ethanol to the copolymer's aqueous solution. LCST increases as the amount of ethanol in the solution increases till the copolymer gets fully soluble at all temperatures and shows no LCST anymore.

A cononsolvency effect (i.e. lower compatibility of the polymer with the solvent at a certain range of solvent composition) is not observed for these copolymers in the system of water-ethanol in contrary to other temperature responsive polymers like PNIPAM [76][80] [185][186] or other thermoresponsive polymers with nitrogen atom as the source of hydrogen bonding [82]. This can be a result of no preference to form water-ethanol interactions rather than water-polymer or polymer-polymer interactions in this system. It is assumed that due to higher interactions of both water and ethanol with the polymer compared to water-ethanol interactions, no hydrophobic hydration of ethanol molecules occurs in this system. According to literature [75][82][186] hydrophobic hydration happens at low fractions of ethanol, when water molecules form a hydration shell around ethanol molecules due to strong hydrogen bonds between them and therefore, there are not enough water molecules to hydrate the polymer. By increasing the ethanol fraction, there are not enough water molecules anymore to hydrate all ethanol molecules. As a result, the mobility of ethanol molecules increases and destroys the water network built by hydrogen bonds. At very high concentrations of ethanol, the water molecules form clusters which are surrounded by ethanol molecules [187][188]. Cononsolvency is also a reason for lower polymer solubility at high alcohol concentration and the appearance of a UCST [84].

6.3 Synthesis of polystyrene-*block*-poly(oligo ethylene oxide methyl ether methacrylate(s)), via ATRP of OEOMA(s) using PS-Br macroinitiator

6.3.1 Synthesis of polystyrene bromide macroinitiators

In this work, amphiphilic stimuli-responsive block copolymers were synthesized via combination of two different polymerization methods. PS as the hydrophobic major block was synthesized via anionic polymerization. The minor temperature responsive block (POEOMA) was subsequently synthesized via ATRP using the PS block as a macroinitiator. As mentioned in section 5.2, after synthesis of PS via anionic polymerization, it was end-functionalized to PS-Br using α-Bromoisobutyryl bromide (BIBB) or α-Bromoisobutyric acid (BriBA). The procedure to synthesized PS-Br was explained in Fig. 16, Fig. 17 and Fig. 18 (section 5.2.3.1 and 5.2.3.2), and summarized in Fig. 45. A two-step approach to synthesize PS-Br as the macroinitiator for ATRP is beneficial to the direct quenching of the living polystyrene anion with α- bromo acid (BIBB), due to the appearance of a bimodal molecular weight distribution in the latter synthesis route [127]. Moreover, the Steglich esterification can be performed under milder conditions and the reagents are less sensitive to impurities such as water and oxygen [189].

To prepare the PS hydrophobic block as a macroinitiator for ATRP of the POEOMA hydrophilic block, a synthesis route including end functionalization of PS with hydroxyl function followed by Steglich esterification with a bromo functionalized carboxylic acid was applied (Fig. 45, route 1). After full consumption of the styrene monomer in anionic polymerization, an excess of propylene oxide was added to generate an alkoxy anion through nucleophilic attack of the carbanion at the lower substituted carbon of the propylene oxide [190][191]. Successively protonation with acetic acid resulted in a hydroxyl end functionalized PS (PS-OH) which was afterwards converted to a PS-Br macroinitiator for ATRP via Steglich esterification [192]. To stimulate the esterification reaction of PS-OH with BriBA, DCC as coupling reagent and DMAP as the catalyst were used. Due to the higher steric shielding of

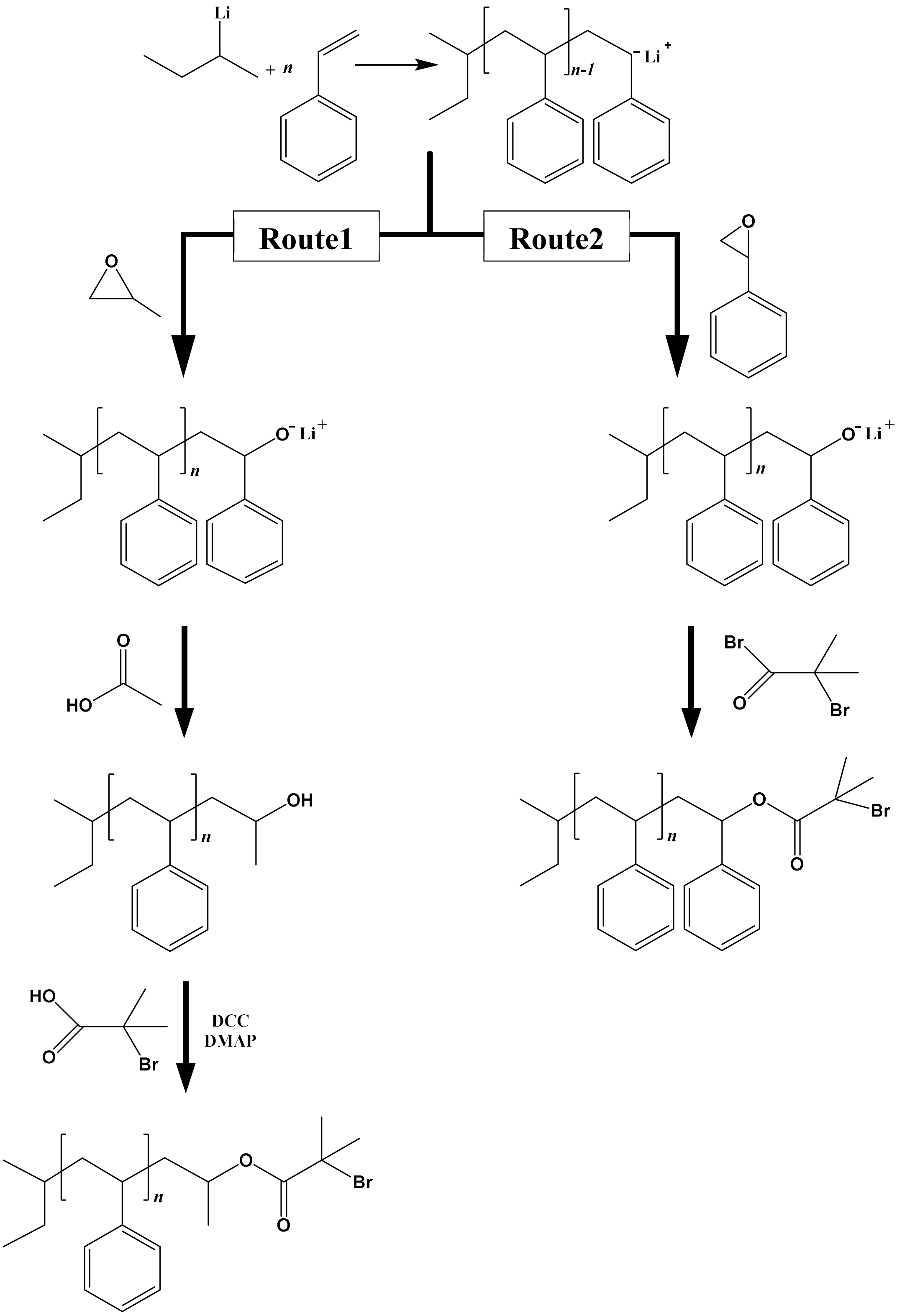

Fig. 45 the summary of synthesis routes for PS-Br synthesis. The first route is via Steglich esterification using PPO and BriBA. The second route uses and SO and BIBB.

the hydroxyl end group, larger polymers with higher molecular weight require a higher excess of acid and coupling reagent to overcome kinetic inhibition [193].

The effective transfer of the hydroxyl group into the ester can be monitored via a downfield shift of the related α-proton as shown in Fig. 46. This proton gives two broad peaks at 3.3 and 3.5 ppm with intensity ratio 1:1 in the case of the alcohol and two peaks at 4.4 and 4.7 ppm with intensity ratios 1:1 for the ester. The appearance of two peaks for both PS-OH and PS-Br is due to the formation of diastereomers during end-functionalization as indicated in Fig. 46.

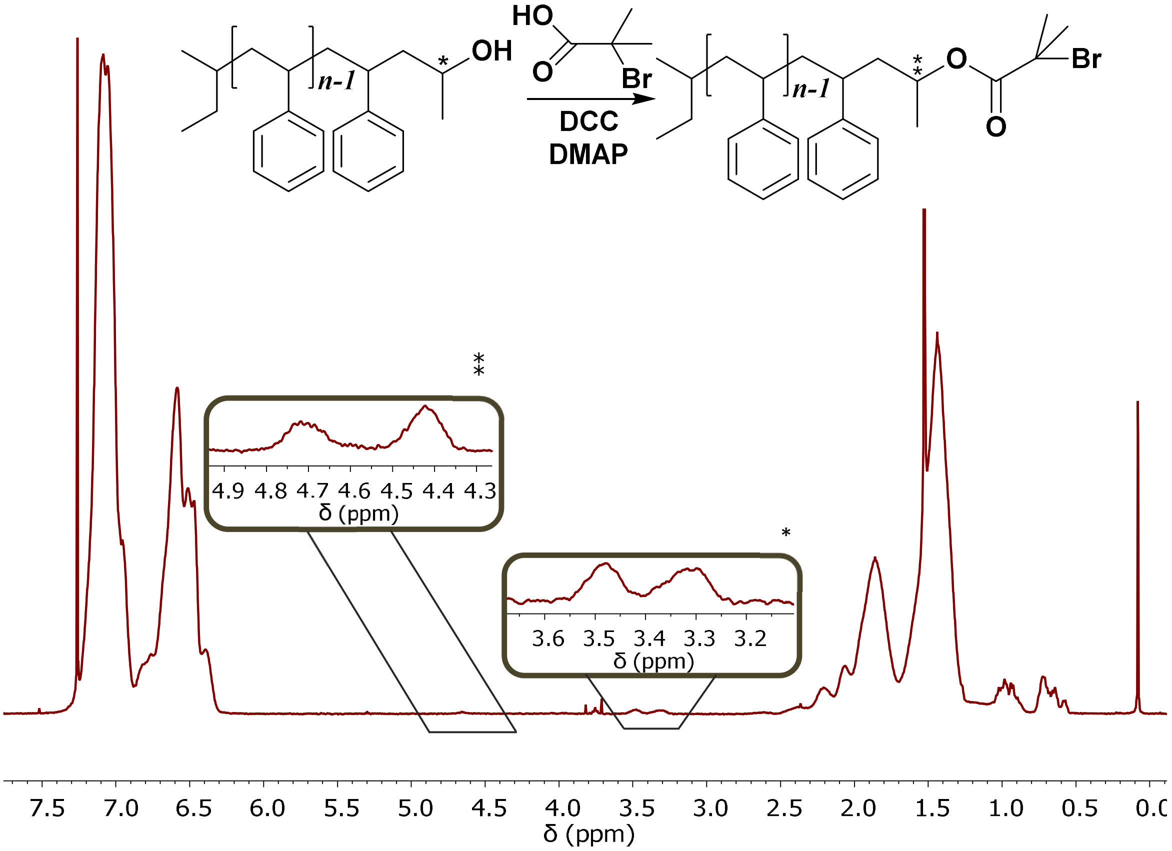

Fig. 46 The synthesis of polystyrene bromide macroinitiator via Steglich esterification; The ^{1}H NMR spectrum of the synthesized PS-OH and the representative peaks of PS-Br. The downfield shift of the α-proton upon esterification is pointed with "*" for PS-OH and with "⁑" for PS-Br.

Consequently, the synthesis of narrowly distributed PS-Br as macroinitiator of ATRP with molecular weights from 20-120 kDa and very low PDI-values (1.012-1.016) was successful. The SEC results of the synthesized macroinitiators presented in Fig. 47 and Table 3 prove the successful polymerization and end-functionalization. The functionalization degree can be determined via ^{1}H NMR spectroscopy by integrating the peaks corresponding to the α-proton of the end-functional group (the region of 3.1-3.7 for PS-OH and 4.3-4.9 for PS-Br) normalized to the 5 protons of the benzyl group of styrene in PS (the region of 6.2-7.4) after subtracting the integration of chloroform peak at 7.26 ppm. The degree of polymerization of PS and the value of the corresponding integration of the protons of the phenyl groups is calculated from SEC results, which are reported in Table 3. All synthesized macroinitiators show a remarkably high degree of functionalization (91-98% of PS).

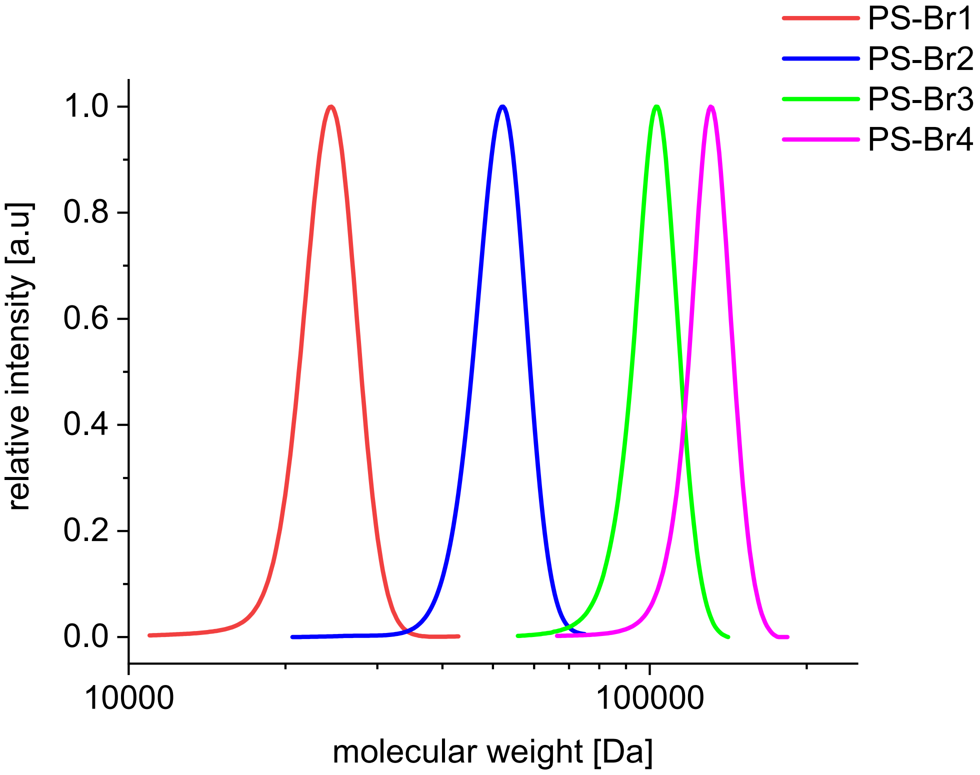

Fig. 47 The SEC graphs of the synthesized PS-Br macroinitiator with molecular weight of around 20000 Da to 120000 Da. The results are summarized in Table 3.

Table 3 The SEC results of the synthesized PS-Br macroinitiators

	M_n [Da]	M_w [Da]	M_w/M_n	functionalization degree (mole % of PS)
PS-Br1	23700	24100	1.014	98
PS-Br2	50500	51300	1.016	94
PS-Br3	100000	101800	1.013	93
PS-Br4	128800	130400	1.012	91

6.3.2 Synthesis of polystyrene-*block*-poly (diethylene oxide methyl ether methacrylate)

PS-*b*-PMEO$_2$MA was synthesized via ATRP of MEO$_2$MA monomer using the bromo-terminated polystyrene as a macroinitiator in the presence of a CuBr/PMDETA catalyst complex at 80˚C (Fig. 48). The experimental procedure and the reaction conditions are explained in section 5.2.3. The main difference between the block copolymerization of POEMAs via ATRP and the homopolymerization is the higher ratio of monomer to initiator, for example 700:1 for ATRP using macroinitiator of 100 kDa molecular weight instead of 200:1 for normal initiator, while aiming similar molecular weight. The reason for this high increase of the monomer is the lower reactivity of the macroinitiator compared to normal initiator due to its high steric shielding which gets more pronounced as the conversion increases and the amount of monomer in the system decreases. With lower ratio of monomer to initiator, the reaction stops at lower conversion and the desired molecular weight is not achieved. The other differences include increasing the ratio of catalyst and ligand to the initiator up to two times the ratio needed for homopolymerization. Since the molecular weight of the macroinitiator is much higher than the normal initiator, same ratio of catalyst and ligand to initiator would result in so small amount that are not physically possible to handle by our experimental devices. Moreover, such less amount of catalyst is easily intoxicated and gets out of the system, leading the reaction to halt or go on with poor control.

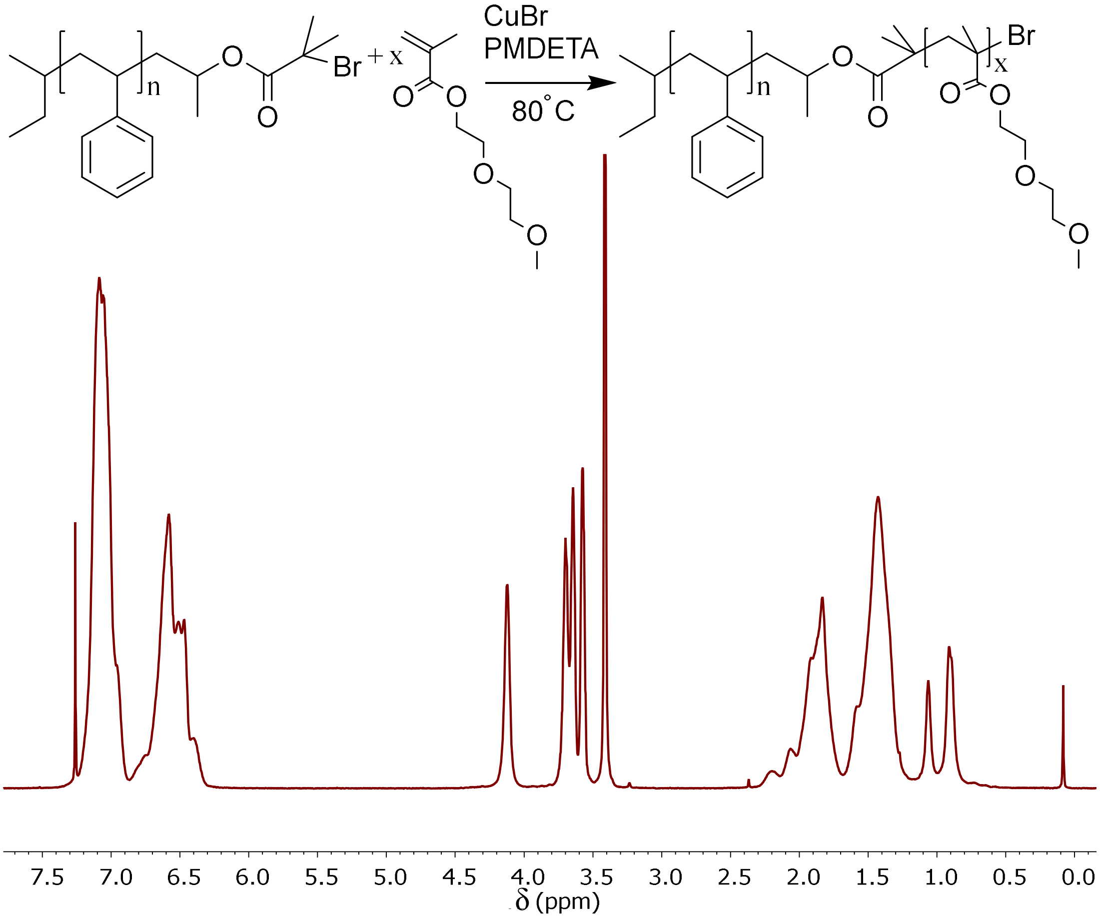

Fig. 48 Synthesis route and the ^{1}H NMR spectrum of PS-*b*-MEO$_2$MA prepared via ATRP using PS-Br as macroinitiator.

Another major difference between using a macroinitiator for block copolymerization and normal ATRP homopolymerization is the solvent. It is obvious that by using macroinitiator the amount of solvent used increases drastically as dissolving the polystyrene macroinitiator needs much more solvent. Furthermore, the solvent itself affects the reaction considerably. Four different solvents are used in this study and their effect on the control over the reaction as well as the reaction progress versus time are studied by ^{1}H NMR spectroscopy. The calculation of the reaction conversion as well as the PMEO$_2$MA's molecular weight via ^{1}H NMR is represented in Fig. 49. Comparing the integral of vinyl protons of the remaining monomers (A & B; 5.45 - 6.12 ppm) to the integration of the region C and Ć (3.9 - 4.4 ppm) which represents the protons next to the ester function of MEO$_2$MA and PMEO$_2$MA respectively, results in polymerization conversion of PMEO$_2$MA via PS-Br as a macroinitiator [158] [159] [194]. The procedure is similar to calculation of POEOMA conversion in ATRP via normal initiator as explained in 6.1.1 and the results are plotted in Fig. 50 and Fig. 51.

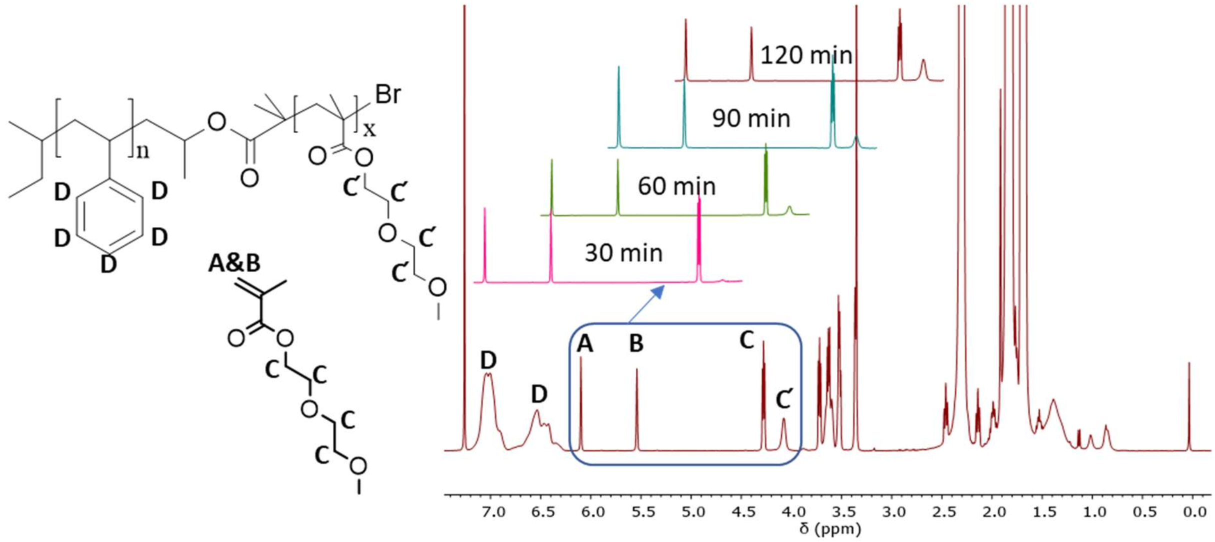

Fig. 49 The change of the NMR spectrum by time during ATRP polymerization of MEO_2MA using PS-Br as a macroinitiator.

The solvents studied in this research include anisole, cyclohexanone, dioxane and a mixture of dioxane and toluene. To analyze the control over reaction in different solvents, the semi-logarithmic plot of monomer conversion i.e. $\ln([M]_0/[M])$ is plotted versus reaction time in Fig. 50 and Fig. 51. The linear part of the semi-logarithmic plots is compared in different reaction systems as a measure of control over reaction. As explained in section 6.1.1, the linearity of $\ln([M]_0/[M])$ versus time indicates that the polymerization rate is proportional to the monomer concentration (first order polymerization with respect to monomer) and the radical concentration is constant during the polymerization, according to eq. (6.1)

$$\frac{R}{[M]} = \frac{1}{t}\ln\left(\frac{[M]_0}{[M]}\right) = k_p K_{eq} \frac{[I]_0[Cu^{I}]}{[Cu^{II}]} = k_{app} \qquad (6.1)$$

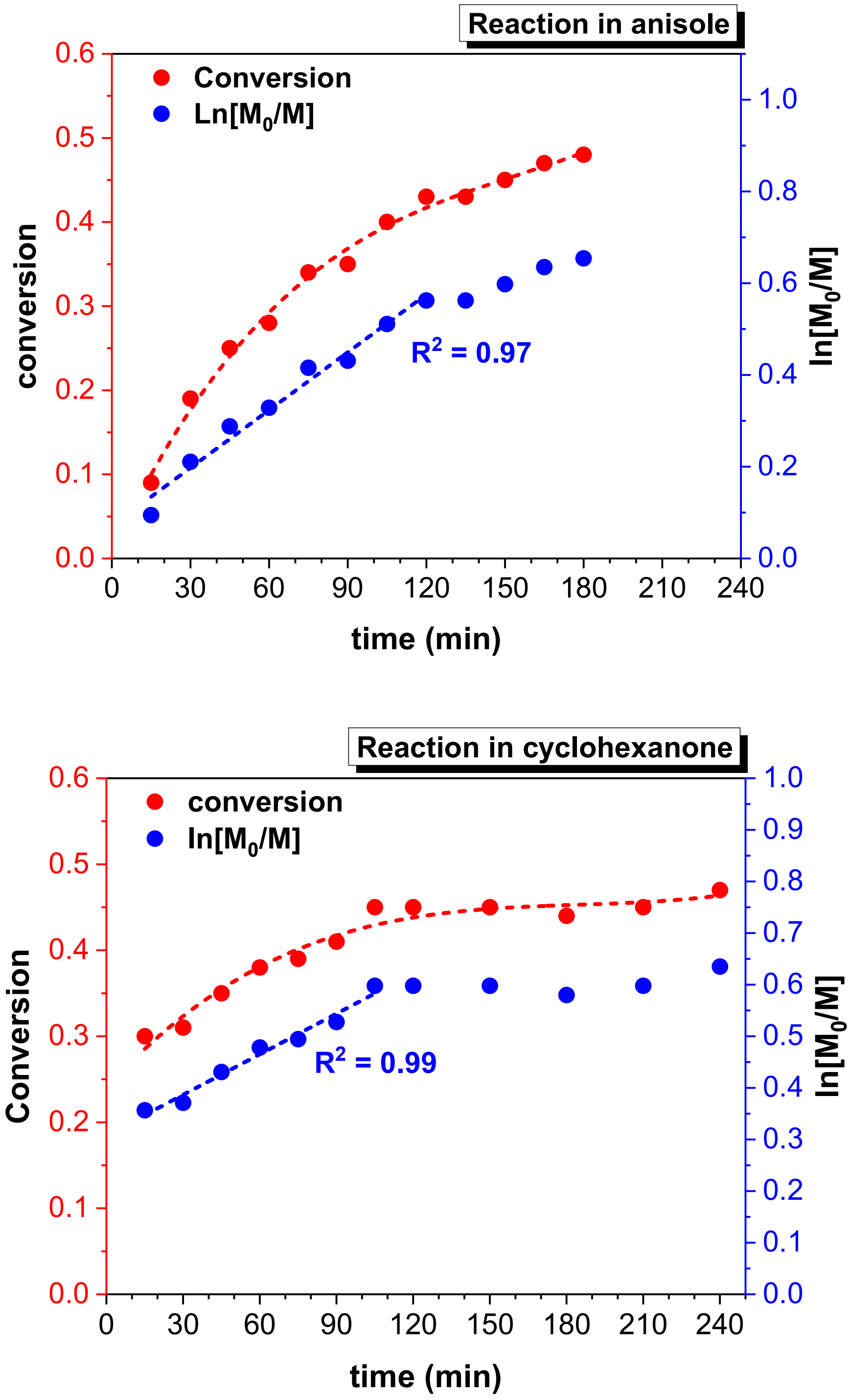

Fig. 50 Comparison of semi-logarithmic plots of monomer conversion vs. time in ATRP of MEO_2MA using PS-Br (M_n = 100 kDa) as a macroinitiator in different solvents. The best control is obsereved for the reaction in a mixture of dioxane and toluene with the volume ratio of 1:3 as solvent, while using pure dioxane as a solvent results in the worsest control.

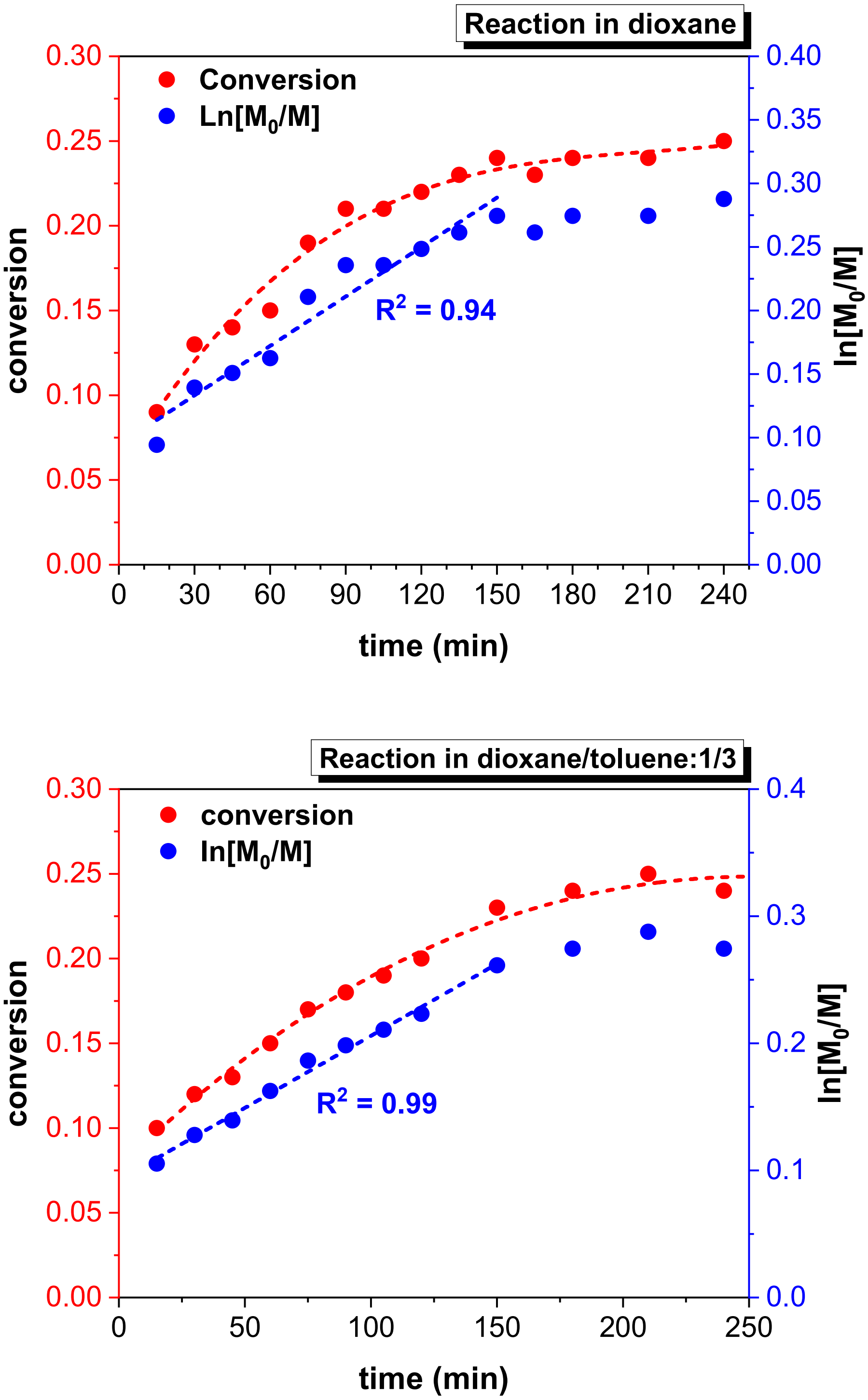

Fig. 51 Comparison of semi-logarithmic plots of monomer conversion vs. time in ATRP of MEO$_2$MA using PS-Br (M_n = 100 kDa) as a macroinitiator in different solvents. The best control is obsereved for the reaction in a mixture of dioxane and toluene with the volume ratio of 1:3 as solvent, while using pure dioxane as a solvent results in the worsest control.

Compared to the synthesis of $PMEO_2MA$ using a simple initiator like α-bromo alkylates [53][194][195], the long chains of high molecular weight PS-Br macroinitiator result in major kinetic inhibition. The growth of radical chains encounters difficulties due to the steric hindrance. In other words, a reduced local monomer concentration around the active chain end due to steric shielding results in chain length dependency of the rate coefficient of chain propagation (k_p) [196]. Therefore, reaction in anisole which has shown very good control in relatively short reaction time for polymerization of MEO_2MA (Fig. 50) using α-bromo alkylates, results in a halt in the growth of molecular weight versus time while using PS-Br as macroinitiator (Fig. 52), as the reaction proceeds very slowly after reaching a certain conversion. The molecular weight of $PMEO_2MA$ was calculated by the ratio of the region of 6.2-7.4 (representing 5 protons of the benzyl group of styrene in PS; D) after subtracting the integration of chloroform peak at 7.26 ppm, to the region of 3.9-4.2 (representing 2 protons in the ethylene oxides in the side chain of $PMEO_2MA$; Ć) (Fig. 49). The diblock copolymer product was precipitated in methanol to remove the remaining monomer, prior to ^1H NMR measurement. The molecular weight of PS was measured by SEC (Fig. 47).

The major role of steric hindrance, in retarding the ATRP polymerization of MEO_2MA using PS-Br macroinitiator can be further proven by addition of ethanol to the reaction solution. Although the ATRP of MEO_2MA in ethanol is very fast due to the higher polarity of solvent that improves the solubility of CuBr catalyst and consequently the redox potential of Cu^I in the system[158] [164] [195], surprisingly the reaction with PS-Br barely proceeds in presence of ethanol. The reason might be the decrease of the solubility of PS-Br macroinitiator in presence of ethanol as a non-solvent for PS.

Considering the solubility of PS-Br macroinitiator to be the cause of hindering the reaction to proceed, toluene as a very good solvent for PS was used. Previous studies show that the synthesis of POEOMAs in toluene is successful and it undergoes a very good control [163][197]. But, in our system the diblock copolymerization does not show any progress in toluene. The reason could be the much lower redox potential of Cu^I catalyst in toluene. Since the concentration of CuBr while using high molecular weight macroinitiator is much lower than in the system using small molecule bromo alkylate initiator, the role of the catalyst solubility and its redox potential gets more emphasized.

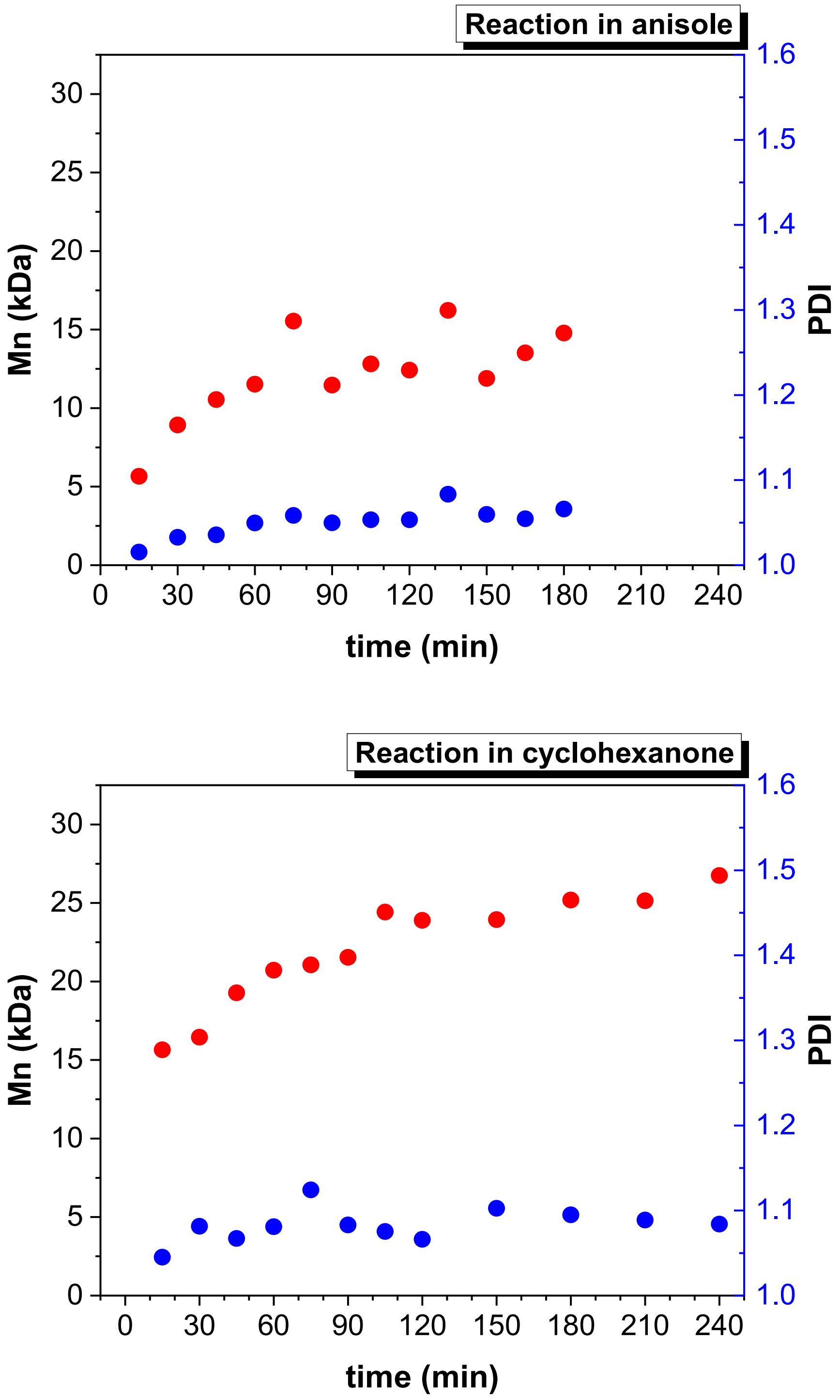

Fig. 52 The increase of the molecular weight versus time during ATRP of MEO_2MA using PS-Br (M_n = 100 kDa) as an initiator in anisole and cyclohexanone as solvents. The desired molecular weight of 25 kDa is not achieved for all the reaction in anisole and for the reaction in cyclohexanone, to reach the desired molecular weight, the reaction should go on to a higher conversion (45 %) which results in lack of control over reaction.

Contemplating the slight success of the diblock copolymerization in anisole, a solvent with similar physical characteristics and compatibility with PS, but with slightly higher polarity could improve the synthesis. Bey *et al.* [192] synthesized Polystyrene-block-poly[methyl methacrylate-random-(1-(2-methyl-15-crown-5)- 1,2,3-triazolyl)methyl methacrylate] (PS-b-P(MMA-r-15C5MA)) with molecular weight around 50 kDa in cyclohexanone. The physical characteristics of cyclohexanone like boiling point and density are similar to anisole, but the value of the normalized empirical parameter of solvent polarity E_T^N is higher (0.198 for anisole and 0.281 for cyclohexanone) [192][198]. As it can be seen in Fig. 51, the reaction proceeds faster in cyclohexanone and is able to reach higher conversion with good control. The results of ^{1}H NMR though, show that for the controlled region of reaction (up to 20% conversion), the achieved molecular weight is lower than theoretical molecular weight calculated from conversion (Fig. 52). There might occur some side reactions producing PMEO$_2$MA homopolymer instead of the diblock copolymer, causing the mismatch of the progress of conversion and molecular weight. Since the homopolymer dissolves in methanol and gets fully separated from the system, it does not appear in the ^{1}H NMR measurement of the diblock product and therefore, the molecular weight calculation via ^{1}H NMR measurement on the diblock products is proven to be accurate.

To solve the problem of PS-Br solubility and the redox potential of the CuBr catalyst, dioxane is used as a solvent for PS-Br and with reasonable polarity for the catalyst to activate (E_T^N= 0.164 [198]). The reaction is able to proceed in dioxane to the desired molecular weight, but the control over the reaction is less than the previous systems as it can be seen from the kinetics studies comparing Fig. 50 and Fig. 51. The semi-logarithmic plot of monomer consumption (ln([M]$_0$/[M])) versus time get further away from a linear graph using dioxane, representing that the polymerization reaction is no longer a first order reaction with respect to monomer (Fig. 53).

To decrease the speed of reaction and improve the control, small amount of toluene is added as a cosolvent. The latter system according to the kinetics, shows very good control over time as well as the possibility to reach the desired molecular weight (Fig. 51 and Fig. 53). Addition of a slight amount of toluene helps the reduction of solvent viscosity and improves the dissolution of the PS-Br macroinitiator [199].

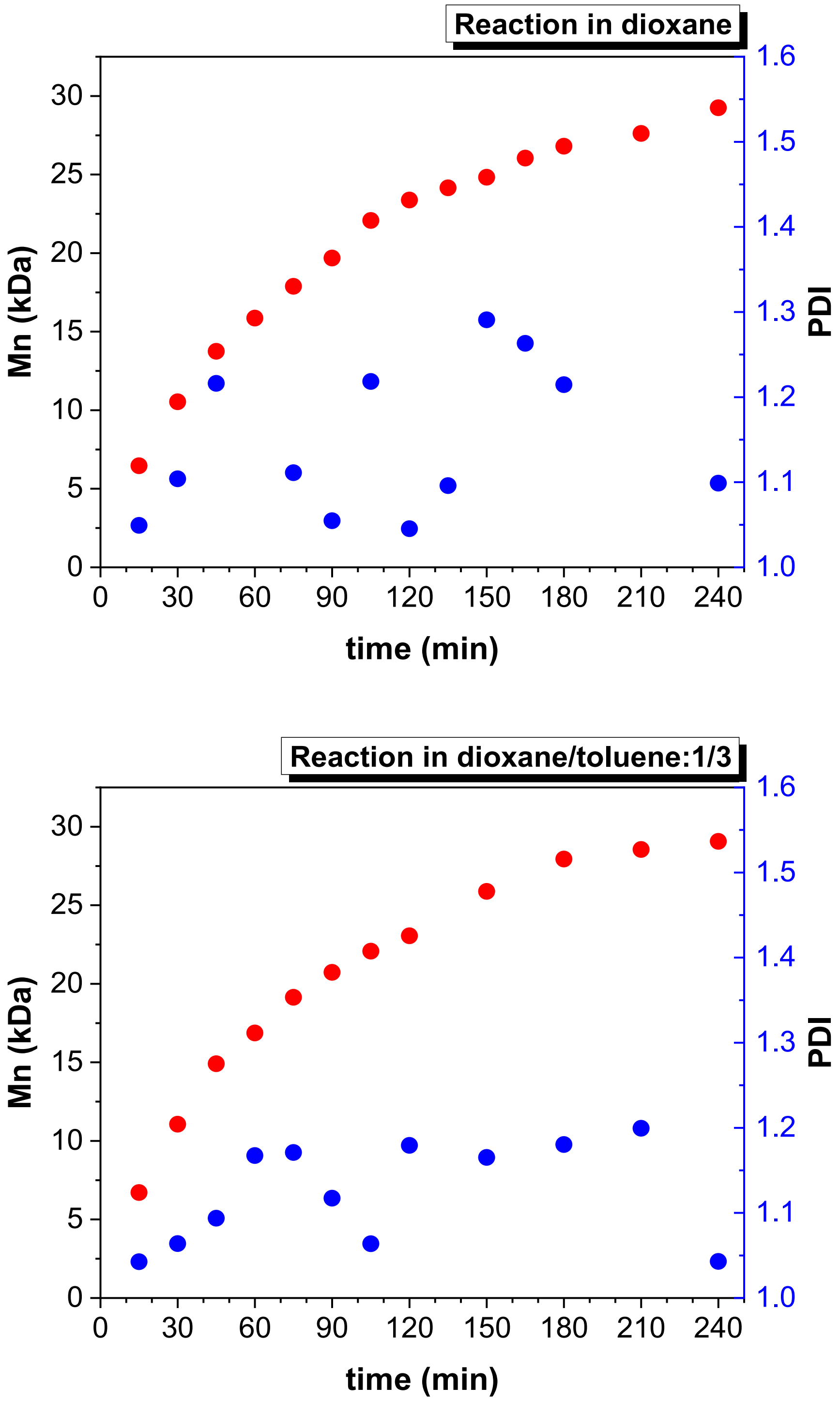

Fig. 53 The increase of the molecular weight versus time during ATRP of MEO_2MA using PS-Br (M_n = 100 kDa) as an initiator in dioxane and dioxane/toluene as solvents. The desired molecular weight of 25 kDa is achieved for both systems.

The shift of SEC traces to lower elution volume proves a successful chain extension of the PS-Br macroinitiator (Fig. 54 and Fig. 55). In all cases, there is a small peak observed at the double molecular weight of the diblocks, which shows a small portion of bimolecular termination. Since the control over reaction is proven to be acceptable and the dispersity index does not increase dramatically (Fig. 52 and Fig. 53), this diminutive portion of bimolecular termination is neglected. Therefore, it can be further proven that the end functionalization of PS is accomplished successfully as well as a successful chain extension of the high molecular weight PS-Br macroinitiator with a PMEO$_2$MA block via a well-controlled ATRP mechanism.

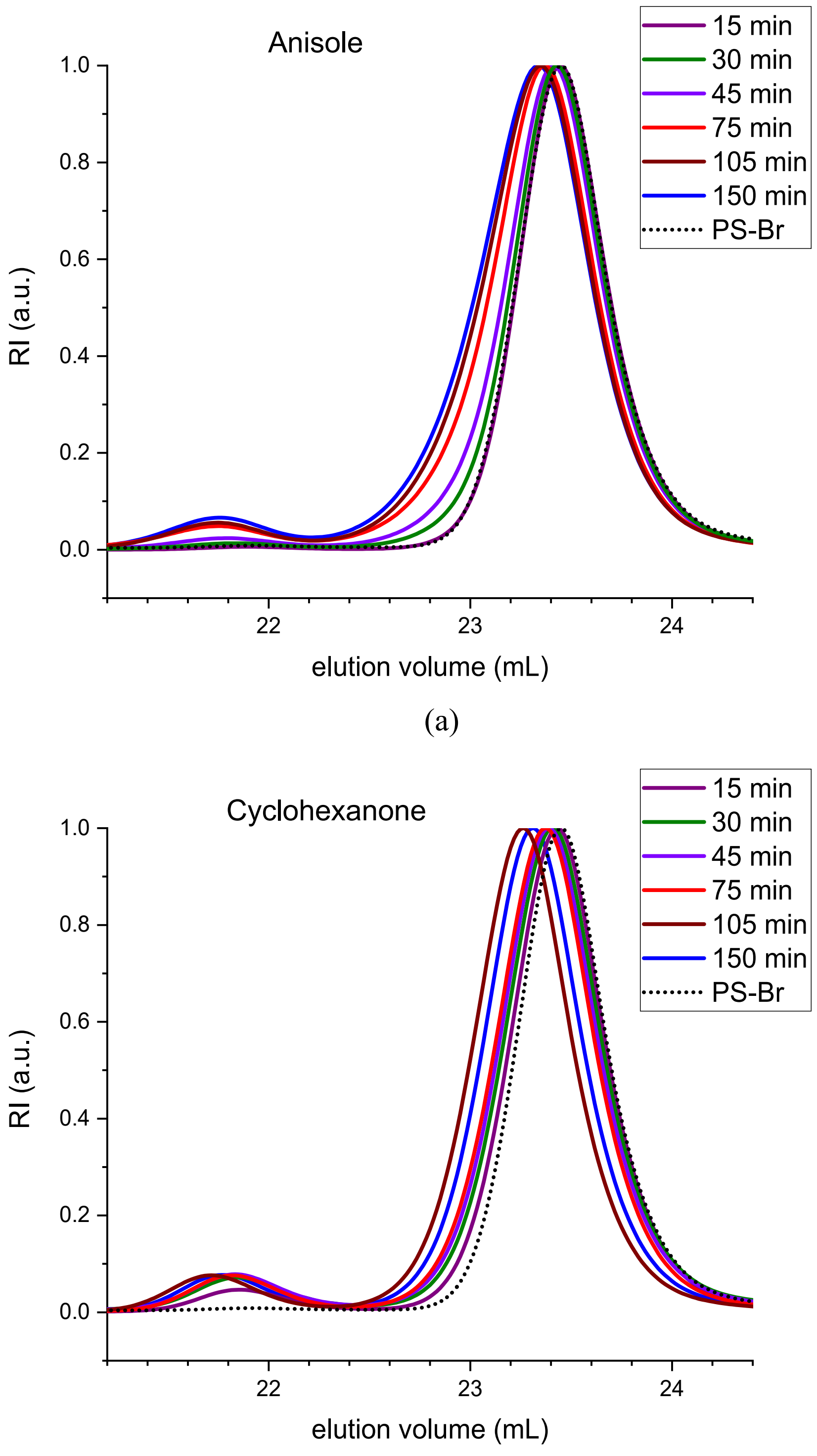

(a)

(b)

Fig. 54 SEC traces of MEO_2MA polymerization in anisole (a) and cyclohexanone (b) as solvents using PS-Br with the molecular weight of 100 kDa as a macroinitiator.

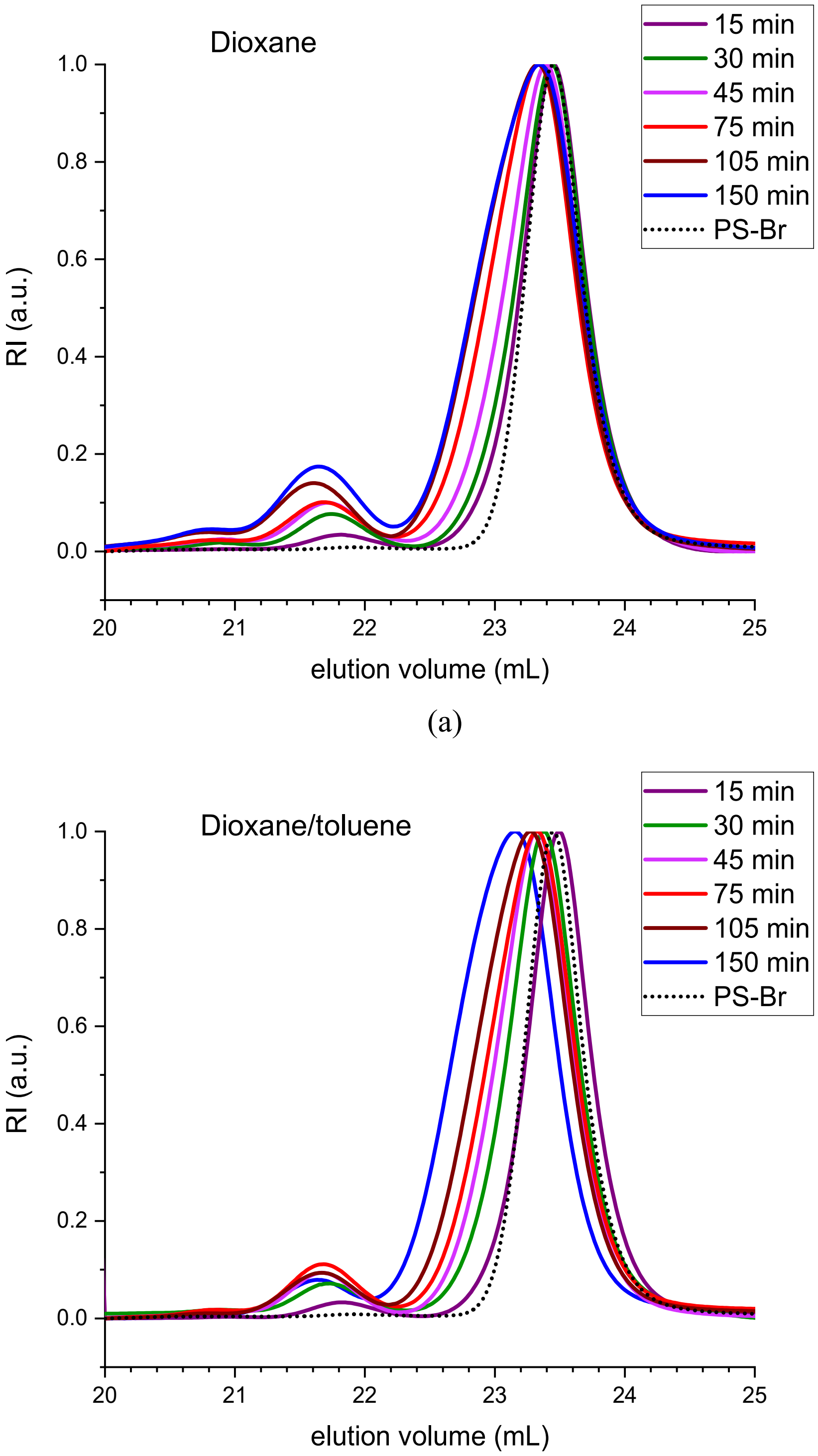

(a)

(b)

Fig. 55 SEC traces of MEO$_2$MA polymerization in dioxane (a) and dioxane/toluene: 3/1 (b) as solvents using PS-Br with the molecular weight of 100 kDa as a macroinitiator.

6.4 Self-assembly of PS-*b*-MEO$_2$MA and PS-*b*-P(MEO$_2$MA-stat-OEOMA) in bulk

To study the morphological properties of PS-*b*-MEO$_2$MA, different diblock copolymers with various composition were synthesized using PS-Br macroinitiators with the molecular weight of 50 or 100 kDa (Table 1, section 6.3.1). Moreover, PS-*b*-P(MEO$_2$MA-*stat*-OEOMA) diblock terpolymers with the MEO$_2$MA: OEOMA molar ratio of 83:17 were synthesized using PS-Br macroinitiators with the molecular weight of 50 or 100 kDa as summarized in Table 4.

Table 4 Specifications of the synthesized diblock copolymers to study the bulk morphology and SNIPS technique for membrane fabrication.

M_n of PS ~ 100 *kDa*	**$M_{n,total}$ (kDa)**	**$M_{n,2nd\ block}$ (kDa)**	**Đ**	**T_g (˚C)***	**χN^{**}**
PS$_{86}$-*b*-P(MEO$_2$MA)$_{14}^{118}$	118	18.0	1.06	101.1	83.4
PS$_{81}$-*b*-P(MEO$_2$MA)$_{19}^{124}$	124	24.2	1.07	101.4	86.0
PS$_{71}$-*b*-P(MEO$_2$MA)$_{29}^{146}$	146	29.0	1.1	98.9	88.0
M_n of PS ~ 50 kDa					
PS$_{84}$-*b*-P(MEO$_2$MA)$_{16}^{64}$	64	16.0	1.06	-	44.6
PS$_{82}$-*b*-P(MEO$_2$MA)$_{18}^{70}$	70	19.9	1.05	99.7	46.2
PS$_{73}$-*b*-P(MEO$_2$MA)$_{27}^{74}$	74	27.3	1.08	96.2	49.3
Second block is a random copolymer					
PS$_{78}$-*b*-P(MEO$_2$MA-*stat*-OEOMA)$_{22}^{134}$	134	34.2	1.06	98.7	86.9
PS$_{79}$-*b*-P(MEO$_2$MA-*stat*-OEOMA)$_{21}^{71}$	71	21.1	1.08	95.9	42.7

[*] Measured via DSC. The DSC graphs will be presented in section 6.4.2.

[**] Determined from the total degree of polymerization (*N*) of the diblock copolymers and the Flory–Huggins-Staverman interaction parameter $\chi_{PS-PMEO_2MA}$= 0.079 (at 25 °C); The calculation of the interaction parameter will be explained in section 6.4.1.

The abbreviated notation PS_x-*b*-$P(MEO_2MA)_y^z$, with x being the weight fraction of the PS block, y being the weight fraction of the $PMEO_2MA$ block and z being the total molecular weight (M_n) of the block copolymer in kDa, is used.

6.4.1 Calculation of the Hansen solubility parameters and interaction parameter

The use of Hansen solubility parameters is quite common in selection of the most compatible solvent to a certain polymer [200]. They are also common tools for studying the miscibility, compatibility, and the phase behaviour of different homopolymer mixtures or different blocks of a copolymer. The basic principle in polymer dissolution is that polymers dissolve better in solvents, which have higher affinities to them. Hansen solubility parameters are defined in order to put numbers in this qualitative idea and make the choice of the right solvent for a certain polymer and in a certain application more quantifiable [200]. To the best of our knowledge, there are no values reported in the literature about the Hansen solubility parameters of either MEO_2MA, OEOMA or their polymers. Therefore, the group contribution method [201][202][203][204] is applied to calculate the Hansen solubility parameters of $PMEO_2MA$ and POEOMA by means of the summation of simple first-order groups' contribution. This calculation is presented in detail in Table 5. The data for the contribution of each structural group in the solubility parameter is taken from the report of Stefanis and Panayiotou [202]. Since POEOMA has more than two ethylene oxide repeating units, its solubility parameters considered to be similar to $PMEO_2MA$.

The calculated solubility parameters for $PMEO_2MA$ are reported in Table 6. The amount of solubility parameters for some of the common solvents are reported as well. The data in Table 6 makes it easier to compare the affinity of different solvents towards the two different blocks (PS and $PMEO_2MA$) and choose a solvent that is the best for dissolving PS-b-$PMEO_2MA$ block copolymers.

To compare the solubility of different solvents for PS or $PMEO_2MA$, beside comparing the solubility parameter of the solvent to the polymer, the interaction parameter between solvent and the polymer can also be calculated to make the comparison more straightforward. The lower, the interaction parameter is, the higher the affinity of the solvent towards the polymer and the better the solubility of that polymer in the solvent. The interaction parameter of the solvent to the polymer were calculated by considering the role of all parts of the solubility parameters (dispersion, δ_D, polarity δ_P, and hydrogen bonding δ_H) [200][205]:

$$\chi_{solvent-polymer} \approx \vartheta_s \frac{(\delta_{D,s}-\delta_{d,p})^2+0.25(\delta_{P,s}-\delta_{P,p})^2+0.25(\delta_{H,s}-\delta_{H,p})^2}{RT} \tag{6.10}$$

$\chi_{solvent-polymer}$ is the interaction parameter between the solvent and the polymer, ϑ_s is the solvent's molar volume, the subscript "*s*" represents the solvent, and the subscript "*p*" represents the polymer. *R* is the gas constant and *T* is the absolute temperature in K.

Table 5 The calculation procedures for Hansen solubility parameter of PMEO$_2$MA

Repeation	Group	Dispersion δ_d	Polarity δ_p	Hydrogen bonding δ_H
2	**-CH$_3$**	−0.9714	−1.6448	−0.7813
3	**-CH$_2$-**	−0.0269	−0.3045	-0.4119
1	**>C<**	1.2686	2.0838	0.0866
1	**-COO-**	0.2039	3.4637	1.1389
2	**-CH$_2$-O-**	0.0310	0.8826	−0.1528
PMEO$_2$MA		16.8	10.5	6.1

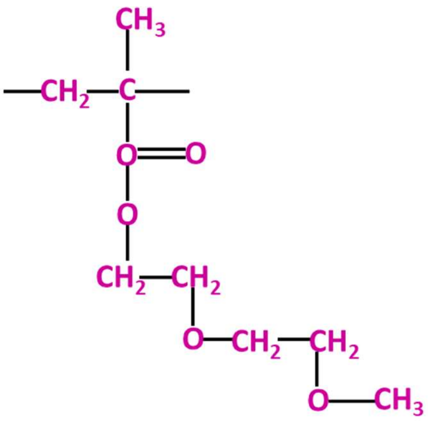

Equation (6.10) considers the role of the substances’ polarity and hydrogen bonding in the interaction parameter and shows the advantage of Hansen solubility parameters to the Hildebrand solubility parameters, which consider only the dispersion between nonpolar materials [200]. The calculated data for the interaction parameter between the common solvents and PS or PMEO$_2$MA are reported in Table 6.

Table 6 Hansen solubility parameters (MPa$^{1/2}$) of PS, PMEO$_2$MA and their common solvents and non solvents.

component	δ_D	δ_P	δ_H	δ	ϑ (cc/mol)	T_b (°C)	$\chi_{\text{Solvent−PS}}$	$\chi_{\text{Solvent−PMEO}_2\text{MA}}$
PS	18.5	4.5	2.9	19.3	99.5	-	-	-
PMEO$_2$MA	16.8	10.5	6.1	20.7	-	-	-	-
Acetone	15.5	10.4	7	19.9	74	56	0.65	0.057
Acetonitrile	15.3	18	6.1	24.4	52.6	82	1.24	0.35
Chloroform	17.8	3.1	5.7	18.9	80.7	61.1	0.096	0.48
Diethyl ether	14.5	2.9	5.1	15.6	104.8	34.6	0.75	0.84
N,N-Dimethyl Acetamide	16.8	11.5	10.2	22.3	92.5	165	1.06	0.17
Dimethyl formamide	17.4	13.7	11.3	24.8	77	153	1.24	0.30
1,4-Dioxane	19	1.8	7.4	20.5	85.7	101	0.25	0.84
Ethanol	15.8	8.8	19.4	26.5	58.5	78.4	1.89	1.08
Ethyl Acetate	15.8	5.3	7.2	18.2	98.5	77.1	0.48	0.32
Pyridine	19	8.8	5.9	21.8	80.9	115.4	0.23	0.18
Sulfolane	20.3	18.2	10.9	29.4	95.7	285	2.55	1.27
Tetrahydrofuran	16.8	5.7	8	19.5	81.7	66	0.22	0.32
Toluene	18	1.4	2	18.2	106.8	110.6	0.12	1.13
Water	15.5	16	42.3	47.8	18	100	3.12	2.45

Solubility parameters of PS and the solvents were taken from Hansen Solubility Parameters' Handbook [200] and the solubility parameters of PMEO$_2$MA was calculated by group contribution method as explained in Table 5.

The comparison of the data in Table 6 proves THF, chloroform and pyridine to be relatively good solvent for both PS and PMEO$_2$MA. Among these solvents, THF is used to dissolve the diblock copolymers for film preparation, since it has good solubility for both blocks, and furthermore, it has lower boiling point and molar volume as well as lower price compared to pyridine and dioxane.

The concepts of solubility parameters have been developed further, not just predicting solubility, which requires high affinity between solvent and solute, but to predict affinities between different polymers leading to compatibility of polymers, and affinities to surfaces to improve dispersion and adhesion [200]. Therefore, the solubility parameters are applied as a tool, using well-defined liquids as energy probes, to measure the similarity, or lack of the same, of key components. Materials that have widely different chemical structure can be very close in affinities.

From the calculated solubility parameters in Table 5, the polymer-polymer interaction parameter (χ) between PS and PMEO$_2$MA can be determined according to the regular solution theory [206][207]:

$$\chi_{A-B} \approx \vartheta_{ref} \frac{[\delta_A^2+\delta_B^2-2\delta_A\delta_B]}{RT} = \frac{\vartheta_{ref}(\delta_A-\delta_B)^2}{RT} \tag{6.11}$$

in which χ_{A-B} is the polymer-polymer interaction parameter between polymer A and B, ϑ_{ref} is the reference molar volume (which is generally the geometric mean of the polymer segment volumes), δ_A and δ_B are the Hansen solubility parameters of polymer A and B respectively, R is the gas constant and T is the absolute temperature in K. The entropic contribution is neglected here as generally for polymer-polymer interaction, the entropic contribution is very low (in the range of 10^{-6}-10^{-2}) and smaller in magnitude than the enthalpic contribution given in the right hand side of equation (6.11). Therefore:

$$\chi_{PS-PMEO_2MA} = \frac{\vartheta_{PS}\left(\delta_{PS}-\delta_{PMEO_2MA}\right)^2}{RT} = \frac{99.5(19.3-20.7)^2}{8.314\times298.15} = 0.079 \tag{6.12}$$

The molar volume of PS is used as a reference volume here instead of the geometric mean of PS and PMEO$_2$MA's segment volumes. since the density of PMEO$_2$MA and P(MEO$_2$MA-stat-OEOMA) are not known, assuming the density of PMEO$_2$MA and P(MEO$_2$MA-stat-OEOMA) to be close to the density of the PS block (ρ =1.05 g/cm^3), the geometric mean should not differ too much from the molar volume of PS.

6.4.2 Investigation of PS-*b*-MEO$_2$MA and PS-*b*-P(MEO$_2$MA-*stat*-OEOMA)'s self-assembly in bulk

To study the miscibility or microphase separation of hydrophobic PS with hydrophilic PMEO$_2$MA or P(MEO$_2$MA-*stat*-OEOMA), DSC measurements are performed on different synthesized block copolymers. The results are presented in Fig. 56. Evaluation of the thermographs in Fig. 56 reveals single glass transition behaviour of polystyrene. Since the polymers have amorphous structure, the glass transition is the only occurrence detected in the thermogram. The experimental values of the glass transition temperature (T$_g$) are included in Table 4, at the introduction of section 6.4.

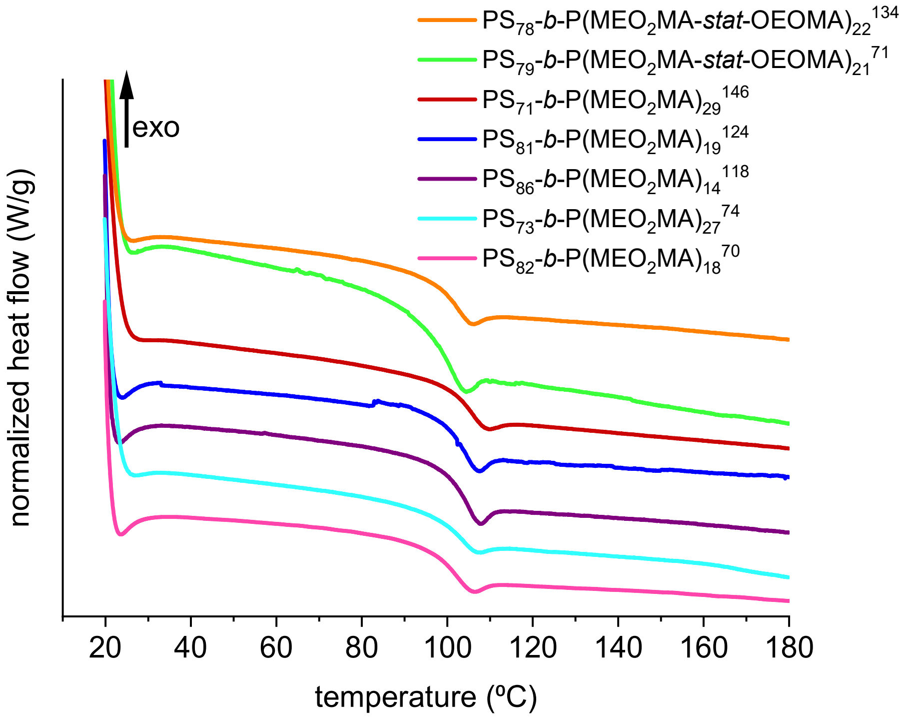

Fig. 56 The DSC results of various PS-*b*-PMEO$_2$MA and PS-b-P(MEO$_2$MA-*stat*-OEOMA) block copolymers with different block ratio and molecular weight.

The glass transition temperature (T_g) of POEOMAs is around -44.8˚C when the M_n is 25 kDa and it decreases as the molecular weight increases [66]. The low value of T_g is most likely due to an increase in mobility of the methacrylate backbone promoted by the flexible two ethylene glycol units of the side chains. Therefore, the T_g of PMEO$_2$MA is out of our measurement range. It is the same for P(MEO$_2$MA-*stat*-OEOMA), since increasing the amount of ethylene oxide in the side chain decreases the T_g even more [52][66]. However, the phase separation observed in bulk (as it will be discussed later) shows that in the melt, the polystyrene block and PMEO$_2$MA/ P(MEO$_2$MA-*stat*-OEOMA) block are not soluble at the temperature range above the room temperature and appear as two distinguishingly separated phases [208]–[210]. This can also be proven by the solubility differences of PS and PMEO$_2$MA (Table 6, section 6.4.1) and the positive value of χ parameter. Moreover, the χN values in Table 4 (at the introduction of section 6.4) indicate that the diblock copolymers lie in the strong segregation regime, since $\chi N \gg 10$ [134].

The glass transition is not changing much with molecular weight, but it becomes more distinguishable (deeper transition) by decreasing the weight ratio of the second block. Moreover, addition of OEOMA units in the second block obviously decreases T_g, while making the glass transition region broader. Such behaviour is attributed to the increase of ethylene oxide units in the side chains which improves the mobility of methacrylate backbone [66] [211].

To investigate the microphase separation of the synthesized Block copolymers (Table 4 at the introduction of section 6.4), thick films with the thickness around 1 mm were prepared via slow solvent evaporation from THF solution. The choice of THF is as explained in section 6.4.1 due to its Hansen solubility parameters which results in THF being a common solvent for both blocks of the diblock copolymers. Furthermore, it's lower price, molar volume and boiling point compared to other optional solvents, favours the choice of THF for film preparation.

The films cast from THF solution of the eight block copolymers reported in Table 4 were explored in terms of their bulk morphologies using AFM and SAXS measurement. AFM of the surface of the cast films helped observing the morphological structure at the interface with air. Moreover, the films were analysed with SAXS which evaluates the characteristic peak positioning of Bragg reflections (depending on the structure factor). Hence, the morphologies (BCC/FCC spheres, hexagonally packed cylinders, or lamellae) of the self-assembled bulk structure can be revealed [212].

The AFM height and phase images of PS-*b*-$PMEO_2MA$ diblock copolymers are plotted in Fig. 57 - Fig. 59. The harder part (brighter area) corresponds to the PS and the softer part (darker area) $PMEO_2MA$. As seen from height images, all films are rather smooth. As $PMEO_2MA$ is considered to be the first block to segregate from solution due to its les solubility in THF, its fraction in the diblock copolymer determines the overall morphology.

The AFM results for the first three PS-*b*-MEO_2MA block copolymers with a PS-Br macroinitiator of 100 kDa molecular weight in Fig. 57 shows that all three samples present hexagonally packed cylinders of $PMEO_2MA$ in PS matrix as indicated by hexagonal pattern of the cylindrical domains in some areas and lying cylinders in other areas of the AFM images. Among these three samples, PS_{86}-*b*-$P(MEO_2MA)_{14}^{118}$ shows a structure consisting of more lying cylinders with very few standing cylinders which appear as small dots in the image. While PS_{81}-*b*-$P(MEO_2MA)_{19}^{124}$ and PS_{71}-*b*-$P(MEO_2MA)_{29}^{146}$ with longer $PMEO_2MA$ show perfectly standing cylinders perpendicular to the surface. The perpendicular orientation of the microstructure for higher ratio of $PMEO_2MA$ in the block copolymer could be attributed to the interaction with solvent. Although, THF is considered to be a good solvent for both PS and MEO_2MA, It is slightly more selective towards PS as can be concluded from the solubility parameters presented in Table 5. Similar behaviour is stated in the reports of Sakurai *et al.* [213]–[220] and Cui *et al.* [221][222]. In these studies, perpendicularly oriented hexagonally packed cylinders in block copolymers' thick films is considered to be a result of the solvent's partial selectivity for the major block. The mechanism is explained as the formation of morphological transition from spheres to cylinders as a result of directional coalescence of spheres normal to the film sample. The direction of the cylinder orientation is guided by the direction of the solvent evaporation which is referred to as an effect of a chemical potential gradient induced by solvent evaporation [213]. The spherical morphology at the start is considered to be the result of non-equilibrium microdomains formed due to the selectivity of the solvent and vitrification of glassy PS microdomain during the solvent evaporation at room temperature. Thermal annealing of the thick film above the glass transition temperatures of both blocks of the copolymer then stimulates the coalescence of non-equilibrium spheres and the block copolymer retrieved its equilibrium domain structures [214][215]. Although the work of Sakurai *et al.* [213]–[220] shows similarity to our work in showing perpendicular orientation in microstructure of block copolymers in thick film, but in our case, the perpendicular structure

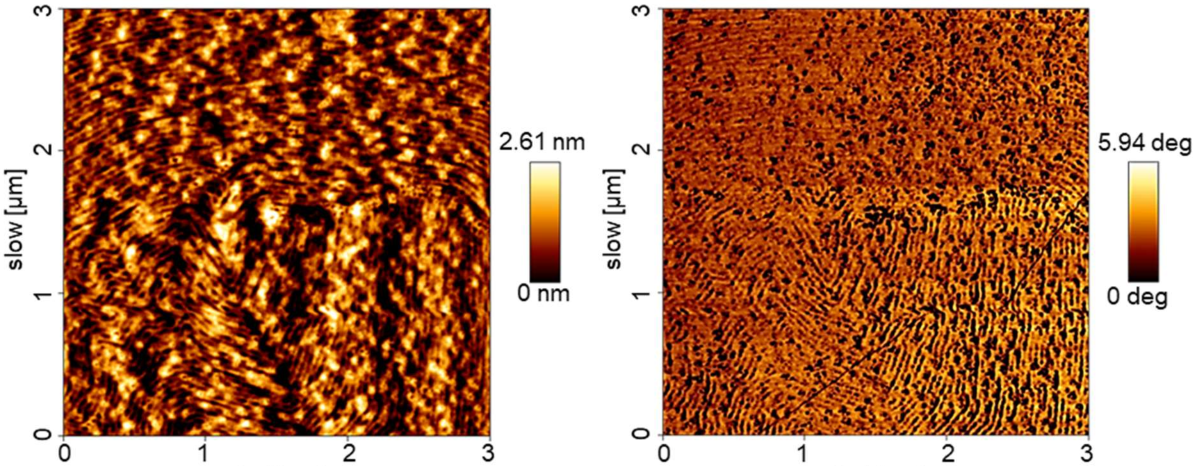

PS$_{86}$-*b*-P(MEO$_2$MA)$_{14}$^{118}

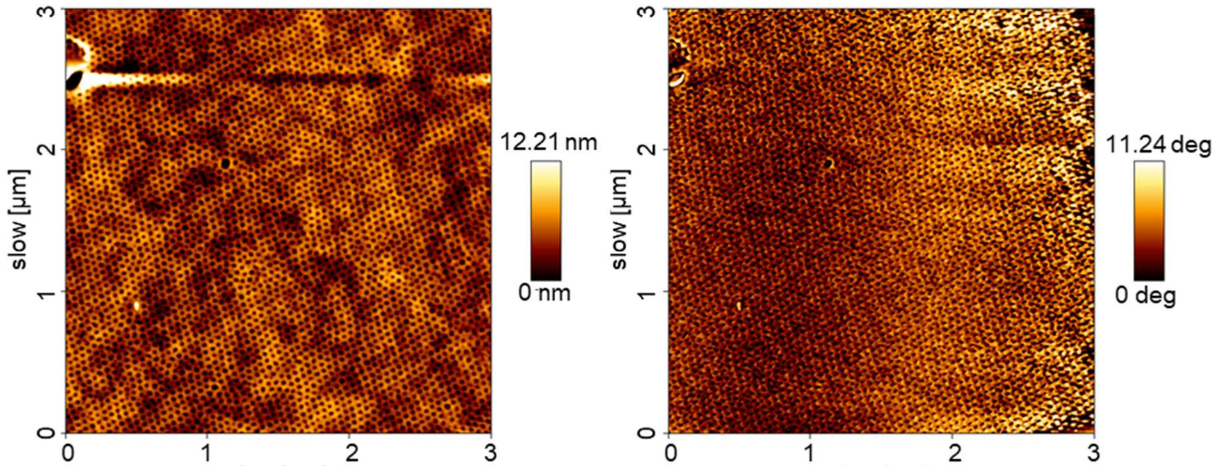

PS$_{81}$-*b*-P(MEO$_2$MA)$_{19}$^{124}

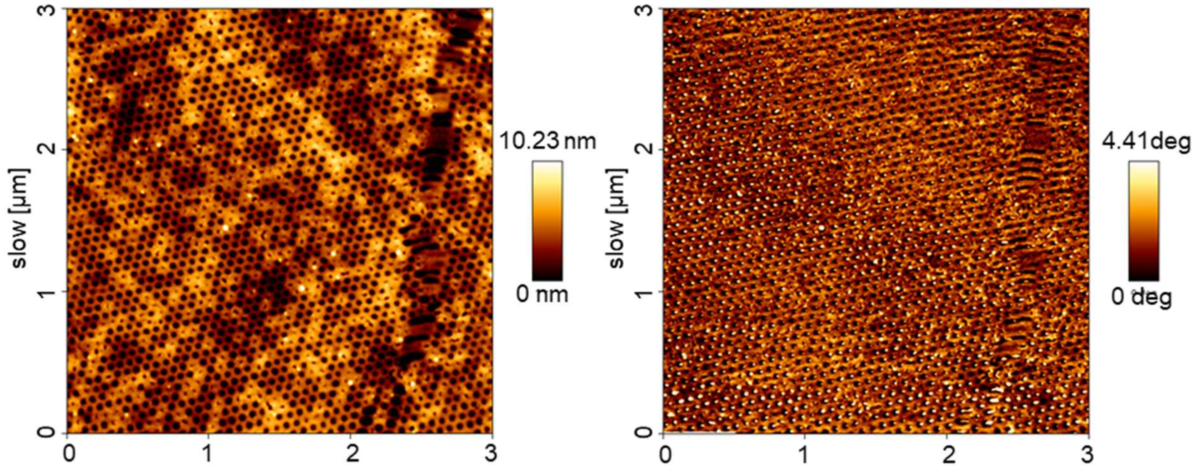

PS$_{71}$-*b*-P(MEO$_2$MA)$_{29}$^{146}

Fig. 57 AFM surface images of the films of PS-*b*-PMEO$_2$MA with PS molecular weight of 100 kDa; The left side is height image and the right side is the phase image.

appears without any further thermal annealing and thus is just the result of solvent evaporation and chemical potential gradient. The appearance of perpendicularly oriented cylinders without thermal annealing also proves that the equilibrium structure in bulk is indeed cylindrical and no non-equilibrium spherical structure is formed.

The zoomed-in images in Fig. 58 show that the arrangement of the cylinders is more uniform, and the phase separation is more pronounced for PS_{71}-*b*-$P(MEO_2MA)_{29}^{146}$ than PS_{81}-*b*-$P(MEO_2MA)_{19}^{124}$. It is also clear that the cylinders' dimensions increase as the composition of $PMEO_2MA$ in the diblock copolymer increases. The average diameter of the cylinder from the AFM image is around 20 nm for PS_{81}-*b*-$P(MEO_2MA)_{19}^{124}$ and 30 nm for PS_{71}-*b*-$P(MEO_2MA)_{29}^{146}$. The distance between the walls of two neighbouring cylinders (as marked by arrows in Fig. 58 is around 40 nm in both PS_{81}-*b*-$P(MEO_2MA)_{19}^{124}$ and PS_{71}-*b*-$P(MEO_2MA)_{29}^{146}$ which is four times the size of PS's radius of gyration according to [193]:

$$R_g = \sqrt{\frac{C_\infty . N . l^2}{6}} = \sqrt{\frac{10 \times \frac{100000}{104.15} \times 0.25^2}{6}} = 10.0\, nm \tag{6.13}$$

Where R_g is the radius of gyration, the value of C_∞ for polystyrene is 10 , N is the degree of polymerization as $\frac{M_n}{M_{styrene}}$ and l is the contribution of one monomer repeating unit of 0.252 nm [193].

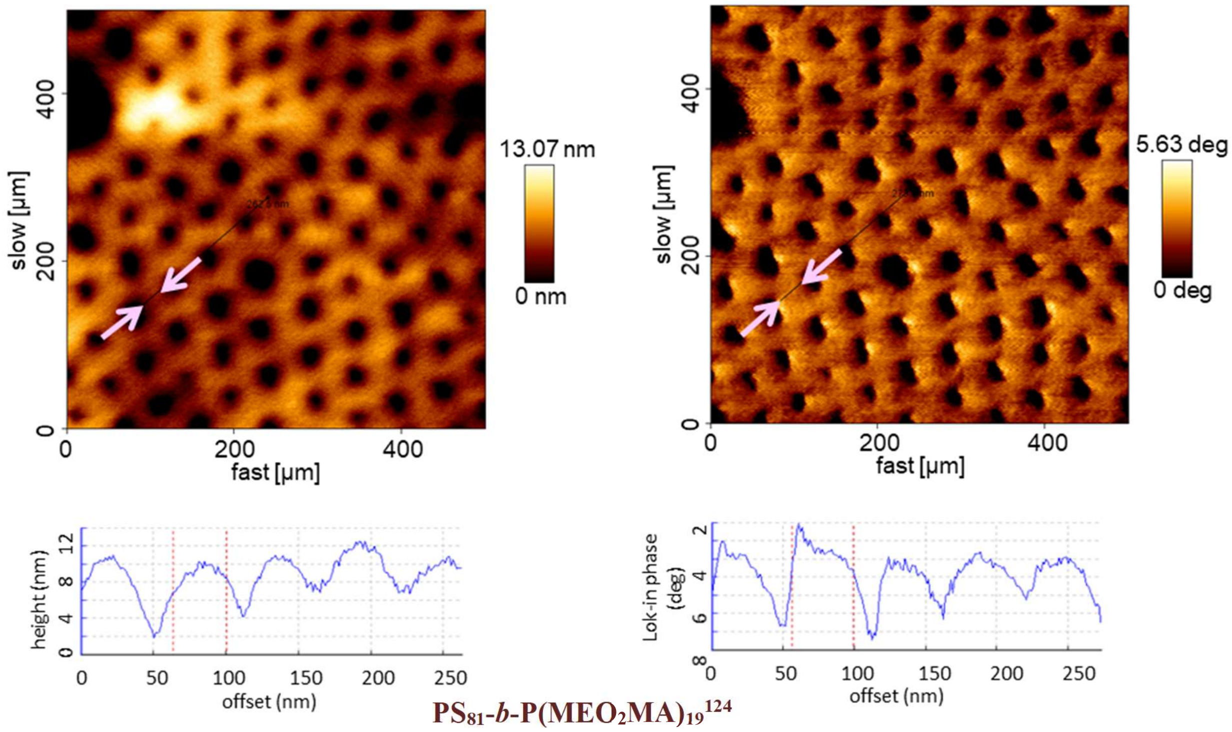

PS_{81}-*b*-$P(MEO_2MA)_{19}$[124]

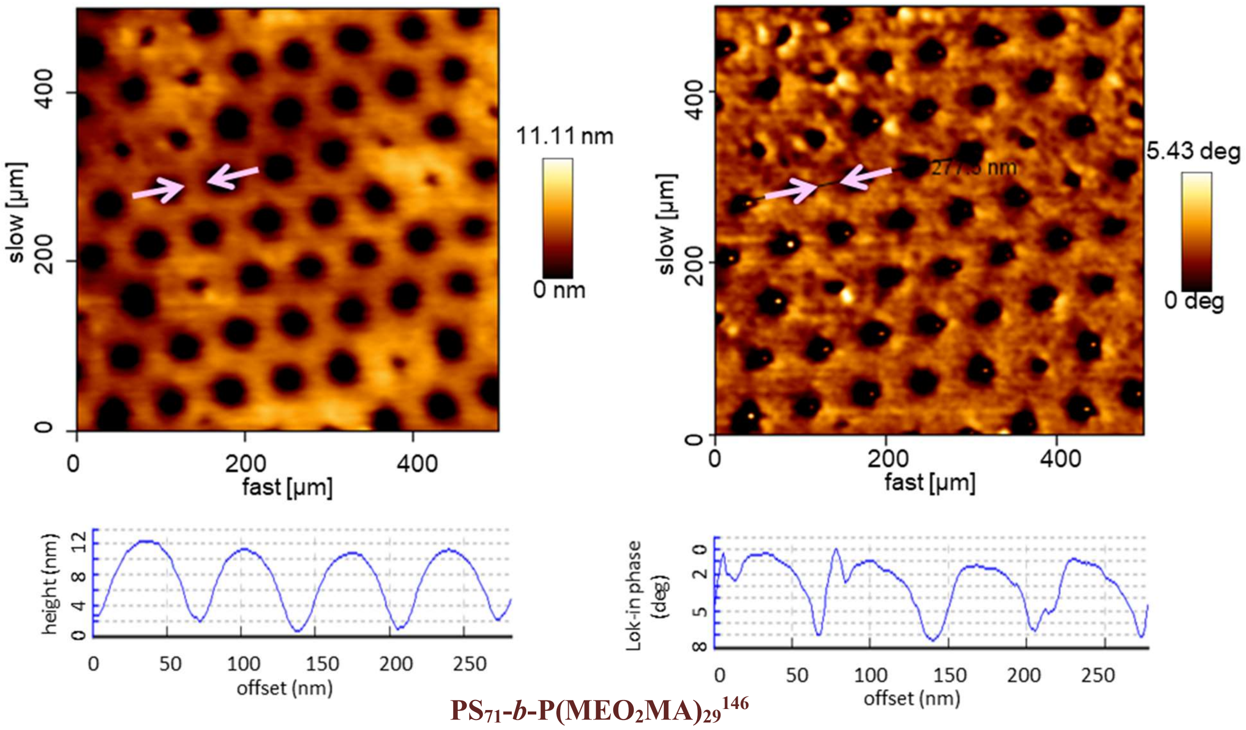

PS_{71}-*b*-$P(MEO_2MA)_{29}$[146]

Fig. 58 The magnified view of the AFM surface height images of the PS-*b*-$PMEO_2MA$ films with PS molecular weight of 100kDa; The left-hand side: the height images of and of PS_{71}-*b*-$P(MEO_2MA)_{29}$[146] polymer films and the right-hand side: the phase images. The arrows in the image show the distance between the walls of two neighbouring cylinders which four times the size of PS's radius of gyration.

To study the relevance of the lateral orientation of the cylinders with the surface energy of PS and PMEO$_2$MA's, thick films of PS-*b*-PMEO$_2$MA with lower molecular weight (half the molecular weight of the previous samples) were prepared under exactly same conditions. The diblock copolymers with smaller molecular weights but similar diblock composition show hexagonally packed cylinders as well (Fig. 59). Different from their higher molecular weight analogues, these copolymers all show only lying cylinders regardless of the diblock composition. The reason might be the lower molecular weight, which makes the entanglement and vitrification of structure in perpendicular orientation more difficult. In other words, the lower molecular weight block copolymers have slightly more freedom in movement due to less entanglement of their chains and therefore can easier arrange themselves lateral to the surface to reduce the surface tension. This proves that the perpendicular structure in high molecular weight PS-*b*-PMEO$_2$MA cannot be attributed to the equality of PS and PMEOMA's surface energy, as the surface energy is not dependant on the molecular weight.

As mentioned before, only the high molecular weight systems show perpendicular alignment. Thermodynamically, lying cylinders with parallel alignment to the surface would be favored, as the diblock copolymers with lower molecular weight indicate. Therefore, it can be concluded that the standing cylinder with the perpendicular alignment to the surface, are in non-equilibrium state. The perpendicular alignment in the non-equilibrium system can be attributed to the solvent gradient and the chemical potential gradient due to solvent evaporation.

The hexagonally packed structure is further proven by SAXS measurement results in Fig. 60-Fig. 61, as all PS-*b*-P(MEO$_2$MA) diblock copolymers show the characteristic peaks of hexagonally packed cylinder structure at q/q^*: 1, $\sqrt{3}$, $\sqrt{4}$, $\sqrt{7}$, $\sqrt{9}$, $\sqrt{12}$, [223]. Multiple Bragg reflections in SAXS measurements indicate a very distinct and long-ranged degree of ordering in the bulk structure of the synthesized block copolymers. Furthermore, it is clear from the AFM images as well as the SAXS results, that the diblock copolymers with shorter chain lengths present lower domain spacing.

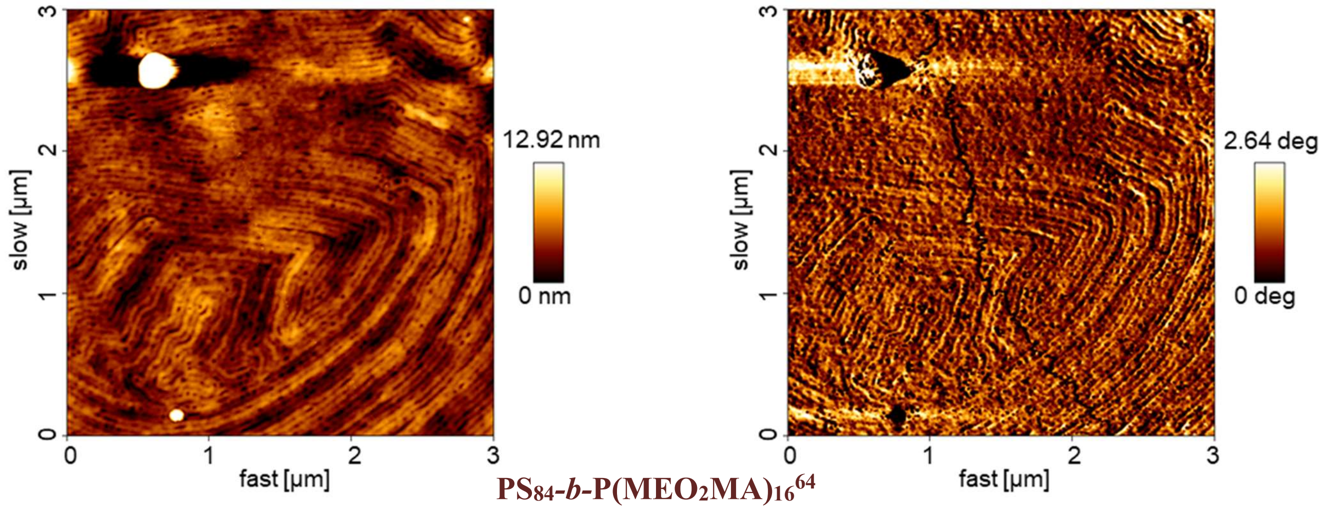

PS$_{84}$-*b*-P(MEO$_2$MA)$_{16}$[64]

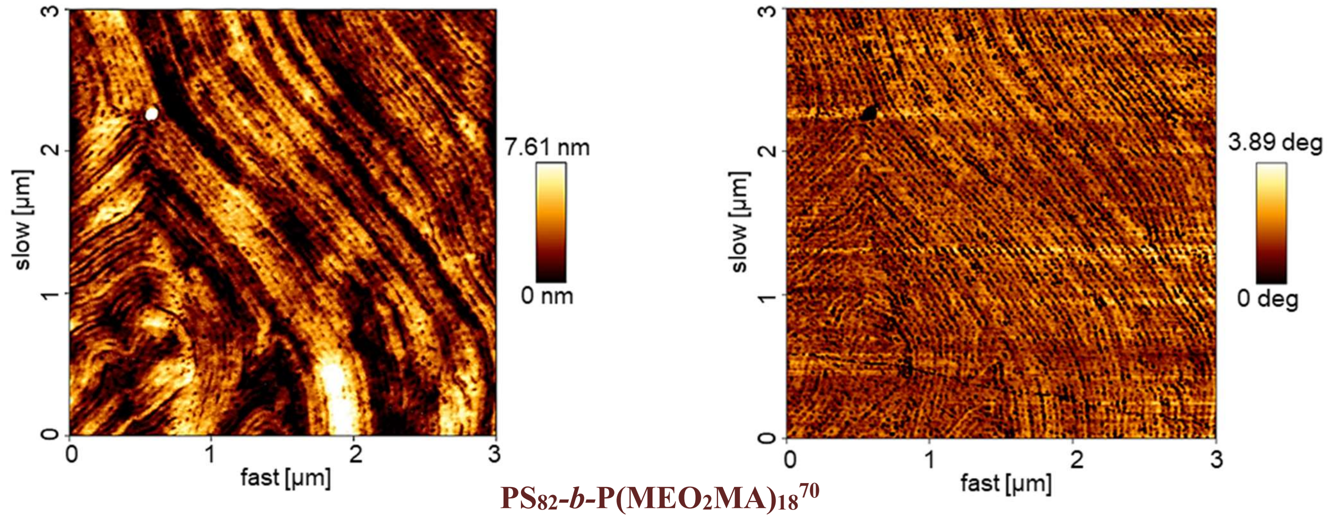

PS$_{82}$-*b*-P(MEO$_2$MA)$_{18}$[70]

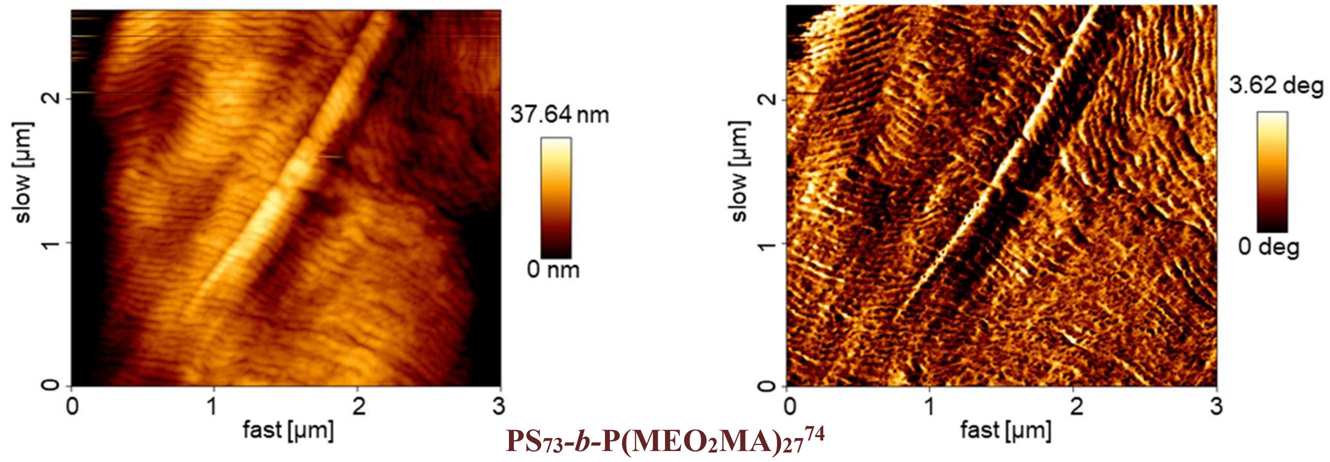

PS$_{73}$-*b*-P(MEO$_2$MA)$_{27}$[74]

Fig. 59 AFM surface images of the films of PS-*b*-PMEO$_2$MA with PS molecular weight of 50 kDa; Left - height image, Right - phase image.

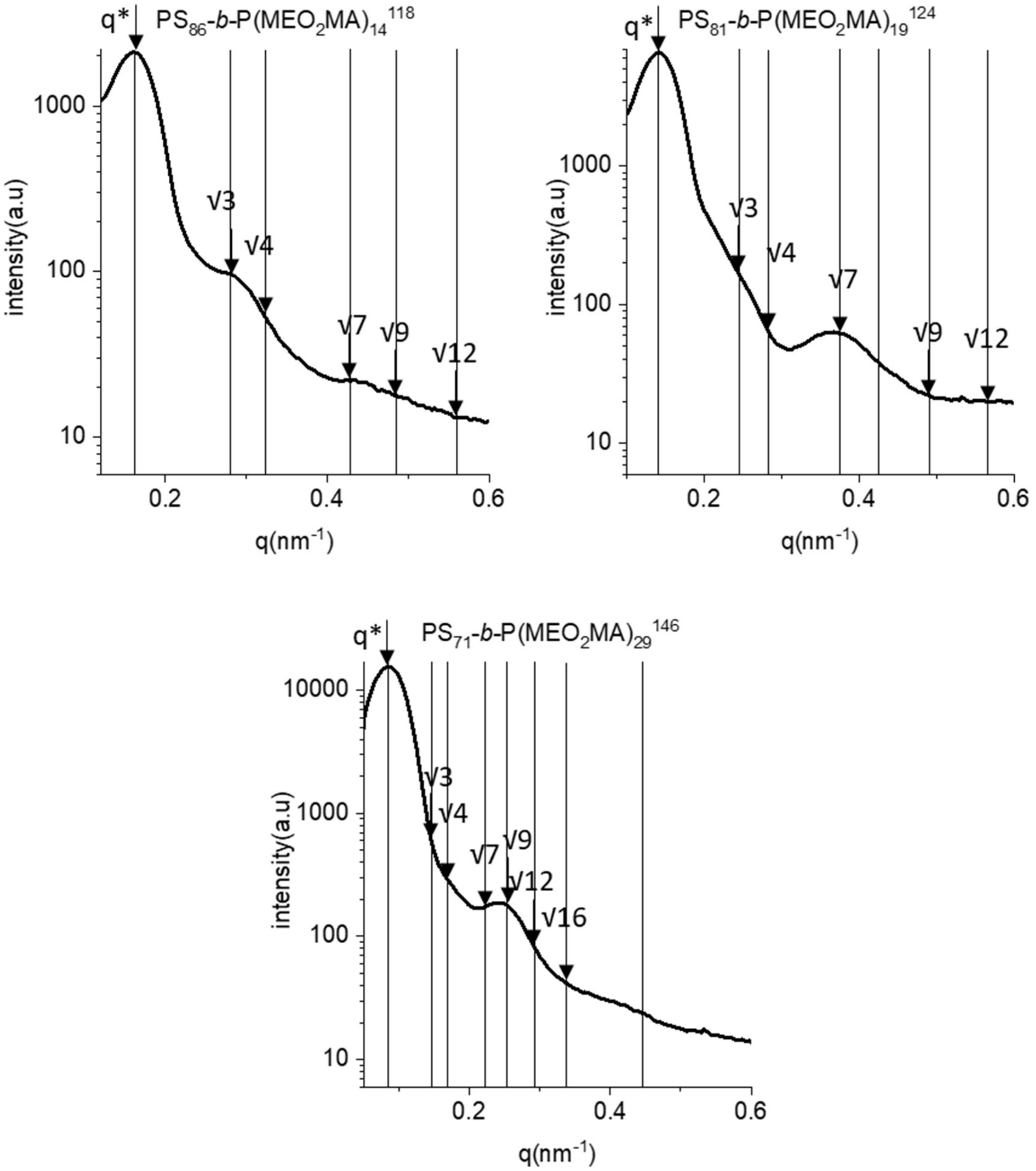

Fig. 60 The results of SAX measurement for PS-*b*-PMEO$_2$MA with PS molecular weight of 100 kDa and various diblock composition, that is mentioned in the legend of each graph.

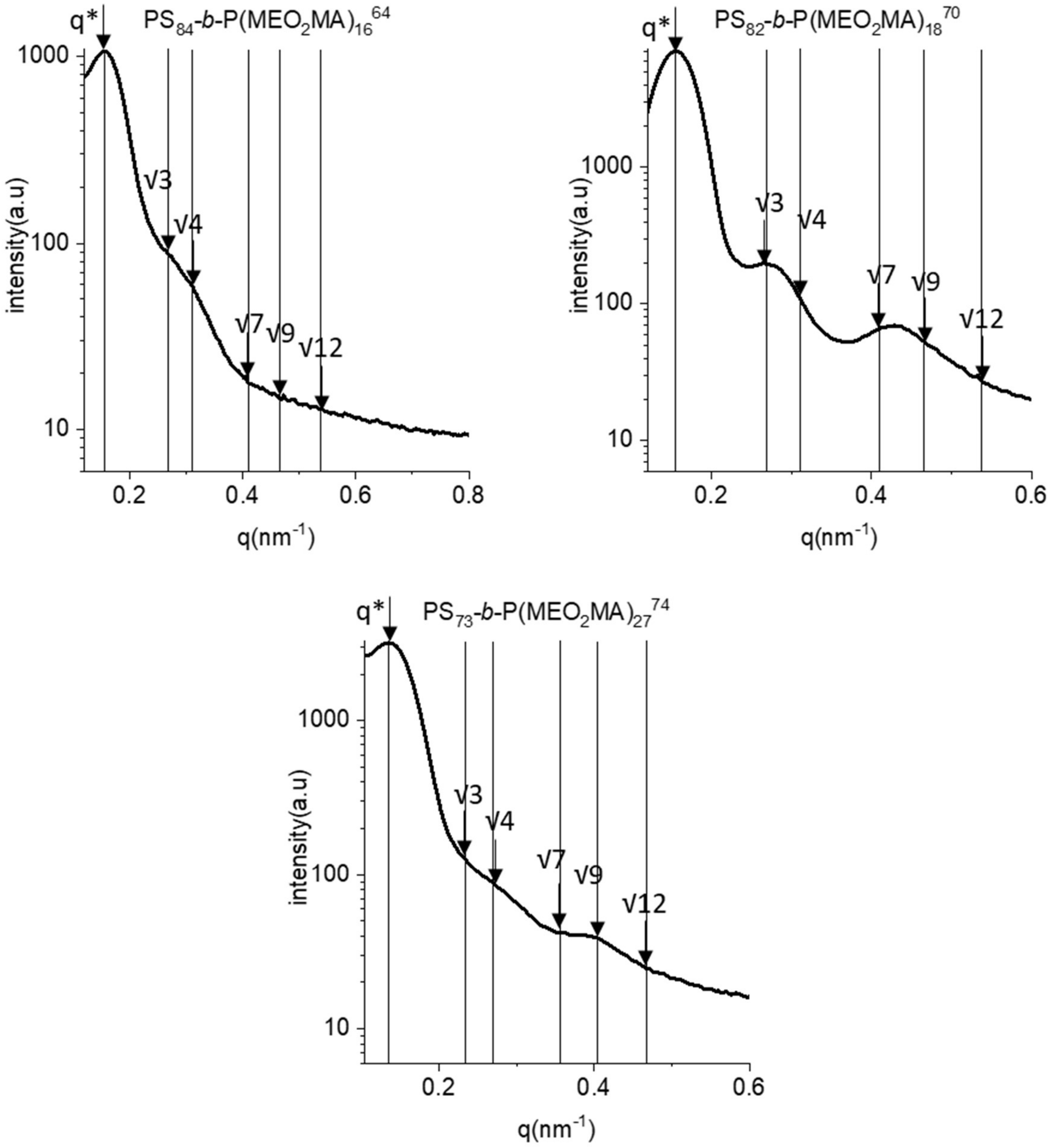

Fig. 61 The results of SAX measurement for PS-*b*-PMEO$_2$MA with PS molecular weight of 50 kDa and various diblock composition, that is mentioned in the legend of each graph.

The AFM images of PS-*b*-P(MEO$_2$MA-*stat*-OEOMA) cast films (Fig. 62) show hexagonally packed cylinders for these terpolymers as well. The cylindrical structure is further proven by SAXS measurement results in Fig. 63. Similar to its diblock copolymer analogues, the terpolymer with higher molecular weight (PS$_{78}$-*b*-P(MEO$_2$MA-*stat*-OEOMA)$_{22}^{134}$), displays hexagonally packed cylinders perpendicular to the surface, while the lower molecular weight sample (PS$_{79}$-*b*-P(MEO$_2$MA$_{83}$-*stat*-OEOMA$_{17}$)$_{21}^{71}$) shows rather a mixture of standing and lying cylinders with more ratio of standing cylinders compared to its diblock analogue. These results express that the increase of the number of ethylene oxide in the side chains of OEOMA is not resulting in a drastic change in the diblock's interaction parameter as well as its solubility parameters. This proves that the randomness and the difference in unit size of the second block does not affect the structure formation and, due to rather high interaction parameter between PS and POEOMA, a clear segregation is observed for PS-*b*-POEMA in bulk. The strong tendency of the two blocks to segregate is caused by their clear difference in chemical structure and, thus, their Hansen solubility parameters which determine the PS and POEMA's high interaction parameter (χ) [200][224]–[226].

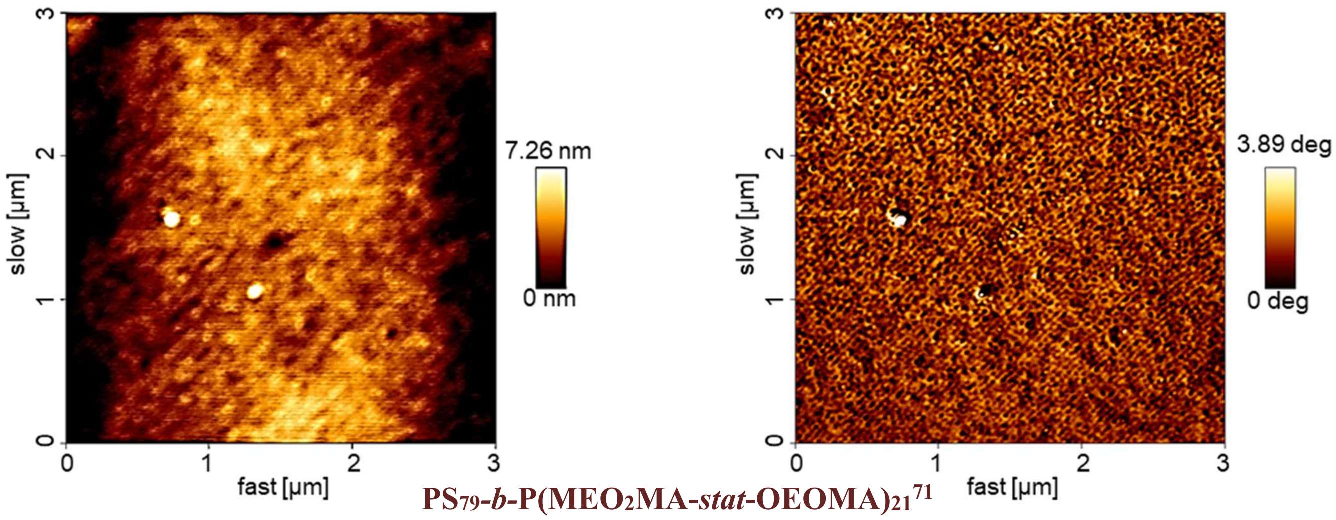

PS$_{79}$-*b*-P(MEO$_2$MA-*stat*-OEOMA)$_{21}$[71]

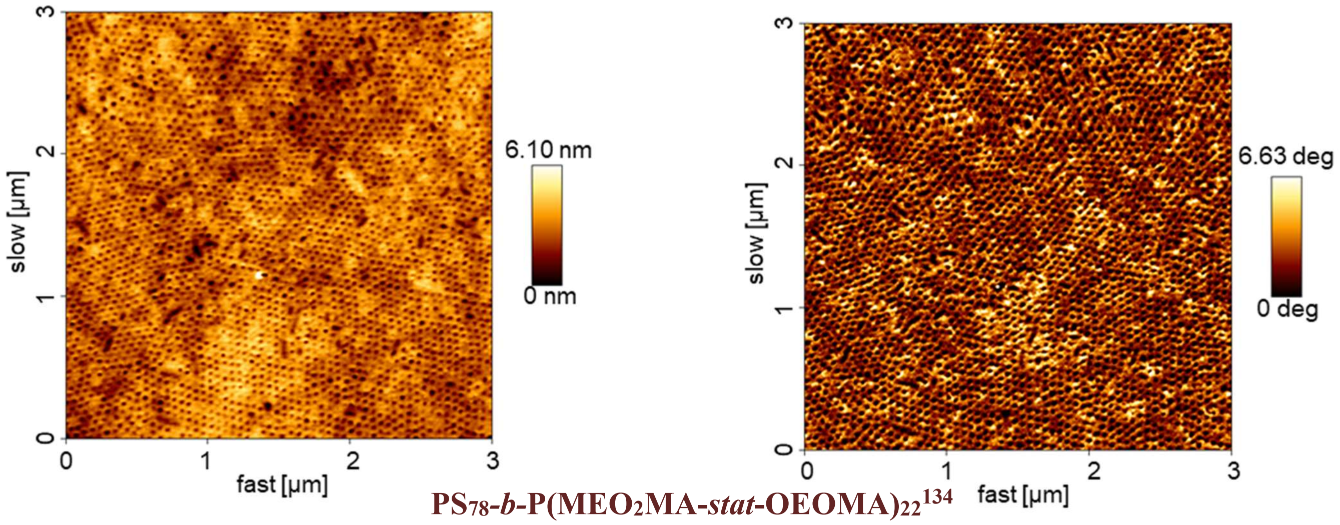

PS$_{78}$-*b*-P(MEO$_2$MA-*stat*-OEOMA)$_{22}$[134]

Fig. 62 AFM surface images of the films of PS-*b*-P(MEO$_2$MA-*stat*-OEOMA) with different molecular weight. The left side is height image, and the right side is the phase image.

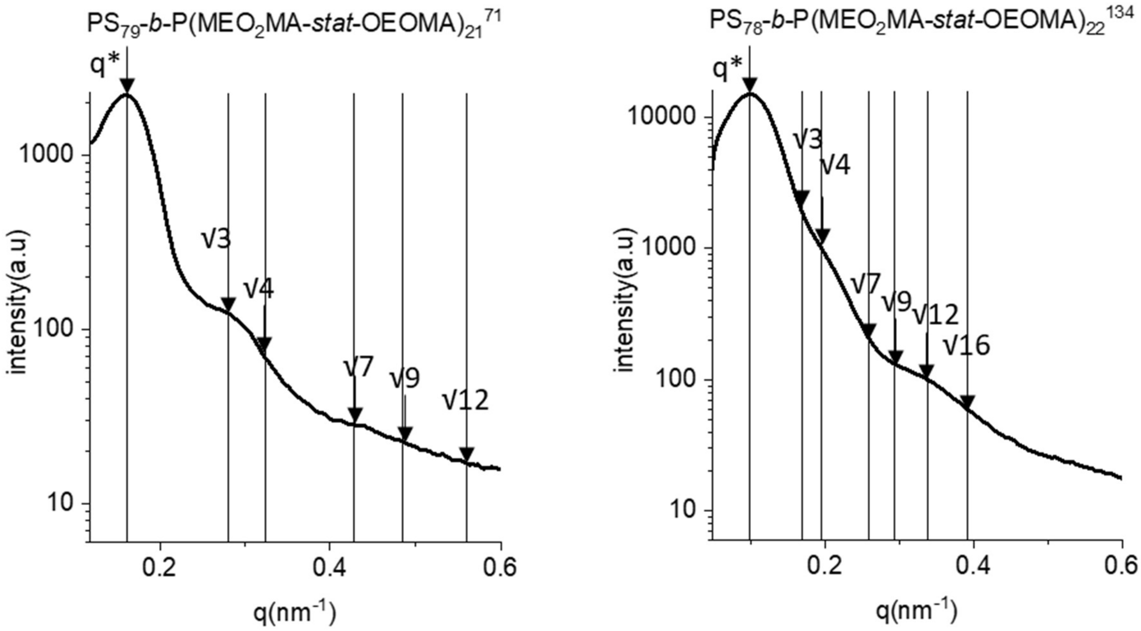

Fig. 63 The results of SAX measurement for PS-*b*-P(MEO$_2$MA-*stat*-OEOMA) with PS molecular weight of 100 kDa or 50 kDa and similar diblock composition, that is mentioned in the legend of each graph.

The illustrated results prove the presented synthesis pathway as a straightforward method for preparation of highly self-assembled materials. The perpendicularly oriented cylindrical structure forming just by simple solvent evaporation is very promising in nanolithographic applications as well as membrane preparation and it is worth thorough studies in future, using more sophisticated techniques such as in situ 2D SAX measurement, TEM cross-section or TEM tomography.

6.5 Isoporous membranes from polystyrene-*b*-poly(oligo ethylene oxide methacrylate)s with tailored pore size and temperature responsivity

As discussed in detail in section 6.4, amphiphilic block copolymers have the ability to self-assemble in various morphologies in bulk and solution. In bulk, depending on the Flory-Huggins interaction parameters and the ratio of the two blocks, they can form spheres, hexagonally packed cylinders, gyroid or lamellar structure [135]. On the other hand, in solution, depending on the selectivity of the solvent(s) used, block copolymers can self-assemble in various forms including spheres, cylinders, vesicles, etc. [227]. Making use of the self-assembly of block copolymers, combined with the traditional phase inversion method, self-assembly non solvent induced phase transition (SNIPS) is used as a straightforward technique to prepare highly porous integral asymmetric membranes. The steps of this method are briefly explained in Fig. 9 in section 3.4. In this technique, first the diblock copolymer is dissolved in a solvent or a mixture of at least two solvents. Each solvent chosen should be selective for one of the blocks and, generally, the solvent selective for the major block has lower boiling point and evaporates faster. The homogenous polymer solution is then cast on glass plate or non-woven using a doctor blade. At this moment, the more volatile solvent starts to evaporate and provides a gradient of concentration perpendicular to the surface of the polymer film. This change of concentration causes the block copolymers to self-assemble in a structure similar to their bulk morphology. If proper time for evaporation is given, hexagonally packed cylinders form perpendicular to the film surface. At this point, the film is put in the precipitation bath, which causes the solvent-nonsolvent exchange. As a result, the top layer structure (generally around 100 nm) freezes immediately by precipitation. The penetration of the nonsolvent through the cylinder channels formed, causes the rest of the polymer film to precipitate as well, forming a spongy or finger like porous structure at the bottom of the thin highly ordered layer. The spongy or finger like structure of the supporting layer, depends on the non-solvent type and the speed of solvent-nonsolvent exchange. If the solvent and non-solvent are completely miscible, the finger like structure is formed and if the solvent and non-solvent are not well miscible, the solvent non-solvent exchange will be slightly delayed, resulting in porous spongy structure [147][148].

Several parameters are crucial in the success of the SNIPS technique. The first factor is the self-assembly of the diblock copolymer which should be guaranteed by choosing the right diblock copolymer with high enough incompatibility between the two blocks which causes them to repel each other and form micelles in the solution. This could be guaranteed by choosing diblock copolymers with high interaction parameters (χ) and the desirable block ratio [135]. As explained in section 6.4, PS-*b*-PMEO$_2$MA and PS-*b*-P(MEO$_2$MA-*stat*-OEOMA) show well separated phases in the cylindrical morphology in bulk when the ratio of the second block is between 14-29 wt.%. To fabricate asymmetric membranes, block copolymers with the weight ratio between 16-29wt.% were used and the total molecular weight was 64-146 kg/mol (Table 4 at the introduction of section 6.4).

To prepare isoporous asymmetric membranes two things about the solvent system are important:

1) The solution must contain a volatile solvent

2) The solution must contain a bad solvent for the micelle core blocks

The volatile solvent is in our case THF. It is needed because it allows an increase in the copolymer concentration on the top layer after the casting of the polymer solution. In principle the self-assembly of highly ordered membranes should be possible also with lower THF concentration but higher polymer concentration. Here the viscosity is a limiting factor. If the viscosity of the polymer solution is too high, firstly the polymer does not dissolve completely and secondly the casting of the polymer solution would be impossible.

The role of the solvents on the micellization and the self-assembly of block copolymers is very important in the formation of membranes with defined structures and pore sizes. That is why the preparation of the polymer solutions with different solvents and solvents compositions and their effect on the surface structure is a big part of this work.

The second factor in success of the SNIPS technique is the solvents chosen for solution preparation. This part is very crucial as choosing the wrong solvent can result in unordered structure. Generally, in the literature, Hansen solubility parameters are used as a guide to compare the selectivity of a certain solvent towards each block of the copolymer. The Hansen solubility parameters of the solvents used in this study as well as the parameters for each of the polymer blocks were listed in Table 6, section 6.4.1. As it was discussed beforehand in section 6.4.1, the most selective solvent for PS are THF and dioxane and one of the most selective solvent for PEO_2MA is DMF. Although, Hansen solubility parameters give an idea about the best possible solvents for casting, mostly the choice of solvents as well as adjusting the rest of casting parameters (like solution concentration and evaporation time) are done by try and error. Therefore, in this work the possibility of using the combination of these solvents is investigated as well. THF or dioxane are evaporating faster than DMF, resulting to higher polymer concentration on the top layer of the cast film and force the block copolymer to phase separate due to the incompatibility of its two blocks. At the same time, the viscosity increases due to the high concentration of the solution as well as micelle formation. Further evaporation of the volatile solvent results in aggregation of micelles in form of hexagonally packed cylinders. After dipping the film in the precipitation bath, the already formed surface structure freezes. The nonsolvent exchanges through the formed pores of the hydrophilic surface by replacing DMF. It also precipitates the less organized layer under the well-organized top layer and forms the sponge or finger-like structure.

The last factor in optimizing SNIPS for a certain block copolymer is the precipitation bath. Here as well, the Hansen solubility parameters can help choosing the best non-solvent with the lowest affinity to both blocks of the copolymer. Furthermore, the boiling point of the non-solvent should be low enough to be able to remove it completely from the fabricated membranes via vacuum. The possibility of using Milli-Q water and dried diethyl-ether as nonsolvent is studied in this research.

6.5.1 Structural investigation of membrane films

As a start for casting, the solvent mixture of THF/DMF is used to determine the limits of other casting parameters, mainly the solution concentration and the evaporation time. This solvent mixture is chosen as it is very common in previous works [110][138][147][148][228] and the high boiling point differences between THF and DMF, provides a bigger window to investigate other casting parameters. The more volatile THF is selective for PS and the much less volatile DMF is more selective for $PMEO_2MA$. The results of the first casting of PS_{81}-*b*-$P(MEO_2MA)_{19}^{124}$ in DMF/THF with volume ratio of 50:50 is plotted in Fig. 64. As it can be observed in Fig. 64 by decreasing the polymer concentration, the film structure changes from

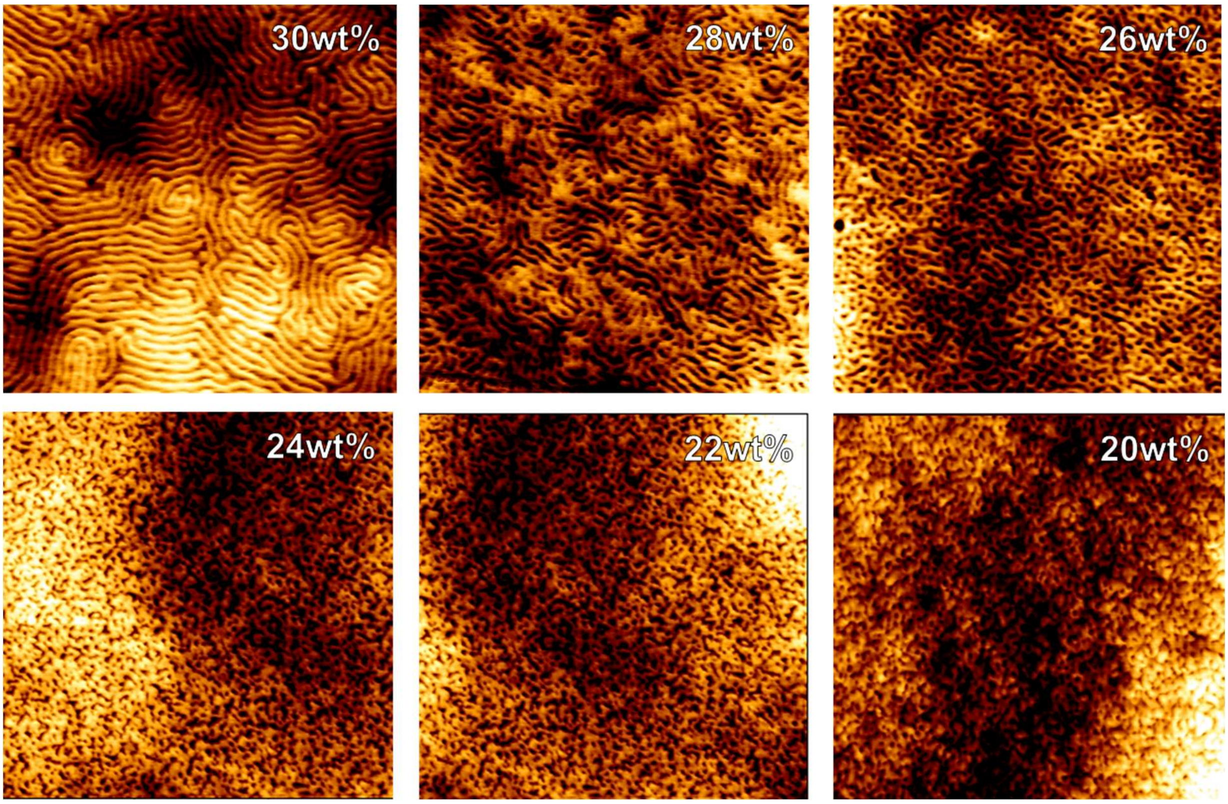

Fig. 64 The AFM images of PS_{81}-*b*-$P(MEO_2MA)_{19}$[124] cast films from solutions of THF/ DMF with the volume ratio of 50/50. The evaporation time was 5 s for all samples. Milli-Q water was used as precipitation bath. All the images are height images in the range of 3 µm * 3 µm.

horizontally oriented cylinders towards a mixture of perpendicular and horizontal cylinders. However, the perfect hexagonally packed cylinders are not observed in any of the cast films. The structure changes from the mixture of standing and lying cylinder to sphere percolation. The reason for such behaviour is that the concentration is too high for the castings over 26 wt% concentration and too less for lower concentration. Therefore, one can conclude that casting at 25 wt.% concentration should result in optimum structure.

The results for casting at the concentration of 25 wt.% as well as the effect of increasing the amount of THF is presented in Fig. 65. These results show that casting the 25 wt.% polymer solution in THF/DMF:50/50, results in a sphere percolated structure with very few perpendicular cylinders. Increasing the amount of THF however increases the amount of perpendicular cylinders as can be seen in Fig. 65. By increasing the amount of THF, the solvent mixture is getting more selective for PS as DMF is more selective for $PMEO_2MA$. Such behaviour is observed for casting of PS-*b*-P2VP in THF/DMF studied by Stegelmeier *et al.* [229]. They studied the structure formation pathways and transient morphologies involved in the formation of mesoporous membranes via SNIPS. Stegelmeier *et al* [229] mapped the topological paths and characteristic transient structures into a ternary phase diagram and focused on the stability region of an ordered pore phase, which is relevant for the generation of integral asymmetric isoporous membranes. They identified several characteristic morphologies including spinodal networks, sphere percolation networks, ordered pore structures, and disordered and ordered cylinder arrangements. Furthermore, they calculated the corresponding composition trajectories in the phase diagram to help optimize suitable experimental conditions for SNIPS technique. According to their work, decreasing the polymer concentration in a certain solvent mixture can lead transition from ordered lying cylinders to an ordered pored network if the chosen solvent composition is proper. In case of reaching spinodal network (like in the present work) from ordered cylinders, change of the solvent composition towards more volatile solvent which is more selective for the larger block could lead to the ordered porous network. Therefore, the structure formed from casting polymer solution in THF/DMF : 50/50 can be better optimized by increasing the amount of THF in the solvent mixture as seen in Fig. 65.

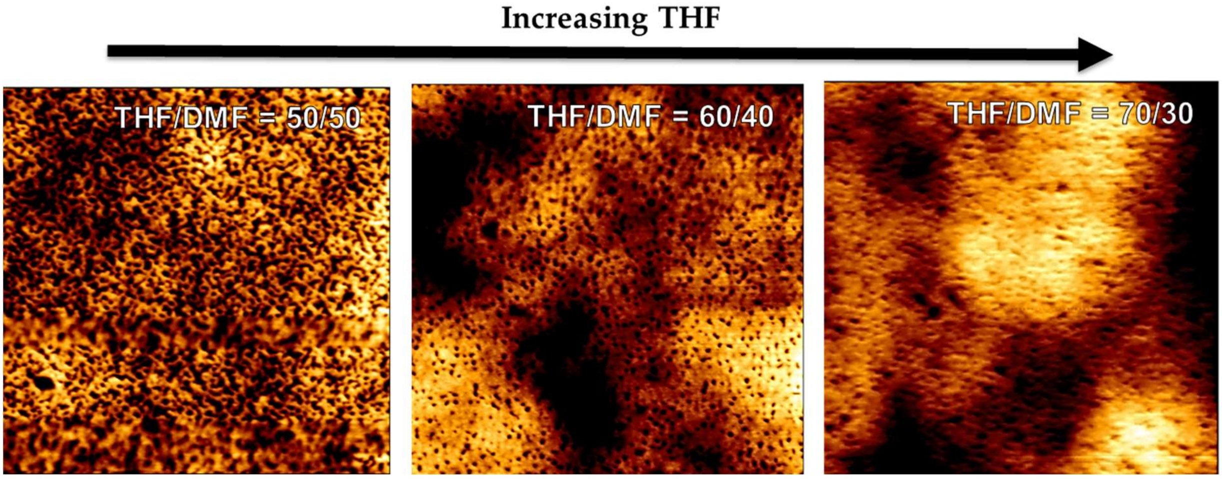

Fig. 65 The AFM images of PS_{81}-*b*-$P(MEO_2MA)_{19}^{124}$ cast films from solutions of THF/ DMF with the different volume rations of 50/50, 60/40 and 70/30 from left to right. The polymer concentration was 25 wt.% and the evaporation time was 5 s for all samples. Milli-Q water is used as precipitation bath. All the images are height images in the range of 3 µm * 3 µm.

The structure formed from casting polymer solution in higher THF amount (THF/DMF : 70/30 can be further improved by increasing the evaporation time before putting the film in the precipitation bath. This helps the cylinders arrange themselves in a well-ordered structure before the structure is frozen by solvent-nonsolvent exchange and immediate precipitation (Fig. 66). However, further increase of the evaporation time results in connected pores and consequently horizontally oriented cylinders. By increasing the evaporation time, more THF is evaporated and the resulted less selective solvent causes the PMEO$_2$MA block to segregate further from PS and form lying cylinders. In a study of the phase separation of polystyrene-*block*-polylactide diblock copolymer, Phillip *et al.* [230] discovered that fast drying a film of a block copolymer solution (less evaporation time) leads to a strong concentration gradient and the microphase separation propagates perpendicular to the surface, resulting in perpendicularly oriented cylinders. While, slow evaporation, results in a parallel alignment of the cylinders.

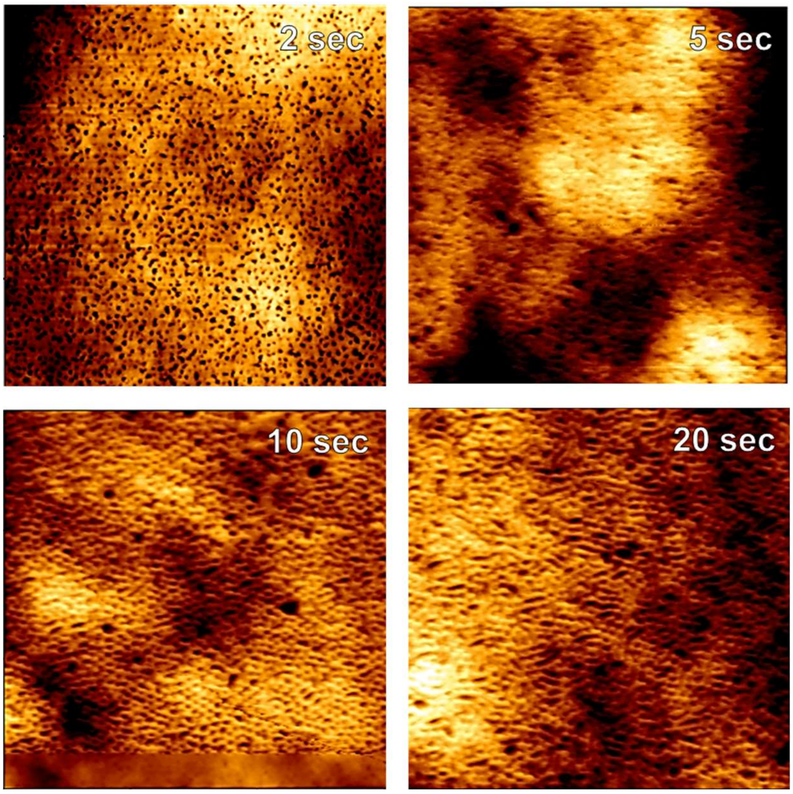

Fig. 66 The AFM images of PS$_{81}$-*b*-P(MEO$_2$MA)$_{19}^{124}$ cast films from solutions of THF/ DMF with the volume ration of 70/30. The evaporation time is increasing from 2 s to 20 s from top left to bottom right. The polymer concentration was 25 wt.% for all samples. Milli-Q water was used as precipitation bath. All the images are height images in the range of 3 μm * 3 μm.

The effect of different solvents on the surface structure of the membrane films fabricated by SNIPS is studied by using three different solvent systems including THF/DMF, DOX/DMF and THF/DOX/DMF. The cast films are investigated via AFM and SEM and the results are plotted in Fig. 67. As it is obvious from Fig. 67, casting in different solvents affects the morphological structure drastically. While casting in THF/DMF is resulting in hexagonally packed perpendicular cylinders, casting in DOX/DMF and THF/DOX/ DMF results in spherical morphology proven by AFM. Furthermore, the uniformity of the pores and pore characteristics in the separation layer is different when different solvent system is used for casting. DOX helps to decrease the solvent quality for the hydrophilic block (PMEO$_2$MA) and facilitates micellization by increasing the interaction between the segments of PMEO$_2$MA block in comparison to the interaction of PMEO$_2$MA and the solvent. The PMEO$_2$MA side of polymer blocks approach to each other and tend to stay closed to form stable pore structures, which reduces the micelle mobility even before dipping the cast film into the precipitation bath [231]. However, the selectivity of DOX compared to the other solvent mixtures does not change the optimum casting concentration in spite of previous studies for PS-P4VP [157]. The reason lays in the completely different selectivity of DOX towards PMEO$_2$MA compared to P4VP. Although DOX is very nonselective solvent for P4VP, its affinity towards PMEO2MA is not that low and it can dissolve the PS-*b*-P(MEO$_2$MA) block copolymer very well. This can be proven by the results of DLS measurements of PS$_{81}$-*b*-P(MEO$_2$MA)$_{19}^{124}$ in different solvents and solvent mixtures as reported in Table 7. The hydrodynamic radius of the block copolymer doesn't change that much in different solvent and solvent mixtures, proving all of these solvent systems to be able to dissolve PS-*b*-P(MEO$_2$MA) copolymers well to form unimers in the solution. According to Table 7, no micellization is observed in any of the solvent systems that studied in this work, since the measured R_h is between 8.8-10.4 nm and it is similar to the radius of gyration (R_g) of PS$_{81}$-*b*-P(MEO$_2$MA)$_{19}^{124}$ calculated by equation (6.13).

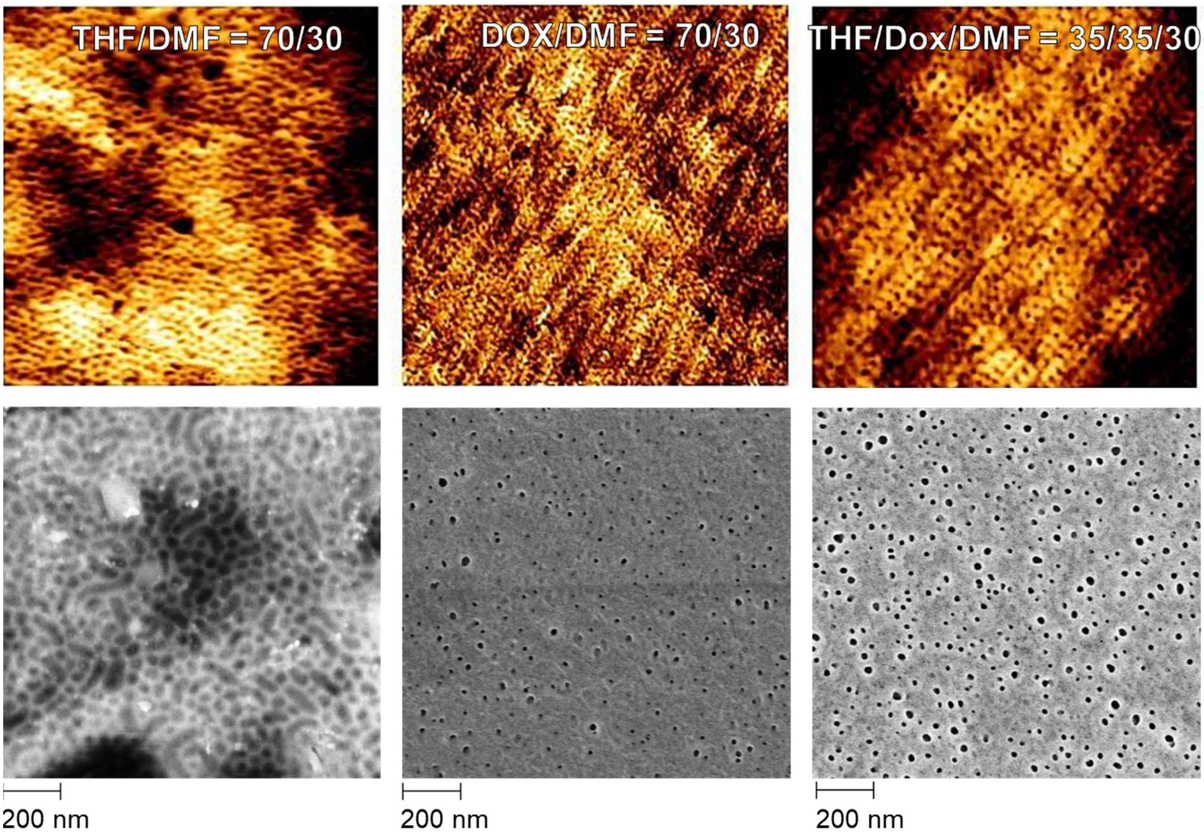

Fig. 67 The AFM (top) and SEM (bottom) images of PS_{81}-*b*-$P(MEO_2MA)_{19}$[124] cast films from solutions of various solvent systems; From left to right: THF/DMF = 70/30, DOX/DMF = 70/30 and THF/DOX/DMF = 35/35/30, the solvent ratios are volume ratio. The polymer concentration was 25 wt.% and the evaporation time was 10 s for all samples. Milli-Q water is used as precipitation bath. All the AFM images are height images in the range of 3 µm * 3 µm and the scale of SEM images are marked under them.

Table 7 Hydrodynamic Radius of 0.1 wt % PS_{81}-*b*-$P(MEO_2MA)_{19}^{124}$ in Different Solvent Systems

Solvent	R_h **(nm)**
Tetrahydrofuran (THF)	10.4
Dimethyl formamide (DMF)	9.2
1,4-Dioxane (DOX)	10.4
THF/DMF: 80/20	9.2
THF/DMF: 70/30	8.8
THF/DMF: 60/40	9.4
THF/DMF: 50/50	9.8
THF/DMF: 40/60	9.6
THF/DMF: 30/70	10.3
THF/DOX/DMF: 35/35/30	9.6

The results of SEM (Fig. 67) however, show that most of the pores on the surface of the cast film are closed, resulting a rather unordered porous structure. The reason for such phenomena lays in the hydrophilicity of $PMEO_2MA$. Hahn *et al.* [232] observed similar behaviour while precipitating PS-*b*-PEO cast film in water. Based on their study, highly polar nonsolvents, for example water, cause the swelling of the PEO-block, leading to a significant increase of the viscosity. Furthermore, the direct precipitation cannot be induced. As a result, the lower mobility of the chains suppresses the structure formation during the phase inversion process. Less polar non solvents, for example, diethyl ether or octanol, ensure the direct precipitation of the diblock without a considerable increase in the viscosity [232]. Therefore, in this work diethyl ether as a less polar nonsolvent is used to induce the precipitation of PS-*b*-$P(MEO_2MA)$, which can prevent any kind of swelling of ethylene oxide in the side chains of $PMEO_2MA$ during the phase inversion resulting in the appearance of closed pores and distorted structure

(Fig. 68). The results of applying diethyl ether as the precipitant prove the importance of the nonsolvent on the surface structure of the cast film. As it will be seen further in Fig. 69, the surface structure of the film precipitated in diethyl ether is well ordered and shows less defects and connected pores.

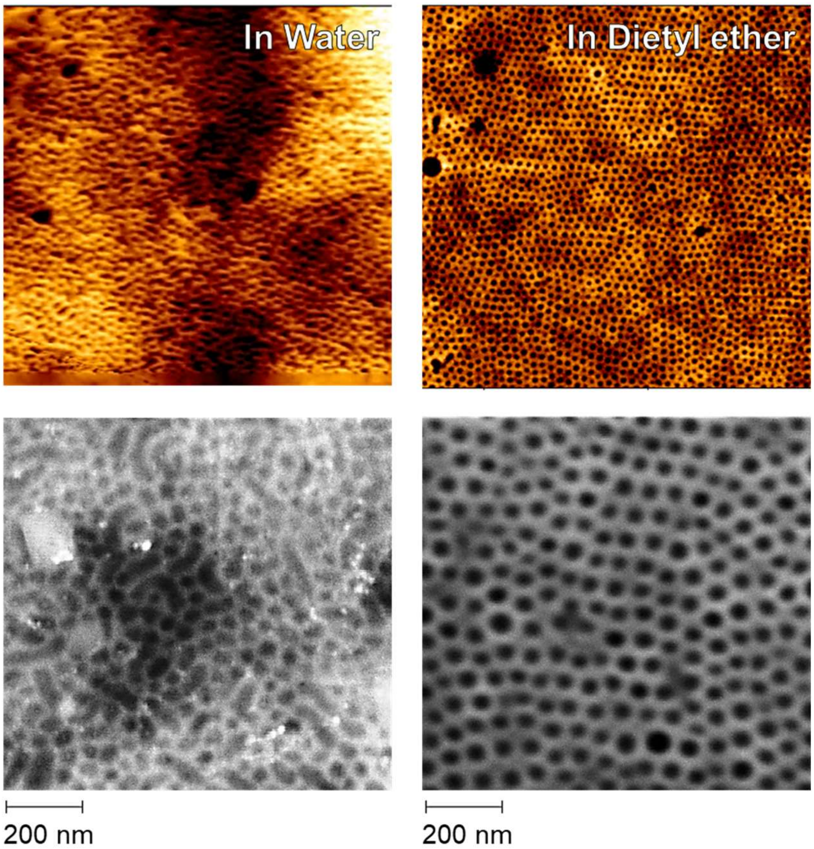

Fig. 68 The AFM (top) and SEM (bottom) images of PS$_{81}$-*b*-P(MEO$_2$MA)$_{19}$[124] cast films from the solutions of THF/DMF with the volume ratio of 70/30. The left side images are from precipitation in Milli-Q water and the right side images are from precipitation in diethyl ether. The polymer concentration in casting solution was 25 wt.% and the evaporation time was 10 s for both samples. The AFM images are height images in the range of 3 µm * 3 µm and the scale of SEM images are marked under them.

In a study, Karunakaran *et al.* [233] reported the successful casting of PS-*b*-PEO in water using THF/DMAC/Sulfulane as solvent mixture. THF is a good solvent for PS while DMAC and Sufulane are better solvent for PEO. Due to their study, sulfulane as a very viscous solvent, helps preserving the structure while precipitating in water, due to its low mobility and therefore results in a structure with open pores. In an attempt we tried to apply the same procedure on PS-*b*-PEMO$_2$MA. The solvent mixture that was selected was THF/DMF/Sulfulane with the volume ratio of 75/13.8/11.2. The solvent ratio was selected in a way that the overall solubility parameter is similar to the one of THF/DMF : 70/30 as calculated by equation (6.14) which results a well ordered structure, while the ratio stays similar to the work of Karunakaran *et al.* [233]. According to literature, the solubility parameter of a liquid mixture (δ_D, δ_P, δ_H) can be represented by the volumetric average of the solubility parameter of the pure compounds [141] [205]:

$$\delta_{i,s} = \frac{\sum_j (x_j \vartheta_j \delta_{i,j})}{\sum_j (x_j \vartheta_j)} \tag{6.14}$$

AFM images of PS_{81}-*b*-$\mathrm{P(MEO_2MA)}_{19}^{124}$ cast films from solutions of THF/DMF/Sul : 75/13.8/11.2 volume ratio are presented in Fig. 70. As it is clear, the casting of the THF/DMF/Sul :75/13.8/11.2 solvent system, results in well-ordered hexagonally packed cylindrical structure in diethyl ether but rather unordered sphere percolation in water. Other attempts of casting with the same solvent system and different solvent ratio, solution concentration or evaporation time were unsuccessful as well. This indicates that although sulfulane shows to be a good choice to preserve the structure of PS-b-PEO film, it has no effect on preserving the structure of PS-*b*-$\mathrm{PMEO_2MA}$ cast film.

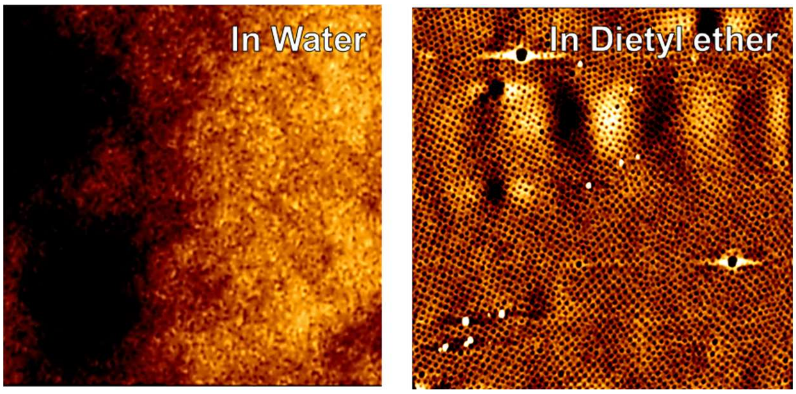

Fig. 69 The AFM images of PS_{81}-*b*-$\mathrm{P(MEO_2MA)}_{19}^{124}$ cast films from solutions of THF/DMF/Sul = 75/13.8/11.2 volume ratio. The left side image is from precipitation in Milli-Q water and the right side image is from precipitation in diethyl ether. The polymer concentration in casting solution was 25 wt.% and the evaporation time was 10 s for both samples. The AFM images are height images in the range of 3 µm * 3 µm.

Fig. 70 shows the cross section of PS_{81}-*b*-$P(MEO_2MA)_{19}^{124}$ cast film from THF/DMF : 70/30 at 10 s evaporation time and precipitated in diethyl ether. The cross section shows a top selective layer of hexagonally packed cylinders and a porous supporting layer with no artifacts. This shows the success of fabricating PS-*b*-$PMEO_2MA$ integral asymmetric membranes via SNIPS.

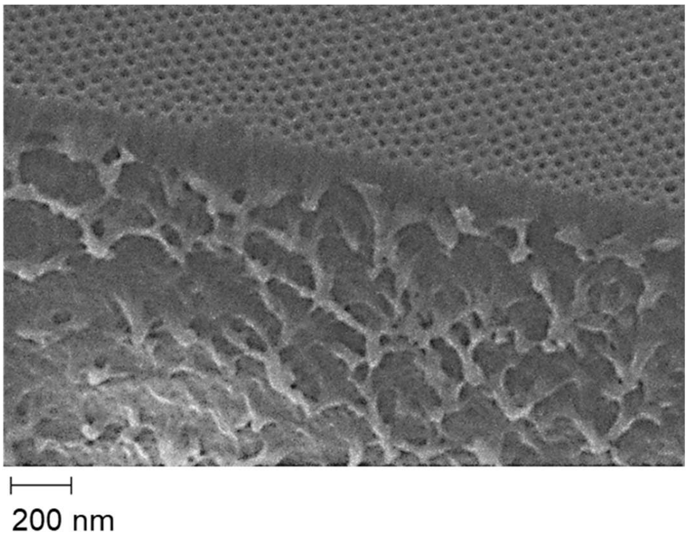

Fig. 70 The cross section of the cast film of PS_{81}-*b*-$P(MEO_2MA)_{19}^{124}$ from the polymer solution in THF/DMF = 70/30 volume ratio. The polymer concentration in casting solution was 25 wt.% and the evaporation time was 10 s. Diethyl ether was used as a precipitation bath.

The casting limits are studied by changing the block ratio of PS and $PMEO_2MA$ from 19 wt.% $PMEO_2MA$ to 29 wt.%. Casting is performed under similar conditions for both block copolymers and the results are plotted in Fig. 71. As it is clear from height AFM images, changing the block ratio affects the pore size of the block copolymers which is in agreement with previous studies on other block copolymers [110][138][139][228]. For a given degree of polymerization, the relative amount of the pore forming block affects the pore size (the larger the block, the larger the pore) [110].

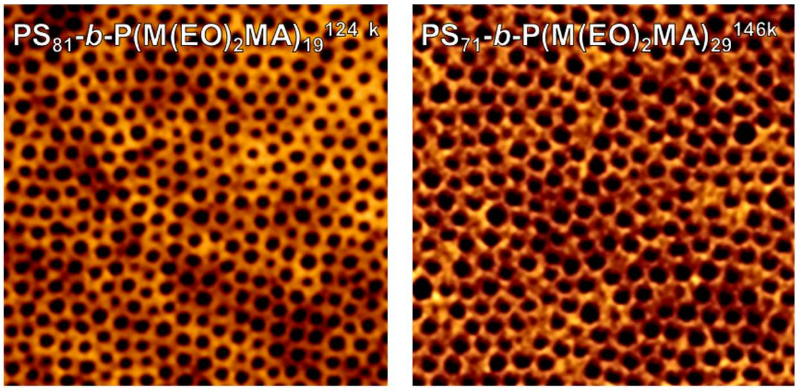

Pore size: 25 nm

Pore size: 30 nm

Fig. 71 AFM height images of the cast films from PS_{81}-*b*-$P(MEO_2MA)_{19}^{124}$ (left side image) and PS_{71}-b-$P(MEO_2MA)_{29}^{146}$ (right side image) solutions in THF/DMF with 70/30 volume ratio. The polymer concentration in the solution was 25 wt.% and the evaporation time was 10 s in both samples. Diethyl ether was used as precipitation bath. The images are in the range of 1 μm * 1 μm.

Another approach to change the membrane pore size is by changing the block copolymer molecular weight. In this study, the total molecular weight of PS-*b*-$PMEO_2MA$ is decreased from 124 kg/mol to 70 kg/mol while keeping the block ratio constant at around 19 wt.% $PMEO_2MA$. As the molecular weight is decreasing, the concentration of polymer solution for casting increases. Therefore, the viscosity is kept almost constant to provide enough entanglement in the polymer cast film and avoid defects. While casting of PS_{81}-*b*-$P(MEO_2MA)_{19}^{124}$ was done at 25 wt.% concentration, PS_{82}-*b*-$P(MEO_2MA)_{18}^{70}$ was cast from a solution of 33 wt.% concentration. The SEM and AFM images of the cast films in Fig. 72 show that by decreasing the molecular weight from 124 kDa to 70 kDa, the pore size (measured by JPK data processing software) is decreasing from around 25 nm to 15 nm. Previous studies on other diblock copolymers show similar results [110][138][234]. However, further investigation would help finding the mathematical relation between the block copolymer molecular's weight and the membrane's pore size.

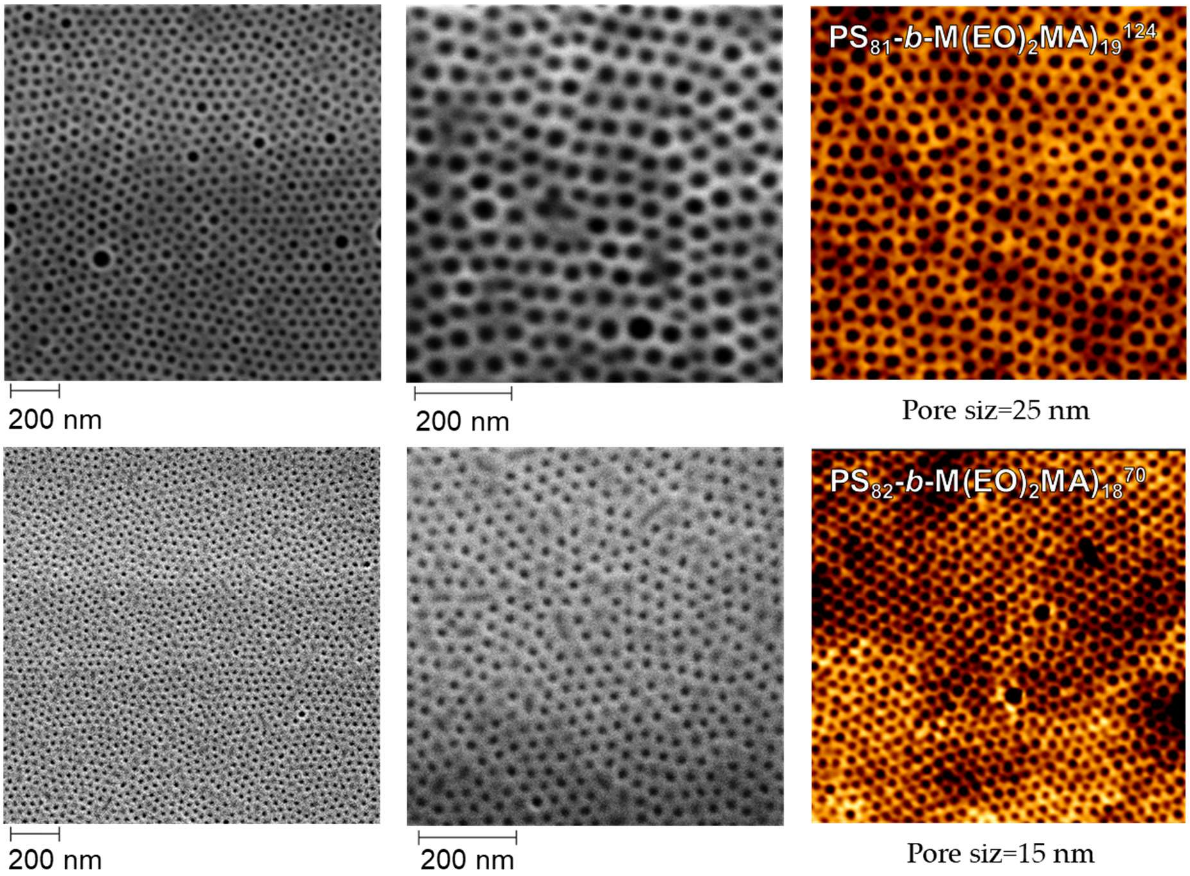

Fig. 72 The SEM and AFM images of PS_{81}-*b*-P(MEO_2MA)$_{19}^{124}$ (top) and PS_{82}-*b*-P(MEO_2MA)$_{18}^{70}$ (bottom) cast films from solutions of THF/DMF with the volume ratio of 70/30. The polymer concentration was 25 wt.% for PS_{81}-*b*-P(MEO_2MA)$_{19}^{124}$ and 33 wt.% for PS_{82}-*b*-MEO_2MA)$_{18}^{70}$. The evaporation time was 10 s in both cases and diethyl ether was used as precipitation bath. The AFM images are in the scale of 3 µm * 3 µm. The scale of SEM images is marked under them. The middle SEM image is a zoomed-in of the left image for better comparison.

PS-*b*-$PMEO_2MA$ block copolymer with lower molecular weight (around 70 kDa) shows further change of the pore size as the block ratio changes. As it was observed for PS-*b*-$PMEO_2MA$ with higher molecular weight (124 kDa), by increasing the ratio of PMO_2MA in the block copolymer, the pores size increases. As can be seen in Fig. 73, the pore size changes from 12 nm for PS_{84}-*b*-P(MEO_2MA)$_{16}^{64}$ to 18 nm for PS_{73}-*b*-P(MEO_2MA)$_{27}^{74}$. However, the change of pore size with changing the ratio of block copolymer is not as high as it was for higher molecular weight block copolymers.

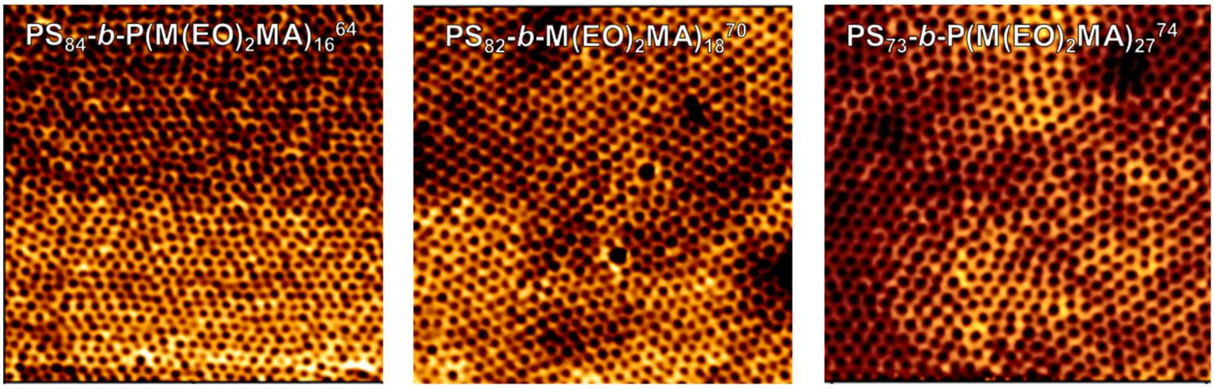

Pore size = 12 nm Pore size = 15 nm Pore size = 18 nm

Fig. 73 AFM height images of the cast films from PS$_{84}$-*b*-P(MEO$_2$MA)$_{16}$ ^{64}, PS$_{82}$-*b*-P(MEO$_2$MA)$_{18}$^{70} and PS$_{73}$-*b*-P(MEO$_2$MA)$_{27}$^{74} solutions, respectively from left to right. The casting solutions were made in THF/DMF with 70/30 volume ratio. The polymer concentration in the solution was 33 wt.% and the evaporation time was 10 s in all samples. Diethyl ether was used as precipitation bath. The images are in the range of 1 µm * 1 µm.

Fig. 74 compares the SEM images of membrane top surfaces cast from 22 wt.% PS$_{78}$-*b*-P(MEO$_2$MA-*stat*-OEOMA)$_{22}$^{134} solution in THF/DOX/DMF: 30/30/35 with 10 s evaporation time and precipitated in water or diethyl ether. For PS-*b*-(MEO$_2$MA)-*stat*-OEOMA) block copolymer, casting from THF/DOX/DMF solution results in less defected films, while casting from DMF/THF is successful as well. Like PS-*b*-PMEO$_2$MA, precipitation in water results in unordered structure, while precipitation in diethyl ether provides well-ordered porous structure with similar pore sizes. This can be explained by higher amount of ethylene oxide in the side chains of OEOMA compared to MEO$_2$MA.

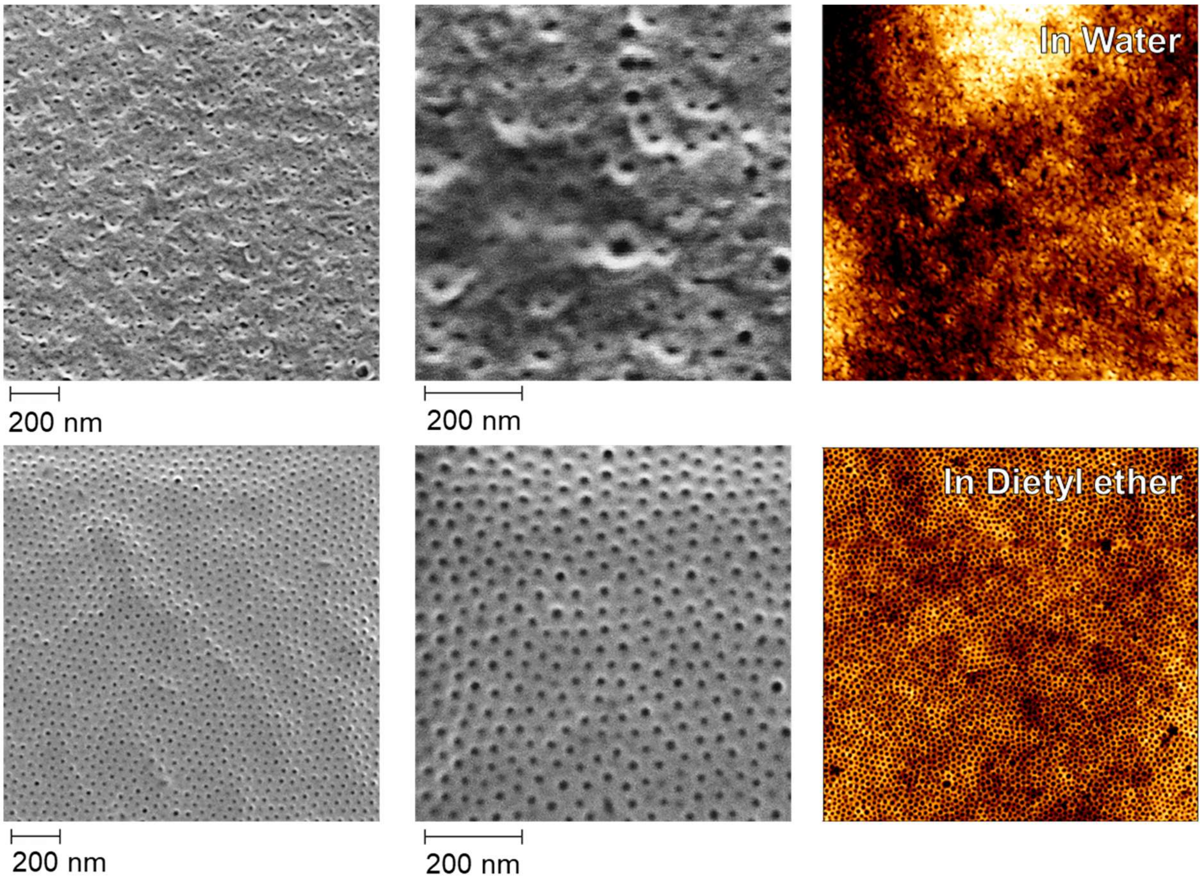

Fig. 74 The AFM and SEM images of PS_{78}-*b*-P(MEO_2MA-*stat*-OEOMA)$_{22}^{134}$ cast films from solutions of THF/Dox/DMF with the volume ratio of 30/30/35. The images at the top are from precipitation in Milli-Q water and the images at the bottom are from precipitation in diethyl ether. The polymer concentration in casting solution was 22 wt.% and the evaporation time was 10 s for both samples. The AFM images are height images in the range of 3 µm * 3 µm and the scale of SEM images are marked under them. The middle SEM image is a zoomed-in of the left image for better comparison.

The change of total molecular weight for PS-*b*-P(MEO_2MA-*stat*-OEOMA), results in pore size change as well (Fig. 75). By varying the molecular weight from 134 kDa to 71 kDa, the pore size decreases from 18 nm to 15 nm. The change of pore size by changing the molecular weight is much less noticeable for PS-*b*-P(MEO_2MA-*stat*-OEOMA) compared to PS-*b*-P(MEO_2MA). This behaviour can be attributed to the long OEO side chains of OEOMA and the statistic P(MEO_2MA-*stat*-OEOMA) as the second block instead of $PMEO_2MA$ homopolymer. The long OEO side chins are occupying much more space in collapsed form compared to $PMEO_2MA$ and result in rather smaller pore size for the membrane films.

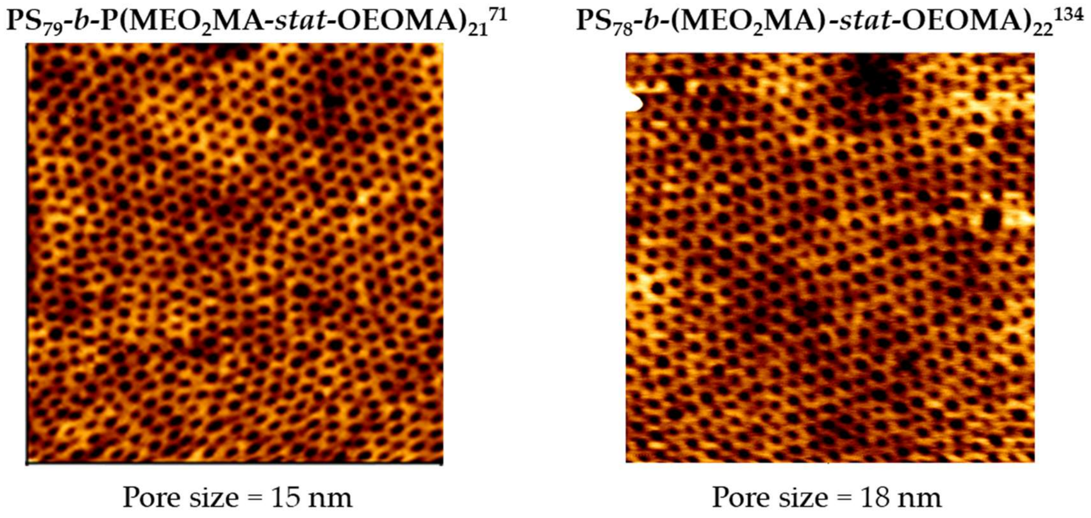

PS$_{79}$-*b*-P(MEO$_2$MA-*stat*-OEOMA)$_{21}$^{71} **PS$_{78}$-*b*-(MEO$_2$MA)-*stat*-OEOMA)$_{22}$^{134}**

Pore size = 15 nm Pore size = 18 nm

Fig. 75 AFM height images of the cast films from PS$_{79}$-*b*-P(MEO$_2$MA-*sta*t-OEOMA)$_{21}$^{71} (left side image) and PS$_{78}$-*b*-P(MEO$_2$MA-*stat*-OEOMA)$_{22}$^{134} (right side image) solutions in THF/DOX/DMF with 30/30/35 volume ratio. The polymer concentration in the solution was 22 wt.% and the evaporation time was 10 s in both samples. Diethyl ether was used as precipitation bath. The images are height image and in the range of 1 µm * 1 µm.

According to AFM images (Fig. 76) casting PS-*b*-P(MEO$_2$MA-*sta*t-OEOMA) from THF/DOX/ DMF solution results in the membrane with spherical surface morphology, while casting from the common solvent mixture of THF/DMF results in hexagonally packed cylinders which is in agreement with the casting results of PS-*b*-P(MEO$_2$MA).

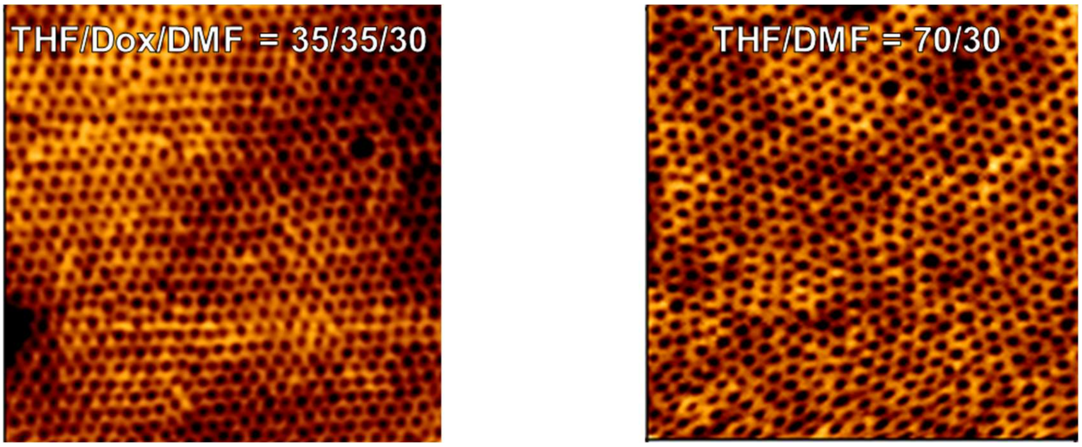

Fig. 76 AFM height images of the cast films from PS$_{79}$-*b*-P(MEO$_2$MA-*sta*t-OEOMA)$_{21}$^{71} solutions in THF/DOX/DMF : 30/30/35 volume ratio (left side image) and THF/DMF : 70/30 volume ratio (right side image). The polymer concentration in the solution was 22 wt.% and the evaporation time was 10 s in both samples. Diethyl ether was used as precipitation bath. The images are height image and in the range of 1 µm * 1 µm.

The presented casting results prove the SNIPS technique to be successful for preparing integral asymmetric porous structure from PS-*b*-P(MEO_2MA) and PS-*b*-P(MEO_2MA-*stat*-OEOMA) copolymers. Optimization of various casting parameters provides the best condition to achieve isoporous polymeric structure via casting in THF/DMF or THF/DOX/ DMF solvent system and diethyl ether as a precipitation bath. While, the pore size can be altered by changing the total molecular weight, block copolymer composition or using a terpolymer as a second block. Such structures are very promising in membrane fabrication, especially for biological application or water treatment.

7 Conclusion

Poly[oligo(ethylene glycol)] (POEOMA) based gradient and random copolymers with various compositions were synthesized via semi-batch Cu-based ATRP. The continuous injection of OEOMA to the system is a very straightforward method of force gradient copolymerization to provide optimized sequence control. Solubility behavior of gradient and random copolymers of MEO$_2$MA and OEOMA with various amounts of OEOMA were investigated by DLS. Both copolymers show reversible thermoresponsivity with a small hysteresis that is slightly higher for gradient copolymers compared to random copolymers. Both copolymers undergo the phase transition in one step, but with different mechanisms. While the random copolymer shows a simple coil to globule transition, the gradient copolymer undergoes micelle formation followed by micelle shrinkage as the temperature increases. By increasing the amount of OEOMA in the copolymer composition, the LCST of both gradient and random copolymers increases linearly, and their values tend to converge.

The effect of different additives including various salts, ethanol and surfactants on the solubility behavior of a gradient and a random copolymer was investigated by DLS. The copolymers show different phase transition behavior in the presence of various additives. While the random copolymer shows a broad transition with a vast change in hydrodynamic radius and normalized scattering intensity, the gradient copolymer displays a rather sharp transition but with less changes in hydrodynamic radius and normalized scattering intensity. The effect of anions on the solubility of both copolymers follows the Hofmeister series. Among the anions studied in this work, SO_4^{2-}, F^-, Cl^- and Br^- show kosmotropic while I^- and SCN^- show chaotropic effect on the solubility of copolymers in pure water. Whereas there is no distinguishable trend observed for the decrease of LCST in presence of various cations. The phase transition behavior of both gradient and random copolymer changes from one-step to two-step phase transition in the presence of salts.

Addition of a good solvent as well as an anionic or cationic surfactant increases the LCST of both gradient and random copolymers. While the gradient copolymer shows a linear increase in LCST vs the amount of ethanol added to the solution, the LCST of the random copolymer changes exponentially. The increase in LCST in the presence of ethanol is attributed to the improvement of polymer’s solubility in presence of ethanol as a good solvent for POEMAs which itself is a result of the competitive interaction with polymer between water and ethanol. There is no cononsolvency observed despite the cononsolvency behavior found for other temperature responsive polymers in presence on ethanol. On the other hand, the addition of surfactants to the aqueous solution of gradient and random copolymers makes the solution more stable by stabilizing the formed micelles and preventing the aggregation. The latter results in a stable solution regardless of temperature over a certain concentration (depending on the copolymer's structural architecture) of surfactant in the system.

The combination of anionic polymerization and ATRP shows a straightforward method to synthesize high molecular weight PS-*b*-PMEO$_2$MA and PS-*b*-P(MEO$_2$MA-*stat*-OEOMA) with very narrow dispersity (<1.1). To best of our knowledge, the resulted molecular weights are much higher than the molecular weights achievable from typical ATRP and are among the highest so far reported for the combination of anionic polymerization and ATRP. This novel synthesis pathway is very versatile for the preparation of block copolymers when the minor block is problematic to undergo living polymerization such as anionic or cationic polymerization.

In this synthesis route, at first, OH-functionalized PS homopolymer was provided via anionic polymerization of styrene followed by chain end reaction with propylene oxide and termination of anions using acetic acid. Further, Steglich esterification was used to transfer the OH- end groups to Br- end groups providing PS-Br as a macroinitiator for ATRP of OEOMAs. Due to the steric hindrance of PS-Br long chains, ATRP of OEOMA appears to be problematic. The hindrance is resolved by changing the reaction solvent from anisole to a mixture of dioxane and toluene, which provides good polarity to preserve Cu-complex's redox potential while dissolving the macroinitiator and radicals very well. Other attempts of using cyclohexanone or pure dioxane as reaction solvent result in lower molecular weight than theory or relatively uncontrolled reaction respectively.

To study the microphase separation in bulk, PS-*b*-PMEO$_2$MA and PS-*b*-P(MEO$_2$MA-*stat*-OEOMA) copolymers with different molecular weight and composition were synthesized. In general, two different PS-Br macroinitiators with the molecular weight of 50 and 100 kDa, respectively, were used. The weight percentage of the second block for both macroinitiators varied from 14% to 29%. All the copolymers synthesized show well-ordered self-assembled hexagonally packed lying or standing cylinders in bulk structure as demonstrated in small-angle x-ray scattering (SAXS) and atomic force microscopy (AFM). This suggests a high interaction parameter between PS and POEOMA which results in a well segregation for PS-*b*-POEMA in bulk. Because of the slight selectivity of THF for PS, the block copolymers with higher ratio of PS and the molecular weight more than 100 kDa, show well defined perpendicularly oriented cylindrical structure. This behavior is similar for both PS-*b*-PMEO$_2$MA and PS-*b*-P(MEO$_2$MA-*stat*-OEOMA) with similar block ratios. The direct self-assembly of block copolymers perpendicularly oriented to the surface is rarely observed in thick films, which makes the PS-*b*-POEOMA copolymers very exceptional in nanotechnological applications such as ultrafiltration membranes or nanolithography.

Iintegral asymmetric isoporous membranes of PS-*b*-PMEO$_2$MA and PS-*b*-P(MEO$_2$MA-*stat*-OEOMA) were fabricated via SNIPS. Different casting parameters are studied to optimize the best casting condition for preparation of a highly ordered structure at the top layer with minimum defects. By changing the solvent system, the best surface structure was achieved by casting in THF/ DMF mixture for PS-*b*-PMEO$_2$MA and casting in THF/DOX/DMF for PS-*b*-P(MEO$_2$MA-*stat*-OEOMA). The study on the influence of polymer concentration and evaporation time shows that a proper polymer concentration depends on the total molecular weight, while evaporation time of 10 s seems to result in the most ordered structure. Diethyl ether as a precipitation bath results in an ordered porous structure with open pores, while precipitation in water results in partially closed pores and distorted structure. The results present a high potential of PS-b-POEOMA for membrane application and open a path for applying novel tailored block copolymers in straightforward SNIPS technique.

8 Outlook

This work has explored and investigated the synthesis and solubility behaviour of POEOMAs in pure water and in presence of various type of additives. Further block copolymerization of OEOMA with styrene to provide biocompatible stimuli responsive block copolymers is investigated as well. Additionally, the possible application of such copolymers in SNIPS for membrane fabrication is investigated and fine-tuned.

ATRP is used for the synthesis of POEOMA homopolymers and also in combination of anionic polymerization for the synthesis of POEOMA minor blocks in block copolymerization. Although the synthesis method in this work is one of the novel methods so far for the synthesis of high molecular weight homopolymers and block copolymers, but thorough degassing via high vacuum technique and requirement of extra pure ingredients make it still not feasible to use in industrial application. Therefore, more industrially friendly methods like “reverse ATRP” or “ARGET ATRP” could be investigated as well. These methods are using $Cu^{II}Br$ as catalyst, which is much less sensitive to oxygen. So far, such methods have not provided the desired polydispersity needed for the stimuli responsive polymers’ high-tech applications and further optimization is needed to be able to utilize them instead of more precise polymerization methods.

Further OEOMAs could be used as stimuli responsive polymers either as homopolymer or in block copolymerization. The change of methacrylate to other functional groups such as styrene or acrylate provides a wide range of responsive materials to be used in vast applications. Moreover, the change of end functional group from methyl to ethyl or hydroxyl changes the temperature responsivity and can provide double responsiveness or fine-tune responsivity to further alter the polymeric materials by demand. As a simpler method, usage of additives can further alter the thermoresponsivity without the need to changing the synthesized material. A vast range of various additives are studied in this work and their effect on the solution behaviour of POEOMA copolymers are discussed. Expanding the library of additives with possible physiological application could improve the use of such polymers in drug delivery, tissue engineering or biosensors. Moreover, such knowledge could help understanding and improving the function of thermo switchable membranes fabricated from these stimuli responsive polymers.

The self-assembly of PS-*b*-POEOMA is studied in this research to investigate the possibility and success of SNIPS technique for membrane fabrication using such polymers. The interesting hexagonally packed standing cylindrical structure though, needs further investigation via more sophisticated techniques such as cryo-TEM or in situ SAX measurement to understand the mechanism of forming such a structure. Further studies on the optimization of SNIPS technique is needed as well to rule out any parameter that could result in a defected structure. Moreover, the separation function of the fabricated membranes (such as water flux and retention) and their stimuli responsivity needs further investigation.

9 Bibliography

[1] D. Roy, J. N. Cambre, and B. S. Sumerlin, "Future perspectives and recent advances in stimuli-responsive materials," *Prog. Polym. Sci.*, vol. 35, no. 1–2, pp. 278–301, 2010.

[2] S. Pavlukhina and S. Sukhishvili, "Polymer assemblies for controlled delivery of bioactive molecules from surfaces," *Adv. Drug Deliv. Rev.*, vol. 63, no. 9, pp. 822–836, 2011.

[3] E. S. Gil and S. M. Hudson, "Stimuli-reponsive polymers and their bioconjugates," *Prog. Polym. Sci.*, vol. 29, no. 12, pp. 1173–1222, 2004.

[4] M. S. Shim and Y. J. Kwon, "Stimuli-responsive polymers and nanomaterials for gene delivery and imaging applications," *Adv. Drug Deliv. Rev.*, vol. 64, no. 11, pp. 1046–1059, 2012.

[5] A. Abdollahi, H. Roghani-Mamaqani, B. Razavi, and M. Salami-Kalajahi, "The light-controlling of temperature-responsivity in stimuli-responsive polymers," *Polym. Chem.*, vol. 10, no. 42, pp. 5686–5720, 2019.

[6] R. P. Shaikh *et al.*, "A review of multi-responsive membranous systems for rate-modulated drug delivery.," *AAPS PharmSciTech*, vol. 11, no. 1, pp. 441–59, 2010.

[7] S. Chatterjee and P. C. Hui, "Review of Stimuli-Responsive Polymers in Drug Delivery and Textile Applicatio," *Molecules*, vol. 24, p. 2547, 2019.

[8] Q. Zhang, N. R. Ko, J. K. Oh, N. Re Ko, and J. Kwon Oh, "Recent advances in stimuli-responsive degradable block copolymer micelles: synthesis and controlled drug delivery applications," *Chem. Commun.*, vol. 48, no. 61, p. 7542, 2012.

[9] A. Saliba, L. Saias, E. Psychari, N. Minc, D. Simon, and F. Bidard, "Microfluidic sorting and multimodal typing of cancer cells in self-assembled magnetic arrays," vol. 107, no. 33, pp. 3–8, 2010.

[10] J. Hu, H. Meng, G. Li, and S. I. Ibekwe, "A review of stimuli-responsive polymers for smart textile applications," *Smart Mater. Struct.*, vol. 21, no. 5, 2012.

[11] A. Abdollahi, Z. Alinejad, and A. R. Mahdavian, "Facile and fast photosensing of polarity by stimuli-responsive materials based on spiropyran for reusable sensors: A physico-chemical study on the interactions," *J. Mater. Chem. C*, vol. 5, no. 26, pp. 6588–6600, 2017.

[12] T. Lu, S. Zhu, Z. Chen, W. Wang, W. Zhang, and D. Zhang, "Hierarchical photonic structured stimuli-responsive materials as high-performance colorimetric sensors," *Nanoscale*, vol. 8, no. 19, pp. 10316–10322, 2016.

[13] S. Jiang, F. Liu, A. Lerch, L. Ionov, and S. Agarwal, "Unusual and Superfast Temperature-Triggered Actuators," *Adv. Mater.*, vol. 27, no. 33, pp. 4865–4870, 2015.

[14] H. Ko and A. Javey, "Smart Actuators and Adhesives for Reconfigurable Matter," *Acc.*

Chem. Res., vol. 50, no. 4, pp. 691–702, 2017.

[15] A. Mourran, H. Zhang, R. Vinokur, and M. Möller, "Soft Microrobots Employing Nonequilibrium Actuation via Plasmonic Heating," *Adv. Mater.*, vol. 29, no. 2, 2017.

[16] P. F. Cao, J. D. Mangadlao, and R. C. Advincula, "Stimuli-Responsive Polymers and their Potential Applications in Oil-Gas Industry," *Polym. Rev.*, vol. 55, no. 4, pp. 706–733, 2015.

[17] V. Abetz, K. Kremer, M. Müller, and G. Reiter, "Functional Macromolecular Systems : Kinetic Pathways to Obtain Tailored Structures," *Macromol. Chem. Phys.*, vol. 220, 2019.

[18] K. Daumann, S. Frost, and M. Ulbricht, "Tunable and switchable nanoparticle separation with thermo-responsive track-etched membranes prepared by controlled surface-initiated polymerization of poly(N-isopropylacrylamide)," *RSC Adv.*, vol. 10, no. 36, pp. 21028–21038, 2020.

[19] M. Hosseini and A. S. Hamdy Makhlouf, *Industrial applications for intelligent polymers and coatings*. Springer International Publishing, 2016.

[20] M. A. Ward and T. K. Georgiou, "Thermoresponsive Polymers for Biomedical Applications," *Polymers (Basel).*, vol. 3, pp. 1215–1242, 2011.

[21] J. F. Lutz, "Thermo-switchable materials prepared using the OEGMA-platform," *Adv. Mater.*, vol. 23, no. 19, pp. 2237–2243, 2011.

[22] Q. Zhang, C. Weber, U. S. Schubert, and R. Hoogenboom, "Thermoresponsive polymers with lower critical solution temperature: From fundamental aspects and measuring techniques to recommended turbidimetry conditions," *Mater. Horizons*, vol. 4, no. 2, pp. 109–116, 2017.

[23] X. Wang, X. Qiu, and C. Wu, "Comparison of the Coil-to-Globule and the Globule-to-Coil Transitions of a Single Poly(N -isopropylacrylamide) Homopolymer Chain in Water," *Macromolecules*, vol. 31, no. 9, pp. 2972–2976, 1998.

[24] X. Wang, X. Qiu, and C. Wu, "Comparison of the Coil-to-Globule and the Globule-to-Coil Transitions of a Single Poly(*N* -isopropylacrylamide) Homopolymer Chain in Water," *Macromolecules*, vol. 31, no. 9, pp. 2972–2976, 1998.

[25] L. Hou and P. Wu, "LCST transition of PNIPAM-b-PVCL in water: Cooperative aggregation of two distinct thermally responsive segments," *Soft Matter*, vol. 10, no. 20, pp. 3578–3586, 2014.

[26] M. Xia, W. Wu, F. Liu, P. Theato, and M. Zhu, "Swelling behavior of thermosensitive nanocomposite hydrogels composed of oligo(ethylene glycol) methacrylates and clay," *Eur. Polym. J.*, vol. 69, pp. 472–482, 2015.

[27] R. Konefal, J. Spevacek, and P. Cernoch, "Thermoresponsive poly(2-oxazoline) homopolymers and copolymers in aqueous solutions studied by NMR spectroscopy and dynamic light scattering," *Eur. Polym. J.*, vol. 100, pp. 241–252, Mar. 2018.

[28] S. Sun and P. Wu, "On the thermally reversible dynamic hydration behavior of oligo(ethylene glycol) methacrylate-based polymers in water," *Macromolecules*, vol. 46, no. 1, pp. 236–246, 2013.

[29] Q. Zhang, C. Weber, U. S. Schubert, and R. Hoogenboom, "Thermoresponsive polymers with lower critical solution temperature: From fundamental aspects and measuring techniques to recommended turbidimetry conditions," *Mater. Horizons*, vol. 4, no. 2, pp. 109–116, 2017.

[30] N. T. Southall, K. A. Dill, and A. D. J. Haymet, "A view of the hydrophobic effect," *J. Phys. Chem. B*, vol. 106, no. 3, pp. 521–533, 2002.

[31] J. Seuring and S. Agarwal, "Polymers with upper critical solution temperature in aqueous solution: Unexpected properties from known building blocks," *ACS Macro Lett.*, vol. 2, no. 7, pp. 597–600, 2013.

[32] S. Fujishige, K. Kubota, and I. Ando, "Phase transition of aqueous solutions of poly(N-isopropylacrylamide) and poly(N-isopropylmethacrylamide)," *J. Mater. Chem.*, vol. 93, pp. 3311–3313, 1989.

[33] L. I. Valuev, V. V. Chupov, O. N. Zefirova, T. L. Lebedeva, and N. a. Plate, "Aqueous solutions of poly-N-alkyl-substituted acrylamides: Structure and properties related to targeted transport," *Pure Appl. Chem.*, vol. 67, no. 6, pp. 963–968, 1995.

[34] Y. Xia, X. Yin, N. a D. Burke, and H. D. H. Sto, "Thermal Response of Narrow-Disperse Poly (N-isopropylacrylamide) Prepared by Atom Transfer Radical Polymerization," *Macromolecules*, no. Scheme 1, pp. 5937–5943, 2005.

[35] C. Scherzinger, P. Lindner, M. Keerl, and W. Richtering, "Cononsolvency of poly(N, N-diethylacrylamide) (PDEAAM) and poly(N-isopropylacrylamide) (PNIPAM) based microgels in water/methanol mixtures: Copolymer vs core-shell microgel," *Macromolecules*, vol. 43, no. 16, pp. 6829–6833, 2010.

[36] M. A. Ward and T. K. Georgiou, "Multicompartment thermoresponsive gels: Does the length of the hydrophobic side group matter?," *Polym. Chem.*, vol. 4, no. 6, pp. 1893–1902, 2013.

[37] M. A. Ward and T. K. Georgiou, "Thermoresponsive terpolymers based on methacrylate monomers: Effect of architecture and composition," *J. Polym. Sci. Part A Polym. Chem.*, vol. 48, pp. 775–783, 2010.

[38] V. Bütün, S. P. Armes, and N. C. Billingham, "Synthesis and aqueous solution properties of near-monodisperse tertiary amine methacrylate homopolymers and diblock copolymers," *Polymer (Guildf).*, vol. 42, no. 14, pp. 5993–6008, 2001.

[39] E. Weißenborn and B. Braunschweig, "Hydroxypropyl cellulose as a green polymer for thermo-responsive aqueous foams," *Soft Matter*, vol. 15, no. 13, pp. 2876–2883, 2019.

[40] Y. Maeda, T. Nakamura, and I. Ikeda, "Hydration and phase behavior of poly(N-vinylcaprolactam) and poly(N-vinylpyrrolidone) in water," *Macromolecules*, vol. 35, no. 1, pp. 217–222, 2002.

[41] V. Kozlovskaya and E. Kharlampieva, " Self-Assemblies of Thermoresponsive Poly(N -vinylcaprolactam) Polymers for Applications in Biomedical Field ," *ACS Appl. Polym. Mater.*, vol. 2, no. 1, pp. 26–39, 2020.

[42] A. Amirova *et al.*, "Synthesis and investigation of thermo-induced gelation of partially cross-linked poly-2-isopropyl-2-oxazoline in aqueous media," *Polymers (Basel).*, vol. 12, no. 3, 2020.

[43] R. Hoogenboom, H. M. L. Thijs, M. J. H. C. Jochems, B. M. Van Lankvelt, M. W. M. Fijten, and U. S. Schubert, "Tuning the LCST of poly(2-oxazoline)s by varying composition and molecular weight: Alternatives to poly(N-isopropylacrylamide)?," *Chem. Commun.*, no. 44, pp. 5758–5760, 2008.

[44] H. G. Schild and D. A. Tirrell, "Microcalorimetric detection of lower critical solution temperatures in aqueous polymer solutions," *J. Phys. Chem.*, vol. 94, no. 10, pp. 4352–4356, 1990.

[45] K. Van Durme, G. Van Assche, H. Rahier, and B. Van Mele, "LCST demixing in poly(vinyl methyl ether)/water studied by means of a High Resolution Ultrasonic Resonator," *J. Therm. Anal. Calorim.*, vol. 98, no. 2, pp. 495–505, 2009.

[46] H. S. Ashbaugh and M. E. Paulaitis, "Monomer hydrophobicity as a mechanism for the LCST behavior of poly(ethylene oxide) in water," *Ind. Eng. Chem. Res.*, vol. 45, no. 16, pp. 5531–5537, 2006.

[47] A. Gandhi, A. Paul, S. O. Sen, and K. K. Sen, "Studies on thermoresponsive polymers: Phase behaviour, drug delivery and biomedical applications," *Asian J. Pharm. Sci.*, vol. 10, no. 2, pp. 99–107, 2015.

[48] P. Masson, G. Beinert, E. Franta, and P. Rempp, "Synthesis of Polyethylene Oxide Macromers," *Polym. Bull.*, vol. 7, pp. 17–22, 1982.

[49] K. Ito, H. Tsuchida, A. Hayashi, E. Yamada, and T. Matsumoto, "Reactivity of poly(ethylene oxide) macromonomers in radical copolymerization," *Polym. J.*, vol. 17, no. 7, pp. 827–839, 1985.

[50] J. F. Lutz, "Polymerization of oligo(ethylene glycol) (meth)acrylates: Toward new generations of smart biocompatible materials," *J. Polym. Sci. Part A Polym. Chem.*, vol. 46, no. 11, pp. 3459–3470, 2008.

[51] J. F. Lutz, Ö. Akdemir, and A. Hoth, "Point by point comparison of two thermosensitive polymers exhibiting a similar LCST: Is the age of poly(NIPAM) over?," *J. Am. Chem. Soc.*, vol. 128, no. 40, pp. 13046–13047, 2006.

[52] S. Han, M. Hagiwara, and T. Ishizone, "Synthesis of Thermally Sensitive Water-Soluble Polymethacrylates by Living Anionic Polymerizations of Oligo(ethylene glycol) Methyl Ether Methacrylates," *Macromolecules*, no. 36, pp. 8312–8319, 2003.

[53] S.-I. Yamamoto, J. Pietrasik, and K. Matyjaszewski, "The Effect of Structure on the Thermoresponsive Nature of Well-Defined Poly(oligo(ethylene oxide) methacrylates) synthesized by ATRP," *J. Polym. Sci. Part A Polym. Chem.*, vol. 46, pp. 194–202, 2008.

[54] P. Kujawa *et al.*, “Impact of End-Group Association and Main-Chain Hydration on the Thermosensitive Properties of Hydrophobically Modified Telechelic Poly(N-isopropylacrylamides) in Water,” *Macromolecules*, vol. 39, pp. 341–348, 2006.

[55] B.-P. Havazelet and S. Gryc, “Binding of Amino Acids to ‘Smart’ Sorbents: Where Does Hydrophobicity Come into Play?,” *Langmuir*, vol. 20, no. 1, pp. 169–174, 2004.

[56] J.-Y. Wu, S.-Q. Liu, P. W.-S. Heng, and Y.-Y. Yang, “Evaluating proteins release from, and their interactions with, thermosensitive poly (N-isopropylacrylamide) hydrogels,” *J. Control. Release*, vol. 10, no. 2, pp. 361–372, 2005.

[57] J.-F. Lutz, K. Weichenhan, Ö. Akdemir, and A. Hoth, “About the phase transitions in aqueous solutions of thermoresponsive copolymers and hydrogels based on 2-(2-methoxyethoxy) ethyl methacrylate and oligo (ethylene glycol) methacrylate,” *Macromolecules*, vol. 40, pp. 2503–2508, 2007.

[58] Y. Maeda, T. Kubota, H. Yamauchi, T. Nakaji, and H. Kitano, “Hydration changes of poly(2-(2-methoxyethoxy)ethyl methacrylate) during thermosensitive phase separation in water,” *Langmuir*, vol. 23, no. 22, pp. 11259–11265, 2007.

[59] Y. Maeda, H. Yamauchi, and T. Kubota, “Confocal micro-Raman and infrared spectroscopic study on the phase separation of aqueous poly(2-(2-methoxyethoxy)ethyl (meth)acrylate) solutions,” *Langmuir*, vol. 25, no. 1, pp. 479–482, 2009.

[60] B. Peng, N. Grishkewich, Z. Yao, X. Han, H. Liu, and K. C. Tam, “Self-assembly behavior of thermoresponsive oligo(ethylene glycol) methacrylates random copolymer,” *ACS Macro Lett.*, vol. 1, no. 5, pp. 632–635, 2012.

[61] B. Zhang, H. Tang, and P. Wu, “In depth analysis on the unusual multistep aggregation process of oligo(ethylene glycol) methacrylate-based polymers in water,” *Macromolecules*, vol. 47, no. 14, pp. 4728–4737, 2014.

[62] Z. L. Yao and K. C. Tam, “Temperature induced micellization and aggregation of biocompatible poly (oligo(ethylene glycol)methyl ether methacrylate) block copolymer analogs in aqueous solutions,” *Polymer (Guildf).*, vol. 53, no. 16, pp. 3446–3453, 2012.

[63] N. S. Ieong, M. Hasan, D. J. Phillips, Y. Saaka, R. K. O’Reilly, and M. I. Gibson, “Polymers with molecular weight dependent LCSTs are essential for cooperative behaviour,” *Polym. Chem.*, vol. 3, pp. 794–799, 2012.

[64] Y. Kudo, H. Mori, and Y. Kotsuchibashi, “Preparation of an ethylene glycol-based block copolymer consisting of six different temperature-responsive blocks,” *Polym. J.*, vol. 50, pp. 1013–1020, 2018.

[65] Y. Ogura, T. Terashima, and M. Sawamoto, “Amphiphilic PEG-Functionalized Gradient Copolymers via Tandem Catalysis of Living Radical Polymerization and Transesterification,” *Macromolecules*, vol. 50, no. 3, pp. 822–831, 2017.

[66] S. Medel, J. M. Garcia, L. Garrido, I. Quijada-Garrido, and R. Paris, “Thermo- and pH-responsive gradient and block copolymers based on 2-(2-methoxyethoxy)ethyl methacrylate synthesized via atom transfer radical polymerization and the formation of

thermoresponsive surfaces," *J. Polym. Sci. Part A Polym. Chem.*, vol. 49, pp. 690–700, 2011.

[67] K.-I. Seno, I. Tsujimoto, S. Kanaoka, and S. Aoshima, "Synthesis of Various Stimuli-Responsive Gradient Copolymers by Living Cationic Polymerization and Their Thermally or Solvent Induced Association Behavior," *J. Polym. Sci. Part A Polym. Chem.*, vol. 46, pp. 6444–6454, 2008.

[68] K.-I. Seno, I. Tsujimoto, T. Kikuchi, S. Kanaoka, and S. Aoshima, "Thermosensitive Gradient Copolymers by Living Cationic Polymerization: Semibatch Precision Synthesis and Stepwise Dehydration-Induced Micellization and Physical Gelation," *J. Polym. Sci. Part A Polym. Chem.*, vol. 46, pp. 6151–6164, 2008.

[69] K.-I. Seno, K. Shokoyoku, and A. Sadahito, "Thermosensitive Diblock Copolymers with Designed Molecular Weight Distribution: Synthesis by Continuous Living Cationic Polymerization and Micellization Behavior," *J. Polym. Sci. Part A Polym. Chem.*, vol. 46, pp. 2212–2221, 2007.

[70] S. Matsumoto, A. Kanazawa, S. Kanaoka, and S. Aoshima, "Dual stimuli-responsive copolymers with precisely arranged degradable units: synthesis by controlled alternating copolymerization of oxyethylene-containing vinyl ethers and conjugated aldehydes," *Polym. Chem.*, vol. 10, pp. 4134–4141, 2019.

[71] S. Eggers, T. Eckert, and V. Abetz, "Double thermoresponsive block-random copolymers with adjustable phase transition temperatures: From block-like to gradient-like behavior," *J. Polym. Sci. Part A Polym. Chem.*, pp. 399–411, 2017.

[72] N. Oleszko-Torbus, A. Utrata-Wesolek, W. Walach, and A. Dworak, "Solution behavior of thermoresponsive random and gradient copolymers of 2-n-propyl-2-oxazoline," *Eur. Polym. J.*, vol. 88, pp. 613–622, 2017.

[73] S. Jaksch *et al.*, "The collapse and aggregation of thermoresponsive poly(2-oxazoline) gradient copolymers: a time-resolved SANS study," *Colloid Polym. Sci.*, vol. 292, no. 10, pp. 2413–3425, 2014.

[74] W. Steinhauer, R. Hoogenboom, H. Keul, and M. Moeller, "Block and gradient copolymers of 2-hydroxyethyl acrylate and 2-methoxyethyl acrylate via RAFT: Polymerization kinetics, thermoresponsive properties, and micellization," *Macromolecules*, vol. 46, no. 4, pp. 1447–1460, 2013.

[75] M. C. M. Costa, S. M. C. Silva, and F. E. Antunes, "Adjusting the low critical solution temperature of poly(N-isopropyl acrylamide) solutions by salts, ionic surfactants and solvents: A rheological study," *J. Mol. Liq.*, vol. 210, pp. 113–118, 2015.

[76] D. Dhara and P. Chatterji, "Phase Transition in Linear and Cross-Linked Poly(N-Isopropylacrylamide) in Water: Effect of Various Types of Additives," *Polym. Rev.*, vol. 40, no. 1, pp. 51–68, 2000.

[77] Y. J. Zhang, S. Furyk, D. E. Bergbreiter, and P. S. Cremer, "Specific Ion effectis on the water solubility of acromolecules: PNIPAM and the Hofmeister series," *J. Am. Chem.*

Soc., vol. 127, no. 23, pp. 14505–14510, 2005.

[78] E. A. Algaer and N. F. A. Van Der Vegt, "Hofmeister ion interactions with model amide compounds," *J. Phys. Chem. B*, vol. 115, no. 46, pp. 13781–13787, 2011.

[79] L. Pérez-Fuentes, D. Bastos-González, J. Faraudo, and C. Drummond, "Effect of organic and inorganic ions on the lower critical solution transition and aggregation of PNIPAM," *Soft Matter*, vol. 14, no. 38, pp. 7818–7828, 2018.

[80] V. I. Michailova *et al.*, "Self-Assembly of a Thermally Responsive Double-Hydrophilic Copolymer in Ethanol-Water Mixtures: The Effect of Preferential Adsorption and Co-Nonsolvency," *J. Phys. Chem. B*, 2018.

[81] S. Eggers, B. Fischer, and V. Abetz, "Aqueous Solutions of Poly[2-(N -morpholino)ethyl methacrylate]: Learning about Macromolecular Aggregation Processes from a Peculiar Three-Step Thermoresponsive Behavior," *Macromol. Chem. Phys.*, vol. 217, no. 6, pp. 735–747, 2015.

[82] N. Lucht, S. Eggers, and V. Abetz, "Cononsolvency in the 'drunken' state: the thermoresponsiveness of a new acrylamide copolymer in water–alcohol mixtures," *Polym. Chem.*, vol. 8, no. 7, pp. 1196–1205, 2017.

[83] M. Dilip, N. J. Bridges, H. Rodriguez, J. F. B. Pereira, and R. D. Rogers, "Effect of Temperature on Salt-Salt Aqueous Biphasic Systems: Manifestations of Upper Critical Solution Temperature," *J. Solution Chem.*, vol. 44, pp. 454–468, 2014.

[84] P. J. Roth, F. D. Jochum, and P. Theato, "UCST-type behavior of poly[oligo(ethylene glycol) methyl ether methacrylate] (POEGMA) in aliphatic alcohols: solvent, co-solvent, molecular weight, and end group dependences," *Soft Matter*, vol. 7, no. 6, p. 2484, 2011.

[85] N. Guang, Shou-xin Liu, X. Li, L. Tian, and M. Hongguang, "Micellization and Gelation of the Double Thermoresponsive ABC-type Triblock Copolymer by One-pot RAFT Synthesis," *Chinese J. Polym. Sci.*, vol. 34, no. 8, pp. 956–980, 2016.

[86] W. Yuan and J. Wang, "Oligo(ethylene glycol) and quaternary ammonium-based block copolymer micelles: from tunable thermoresponse to dual salt response," *RSC Adv.*, vol. 4, p. 38855, 2014.

[87] Q. Fang, T. Chen, Q. Zhong, and J. Wang, "Thermoresponsive polymers based on oligo(ethylene glycol) methyl ether methacrylate and modified substrates with thermosensitivity," *Macromol. Res.*, vol. 25, no. 3, pp. 206–213, 2017.

[88] T. J. Murdoch *et al.*, "Enhanced specific ion effects in ethylene glycol-based thermoresponsive polymer brushes," *J. Colloid Interface Sci.*, vol. 490, pp. 869–878, 2017.

[89] N. Badi and J. F. Lutz, "Sequence control in polymer synthesis.," *Chem. Soc. Rev.*, vol. 38, no. 12, pp. 3383–3390, 2009.

[90] M. Kamigaito, T. Ando, and M. Sawamoto, *Metal-catalyzed living radical*

polymerization, vol. 101, no. 12. 2001.

[91] W. A. Braunecker and K. Matyjaszewski, “Controlled/living radical polymerization: Features, developments, and perspectives,” *Prog. Polym. Sci.*, vol. 32, no. 1, pp. 93–146, 2007.

[92] A. H. E. Müller and K. Matjaszewski, *Controlled and Living Polymerizations: From Mechanisms to Applications*. Wiley-VCH Verlag, Weinheim, 2009.

[93] J. Nicolas and Y. Guillaneuf, “Encyclopedia of Polymeric Nanomaterials,” in *Encyclopedia of Polymeric Nanomaterials*, Springer-Verlag Berlin Heidelberg, 2014.

[94] X. Tian, J. Ding, B. Zhang, F. Qiu, X. Zhuang, and Y. Chen, “Recent advances in RAFT polymerization: Novel initiation mechanisms and optoelectronic applications,” *Polymers (Basel).*, vol. 10, no. 1–26, 2018.

[95] S. Perrier, “50th Anniversary Perspective: RAFT Polymerization - A User Guide,” *Macromolecules*, vol. 50, pp. 7433–7447, 2017.

[96] X. Hu, N. Zhu, and K. Guo, “Advances in Organocatalyzed Atom Transfer Radical Polymerization,” *Adv. Polym. Technol.*, vol. 2019, pp. 1–9, 2019.

[97] N. Ayres, “Atom transfer radical polymerization: A robust and versatile route for polymer synthesis,” *Polym. Rev.*, vol. 51, pp. 138–162, 2011.

[98] T. G. Ribelli, F. Lorandi, M. Fantin, and K. Matyjaszewski, “Atom Transfer Radical Polymerization: Billion Times More Active Catalysts and New Initiation Systems,” *Macromol. Rapid Commun.*, vol. 40, no. 1, pp. 1–44, 2019.

[99] G. Odian, *Principles of polymerization*. Wiley interscience, 2004.

[100] V. Abetz and A. Boschetti-de-Fierro, *Block Copolymers in the Condensed State*, vol. 7. Elsevier B.V., 2012.

[101] M. Szwarc, “Living polymers,” *Nature*, vol. 178, no. 4543, pp. 1168–1169, 1956.

[102] R. Waack, A. Rembaum, J. D. Coombes, and M. Szwarc, “Molecular weights of ‘living’ polymers,” *J. Am. Chem. Soc.*, vol. 79, no. 8, pp. 2026–2027, 1957.

[103] H. Brody, M. Ladacki, R. Milkovitch, and M. Szwarc, “Molecular Peight of Living Polymers. Polybutadiene and Polyisoprene,” *J. Polym. Sci.*, no. 25, pp. 221–224, 1957.

[104] C. L. Lee, J. Smid, and M. Szwarc, “The mechanism of formation of living α-methylstyrene dimer and tetramer,” *J. Phys. Chem.*, vol. 66, pp. 904–907, 1962.

[105] D. H. Richards and R. L. Williams, “Structure of the tetramer of α-methylstyrene.pdf,” *J. Polym. Sci. Polym. Chem. Ed.*, pp. 89–104, 1973.

[106] M. Morton and F. R. Ells, “Absolute rates in anionic copolymerization,” *J. Polym. Sci.*, vol. 61, pp. 25–29, 1962.

[107] M. Morton and L. J. Fetters, “Homogeneous anionic polymerization. V. Association

phenomena in organolithium polymerization," *J. Polym. Sci. Part A Gen. Pap.*, vol. 2, pp. 3311–3326, 1964.

[108] C. M. Selman and H. L. Hsieh, "Effect of aggregate size on alkyllithium initiated polymerizations," *J Polym Sci Part B Polym Lett*, vol. 9, pp. 219–224, 1971.

[109] A. Hirao, R. Goseki, and T. Ishizone, "Advances in living anionic polymerization: From functional monomers, polymerization systems, to macromolecular architectures," *Macromolecules*, vol. 47, no. 6, pp. 1883–1905, 2014.

[110] V. Abetz, "Isoporous Block Copolymer Membranes," *Macromol. Rapid Commun.*, vol. 36, pp. 10–22, 2015.

[111] F. H. Schacher, P. A. Rupar, and I. Manners, "Functional block copolymers: Nanostructured materials with emerging applications," *Angew. Chemie - Int. Ed.*, vol. 51, no. 32, pp. 7898–7921, 2012.

[112] N. Hadjichristidis, H. Iatrou, S. Pispas, and M. Pitsikalis, "Anionic polymerization: high vacuum techniques," *J. Polym. Sci. Part A Polym. Chem.*, vol. 38, no. 18, pp. 3211–3234, 2000.

[113] J. S. Wang and K. Matyjaszewski, "Controlled/"living" radical polymerization. Atom transfer radical polymerization in the presence of transition-metal complexes," *J. Am. Chem. Soc.*, vol. 117, pp. 5614–5615, 1995.

[114] M. Sawamoto and T. Higashimura, "Polymerization of Methyl Methacrylate with the Carbon Tetrachloride/Dichlorotris-(triphenylphosphine)ruthenium(II)/Methylaluminum Bis(2,6-di-tert-butylphenoxide) Initiating System," vol. 28, pp. 1721–1723, 1995.

[115] R. J. Young and P. A. Lovell, *Introduction to polymers*, Third. CRC Press Taylor & Francis Group, 2011.

[116] K. Matyjaszewski, "Atom Transfer Radical Polymerization (ATRP): Current Status and Future Perspectives," *Macromolecules*, vol. 45, no. 10, pp. 4015–4039, 2012.

[117] K. Matyjaszewski, "Mechanistic and synthetic aspects of atom transfer radical polymerization," *J. Macromol. Sci. - Pure Appl. Chem.*, vol. 34, pp. 1785–1801, 1997.

[118] K. Matyjaszewski and J. Xia, "Atom transfer radical polymerization.," *Chem. Rev.*, vol. 101, pp. 2921–2990, 2001.

[119] G. Coullerez, A. Carlmark, E. Malmström, and M. Jonsson, "Understanding copper-based atom-transfer radical polymerization in aqueous media," *J. Phys. Chem. A*, vol. 108, no. 35, pp. 7129–7131, 2004.

[120] H. Fischer, "The persistent radical effect: A principle for selective radical reactions and living radical polymerizations," *Chem. Rev.*, vol. 101, no. 12, pp. 3581–3610, 2001.

[121] W. Tang, Y. Kwak, W. Braunecker, N. V. Tsarevsky, M. L. Coote, and K. Matyjaszewski, "Understanding atom transfer radical polymerization: Effect of ligand

and initiator structures on the equilibrium constants,” *J. Am. Chem. Soc.*, vol. 130, no. 32, pp. 10702–10713, 2008.

[122] A. A. Isse, C. Y. Lin, M. L. Coote, and A. Gennaro, “Estimation of standard reduction potentials of halogen atoms and alkyl halides,” *J. Phys. Chem. B*, vol. 115, no. 4, pp. 678–684, 2011.

[123] N. V. Tsarevsky, W. A. Braunecker, S. J. Brooks, and K. Matyjaszewski, “Rational selection of initiating/catalytic systems for the copper-mediated atom transfer radical polymerization of basic monomers in protic media: ATRP of 4-vinylpyridine,” *Macromolecules*, vol. 39, no. 20, pp. 6817–6824, 2006.

[124] T. Pintauer and K. Matyjaszewski, “Structural aspects of copper catalyzed atom transfer radical polymerization,” *Coord. Chem. Rev.*, vol. 249, pp. 1155–1184, 2005.

[125] Y. Yagci and M. A. Tasdelen, “Mechanistic transformations involving living and controlled/living polymerization methods,” *Prog. Polym. Sci.*, vol. 31, no. 12, pp. 1133–1170, 2006.

[126] S. Reinicke and H. Schmalz, “Combination of living anionic polymerization and ATRP via ‘click’ chemistry as a versatile route to multiple responsive triblock terpolymers and corresponding hydrogels,” *Colloid Polym. Sci.*, vol. 289, no. 5–6, pp. 497–512, 2011.

[127] M. H. Acar and K. Matyjaszewski, “Block copolymers by transformation of living anionic polymerization into controlled/"living’ atom transfer radical polymerization,” *Macromol. Chem. Phys.*, vol. 200, no. 5, pp. 1094–1100, 1999.

[128] A. Ramakrishnan and R. Dhamodharan, “a Novel and Simple Method of Preparation of Poly(Styrene-B-2-Vinylpyridine) Block Copolymer of Narrow Molecular Weight Distribution: Living Anionic Polymerization Followed By Mechanism Transfer To Controlled/‘Living’ Radical Polymerization (Atrp),” *J. Macromol. Sci. Part A*, vol. 37, no. 6, pp. 621–631, 2000.

[129] J. yeop Lee *et al.*, “Poly(styrene-r-butadiene)-b-poly(poly(ethylene glycol) methyl ether methacrylate) as a silica dispersant in rubber compounds,” *Polym. Int.*, vol. 63, no. 5, pp. 908–914, 2014.

[130] V. Abetz, A. Boschetti-de-Fierro, and J. Gohy, “Morphologies in Block Copolymers,” in *Controlled and Living Polymerizations: From Mechanisms to Applications*, Wiley-VCH Verlag GmbH & Co. KGaA, 2009, pp. 493–554.

[131] V. Abetz and P. F. W. Simon, “Phase behaviour and morphologies of block copolymers,” *Adv. Polym. Sci.*, vol. 189, no. 1, pp. 125–212, 2005.

[132] Y. Mai and A. Eisenberg, “Self-assembly of block copolymers,” *Chem. Soc. Rev.*, vol. 41, no. 18, pp. 5969–5985, 2012.

[133] V. Abetz and T. Goldacker, “Formation of superlattices via blending of block copolymers,” *Macromol. Rapid Commun.*, vol. 21, no. 1, pp. 16–34, 2000.

[134] G. H. F. F. S. Bates, “BLOCK COPOLYMER THERMODYNAMICS : Theory and

Experiment," *Annu. Rev. Phys. Chem.*, pp. 525–557, 1990.

[135] F. S. Bates, "Polymer-Polymer Phase Behavior," *Science (80-.).*, vol. 251, pp. 898–905, 1991.

[136] M. W. Matsen and F. S. Bates, "Block copolymer microstructures in the intermediate-segregation regime," *J. Chem. Phys.*, vol. 106, no. 1997, pp. 2436–2448, 1999.

[137] J. W. Lee, J. H. Kim, J. K. Lee, N. Kim, and S. H. Kim, "Mesoporous Composite Membrane Based on Block Copolymer Self-Assembly," *Macromol. Res.*, vol. 27, no. 10, pp. 974–981, 2019.

[138] S. Rangou *et al.*, "Self-organized isoporous membranes with tailored pore sizes," *J. Memb. Sci.*, vol. 451, pp. 266–275, 2014.

[139] Y. Zhang, J. L. Sargent, B. W. Boudouris, and W. A. Phillip, "Nanoporous membranes generated from self-assembled block polymer precursors: Quo Vadis?," *J. Appl. Polym. Sci.*, vol. 132, no. 21, pp. 1–17, 2015.

[140] A. Volker, "Isoporous Block Copolymer Membranes," *Macromol. Rapid Commun.*, vol. 36, no. 1, pp. 10–22, 2015.

[141] Q. Zhang, Y. Mun, Y. Gu, R. Mika, and U. Wiesner, "Tuning substructure and properties of supported asymmetric triblock terpolymer membranes," *Polymer (Guildf).*, vol. 107, pp. 398–405, 2016.

[142] S. Ramakrishna, Z. Ma, and T. Matsuura, *Polymer Membranes in Biotechnology: Preparation, Functionalization and Application*. World Scientific, 2011.

[143] J. F. Gohy, "Block Copolymer Micelles," *Adv. Polym. Sci.*, vol. 190, pp. 65–136, 2005.

[144] W. A. Phillip, B. O'neill, M. Rodwogin, M. A. Hillmyer, and E. L. Cussler, "Self-assembled block copolymer thin films as water filtration membranes," *ACS Appl. Mater. Interfaces*, vol. 2, no. 3, pp. 847–853, 2010.

[145] Y. Matsushita, "Microphase Separation (of Block Copolymers)," in *Encyclopedia of Polymeric Nanomaterials*, S. Kobayashi and K. Müllen, Eds. Berlin, Heidelberg: Springer Berlin Heidelberg, 2014, pp. 1–6.

[146] A. P.T.P and I. G. Wenten, "HUMIC SUBSTANCES REMOVAL BY POLYSULFONE-BASED ULTRAFILTRATION MEMBRANE : A REVIEW." 2015.

[147] F. Schacher, T. Rudolph, F. Wieberger, M. Ulbricht, and A. H. E. Müller, "Double stimuli-responsive ultrafiltration membranes from polystyrene-block-poly(N, N -dimethylaminoethyl methacrylate) diblock copolymers," *ACS Appl. Mater. Interfaces*, vol. 1, no. 7, pp. 1492–1503, 2009.

[148] S. Saleem, S. Rangou, C. Abetz, B. Lademann, V. Filiz, and V. Abetz, "Block copolymer membranes from polystyrene-b-poly(solketal methacrylate) (PS-b-PSMA) and amphiphilic polystyrene-b-poly(glyceryl methacrylate) (PS-b-PGMA)," *Polymers (Basel).*, vol. 9, no. 6, 2017.

[149] X. Shen, T. Xie, J. Wang, and F. Wang, "Improved fouling resistance of poly(vinylidene fluoride) membrane modified with poly(acryloyl morpholine)-based amphiphilic copolymer," *Colloid Polym. Sci.*, vol. 295, no. 7, pp. 1211–1221, 2017.

[150] S. Mazinani, S. Darvishmanesh, A. Ehsanzadeh, and B. Van der Bruggen, "Phase separation analysis of Extem/solvent/non-solvent systems and relation with membrane morphology," *J. Memb. Sci.*, vol. 526, no. October 2016, pp. 301–314, 2017.

[151] A. K. Hołda and I. F. J. Vankelecom, "Understanding and guiding the phase inversion process for synthesis of solvent resistant nanofiltration membranes," *J. Appl. Polym. Sci.*, vol. 42130, pp. 1–17, 2015.

[152] H. Sai *et al.*, "Hierarchical Porous Polymer Scaffolds from Block Copolymers," vol. 341, no. 6145, pp. 530–534, 2020.

[153] A. Troy and J. Scott, "Refractive Index of Ethanol-Water Mixtures and Density and Refractive Index of Ethanol-Water- Ethyl ether Mixtures," *J. Phys. Chem.*, vol. 50, pp. 406–412, 1946.

[154] J. . V. Herraez and R. Belda, "Viscous Synergy of Pure Monoalcohol Mixtures in Water and its Relation to Concentration," *J. Solution Chem.*, vol. 33, no. 2, pp. 117–129, 2004.

[155] Y. Tanaka, Y. Matsuda, H. Fujiwara, H. Kubota, and T. Makita, "Viscosity of (water + alcohol) mixtures under high pressure," *Int. J. Thermophys.*, vol. 8, no. 2, pp. 147–163, 1987.

[156] Y. Tanaka, T. Yamamoto, Y. Satomi, H. Kubota, and T. Makita, "Specific Volume and Viscosity of Ethanol-Water Mixtures under High Pressure," *Rev. Phys. Chem. Japan*, vol. 47, no. 1, pp. 12–24, 1977.

[157] M. Radjabian, C. Abetz, B. Fischer, A. Meyer, and V. Abetz, "Influence of Solvent on the Structure of an Amphiphilic Block Copolymer in Solution and in Formation of an Integral Asymmetric Membrane," *ACS Appl. Mater. Interfaces*, vol. 9, no. 37, pp. 31224–31234, 2017.

[158] J. F. Lutz and A. Hoth, "Preparation of Ideal Analoues with a Tunable Thermosensitivity by Controlled Radical Copolymerization of 2-(2-Methoxyethoxy)ethyl Methacrylate and Oligo(ethylene glycol) Methacrylate," *Macromolecules*, vol. 39, pp. 893–896, 2006.

[159] X. Wang and S. P. Armes, "Facile Atom Transfer Radical Polymerization of Methoxy-Capped Oligo (ethylene glycol) Methacrylate in Aqueous Media at Ambient Temperature," *Macrolecules*, vol. 33, pp. 6640–6647, 2000.

[160] L. Xue, U. S. Agarwal, and P. J. Lemstra, "High molecular weight PMMA by ATRP," *Macromolecules*, vol. 35, no. 22, pp. 8650–8652, 2002.

[161] C. Reichardt and T. Welston, *Solvents and Solvent Effects in Organic Chemistry*, 4th ed. wiley-VCH, 2011.

[162] G. Coullerez, A. Carlmark, E. Malmström, and M. Jonsson, "Understanding copper-based Atom Transfer Radical Polymerization in aqueous media," *J. Phys. Chem.*, vol.

108, no. 35, pp. 1–4, 2004.

[163] H. Bergenudd, G. Coullerez, M. Jonsson, and E. Malmström, “Solvent effects on ATRP of oligo(ethylene glycol) methacrylate. exploring the limits of control,” *Macromolecules*, vol. 42, no. 9, pp. 3302–3308, 2009.

[164] M. Horn and K. Matyjaszewski, “Solvent effects on the activation rate constant in atom transfer radical polymerization,” *Macromolecules*, vol. 46, no. 9, pp. 3350–3357, 2013.

[165] K. Matyjaszewski, B. Go1belt, H. Paik, and C. P. Horwitz, “Tridentate Nitrogen-Based Ligands in Cu-Based ATRP: A Structure - Activity Study,” *Macrolecules*, vol. 34, pp. 430–440, 2001.

[166] K. Matyjaszewski, “Structure-reactivity correlation in Atom Transfer Radical Polymerization,” *Macromol. Symp.*, vol. 182, pp. 209–224, 2002.

[167] J. Qiu, K. Matyjaszewski, L. Thouin, and C. Amatore, “Cyclic voltammetric studies of copper complexes catalyzing atom transfer radical polymerization,” *Macromol. Chem. Phys.*, vol. 201, no. 14, p. 1625, 2000.

[168] K. Matyjaszewski, M. J. Ziegler, S. V Arehart, D. Greszta, and T. Pakula, “Gradient copolymers by atom transfer radical copolymerization,” *J. Phys. Org. Chem.*, vol. 13, pp. 775–786, 2000.

[169] F. Hofmeister, “Zur Lehre von der Wirkung der Salze - Dritte Mittheilung,” *Arch. für Exp. Pathol. und Pharmakologie*, vol. 25, no. 1, pp. 1–30, 1889.

[170] W. Kunz, J. Henle, and B. W. Ninham, “‘Zur Lehre von der Wirkung der Salze’ (about the science of the effect of salts): Franz Hofmeister’s historical papers,” *Curr. Opin. Colloid Interface Sci.*, vol. 9, pp. 19–37, 2004.

[171] J. Heyda and J. Dzubiella, “Thermodynamic Description of Hofmeister Effects on the LCST of Thermosensitive Polymers,” *J. Phys. Chem. B*, vol. 118, pp. 10979–10988, 2014.

[172] Y. Zhang and P. S. Cremer, “Chemistry of Hofmeister anions and osmolytes.,” *Annu. Rev. Phys. Chem.*, vol. 61, pp. 63–83, 2010.

[173] T. S. Peter H. von Hippel, “Ion effects on the Solution Structure of Biological macromolecules,” *Acc. Chem. Res.*, vol. 2, pp. 257–265, 1969.

[174] Y. Q. Gao, “Simple Theory for Salt Effects on the Solubility of Amide,” *J. Phys. Chem. B*, vol. 116, p. 9934−9943, 2012.

[175] A. Ciferri and A. Perico, *Ionic interations in Natural and Synthetic Macromolecules*. Wiley, 2012.

[176] P. M. and K. J. Mysels, *Mukerjee, P. and Mysels, K.J. (1971) Critical Micelle Concentration of Aqueous Surfactant Systems. Vol. 36, US Government Printing Office, Washington DC.*, vol. 36. US Government Printing Office, 1971.

[177] J. M. Neugebauer, “Detergents: An overview,” *Methods in Enyzmology*, vol. 182, pp. 239–253, 1990.

[178] S. Roe, *Protein Purification Application: A Practical Approach*. Oxford University Press, 1990.

[179] T. B. R. Walter, J.Ricka, Ch. Quellet, Ch. Nyffenegger, “Coil−Globule Transition of Poly(N-isopropylacrylamide), A Study of Polymer−Surfactant Association.pdf,” *Macromolecules*, vol. 29, pp. 4019–4028, 1996.

[180] C. Wu and S. Zhou, “Effects of surfactants on the phase transition of poly(N-isopropylacrylamide) in water,” *J. Polym. Sci. Part B Polym. Phys.*, vol. 34, no. 9, pp. 1597–1604, 1996.

[181] M. Sakai, N. Satoh, K. Tsujii, Y. Q. Zhang, and T. Tanaka, “Effects of Surfactants on the Phase Transition of a Hydrophobic Polymer Gel,” *Langmuir*, vol. 11, no. 7, pp. 2493–2495, 1995.

[182] E. Kokufuta, Y.-Q. Zhang, T. Tanaka, and A. Mamada, “Effects of surfactants on the phase transition of poly(N-isopropylacrylamide) Gel,” *Macromolecules*, vol. 26, pp. 1053–1059, 1996.

[183] H. G. Schild and D. A. Tirrell, “Interaction of Poly(N-isopropylacrylamide) with Sodium n-Alkyl Sulfates in Aqueous Solution,” *Langmuir*, vol. 7, no. 4, pp. 665–671, 1991.

[184] Q. Fang, T. Chen, Q. Zhong, and J. Wang, “Thermoresponsive polymers based on oligo(ethylene glycol) methyl ether methacrylate and modified substrates with thermosensitivity,” *Macromol. Res.*, vol. 25, no. 3, pp. 206–213, 2017.

[185] K. Kyriakos *et al.*, “Quantifying the Interactions in the Aggregation of Thermoresponsive Polymers: The Effect of Cononsolvency,” *Macromol. Rapid Commun.*, vol. 37, no. 5, pp. 420–425, 2016.

[186] R. O. . Costa and R. F. . Freitas, “Phase behavior of poly(N-isopropylacrylamide) in binary aqueous solutions,” *Polymer (Guildf).*, vol. 43, no. 22, pp. 5879–5885, 2002.

[187] S. Y. Noskov, G. Lamoureux, and B. Roux, “Molecular dynamics study of hydration in ethanol-water mixtures using a polarizable force field,” *J. Phys. Chem. B*, vol. 109, no. 14, pp. 6705–6713, 2005.

[188] P. J. Roth, M. Collin, and C. Boyer, “Advancing the boundary of insolubility of non-linear PEG-analogues in alcohols: UCST transitions in ethanol-water mixtures,” *Soft Matter*, vol. 9, no. 6, pp. 1825–1834, 2013.

[189] N. V Tsarevsky, T. Sarbu, B. Go, and K. Matyjaszewski, “Synthesis of Styrene - Acrylonitrile Copolymers and Related Block Copolymers by Atom Transfer Radical Polymerization,” *Macromolecules*, vol. 35, no. 16, pp. 6142–6148, 2002.

[190] R. P. Quirk, D. L. Pickel, and H. Hasegawa, “Anionic polymerization chemistry of epoxides: Electron-transfer processes,” *Macromol. Symp.*, vol. 226, pp. 69–77, 2005.

[191] R. P. Quirk and G. M. Lizárraga, “Investigation of the Reaction of Poly(styryl)lithium with Propylene Oxide,” *Macromolecules*, vol. 31, no. 11, pp. 3424–3430, 1998.

[192] A. Bey, O. Dreyer, and V. Abetz, “Thermodynamic analysis of alkali metal complex formation of polymer-bonded crown ether,” *Phys. Chem. Chem. Phys.*, vol. 19, pp. 15924–15932, 2017.

[193] K. S. Pafiti, C. S. Patrickios, V. Filiz, S. Rangou, C. Abetz, and V. Abetz, “Styrene-vinyl pyridine diblock copolymers: Achieving high molecular weights by the combination of anionic and reversible addition-fragmentation chain transfer polymerizations,” *J. Polym. Sci. Part A Polym. Chem.*, vol. 51, no. 1, pp. 213–221, 2013.

[194] M. Bozorg, B. Hankiewicz, and V. Abetz, “Solubility behaviour of random and gradient copolymers of di- And oligo(ethylene oxide) methacrylate in water: Effect of various additives,” *Soft Matter*, vol. 16, no. 4, pp. 1066–1081, 2020.

[195] M. Bozorg, B. Hankiewicz, and V. Abetz, “Solubility behaviour of random and gradient copolymers of di- and oligo(ethylene oxide) methacrylate in water: Effect of various additives,” *Soft Matter*, 2019.

[196] A. A. Gridnev and S. D. Ittel, “Dependence of free-radical propagation rate constants on the degree of polymerization,” *Macromolecules*, vol. 29, no. 18, pp. 5864–5874, 1996.

[197] D. Neugebauer, Y. Zhang, T. Pakula, S. S. Sheiko, and K. Matyjaszewski, “Densely-grafted and double-grafted PEO brushes via ATRP. A route to soft elastomers,” *Macromolecules*, vol. 36, no. 18, pp. 6746–6755, 2003.

[198] C. Reichardt and T. Welton, *Solvents and Solvent Effects in Organic Chemistry: Fourth Edition*. 2003.

[199] T. Ishizone, S. Han, M. Hagiwara, and H. Yokoyama, “Synthesis and surface characterization of well-defined amphiphilic block copolymers containing poly [oligo(ethylene glycol) methacrylatel segments,” *Macromolecules*, vol. 39, no. 3, pp. 962–970, 2006.

[200] C. M. Hansen, *Hansen Solubility Parameters A User’s Handbook*. CRC Press Taylor & Francis Group, 2007.

[201] V. D. W. Krevelen, *Properties of Polymers*. 1990.

[202] E. Stefanis and C. Panayiotou, “Prediction of hansen solubility parameters with a new group-contribution method,” *Int. J. Thermophys.*, vol. 29, no. 2, pp. 568–585, 2008.

[203] C. M. Hansen, “Solubility Parameters — An Introduction,” *Hansen Solubility Parameters A User’s Handb.*, pp. 1–24, 2000.

[204] E. Stefanis, L. Constantinou, and C. Panayiotou, “A Group-Contribution Method for Predicting Pure Component Properties of Biochemical and Safety Interest,” *Ind. Eng. Chem. Res. 2004,* vol. 43, pp. 6253–6261, 2004.

[205] P. Vandezande, X. Li, L. E. M. Gevers, and I. F. J. Vankelecom, “High throughput study

of phase inversion parameters for polyimide-based SRNF membranes," vol. 330, pp. 307–318, 2009.

[206] M. Rubinstein and R. H. Colby, *Polymer Physics*. New York: Oxford, university press, 2003.

[207] E. A. G. J. Brandrup, E. H. Immergut, *Polymer Handbook*. JOH N WILE Y & SONS , INC .

[208] T. G. Haenelt *et al.*, "Morphology and elasticity of polystyrene-Block-polyisoprene diblock copolymers in the melt," *Korea Aust. Rheol. J.*, vol. 26, no. 3, pp. 263–275, 2014.

[209] S. Chaudhury, J. Gaalken, J. Meyer, and M. Ulbricht, "Calorimetric studies of PEO-b-PMMA and PEO-b-PiPMA diblock copolymers synthesized via atom transfer radical polymerization," *Polym. (United Kingdom)*, vol. 139, pp. 11–19, 2018.

[210] D. J. T. Hill, A. K. Whittaker, and K. W. Wong, "Miscibility and specific interactions in blends of poly(4-vinylphenol) and poly(2-ethoxyethyl methacrylate)," *Macromolecules*, vol. 32, no. 16, pp. 5285–5291, 1999.

[211] J. Yamanaka, T. Kayasuga, M. Ito, H. Yokoyama, and T. Ishizone, "Synthesis of water-soluble poly[oligo(ethylene glycol) methacrylate]s by living anionic polymerization of oligo(ethylene glycol) vinyl ether methacrylates," *Polym. Chem.*, vol. 2, no. 8, p. 1837, 2011.

[212] S. Förster *et al.*, "Scattering curves of ordered mesoscopic materials," *J. Phys. Chem. B*, vol. 109, no. 4, pp. 1347–1360, 2005.

[213] S. Sakurai, H. Fujiwara, G. Kimura, and Y. Mizuno, "Perpendicular orientation of cylindrical nanodomains in a block copolymer thick film," in *Pacifichem 2010*, 2010, p. MACRO-345.

[214] S. Sakurai, G. Kimura, H. Yamanishi, and H. Yoshida, "Spontaneous perpendicular orientation of cylindrical microdomains in a thick film of block copolymers," *IOP Conf. Ser. Mater. Sci. Eng.*, vol. 14, p. 012004, 2010.

[215] S. Sakurai *et al.*, "Spontaneous perpendicular orientation of cylindrical microdomains in a block copolymer thick film," *Macromolecules*, vol. 42, no. 6, pp. 2115–2121, 2009.

[216] H. Ohnogi, S. Sasaki, and S. Sakurai, "Evaluation of Grain Size by Small-Angle X-Ray Scattering for a Block Copolymer Film-Perpendicularly Oriented.pdf," *Macromol. Symp.*, vol. 366, pp. 35–41, 2016.

[217] H. Ohnogi, T. Isshiki, S. Sasaki, and S. Sakurai, "Intriguing transmission electron microscopy images observed for perpendicularly oriented cylindrical microdomains of block copolymers," *Nanoscale*, vol. 6, no. 18, pp. 10817–10823, 2014.

[218] S. Tomita, H. Urakawa, I. Wataoka, S. Sasaki, and S. Sakurai, "Complete and comprehensive orientation of cylindrical microdomains in a block copolymer sheet," *Polym. J.*, vol. 48, no. 12, pp. 1123–1131, 2016.

[219] S. Tomita, N. Shimizu, N. Igarashi, H. Takagi, S. Sasaki, and S. Sakurai, "Coalescence of non-equilibrium spheres through thermal annealing in a polystyrene-block-poly(ethylene-co-butylene)-block-polystyrene triblock copolymer film under a uniaxially stretched state," *Polym. J.*, vol. 49, no. 6, pp. 519–526, 2017.

[220] S. Tomita, N. Shimizu, N. Igarashi, H. Takagi, S. Sasaki, and S. Sakurai, "Time-resolved 2d-SAXS measurements to reveal mechanism of cylinder orientation upon sphere-to-cylinder transition under a planar flow in an SEBS triblock copolymer sheet," *Eur. Polym. J.*, vol. 93, no. May, pp. 382–389, 2017.

[221] G. Cui *et al.*, "Perpendicular oriented cylinders via directional coalescence of spheres embedded in block copolymer films induced by solvent annealing," *Polymer (Guildf).*, vol. 55, no. 6, pp. 1601–1608, 2014.

[222] G. Cui *et al.*, "Macroscopic alignment of cylinders via directional coalescence of spheres along annealing solvent permeation directions in block copolymer thick films," *Macromolecules*, vol. 47, no. 17, pp. 5989–5999, 2014.

[223] I. W. Hamley and V. Castelletto, *Small-angle scattering of block copolymers in the melt, solution and crystal states*, vol. 29, no. 9. 2004.

[224] S. Eggers, F. Lauterbach, and V. Abetz, "Synthesis and self-assembly of high molecular weight polystyrene-block-poly[2-(N-morpholino)ethyl methacrylate]: A story about microphase separation, amphiphilicity, and stimuli-responsivity," *Polym. (United Kingdom)*, vol. 107, no. 107, pp. 357–367, 2016.

[225] I. W. Hamley, "Structure and flow behaviour of block copolymers," *J. Phys. Condens. Matter*, vol. 13, no. 33, 2001.

[226] M. W. Matsen and F. S. Bates, "Origins of complex self-assembly in block copolymers," *Macromolecules*, vol. 29, no. 23, pp. 7641–7644, 1996.

[227] E. B. Zhulina and O. V. Borisov, "Theory of block polymer micelles: Recent advances and current challenges," *Macromolecules*, vol. 45, no. 11, pp. 4429–4440, 2012.

[228] M. Radjabian and V. Abetz, "Tailored pore sizes in integral asymmetric membranes formed by blends of block copolymers," *Adv. Mater.*, vol. 27, no. 2, pp. 352–355, 2015.

[229] C. Stegelmeier *et al.*, "Supporting Information Transient block copolymer topologies for generating nanoporous polymer membranes," pp. 1–8.

[230] W. A. Phillip, M. A. Hillmyer, and E. L. Cussler, "Cylinder orientation mechanism in block copolymer thin films upon solvent evaporation," *Macromolecules*, vol. 43, no. 18, pp. 7763–7770, 2010.

[231] S. P. Nunes *et al.*, "From micelle supramolecular assemblies in selective solvents to isoporous membranes," *Langmuir*, vol. 27, no. 16, pp. 10184–10190, 2011.

[232] J. Hahn *et al.*, "Structure formation of integral-asymmetric membranes of polystyrene-block-Poly(ethylene oxide)," *J. Polym. Sci. Part B Polym. Phys.*, vol. 51, no. 4, pp. 281–290, 2013.

[233] M. Karunakaran, S. P. Nunes, X. Qiu, H. Yu, and K. V. Peinemann, “Isoporous PS-b-PEO ultrafiltration membranes via self-assembly and water-induced phase separation,” *J. Memb. Sci.*, vol. 453, pp. 471–477, 2014.

[234] R. M. Dorin, W. A. Phillip, H. Sai, J. Werner, M. Elimelech, and U. Wiesner, “Designing block copolymer architectures for targeted membrane performance,” *Polym. (United Kingdom)*, vol. 55, no. 1, pp. 347–353, 2014.

10 Appendix

10.1 results of DLS measurements of gradient and random copolymers of MEO_2MA and OEOMA in aqueous solution in presence of various additives

In the following, the results of DLS measurements of gradient and random copolymers MEO_2MA and OEOMA containing around 20 mol% OEOMA in aqueous solution and in presence of various additives is shown. In all cases, the lower graphs show the normalized scattering intensity and the upper ones, the hydrodynamic radius. The dashed lines show the LCST. The type of additive as well as the additive concentration is mentioned on each graph. To make the comparison easier, for each additive the results for random and gradient copolymers are plotted after each other.

More than two-step aggregation is observed in the phase transition behavior of gradient and random copolymers in the presence of different salts indicating their high interaction with the polymer chain. In presence of kosmotropic salts, the second phase transition temperature is also decreasing by the increase of salt concentration. Three phase transition temperatures are observed in the case of strong kosmotropic cations.

10.1.1 The effect of anions

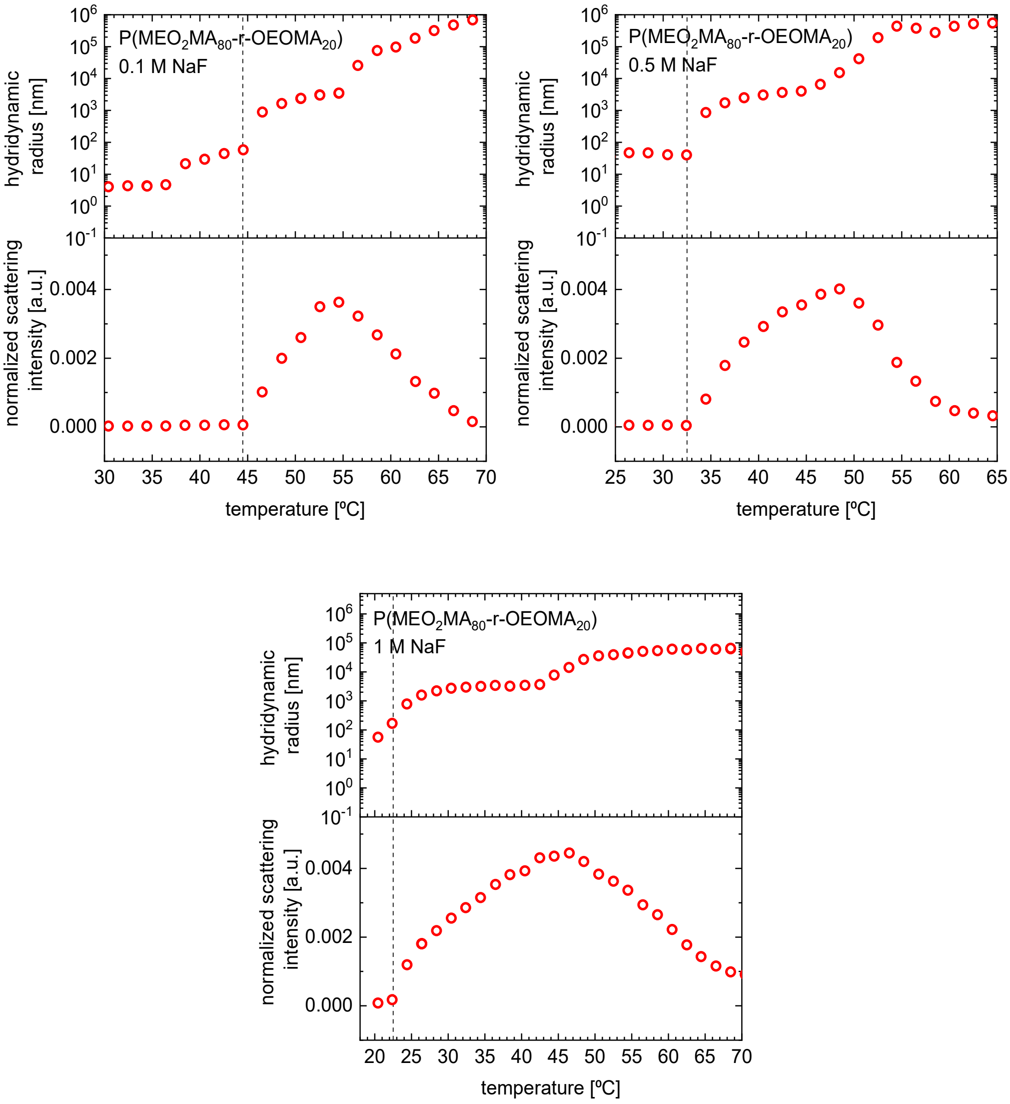

Fig. A1 DLS measurements of the random copolymer P(MEO$_2$MA$_{80}$-*r*-OEOMA$_{20}$), M_n = 15.96 kDa, Đ = 1.17) in NaF aqueous solution. The vertical dashed lines point out the abrupt change in the hydrodynamic radius (upper graph) and the normalized scattering intensity (lower graph) and indicates the LCST.

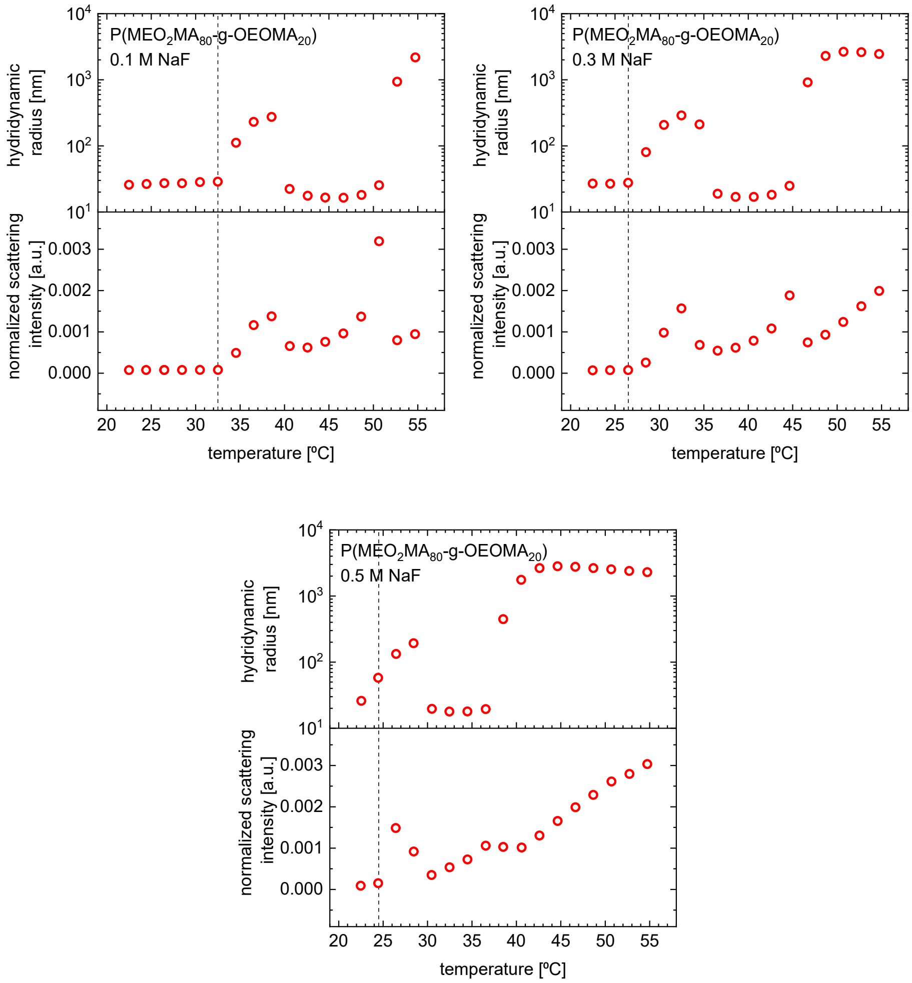

Fig. A2 DLS measurements of the gradient copolymer P(MEO$_2$MA$_{80}$-*g*-OEOMA$_{20}$), M_n = 15.21 kDa, Đ = 1.24 in NaF aqueous solution. The vertical dashed lines point out the abrupt change in the hydrodynamic radius (upper graph) and the normalized scattering intensity (lower graph) and indicates the LCST.

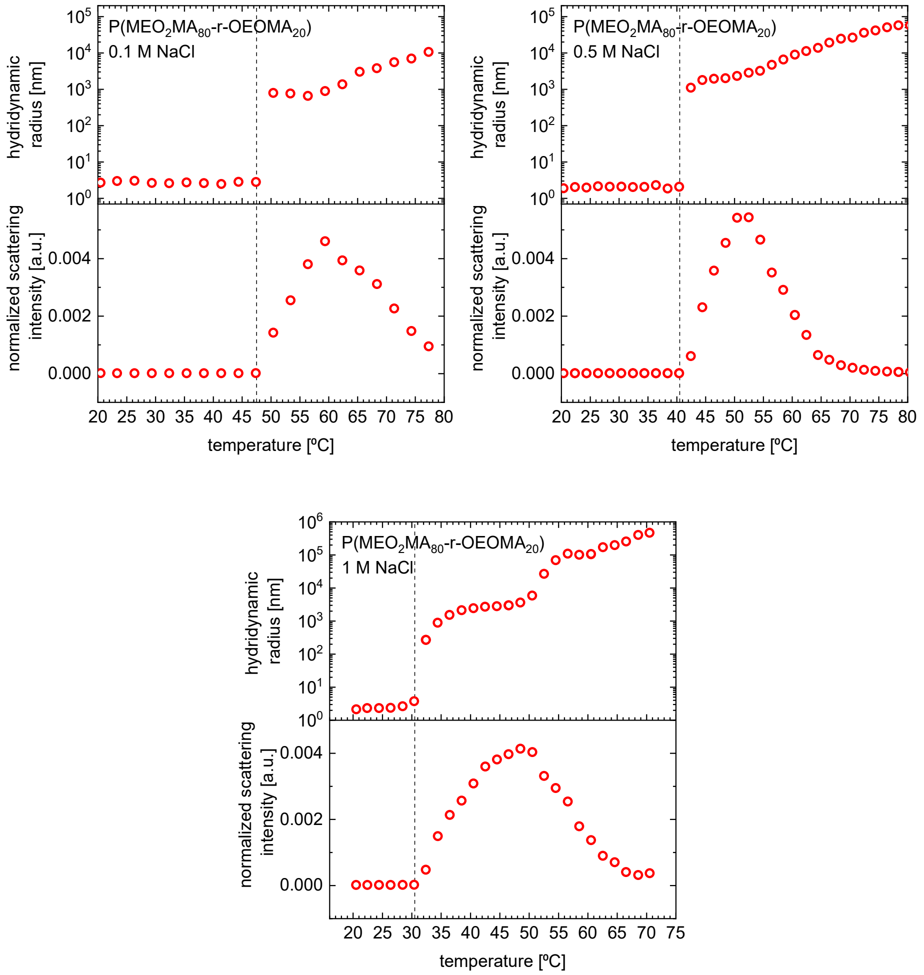

Fig. A3 DLS measurements of the random copolymer P(MEO$_2$MA$_{80}$-*r*-OEOMA$_{20}$), M_n = 15.96 kDa, Đ = 1.17) in NaCl aqueous solution. The vertical dashed lines point out the abrupt change in the hydrodynamic radius (upper graph) and the normalized scattering intensity (lower graph) and indicates the LCST.

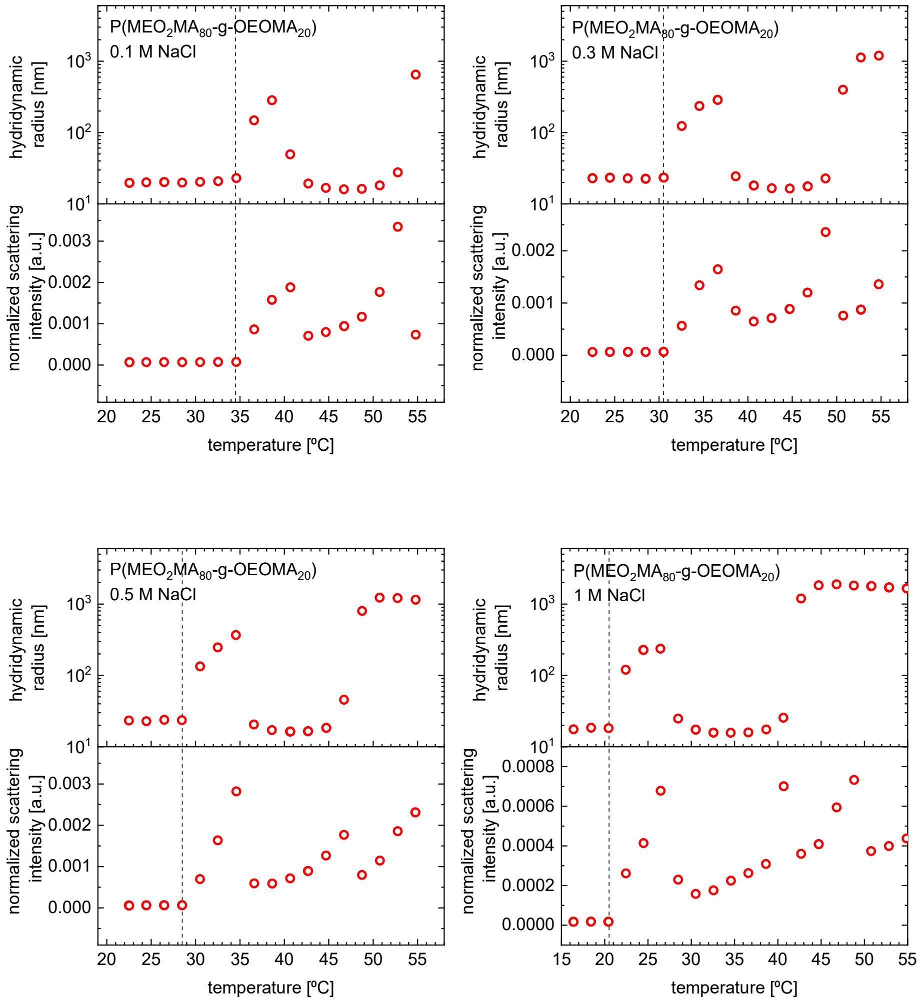

Fig. A4 DLS measurements of the gradient copolymer P(MEO$_2$MA$_{80}$-g-OEOMA$_{20}$), M$_n$ = 15.21 kDa, Đ = 1.24 in NaCl aqueous solution. The vertical dashed lines point out the abrupt change in the hydrodynamic radius (upper graph) and the normalized scattering intensity (lower graph) and indicates the LCST.

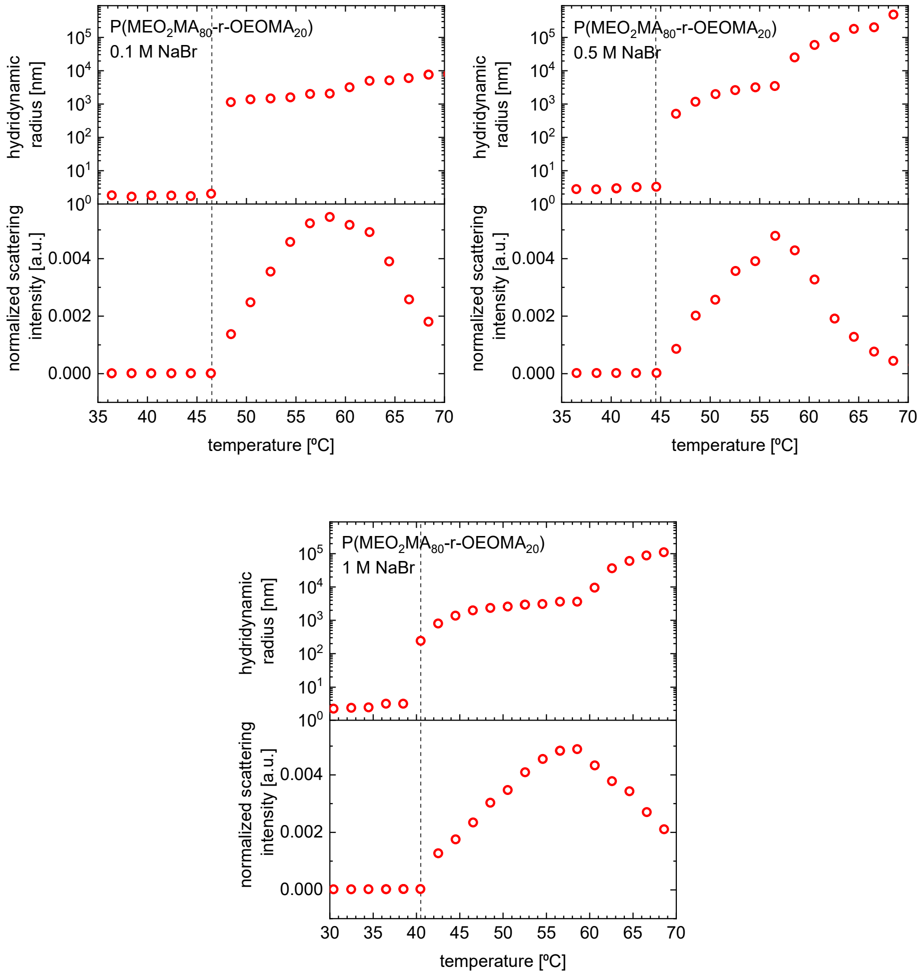

Fig. A5 DLS measurements of the random copolymer P(MEO_2MA_{80}-*r*-$OEOMA_{20}$), M_n = 15.96 kDa, Đ = 1.17) in NaBr aqueous solution. The vertical dashed lines point out the abrupt change in the hydrodynamic radius (upper graph) and the normalized scattering intensity (lower graph) and indicates the LCST.

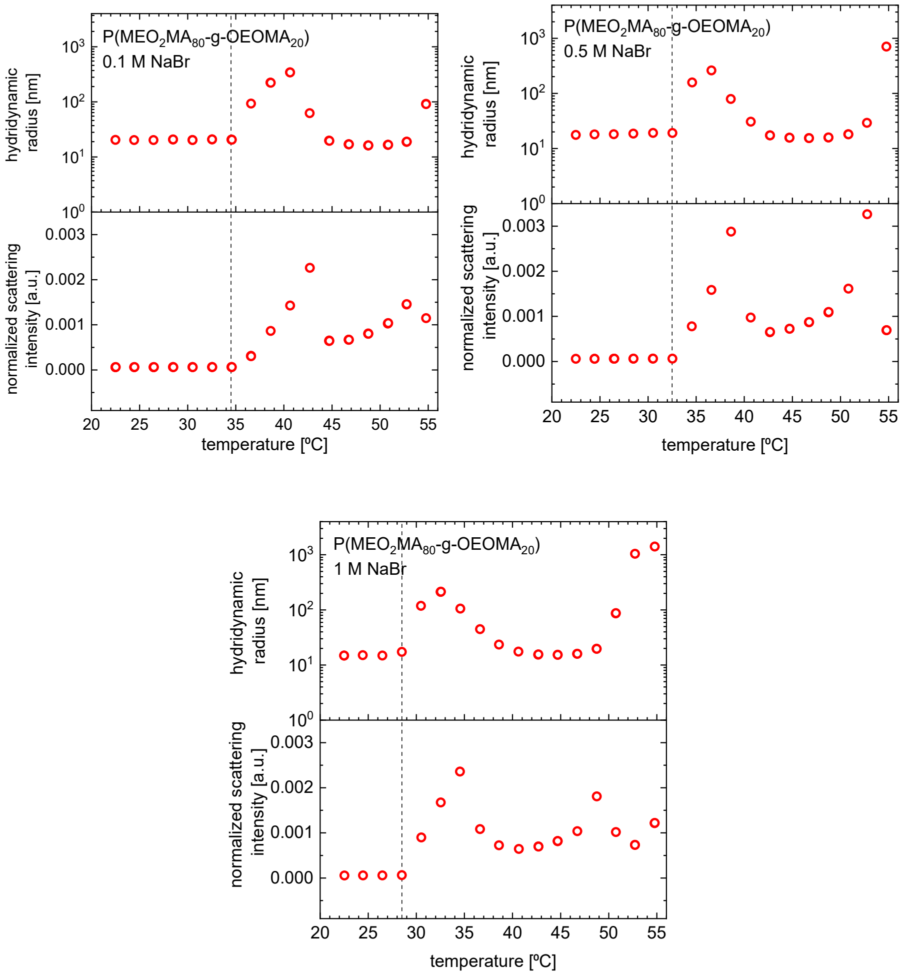

Fig. A6 DLS measurements of the gradient copolymer P(MEO$_2$MA$_{80}$-*g*-OEOMA$_{20}$), M_n = 15.21 kDa, Đ = 1.24 in NaBr aqueous solution. The vertical dashed lines point out the abrupt change in the hydrodynamic radius (upper graph) and the normalized scattering intensity (lower graph) and indicates the LCST.

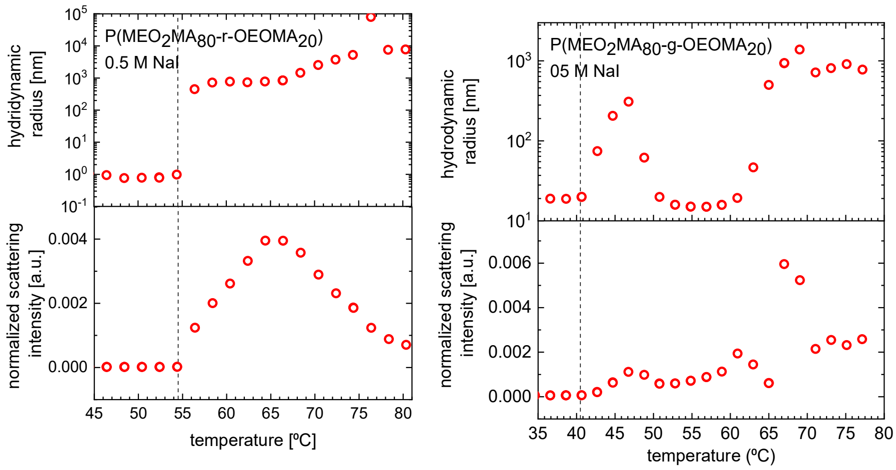

Fig. A7 DLS measurements of the random copolymer P(MEO$_2$MA$_{80}$-*r*-OEOMA$_{20}$), M$_n$ = 15.96 kDa, Đ = 1.17 (left) and gradient copolymer P(MEO$_2$MA$_{80}$-*g*-OEOMA$_{20}$), M$_n$ = 15.21 kDa, Đ = 1.24 (right) in NaI aqueous solution. The vertical dashed lines point out the abrupt change in the hydrodynamic radius (upper graph) and the normalized scattering intensity (lower graph) and indicates the LCST.

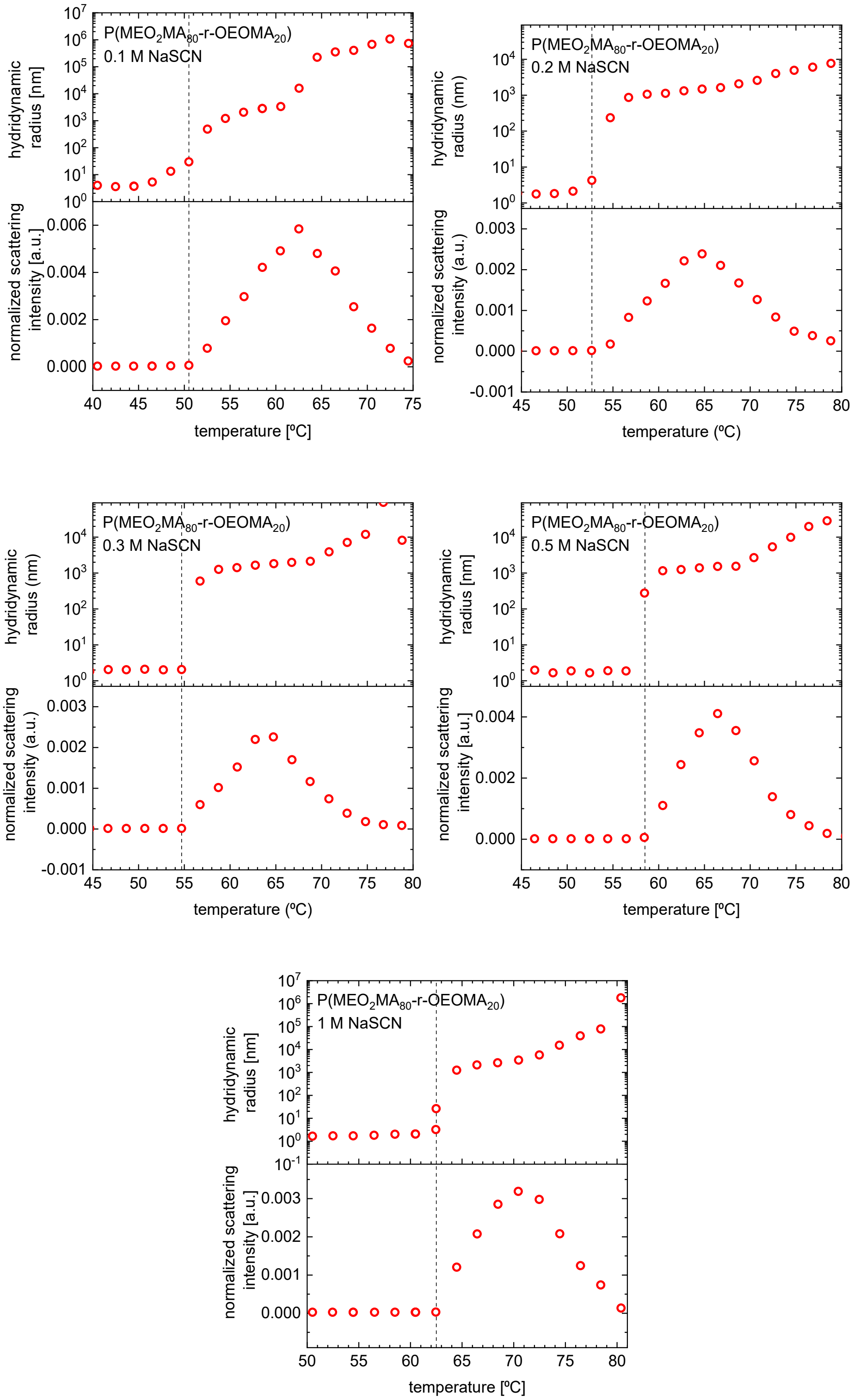

Fig. A8 DLS measurements of the random copolymer P(MEO2MA$_{80}$-*r*-OEOMA$_{20}$), M$_n$ = 15.96 kDa, Đ = 1.17) in NaSCN aqueous solution. The vertical dashed lines point out the abrupt change in the hydrodynamic radius (upper graph) and the normalized scattering intensity (lower graph) and indicates the LCST.

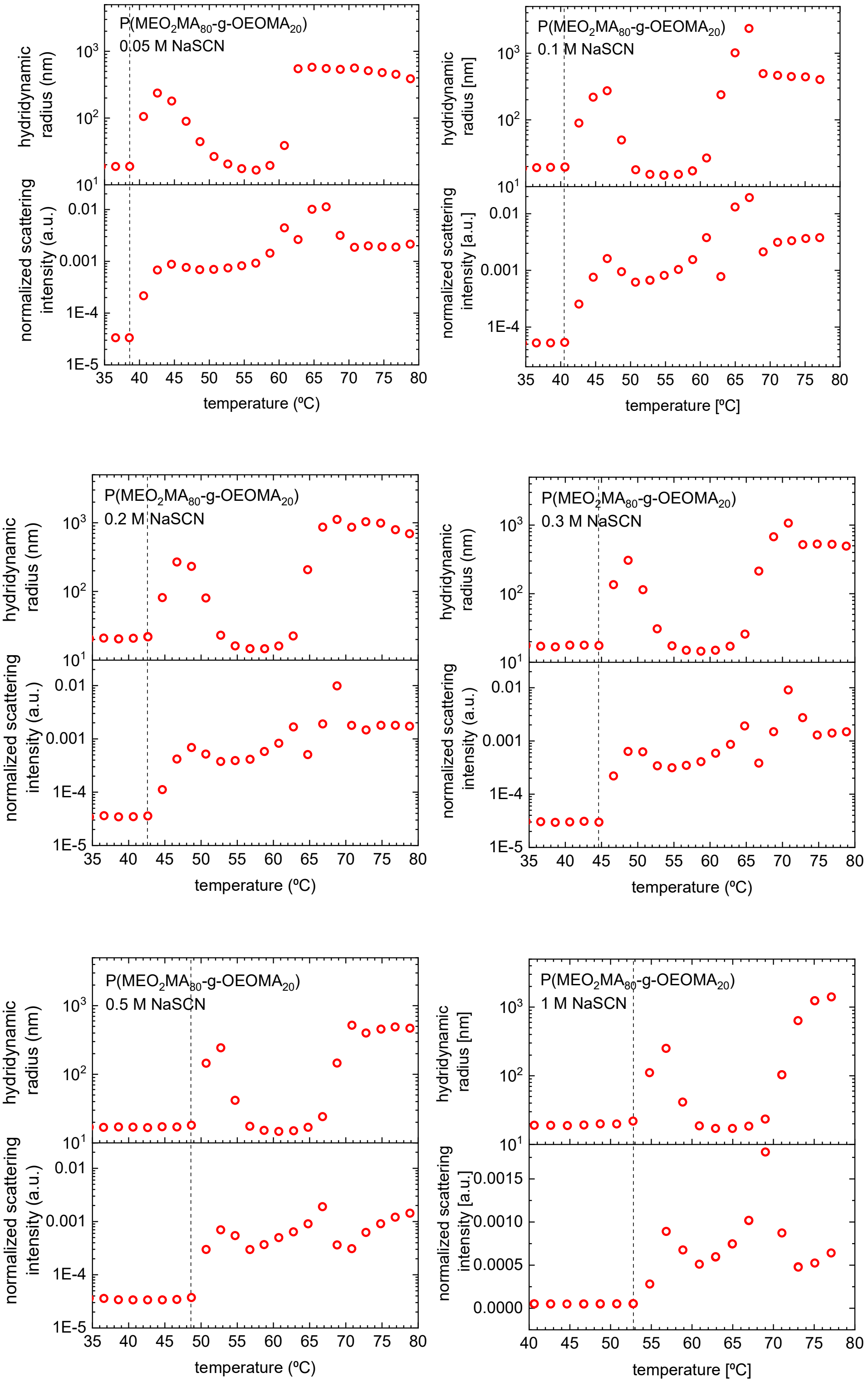

Fig. A9 DLS measurements of the gradient copolymer P(MEO$_2$MA$_{80}$-*g*-OEOMA$_{20}$), Mn = 15.21 kDa, Đ = 1.24 in NaSCN aqueous solution. The vertical dashed lines point out the abrupt change in the hydrodynamic radius (upper graph) and the normalized scattering intensity (lower graph) and indicates the LCST.

10.1.2 The effect of cations

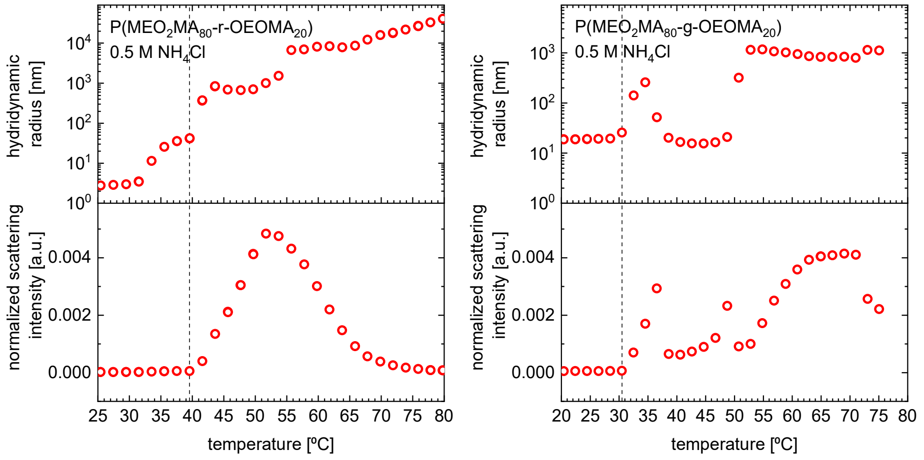

Fig. A10 DLS measurements of the random copolymer P(MEO$_2$MA$_{80}$-*r*-OEOMA$_{20}$), M$_n$ = 15.96 kDa, Đ = 1.17 (left) and gradient copolymer P(MEO$_2$MA$_{80}$-*g*-OEOMA$_{20}$), M$_n$ = 15.21 kDa, Đ = 1.24 (right) in NH$_4$Cl aqueous solution. The vertical dashed lines point out the abrupt change in the hydrodynamic radius (upper graph) and the normalized scattering intensity (lower graph) and indicates the LCST.

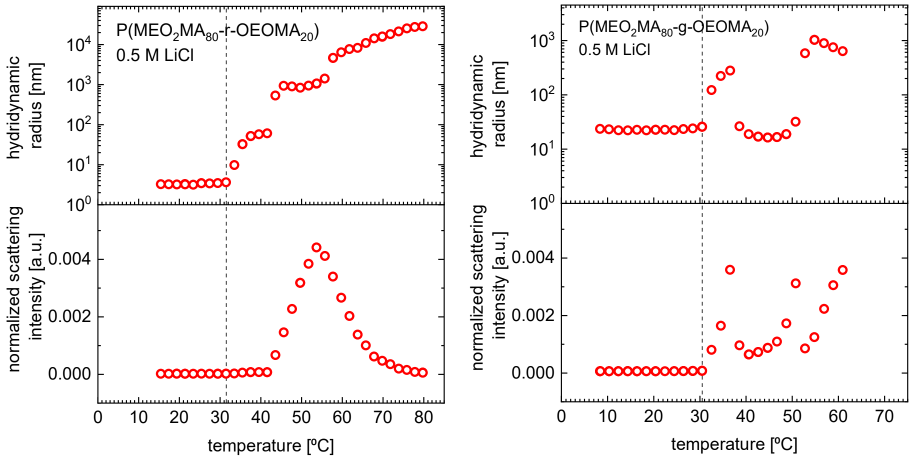

Fig. A11 DLS measurements of the random copolymer P(MEO$_2$MA$_{80}$-*r*-OEOMA$_{20}$), M$_n$ = 15.96 kDa, Đ = 1.17 (left) and gradient copolymer P(MEO$_2$MA$_{80}$-*g*-OEOMA$_{20}$), M$_n$ = 15.21 kDa, Đ = 1.24 (right) in LiCl aqueous solution. The vertical dashed lines point out the abrupt change in the hydrodynamic radius (upper graph) and the normalized scattering intensity (lower graph) and indicates the LCST.

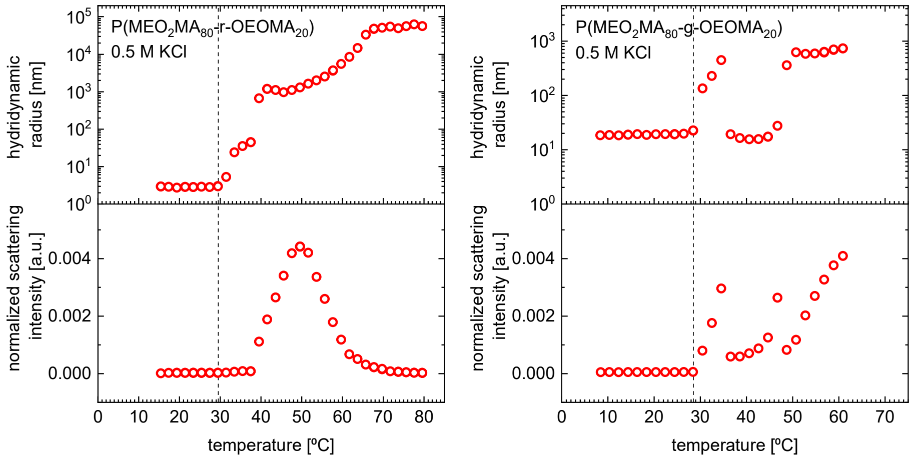

Fig. A12 DLS measurements of the random copolymer P(MEO$_2$MA$_{81}$-*r*-OEOMA$_{19}$), M$_n$ = 15.96 kDa, Đ = 1.17 (left) and gradient copolymer P(MEO$_2$MA$_{80}$-*g*-OEOMA$_{20}$), M$_n$ = 15.21 kDa, Đ = 1.24 (right) in KCl aqueous solution. The vertical dashed lines point out the abrupt change in the hydrodynamic radius (upper graph) and thenormalized scattering intensity (lower graph) and indicates the LCST

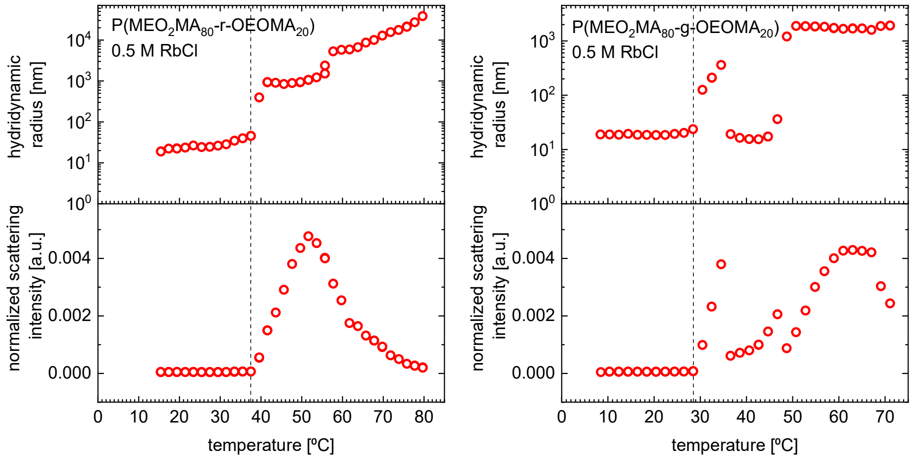

Fig. A13 DLS measurements of the random copolymer P(MEO$_2$MA$_{80}$-*r*-OEOMA$_{20}$), M$_n$ = 15.96 kDa, Đ = 1.17 (left) and gradient copolymer P(MEO$_2$MA$_{80}$-*g*-OEOMA$_{20}$), Mn = 15.21 kDa, Đ = 1.24 (right) in RbCl aqueous solution. The vertical dashed lines point out the abrupt change in the hydrodynamic radius (upper graph) and the normalized scattering intensity (lower graph) and indicates the LCST.

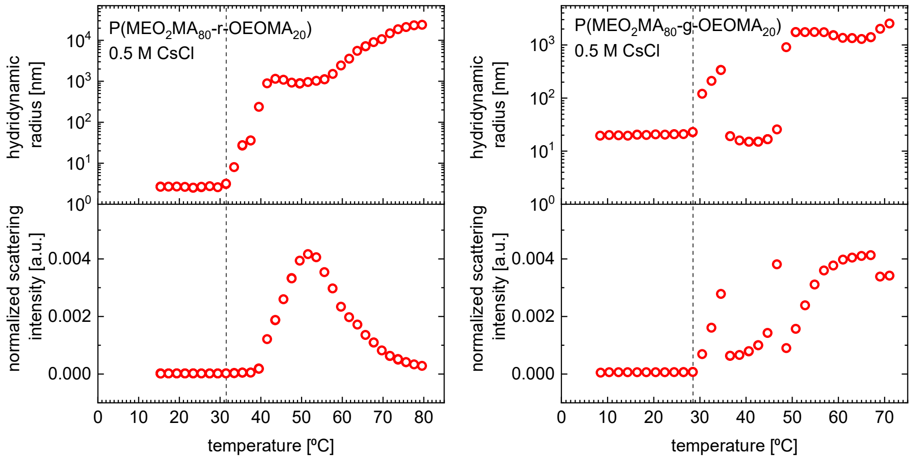

Fig. A14 DLS measurements of the random copolymer P(MEO2MA$_{80}$-*r*-OEOMA$_{20}$), M$_n$ = 15.96 kDa, Đ = 1.17 (left) and gradient copolymer P(MEO$_2$MA$_{80}$-*g*-OEOMA$_{20}$), M$_n$ = 15.21 kDa, Đ = 1.24 (right) in CsCl aqueous solution. The vertical dashed lines point out the abrupt change in the hydrodynamic radius (upper graph) and the normalized scattering intensity (lower graph) and indicates the LCST.

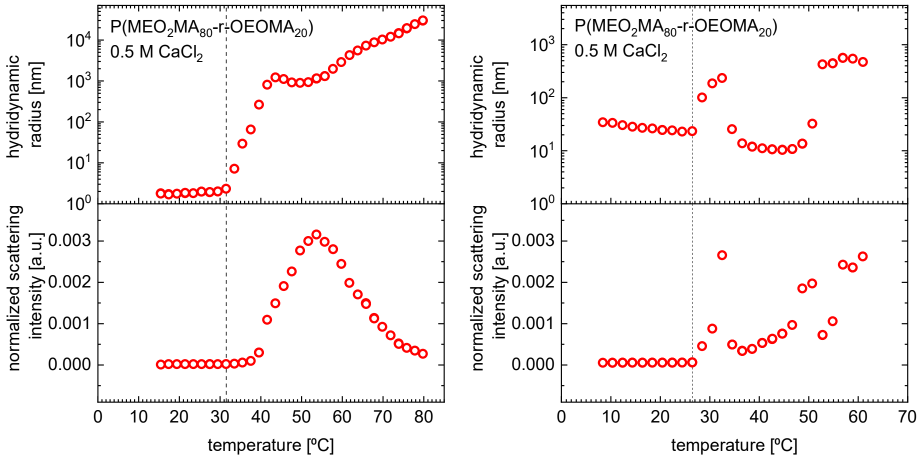

Fig. A15 DLS measurements of the random copolymer P(MEO$_2$MA$_{80}$-*r*-OEOMA$_{20}$), M$_n$ = 15.96 kDa, Đ = 1.17 (left) and gradient copolymer P(MEO$_2$MA$_{80}$-*g*-OEOMA$_{20}$), M$_n$ = 15.21 kDa, Đ = 1.24 (right) in CaCl$_2$ aqueous solution. The vertical dashed lines point out the abrupt change in the hydrodynamic radius (upper graph) and the normalized scattering intensity (lower graph) and indicates the LCST.

10.1.3 The effect of surfactants

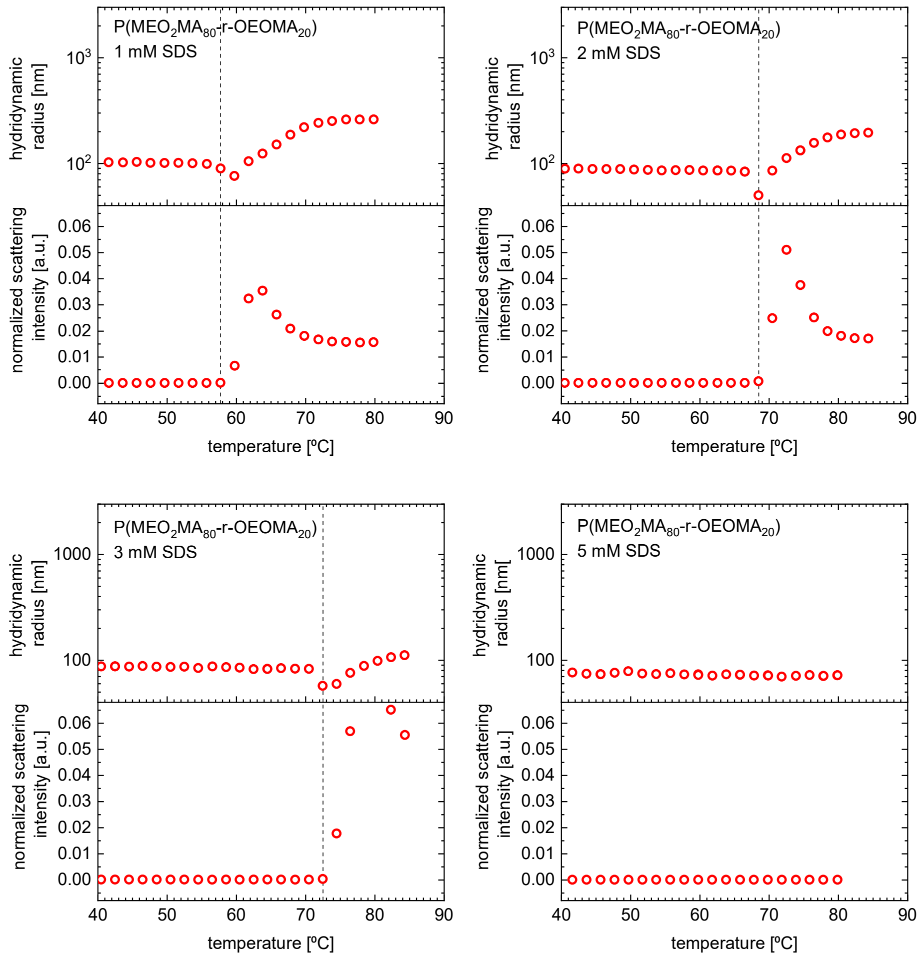

Fig. A16 DLS measurements of the random copolymer P(MEO$_2$MA$_{80}$-r-OEOMA$_{20}$), M_n = 15.96 kDa, Đ = 1.17 in SDS aqueous solution. The vertical dashed lines point out the abrupt change in the hydrodynamic radius (upper graph) and the normalized scattering intensity (lower graph) and indicates the LCST.

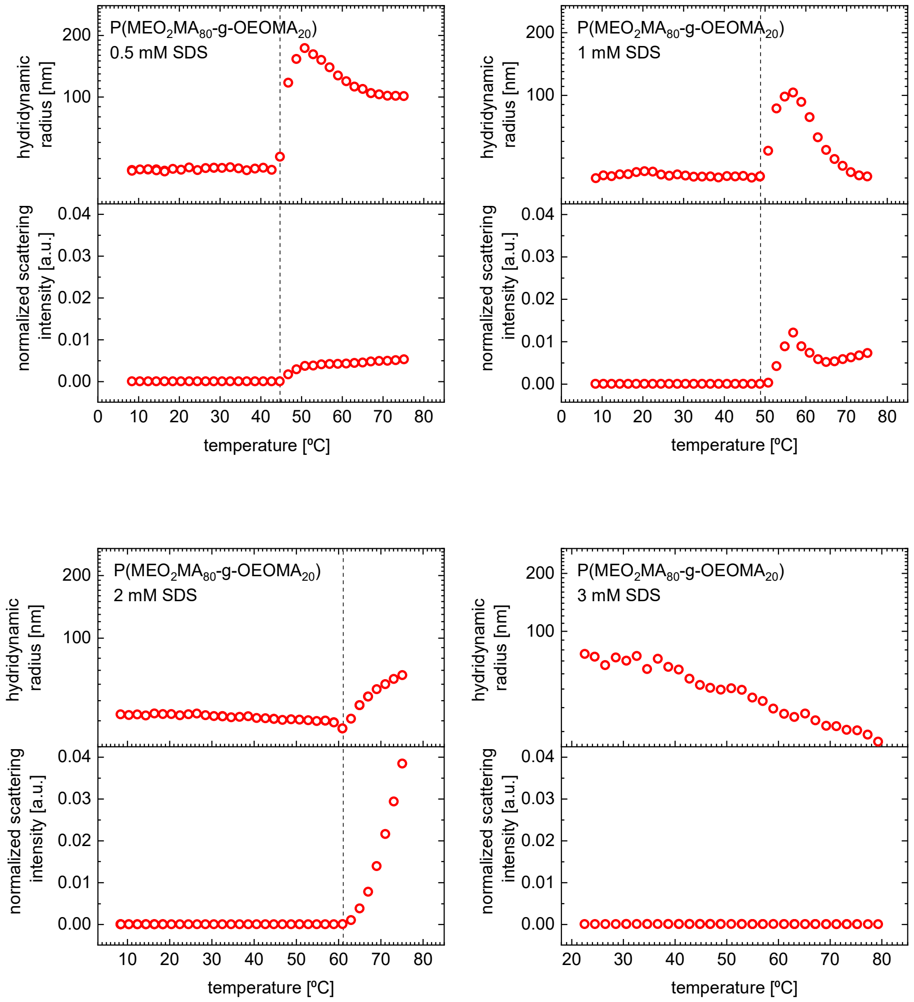

Fig. A17 DLS measurements of the gradient copolymer P(MEO_2MA_{80}-*g*-$OEOMA_{20}$), M_n = 15.21 kDa, Đ = 1.24 in SDS aqueous solution. The vertical dashed lines point out the abrupt change in the hydrodynamic radius (upper graph) and the normalized scattering intensity (lower graph) and indicates the LCST.

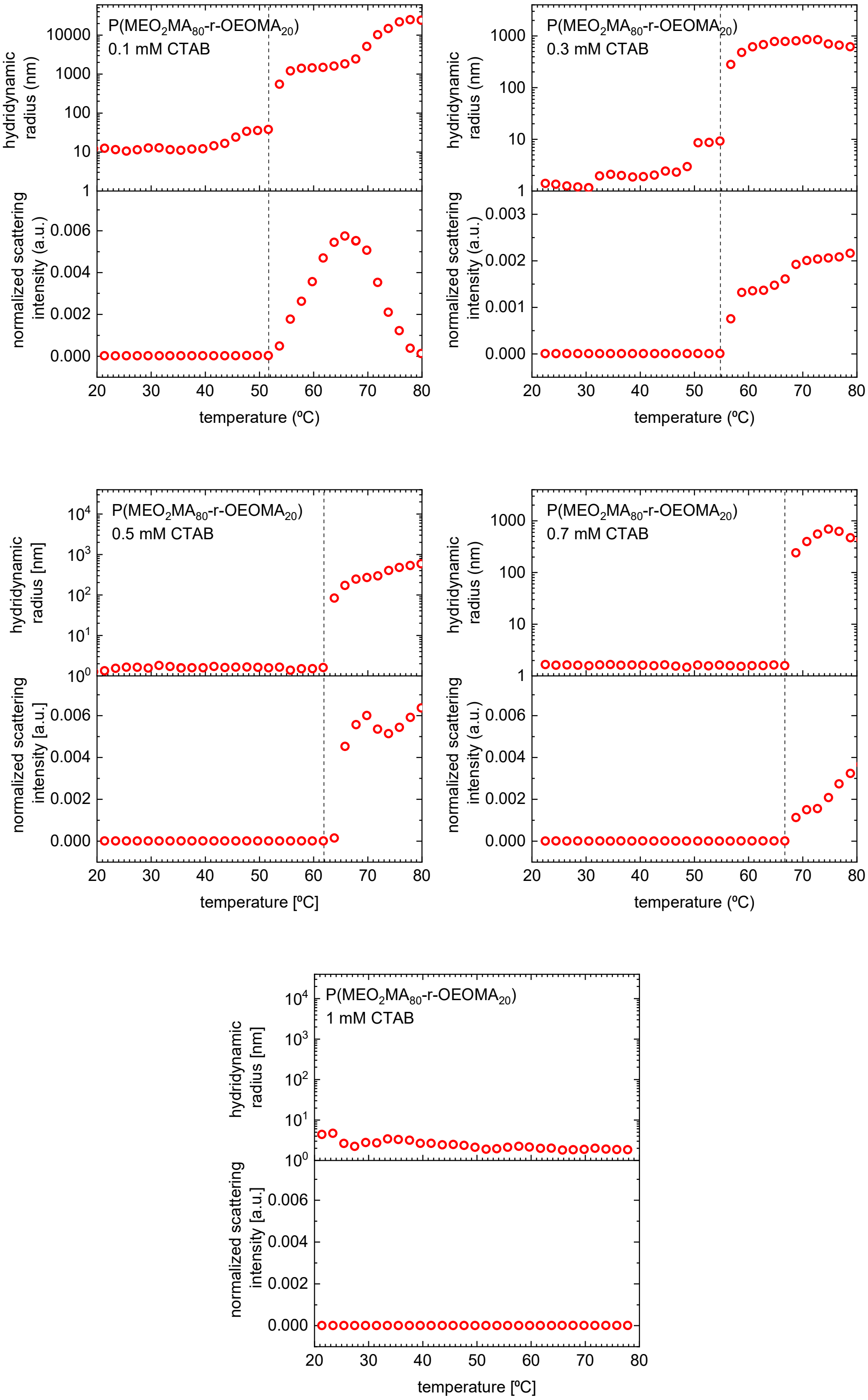

Fig. A 18 DLS measurements of the random copolymer P(MEO$_2$MA$_{80}$-*r*-OEOMA$_{20}$), M$_n$ = 15.96 kDa, Đ = 1.17 in SDS aqueous solution. The vertical dashed lines point out the abrupt change in the hydrodynamic radius (upper graph) and the normalized scattering intensity (lower graph) and indicates the LCST.

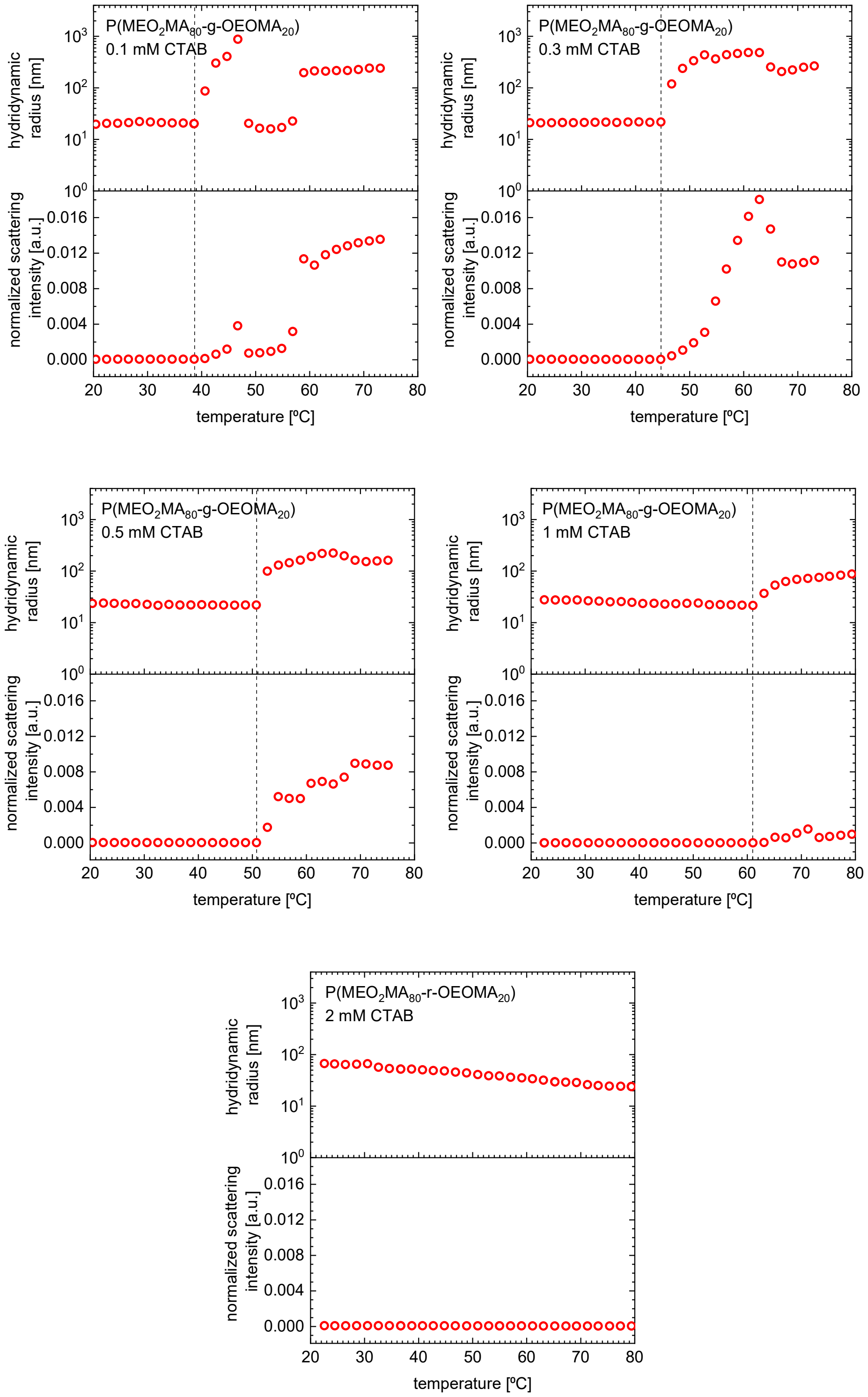

Fig. A19 DLS measurements of the gradient copolymer P(MEO_2MA_{80}-*g*-$OEOMA_{20}$), M_n = 15.21 kDa, Đ = 1.24 in CTAB aqueous solution. The vertical dashed lines point out the abrupt change in the hydrodynamic radius (upper graph) and the normalized scattering intensity (lower graph) and indicates the LCST.

10.1.4 The effect of ethanol

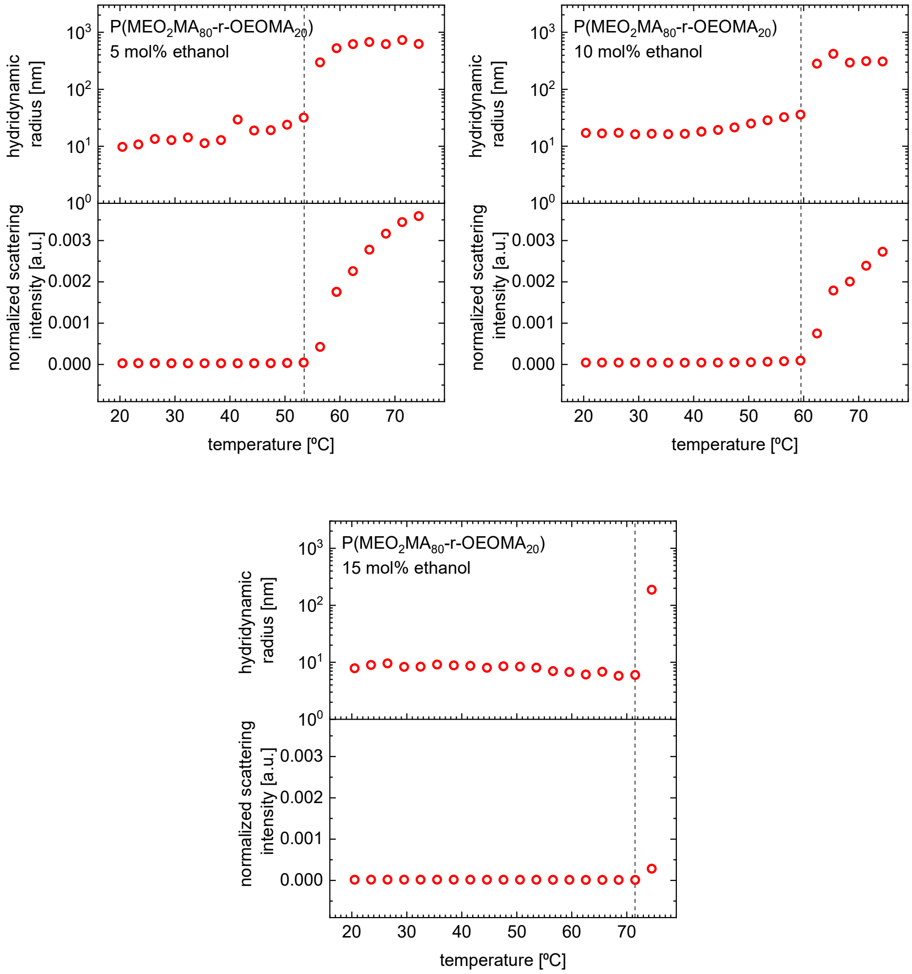

Fig. A20 DLS measurements of the random copolymer P(MEO_2MA_{80}-*r*-$OEOMA_{20}$), $M_n = 15.96$ kDa, Đ = 1.17 in ethanol-water mixture. The vertical dashed lines point out the abrupt change in the hydrodynamic radius (upper graph) and the normalized scattering intensity (lower graph) and indicates the LCST.

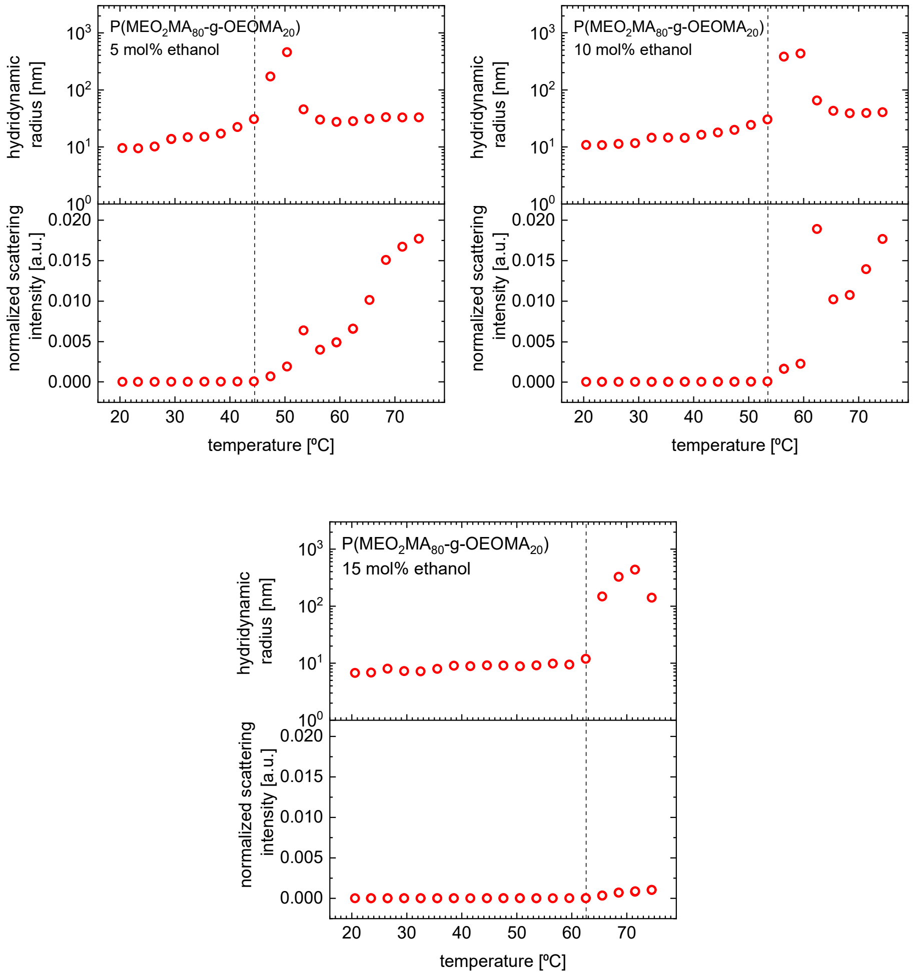

Fig. A21 DLS measurements of the gradient copolymer P(MEO$_2$MA$_{80}$-*g*-OEOMA$_{20}$), M_n = 15.21 kDa, Đ = 1.24 in ethanol-water mixture. The vertical dashed lines point out the abrupt change in hydrodynamic radius (upper graph) and normalized scattering intensity (lower graph) and indicates the LCST.

10.2 Used hazardous substances according to GHS

compound	**symbol**	**hazard statements**	**precautionary statements**
acetone		225–319–336– EUH066	210–240– 305+351+338– 403+233
aluminum oxide (basic)		————————	————————
aluminum oxide (neutral)		————————	————————
ammonium chloride		302–319	264–270–280–301+312– 305+351+338–337+ 313
anisole		226–336	210–233–240–241–242–243

			
argon		280	410+403
α-bromoisobutyric acid		314	280–305+351+338–310
α-bromoisobutyryl bromide		314	280–301+330+331–303+361+353–305+351+338+310
***sec*-butyllithium (1.4 M in cyclohexane)**	    	225–250–260–304–314–336–410	210–222–223–231+232–370+378–422
calcium chloride		319	264–280–305+351+338–337+313

calcium hydride		260	260
Cesium chloride		361f	201–308+313
cetyltrimethylammonium bromide	   	302–315–318– 335–373–410	273–280–301+312– 302+352–305+351+338–314
chloroform	  	302–331–315– 319–351– 361d–336–372	261–281– 305+351+338–311
copper(I) bromide		315–319–335	261–305+351+338

copper(II) bromide	  	302–314–410	260–273–280–303+361+353–304+340+310-305+351+338+310-391
cyclohexane	   	225–304–315–336–410	210–261–273–301+310–331–501
cyclohexanone	  	226–302+312+332–315–318	210–280–301+312–303+361+353–304+340+312–305+351+338

di ethylene oxide methyl ether methacrylate		315–317–319–335	280 - P302 + 352 - 305 + 351 + 338
di-*n*-butylmagnesium (1 M in *n*-heptane)	    	225–250–260–304–314–336–410	210–231+232–280–305+351+338–370+378–422
dichloromethane	 	315–319–335–336–351–371	260–280–305+351+338
***N,N'*-dicyclohexylcarbodiimide**	 	302–311–318–317	280–305+352–305+351+338–309+310

diethyl ether	 	224–302–336	210–261
4-(dimethylamino)pyridine		301–310–315–319–335	280–301+310+330–302+352+310–304+340+312–305+351+338–337+313
***N,N*-dimethylformamide**	  	226–312+332–319–360d	201–210–261–280–308+313–370+378
4,4′-dinonyl-2,2′-bipyridine		315–319–335	302+352–305+351+338

1,4-dioxane	  	225–319–335–351	210–280–305+351+338–370+378–403+235
ethanol	 	225–319	210–240–305+351+338–403+233
ethyl acetate	 	225–319–336	210–305+351+338–370+378–403+235
ethyl α-bromoisobutyrate	  	226 –302 –318	210–280–301+312+330–305+351+338+310

***N*-isopropylacrylamide**		302–319	305+351+338
lithium chloride		302–315–319	301+312+330– 305+351+338
methanol	  	225–301–311– 331–370	210–233–280– 302+352– 304+340– 308+310–403+235
oligo ethylene oxide methyl ether methacrylate		315–317–319– 335	261–264–271–280– 302+352–305+351+338
***N,N,N‘,N‘‘,N‘‘*- Pentamethyl diethylenetriamine**	 	302–311–314	260–280– 301+312+330– 303+361+353– 304+340+310– 305+351+338

2-propanol	 	225–319–336	210–305+351+338– 370+378–403+235
propylene oxide	  	224–302– 311+331–315– 319–335–340– 350	201–210–261– 280– 305+351+338– 308+313
Sodium dodecyl sulfate	  	228–302–315– 318–335–412	210–273–280– 301+312+330–302+352– 305+351+338 +310
sodium fluoride		301–315–319– EUH032	302+352– 305+351+338– 308+310
sodium iodide		400	273

sodium thiocyanate		302+312+332–319–412–EUH032	273–280–305+351+338
sulfolane		302	301+312+330
styrene	  	226–315–319–332–361d–372	201–210–261–280–304+340+312–308+313
styrene oxide	 	312–315–317–319–331–340–350	201–261–280–305+351+338–311

tetrahydrofuran		225–302–319–335–351	210–280–301+312+330–305+351+338–370+378–403+235
toluene		225–304–315–336–361d–373	210–260–280–301+310–370+378–403+235

11 Aknowledegement

I have been supported by several people during this PhD work and I'd like to thank and acknowledge them for their scientific and moral support. First of all, I thank prof. Volker Abetz for providing me the opportunity to pursue my PhD work at the university of Hamburg on such a challenging topic. I really appreciate the helpful scientific discussions and positive feedback on my work.

There were several people who proofread this thesis prior to submission. I thank Lucian Blaga, Maryam Radjabian, Felix Lauterbach, Niklas Lucht, Stephan Hinrichs and Iklima Oral very much.

I've used several facilities at the department of chemistry, university of Hamburg which were crucial for the progress of the work. I specially thank Birgit Hankiewicz for the help with analyzing the results of light scattering. I thank Margarethe Fritz and Andreas Meier for the help with AFM measurement. I also appreciate the help of Andreas Meier for SAX measurement and the help with analyzing the results. Margarethe Fritz and Nina Schober are thanked for performing all the SEC measurements. Martin Kehden is thanked for the DSC measurements. I'm also very thankful to him and Margarethe Fritz for laboratory technical support. Alexandra bey introduced me to anionic polymerization and ATRP in the lab. I'm very thankful for her generosity in sharing knowledge, our fruitful scientific discussions and brainstorming and endless moral support. I'm also very thankful to Daniela Weinert, Robert Schön and Andreas Kornowski from the group of Prof. Horst Weller for SEM measurements.

I'd like to specially thank Sigrid Zeckert, our secretory in the group of Prof. Abetz for her support in administrative work. I'm also extremely thankful for her great understanding and kindness. The charm of fresh coffee in the morning always reminds me of you.

I'm also very thankful to Nina Schober for the help to settle down in Germany from finding a place to stay to going through complicated bureaucratic procedures, for

reading and translating all my German documents so kindly at the start of my work and for her unconditional friendship.

Taida Gil-Haenelt, Alexandra Bey, Elaine Rahmstohf, Doreen Alisch, Steffen Eggers, Elizabeth Wittenberg, Iklima Oral, Stephan Hinrics, Niklas Lucht, Felix Lauterbach, Merlina Thiessen, Birgit Hankiewics, Melanie Bencken, Margarethe Fritz, Nina shober, Martin Kehden and Ulf König are thanked for being such great colleagues and providing a friendly atmosphere to work with pleasure. I've learnt a lot from you and I always appreciate the way you helped me grow scientifically and personally.

During my PhD, I was additionally assisted by students who did their bachelor's thesis or a student laboratory course with me. Hence, I thank Simon Bittman, Janina Krügel, Moritz Münzmey Simon Doerner, Mitra Zolfagharikhani and in particular Iklima Oral and Stephan Hinrichs for their great work.

In the end I'd like to thank my family for always believing in me, supporting me and for the great motivation they inspired. And last but not least, a big thank you to my husband Lucian Blaga, who has been always there for me in the rainy and sunny days of our lives.

12 Decleration of oath

I hereby declare on oath, that I have written the present dissertation by my own and have not used other than the acknowledged resources and aids. The submitted written version corresponds to the version on the electronic storage medium. I hereby declare that I have not previously applied or pursued for a doctorate (Ph.D. studies).

Maryam
Bozorg

08.03.2021